NASA Conference Publication 2080

12th Aerospace Mechanisms Symposium
NASA, Cal-Tech, Lockheed

A Symposium held at
Ames Research Center
Moffett Field, California
April 27-28, 1978

NASA

NASA Conference Publication 2080

12th Aerospace Mechanisms Symposium
NASA, Cal-Tech, Lockheed

A Symposium held at
Ames Research Center
Moffett Field, California
April 27-28, 1978

National Aeronautics
and Space Administration

**Scientific and Technical
Information Office**

1979

CONTENTS - AGENDA

CONTENTS - AGENDA (Continued)

April 28, 1978
MORNING SESSIONS

Peter T. Lyman, Session Chairman, Jet Propulsion Laboratory

James H. Parks, Session Chairman, NASA Langley Research Center

Frank T. Martin, Session Chairman, NASA Goddard Space Flight Center

CONTENTS - AGENDA (Concluded)

AFTERNOON SESSIONS

Mervin Briscoe, Session Chairman, SPACEUROP, The Netherlands

Tour of NASA Ames Research Center: World's Largest Wind Tunnel, Aircraft Simulation Facilities, and the Ames Aircraft Flight Line

PREFACE

The Aerospace Mechanisms Symposium is devoted exclusively to the interchange of information relative to aerospace mechanisms. Information gathered from the formal presentations is but one of the benefits to be gained from this two-day meeting. Another important reward is gained from the professional and technical discussions and associations which begin here and are carried on long after the 12th Symposium is brought to a close. It is our sincere desire that you profit from the many opportunities presented during the planned break periods and social activities.

We hope your visit to the Ames Research Center is both enjoyable and rewarding.

Angelo Giovannetti
Host Chairman

ORGANIZING COMMITTEE

Charles W. Coale, General Chairman, LMSC
Ernest E. Sechler, Administrative Chairman, CIT
Alfred L. Rinaldo, Operations Chairman, LMSC
Angelo Giovannetti, Host Chairman, ARC

Paul W. Bomke, NASA-JPL
Aleck C. Bond, NASA-JSC
Mervin Briscoe, SPACEUROP
Kenneth S. Bush, NASA-LRC
Kenneth C. Curry, NASA-JPL
David F. Engelbert, NASA-ARC
John D. Ferrera, NASA-JPL
James H. Parks, NASA-LRC
Bowden W. Ward, Jr., NASA-GSFC
David F. Welch, CIT

Symposium potpourri

Dr. Ernest E. Sechler opens the symposium.

OPENING REMARKS

Dr. Ernest E. Sechler
CALTECH

It is my privilege to be the first speaker on this, the 12th Aerospace Mechanisms Symposium. A little over a decade ago Dr. George Herzl of Lockheed came to the conclusion that the people who really were responsible for the successes of the various Aerospace programs had no forum in which they could discuss their problems, their successes, and their failures. These people were those who designed and helped develop the various mechanisms which were the sinews and the muscles which actually did the work called for by some human or computer brain. He convinced two others that something should be done and the three original founders, George Herzl, Richard Pefley, and William Schimandle, conceived the idea of an annual meeting of people interested in mechanisms of all kinds where ideas could be interchanged in an atmosphere of mutual respect and understanding. This is the twelfth of such meetings.

The three sponsors of each meeting have been:

1. One of the NASA Centers - representing the interest of the Government Research Centers in mechanisms of all kinds.
2. Lockheed - representing the industrial complex whose successes depend on mechanisms performing in a specified manner, and
3. Academia - first represented by Santa Clara University and now by CALTECH.

We are pleased that some of the original organizing committee members are present at this meeting, among them being Lloyd Jones, Pete Lyman, and Jim Adams. Also, we welcome officially a new committee member from abroad, Mervin Briscoe of the European Space Agency, who has been instrumental in making these symposia of international interest.

Only one more item - we are holding an attractive carrot before all of our speakers. At the end of Friday's meeting, the Committee will vote on the best presentation made at this symposium. The winning speaker will then be awarded the George Herzl Plaque for his presentation.

DEVELOPMENT OF A BEDREST MUSCLE STRESS APPARATUS

By Cletis R. Booher
NASA Johnson Space Center

Sonne L. Hooper and Drel N. Setzer
Nelson & Johnson Engineering, Incorporated

ABSTRACT

In attempting further to define the deleterious effects of spaceflight on the human body, measurement systems and techniques were devised to determine the loss of skeletal muscle strength and tone as a result of spaceflight exposure. In order to determine how the muscle degradation process progresses with time during nonuse, a system for measuring muscle stress during bedrest was developed. The Bedrest Muscle Stress Apparatus (BRMSA) is configured to slip snugly over the foot board of a standard hospital bed. Data collected with this device correlated well with pre- and post-bedrest data collected with the original skeletal muscle stress apparatus (SMSA).

****

Since man first ventured into the strange, new environment created by space travel, medical doctors and physiologists have been trying to determine the basis and extent of the physiological changes which living organisms, particularly the human body, experience in these surroundings. These studies have encompassed experimental systems and protocols covering a wide range of types and complexity. These efforts have progressed from the very simple types of "bungee" exercisers utilized in the early Mercury and Gemini flights to the very sophisticated medical experiment systems flown during the Skylab program. The Skylab equipment was designed to quantify precisely, among other measurements: metabolic rate, cardiovascular function, vestibular response, and sleep effectivity.

During the latter stages of the Skylab program and the Apollo-Soyuz Test Project (ASTP) a group of investigators at Johnson Space Center (JSC) began to reason that another possibly significant aspect of the overall physiological effect of the space environment might be determined by measuring the changes which occur in muscle strength and efficiency during spaceflight. A great amount of one-G research, utilizing various types of muscle stress techniques and electromyographic (EMG) recording systems, had been conducted to gather this type of data, and the applicability to zero-G effects seemed obvious.

A method for developing roughly reproducible stress levels in the gastrocnemius muscle with minimal external devices in the one-G environment was utilized to measure the change in strength and efficiency in the crew of the second Skylab mission during their 59-day flight. The measurement consisted of having the subject balance on the ball of his foot on the leg of interest for a specified period of time both with and without holding an additional 40-pound weight. The gastrocnemius is the muscle located on the back of the lower leg just above the Achilles tendon.[1]

A Skeletal Muscle Stress Apparatus (SMSA) which allows relative isolation

of the muscle or muscle groups of interest such that they can have known forces applied to them was developed to gather muscle strength and efficiency data from the American contingent of the ASTP crew. The basic SMSA consists of chair and pedestal assemblies which are structurally tied together at their bases to form an integral system (see Fig. 1). The pedestal assembly, located in front of the chair, is adjustable fore and aft and to the left and right with respect to the chair for the purpose of accommodating 5th through 95th anthropometric percentile subjects and utilization of either left or right limbs. A treadle which is suspended in the pedestal assembly approximately 16 inches above the floor is coupled to a Statham Instruments Model UL3 universal transducing cell through a model UL4, 0 to 200 pounds load cell accessory. The treadle is also coupled, through a cable and bell crank system, to a wrist strap.

Measurements are made on the gastrocnemius and soleus muscles in the leg by the subject seating himself in the chair assembly and placing the foot of interest in the treadle, the EMG electrodes having been previously located properly on the leg. The treadle is constructed such that the point around which it pivots coincides approximately with the subject's ankle position. The pedestal assembly is located with respect to the chair such that the knee stop may be brought down confortably on the subject's knee and locked firmly into place on the pedestal assembly for the purpose of inhibiting movement in the subject's leg when the experimental data is being gathered. Pressure against the treadle by the ball of the subject's foot is measured by the force cell and displayed on a meter in the field of view of the subject, usually on top of the knee stop.

Measurements are made on the biceps brachii and brachioradialis muscles by placing the wrist of the properly electroded arm through the wrist strap. The elbow rest and wrist strap tie strap are adjusted to allow the subject to sit in a comfortable, upright position with his forearm at a right angle to his body truck and no input being registered by the force cell. Force applied by the subject at his wrist in an upward direction is measured by the force cell and displayed on the meter. The force measurement system is calibrated with a cantilever weight device which is designed to attach directly to the bell crank in lieu of the wrist strap tie strap.

The SMSA was successfully utilized on the American ASTP crewmembers for preflight measurements, but the exposure of this crew to toxic gas during descent and the subsequent concern for crew health prevented muscle characteristic data from being collected on all but one of the crewmembers post recovery.[2] The SMSA was also utilized as an onboard experiment in a simulated dedicated Life Sciences Spacelab mission in January 1976.[3]

EMG data reduced from the studies conducted during the second Skylab and ASTP missions indicated that the anti-G muscles become very susceptible to fatigue when subjected to weightless conditions. These effects apparently start early in the weightless period and increase in severity as the weightlessness continues. The time course of these characteristics was not, however, easily definable with just the two sets of data - the second of which (post-ASTP) was rather sketchy anyway. It became obvious that the only way to get good information relative to the time sequence of changes in the anti-G muscle characteristics was to devise a system to determine these changes in real-time.

The best currently known analogy to spaceflight conditions relative to physiological changes which can be easily implemented in ground-based testing is bed rest. Although many investigators argue - probably correctly - that various phenomena which significantly affect specific physiological changes during spaceflight are absent from bedrest situations, the overall deconditioning effect is still strikingly similar. Since no U.S. spaceflights were being scheduled following the ASTP mission, and since in the interim several bedrest studies were, it was determined by the investigators that a device to determine muscle degradation in bedrest subjects would be very useful.

Since one very important requirement of bedrest studies is that the subjects must remain in a supine position at all times, a basic design constraint for any type of Bedrest Muscle Stress Apparatus (BRMSA) would have to be that it must be usable without requiring the subjects to arise from bed. It also seemed desirable to provide a device which could be easily moved from one bed to another so that minimal disturbance of the bed-resting subjects would be required while performing the muscle stress tests. The initial response to these requirements was a concept of a system which could easily be slipped onto the footboard of the bed on which the subject was lying. Although this is the concept which was incorporated into the final BRMSA design, actual utilization of the equipment turned out to be not as simple as originally conceived and the ease of movement between beds concept was essentially negated during operational use.

After careful study of the beds utilized by the hospital in which the initial bedrest study was to be conducted, the basic BRMSA design was developed. The basic frame is devised to fit snugly over the footboard with one end placed directly over the main supporting corner post of the bed. The frame is symmetrical so that it can be placed at either side of the footboard to allow the subject to be tested on either his right or left limbs.

A treadle almost identical to the one utilized in the original SMSA, particularly with respect to subject interface, is suspended in the middle of the frame and coupled to a load cell and transducer identical to that utilized in the SMSA. The treadle is configured with multiple holes around the perimeter to interface with the load cell force bar such that adjustment of the treadle base angle relative to the orientation of the subject's leg can be accomplished (see Fig. 2). The Principal Investigator desired this adjustment in order to allow testing to be accomplished with the subject's foot placed at various angles relative to his leg - in particular, toe-down angles.

The arm stress interface with the treadle load cell system is accomplished by providing an adjustable-length rod which attaches to a cloth strap around the subject's wrist on one end and one side of the treadle on the other end. Multiple holes are provided in the treadle side for this interface, also to allow adjustment relative to the angle of the rod, determined by the subject's forearm length, with respect to the treadle height above the top of the mattress. The direction of pull on the rod exerted by the subject's wrist was to be kept perpendicular to a line from the treadle pivot point to the rod attach point.

One of the most perplexing aspects of the BRMSA development program was devising a method for restraining the subject's body against the isometric forces he would be exerting. Several concepts were examined and discarded before the final configuration was developed and implemented. The restraint

system had to be reasonably comfortable on the subject while he maintained his supine position during the test period, and fairly easy to don in this position also. It could not interfere significantly with the various physiological sensors placed on the subject's body, and still had to withstand the reaction to the isometric forces applied by the subject which were to range up to 300 pounds and more.

Anthropometric data indicated that a restraint system which would distribute the force at both the waist and shoulders would be the most efficient and the most comfortable for the subject. The waistband portion of the final restraint configuration was a custom-built unit based on the concept of a backpack waistband, but with longer pads to extend entirely around the subject's waist. Attach points were very securely sewn into the top and bottom of the band to accept the shoulder straps and subject restraint cables, respectively. The shoulder straps were of a padded adjustable type - lengthened versions, as a matter of fact, of the shoulder straps developed for the Skylab bicycle ergometer restraint system. These straps were crossed across the subject's chest in use and when they and the restraint cables were cinched down to allow minimal movement of the subject against the isometric forces he exerted during testing, the entire restraint system felt reasonably comfortable and quite secure. The restraint cables attached to each side of the BRMSA frame close to the top with pip pins which passed through a multi-hole metal strap on the end of the cables.

The inside surfaces of the frame "legs" which contacted the footboard were covered with a hard, slick rubber-like material to facilitate installation and removal of the BRMSA on and off the footboard. The instrumentation package which contained the electronic circuitry to perform the force and EMG measurements was mounted on a flat plate which had hooks at one end to engage mating holes located on the top of the BRMSA frame, allowing this package to hang down along the outer side of the BRMSA.

The muscle force output from the universal transducing cell was fed into a Statham Instruments Model SC1100 bridge amplifier. An additional stage of gain was added so that the output from the bridge amplifier could be optionally increased when measuring low force levels. A meter, with scales calibrated in pounds of force, was mounted on a small metal box. This box was then placed in a location from which the subject could easily monitor the reading and thus maintain the fixed force levels required by the test protocol.

Captured pins, the ends of which fell approximately 1 inch below the main box section of the BRMSA frame, were located at each end of the frame between each pair of "legs" such that the pin at the end of the frame located at the extreme end of the footboard would engage the hole located on the top of the footboard at this point. This arrangement prevented any possible lateral movement of the BRMSA along the footboard. Two handles located at each end of the BRMSA frame to facilitate placement and removal of the unit on and from the footboard complete the BRMSA design configuration.

Calibration is accomplished through the use of a calibrator arm which hooks under the treadle pivot point on each side and rests on the force cell linkage in a horizontal position. The distances between the pivot point and the effective center of gravity of the calibrator arm are calculated to impart the known 100-pound calibration force to the force measurement system.

A typical use sequence of the BRMSA would proceed in the following manner:

Sensoring - EMG and sensors for other measurements which may be made before, during, between, or after stress sequences which require electrical contact with the body are attached at appropriate locations on the body. These other measurements may include electrocardiogram, vectorcardiogram and/or electroencephalogram. Also, sensors which will be located in proximity to or underneath the restraint system are usually applied at this time. These may include a pneumogram strain gauge, a phonocardiogram sensor, leg volume cuff assembly, and other trunk or leg-mounted sensors.

System configuring - The BRMSA is mounted at the appropriate side of the footboard. The instrumentation package is hung on the outboard side of the BRMSA, appropriate power and signal connections are made, and the system is turned on. Other instrumentation appropriate to the particular investigation being conducted will probably be connected and powered up at this time also.

Calibration - The calibration arm is placed on the BRMSA in the appropriate location and all systems and real-time readouts are adjusted to reflect the 100-pound calibration value. Other systems utilized in the particular investigation are usually calibrated as appropriate at this time. The calibration arm is removed from the BRMSA at the conclusion of this sequence.

Restraint donning - The subject is rolled to one side or the other as convenient and the restraint belt and shoulder straps are placed on the bed in such a manner that they can easily be wrapped around the subject and secured when he rolls onto his back again. The shoulder straps are loosely attached to the belt and the restraint cables are adjusted to give a good pull against the isometric forces. The restraint cables can most easily be attached to the BRMSA (after being attached to the belt) if the subject allows his knee to bend up slightly, then be straightened back out to check the cable length adjustment. The shoulder straps are then cinched down snugly and the entire restraint system is checked for tightness and comfort and further adjusted as necessary.

Final configuring - Any additional sensors appropriate to the investigation being pursued, such as a blood pressure cuff and microphone, are placed on the subject and all sensors are connected to their appropriate instrumentation systems. The subject places his appropriate limb in place, his foot in the treadle or his wrist through the wrist strap, which will have been connected to the treadle via the adjustable rod. With the subject relaxed (to the extent possible), any force values being registered in the system due to the tightness of the restraint system is nulled out.

Force application - Force is applied against the treadle with the foot by the subject pushing with the ball of his foot only. Force is applied with the arm by the subject pulling straight up (toward his head) with his elbow only. Force is usually applied for a few seconds up to a minute in a sequence of percentages of a previously-determined maximum voluntary contraction (MVC) value. The MVC value is determined by the subject pushing with the maximum force possible for a very short length of time in each of the test configurations desired. The MVC is many times re-checked at the conclusion of a stress sequence.

A typical sequence for leg muscle stress levels might be as follows:

10 seconds at 30% MVC
20 seconds rest
10 seconds at 40% MVC
20 seconds rest
10 seconds at 20% MVC
20 seconds rest
60 seconds at 50% MVC
60 seconds rest
MVC
Relax

The subject maintains these fixed percentage MVC levels by monitoring the force level meter at the levels prescribed by the test conductor.

Initial utilization of the BRMSA showed all of the basic concepts incorporated into the system design to be sound. There were, however, a few shortcomings which had to be rectified before the system could be utilized to its fullest extent. When pressure was first applied by a test subject against the treadle, it became immediately obvious that the backplate against which the heel rested came up too far from the soleplate and caused interference by bearing against the Achilles tendon. This problem was rectified for the "foot flat" test position (the foot approximately perpendicular to the leg) by placing a piece of foam rubber between the subject's leg and this plate. This situation, however, rendered the BRMSA totally useless for any type of toe down testing.

A couple of MVCs by the (fortunately) rather large test subject during initial checkout of the BRMSA quickly revealed several less than adequate components in the initially-devised subject restraint system. The hooks which attached the restraint cables to the subject restraint harness had to be upgraded considerably, and the restraint waistband attach points had to be strengthened also.

As the first of the actual in-bed tests were being accomplished, it was observed that, despite the apparent sturdiness of the hospital beds being utilized and the theoretical offsetting of the forces being generated by the subject with the subject restraint system, there was indeed considerable movement being effected between the footboard and the bedrails. It therefore became necessary to devise an additional restraint system for use between the footboard and the bedrails to prevent movement between these components of the bed. Two cables with turnbuckles at one end and terminations which could be attached quickly to the footboard (one actually attached to the BRMSA frame) and the rails were fabricated and installed. This extra bracing effectively eliminated a large portion of the footboard-to-bedrail movement.

As the procedures and techniques for setting up and operating the BRMSA and other systems associated with the bedrest study became more coordinated and streamlined, it became apparent that setting the system up on one bed and then shifting subjects in and out of that bed, rather than moving the equipment from bed to bed, was a much more efficient mode of operation. This was due mainly to the quantity of equipment to be moved rather than any problems with moving the BRMSA itself from one bed to another.

Data collected with the BRMSA correlated well with pre- and post-bedrest

data collected with the original SMSA. The absolute values of the data obtained from the BRMSA were slightly higher than the SMSA data due to a better mechanical advantage for the subjects in the supine position, but all frequency and trend data correlated very well between the two units.[4]

In addition to its proven value for gathering in-test muscle stress data during bedrest simulations of the zero-G environment, it would appear that the BRMSA might also have definite application in certain clinical situations. Since long-term confinement of patients in bed does have the precise deleterious effect on the cardiovascular and skeletal muscle system which makes it a valuable corollary to the zero-G environment, it would seem that a system of this type would be useful at least to keep track of a long-term bedridden patient's muscle strength deterioration, if not also to provide therapeutic assistance in maintaining a minimal level of skeletal muscle and cardiovascular system tone. It is the contention of many cardiologists that isometric exercise is one of the best adjuncts to building and maintaining a health cardiovascular system, in addition to its obvious positive effects on the skeletal muscle system.

In conclusion, the authors wish to acknowledge several individuals without whose inputs and efforts this program would never have existed or been accomplished. Earl V. LaFevers, Ph.D., recently with JSC's Bioengineering Systems Division and now a human factors consultant, was Principal Investigator and prime mover on all of the muscle stress studies conducted at JSC over the past 4 years. It was at his behest that the BRMSA was devised, and without his constant encouragement (and in some cases, harassment) it would never have been built. Mr. James S. Arthur of JSC's Equipment Engineering Branch handled the myriad administrative details involved with the contract under which Mr. Hooper and Mr. Setzer accomplished the detailed design of the system, and in conjunction with Mr. Dave Mullins of the Planning and Scheduling Office, administered the fabrication contract for the BRMSA. Mr. Eugene K. Wendler of JSC's Crew Systems Division is to be commended for his tireless hours spent in designing, redesigning, and repairing the subject restraint harness. Mr. Joe Baker, Mr. William N. Crozier, and Mr. John Donaldson of Technology, Incorporated's Cardiovascular Laboratory support group at JSC are also to be given a large amount of thanks for their diligent work in the design, fabrication, maintenance, and operation of the BRMSA instrumentation system.

References

1. LaFevers, E. V., Nicogossian, A. E., Hoffler, G. W., Hursta, W. N. and Baker, J. Spectral Analysis of Skeletal Muscle Changes Resulting from 59 Days of Weightlessness in Skylab II. NASA TM X-58171, 1975.

2. LaFevers, E. V., Nicogossian, A. E. and Hursta, W. N. Electromyographic Analysis of Skeletal Muscle Changes Arising from 9 Days of Weightlessness in the Apollo Soyuz Space Mission. NASA TM X-58177, 1976.

3. Life Sciences Spacelab Mission Simulation II Science Report; pp. 163-182, 1977.

4. LaFevers, E. V., Booher, C. R., Crozier, W. N. and Donaldson, J. Effects of 28 Days of Bedrest Immobilization on the Responses of Skeletal Muscle to Isometric Stress. JSC Final Report, unpublished, 1976.

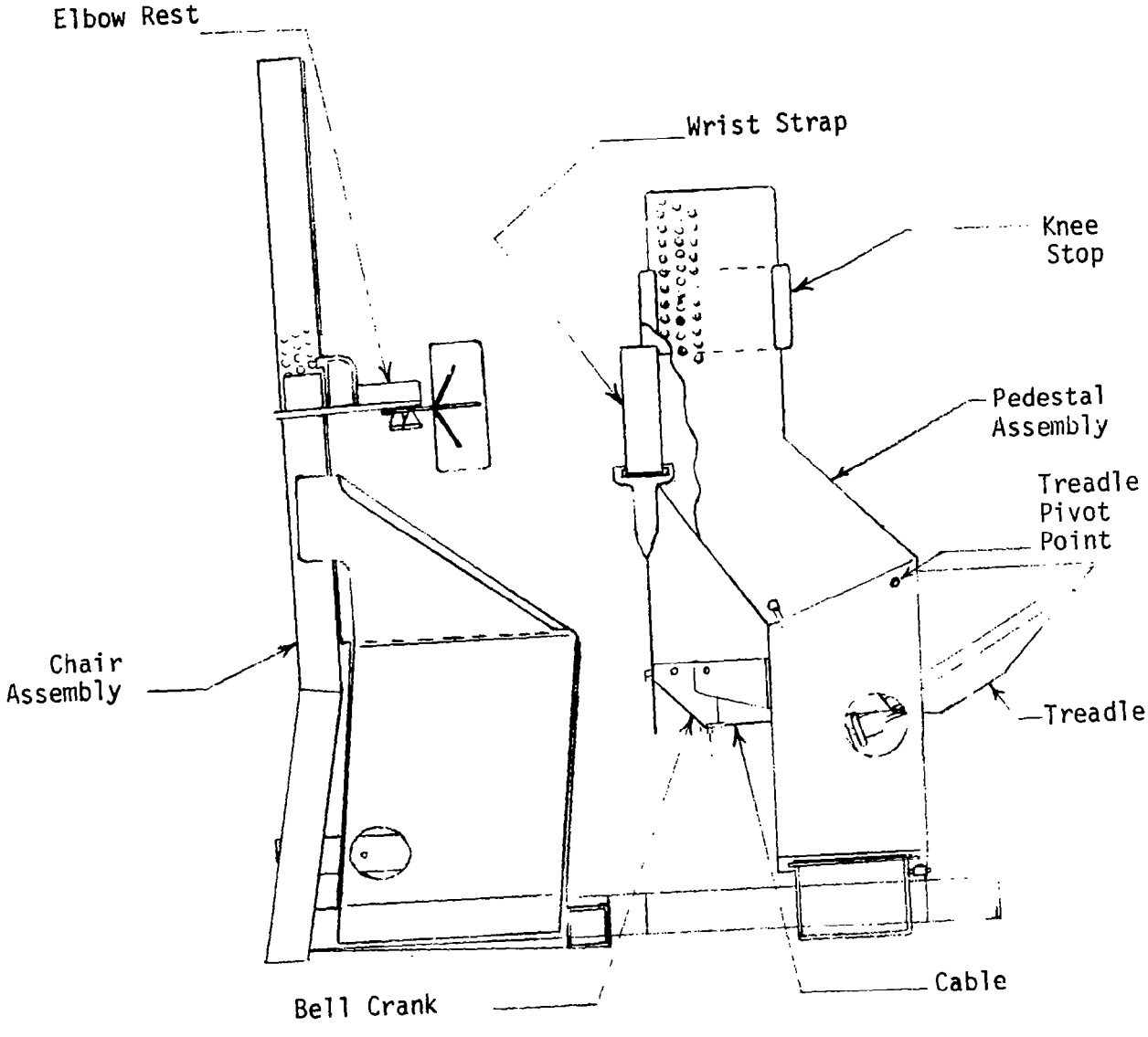

FIGURE 1 - SKELETAL MUSCLE STRESS APPARATUS

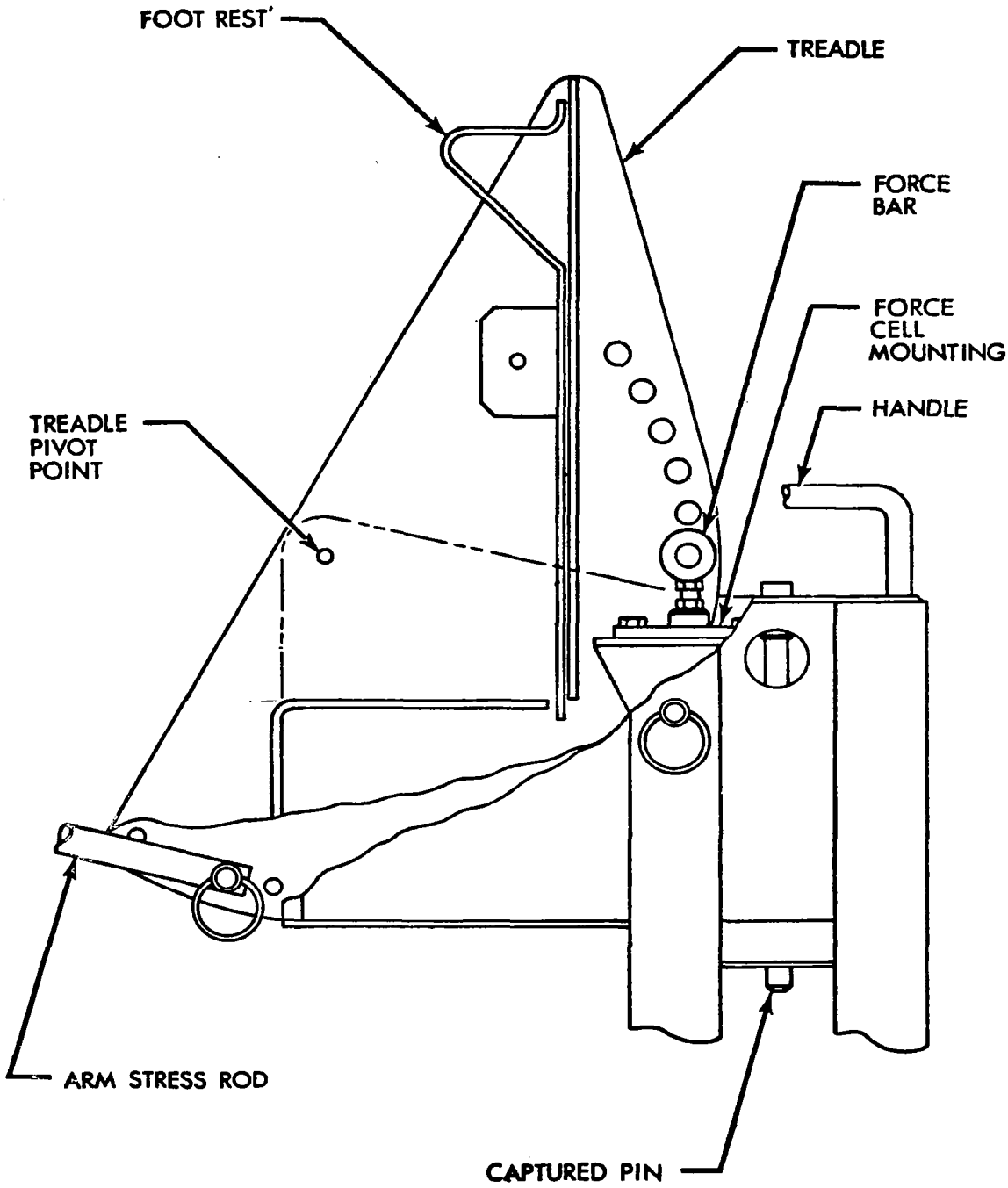

FIGURE 2 – BED REST MUSCLE STRESS APPARATUS

ULTRA HIGH RESOLUTION STEPPER MOTORS

DESIGN, DEVELOPMENT, PERFORMANCE

AND APPLICATION

By
H. Moll
G. Röckl

T E L D I X GmbH
Heidelberg/Germany

ABSTRACT

The design and development of stepper motors with steps in the 10 arc sec to 2 arc min range is described with detailing some of the problem areas, e.g. rotor suspension, tribology aspects and environmental conditions.

A summary of achieved test results and the employment in different mechanisms already developed and tested will be presented to give some examples of the possible use of this interesting device. Adaptations to military and commercial requirements have been proposed and show the wide range of possible applications.

INTRODUCTION

The stringent requirements to be met by actuators for space applications inevitably increased the work concerning the design and manufacture of such mechanisms.

Communications satellites which provide certain regions of the world with a communications service via radio relay stations have to meet stringent requirements concerning the positioning accuracy of their antennas. Depending on the system configuration there is, for instance, the possibility of tilting the complete satellite including its antennas by means of momentum exchange devices or only the antennas by means of antenna pointing systems. In both cases, high alignment accuracies ($<0.1^{\circ}$) have to be met by the actuators.

Furthermore, high positioning accuracies are mandatory for actuators and alignment mechanisms used for solar panels and space experiments.

Besides the requirement for high angular resolution and positioning accuracy, a high actuating torque is required in many cases. Conventional actuators can only meet these requirements by an additional input, i.e. by high-quality gears and a high-accuracy angular sensor with the pertinent feedback electronics. However, this input increases the size, the weight and the power consumption, and reduces the system reliability considerably.

DEVELOPMENT

General

Within the scope of a DFVLR contract (Development of a Gimbal System for the Gimbal Suspension of Momentum Wheels) Teldix started in 1972 the development of stepper motors of the type SMR (friction-type version), based on a principle conceived by Prof. Kleinwächter. Further development studies within the scope of ESTEC contracts (Development of a Single Gimbal Momentum Wheel, Development of an Actuator Mechanism for Solar Panels) led to stepper motors of the SMZ type (tooth-type version).

Requirements

Depending on the configuration, the following requirements are to be met by the stepper motors:

High angular resolution

High stepping accuracy

Good step angle reproducibility

High holding torque

High dynamic motor torque

Low power consumption

Low volume and special construction

Low weight and high reliability during the specified mission time

Based on the different requirements the following stepper motors have been realized:

Type SMR 1-0

Stepper motor, friction-type version, O.D. 110 mm. This motor is designed to perform angular steps of about 10 seconds of arc to an actuating torque of ≤ 0.5 Nm.

Type SMZ 1-0
Stepper motor, tooth-type version, O.D. 110 mm. This motor is designed to operate at an actuating torque of $\leq$ 0.8 Nm angular steps (2 minutes of arc) at a high accuracy (< 20 % deviation from nominal step); a good step reproducibility (better than 10 % in relation to the nominal step) is desired, too.

Type SMZ 2-0 (see Fig. 1)
Stepper motor, tooth-type version, O.D. 150 mm. This motor features a high actuating torque of > 1 Nm and a lower angular step accuracy (< 50 % in relation to the nominal step).

Motor Concept

The constructional requirements set forth for these motors resulted in a pancake design. These motors of circular construction, feature a relatively large center hole. Independent of their function, these motors show further common design characteristics.

Besides the motor drive electronics, the motors consist of two assemblies, the stator and the rotor. The stator consists of a certain number of electromagnets mounted in a circular array and, depending on the motor type, of a conical running surface facing the rotor or of bevel gear teeth on which the rotor rolls off. The electric circuitry of the electromagnets is built into the stator.

Basically, the rotor consists of a specially designed flexible disk (diaphragm) mounted vertically to the motor's inner shaft. The circumference of this flexible disk is provided with a soft magnetic ring having a plane running surface or with bevel gear teeth. The coaxial suspension of the rotor with respect to the stator can be realized either by using a motor support in the system or by a suspension being part of the motor.

Motor Function

After switching one of the electromagnets, the rotor segment facing the electromagnet is attracted (see Fig. 3). Thus, a positive connection between rotor and stator is obtained with the tooth-type version and a non-positive one with the friction-type version. In order to increase the non-positive connection of the latter version, at least two opposite magnets are switched at a time. With sequential excitation of the solenoids, the rim of the rotor rolls off the stator rim acting like a swash plate.

Angular displacement of the rotor with the tooth-type version is obtained by applying a different number of teeth on stator and rotor. If, for instance, the number of teeth differs just by one, the rotor proceeds by the angle of one circular pitch while the magnetic field is performing one complete revolution. This comparatively small angle can therefore be subdivided into as many defined steps as magnets are mounted on the circumference of the stator.

With the friction-type version, angular displacement is achieved in that the rotor diaphragm rolls off at a smaller radius than that of the stator because of the diagonal bending of the rotor. This difference in the circumference of rotor and stator results in a very small displacement with each revolution of the magnetic fields. As with the tooth-type version, the step angle is calculated on the number of the solenoids.

The holding torque with the motor at standstill and the stepping torque with the motor proceeding are obviously higher with the tooth-type version than with the friction-type version. Besides, the latter shows a slight change in the step angle as a function of the load torque.

The tooth-type version features good reproducibility of the step angle (see Fig. 4) and no step angle error accumulation. Thus, it is possible to obtain precisely any angular position simply by counting the number of steps. The step angle, however, cannot be reduced infinitely because of the minimum tooth module necessary.

As mentioned above, the stepper motor is operated by use of an external electronic drive unit. The system electronics unit furnishes a digital signal to the electronic drive unit for the control of motor speed and sense of rotation.

Design of the Electronic Drive Unit

The electronic drive unit incorporates integrated C-MOS components. The command signal for CW and CCW rotation is fed to a ring counter. Power transistors used to switch the solenoids in the stator are controlled via a decoder and logic circuits.

Special Problems Encountered with the Stepper Motor Development

The motor design and its application for space missions required the clarification of the following aspects.

Mechanical Load

The motors have to be designed such that they are capable of withstanding the high mechanical loads occurring during the launch phase. This applies especially to the elastic rotor suspension and to the running surfaces on rotor and stator. It has been proven that maximum stepper motor performance is ensured by using several diaphragms that are screwed or riveted together. The internal friction mechanism of such a packaged rotor suspension also contributes to the damping of possible rotor Q factors.

Oxydation Problems

Oxydation especially occurring on the running surfaces of rotor and stator lead to a decrease in the motor efficiency. To eliminate such a degradation, it is recommended to provide the running surfaces of rotor and stator with a precious metal finish. Hereby, it is to be taken into consideration that the plating thickness has to be very thin because of the magnetic resistance and that there is no change in the friction coefficient between the contacting surfaces. Tests performed with a hard gold plating, Vickers hardness of approx. 1600 N/mm^2, showed good results.

Cold Welding

Under hard vacuum conditions, the problem of cold welding between the contacting surfaces on rotor and stator cannot be excluded. Investigations under vacuum (5×10^{-8} torr) showed that hard-gold plated surfaces do not indicate any signs of cold welding.

Tests

Besides the performance tests, a number of environmental tests have been performed to simulate the loads occurring during the launch phase and the long-term operation under ultra high vacuum conditions. These tests have been performed on individual stepper motors and on motors installed in gimbal systems (see Fig. 5).

Fig. 2 shows the motor torque as a function of the stepping frequency for the stepper motor type SMZ 1-0 installed in the inner gimbal system.

STATUS

SMR Type Stepper Motor

Development funded by DFVLR. Engineering Models subjected to environmental tests with qualification level. Life Test in ultra high vacuum, one motor $25 \cdot 10^6$ steps, alternating direction, against a spring load; two other motors $3 \cdot 10^6$ steps each. Employed for Gimbal System, proposed for Bearing and Power Transfer Assemblies and Antenna Pointing Mechanisms.

High Resolution Stepper Motor (size 155)
ESTEC contract successfully completed.

Single Gimbal Mechanism (Stepper Motor size 110)
ESTEC contract, Breadboard Model completed.

Single Gimbal Mechanism (Stepper Motor size 110)
ESTEC contract for Engineering Model completed.

Ultra high Resolution Stepper Motor (size 155)
ESTEC contract completed.

Employed in Single Gimbal Momentum Wheel and Double Gimbal Momentum Wheel with Self-locking Actuator.

Proposed for:
Bearing and Power Transfer Assembly (BAPTA);
Antenna Pointing Mechanism (APM).

Military applications:
Actuating mechanism for fin control and antennas of missiles.

Commercial applications:
Actuating mechanism for angular control, digital interface.

SUMMARY

The development results obtained with the three motor types SMR 1-0, SMZ 1-0 and SMZ 2-0 show that the requirements set forth for these motors have been met.

As to certain motor parameters, such as motor torque, stepping speed, angular resolution and angular accuracy, it has been shown that the parameter limits have not yet been reached, especially what the SMZ type version is concerned.

Further statements on the motor limits will be possible after competion of the scheduled qualification tests.

REFERENCES

1. Kleinwächter and Dröge, "Schrittmotor für Stell-DRALLRAD, Type SDR 20".

2. Hildebrand, S., "Feinmechanische Bauelemente". Carl Hauser Verlag, München.

3. Bowden and Tabor, " Reibung und Schmierung fester Körper". Springer-Verlag, Heidelberg.

4. Several DFVLR and ESTEC Reports.

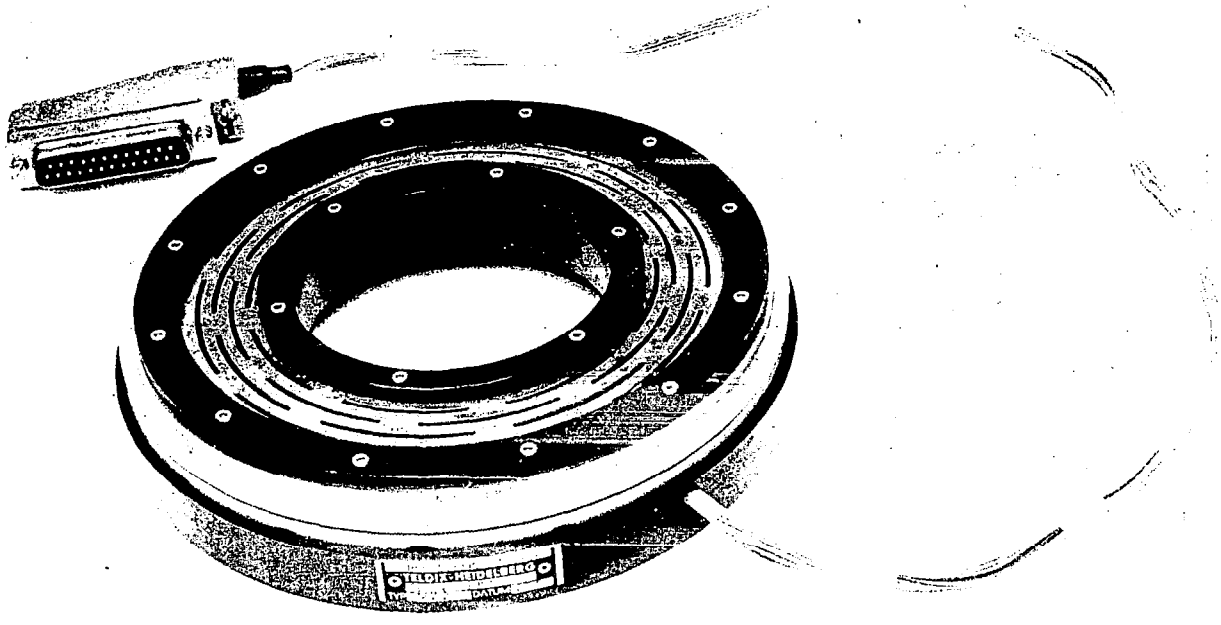

Figure 1 Stepper Motor Type SMZ 2-0 developed for solar pannel attitude control mechanism

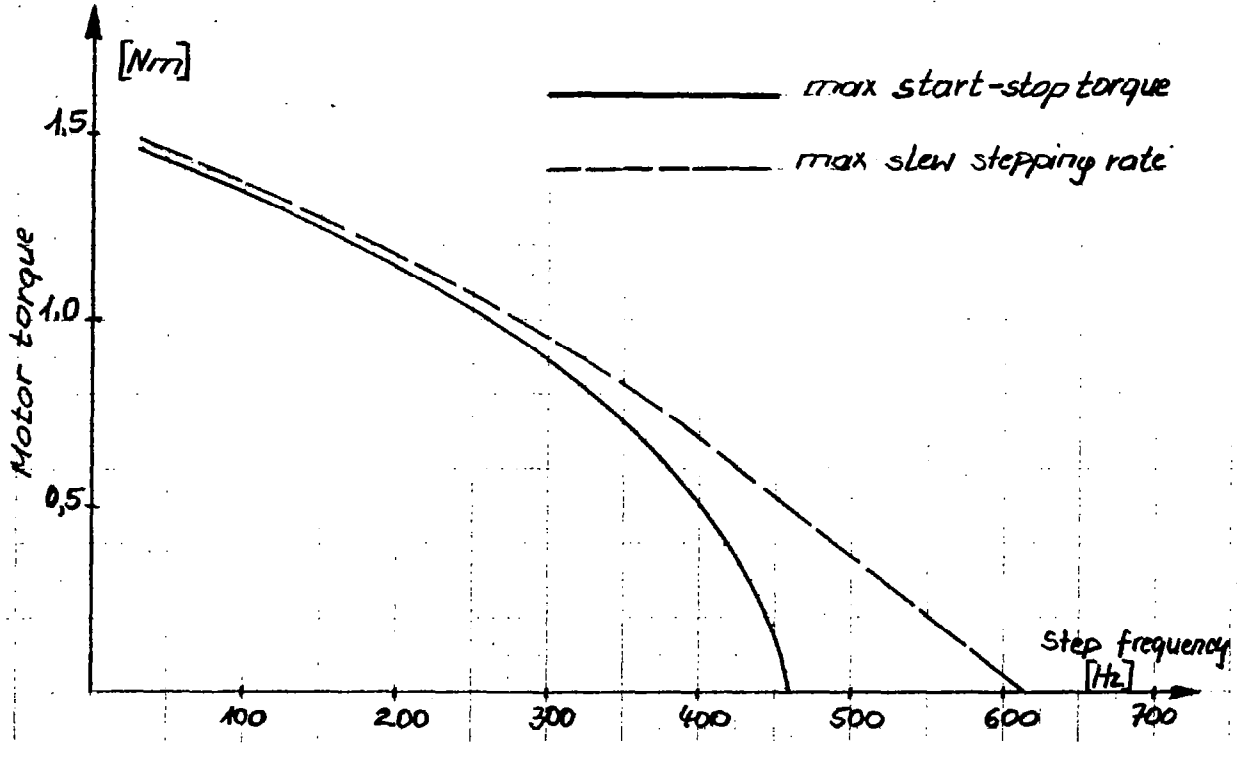

Figure 2 Motor torque as a function of the stepping frequency for the stepper motor SMZ 1-0 installed in an inner gimbal system

Motor de-energized:

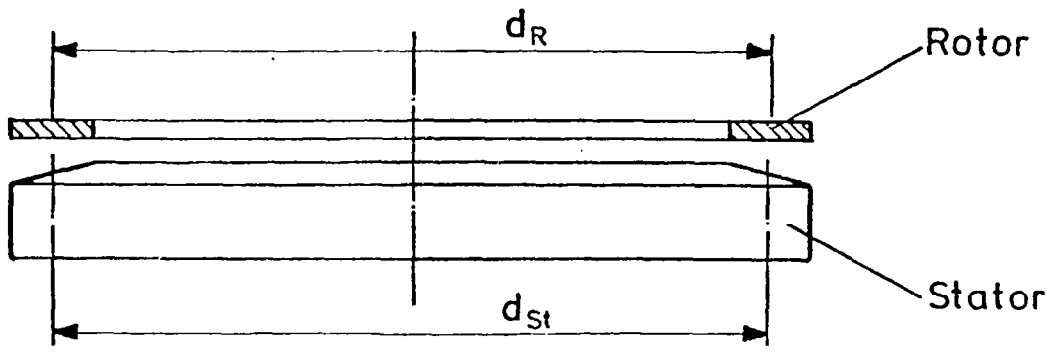

Tooth-type Version: Rotor engaged unilaterally:

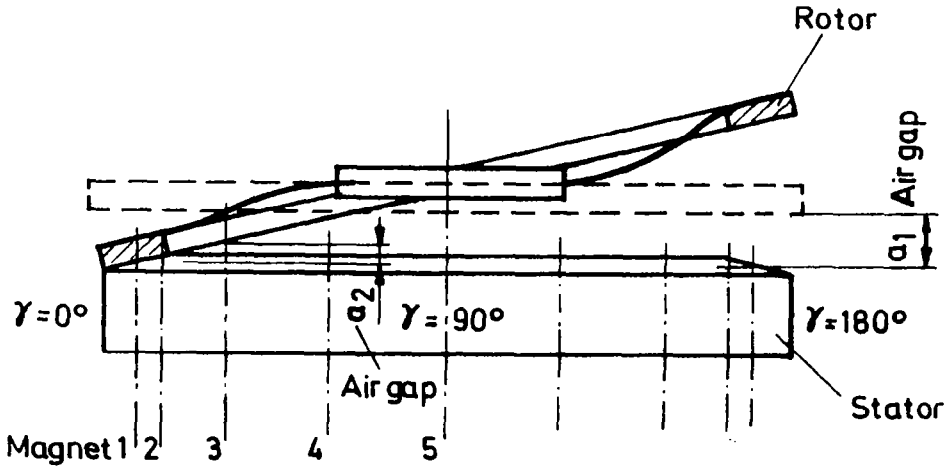

Friction-type Version: Rotor engaged diametrically:

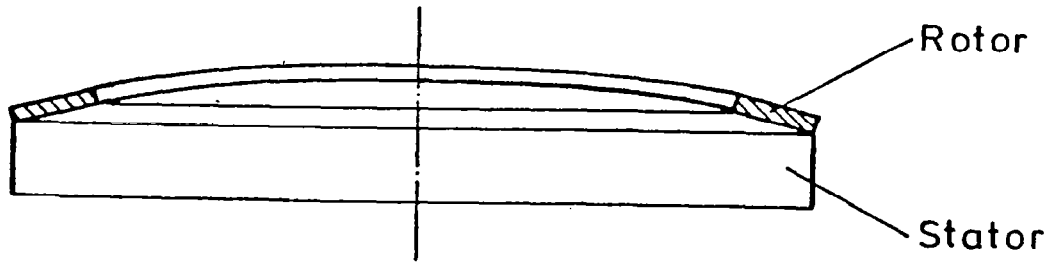

Figure 3 Principle of operation of the stepper motor

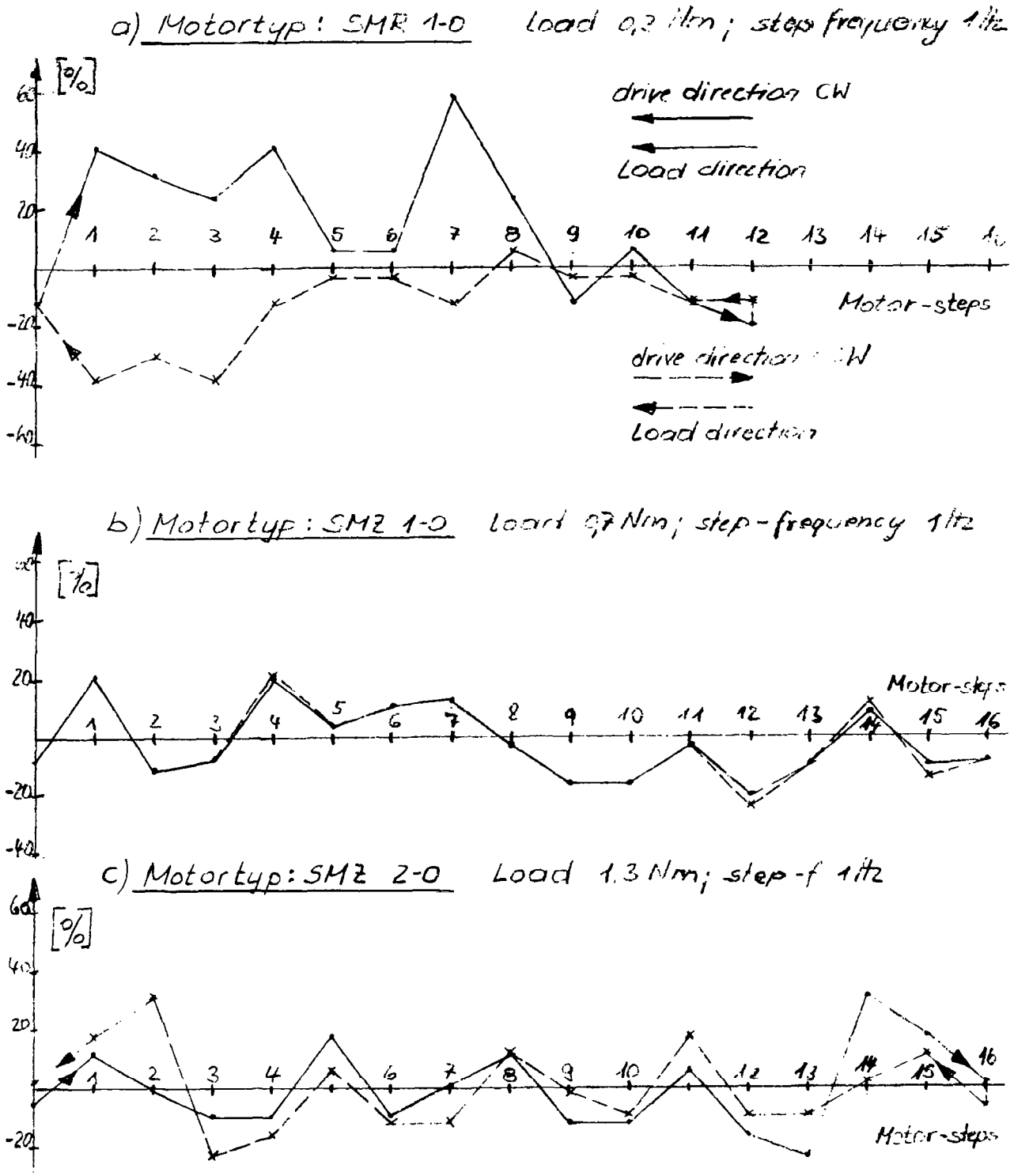

Figure 4 Deviation of the individual step angle from the nominal step angle

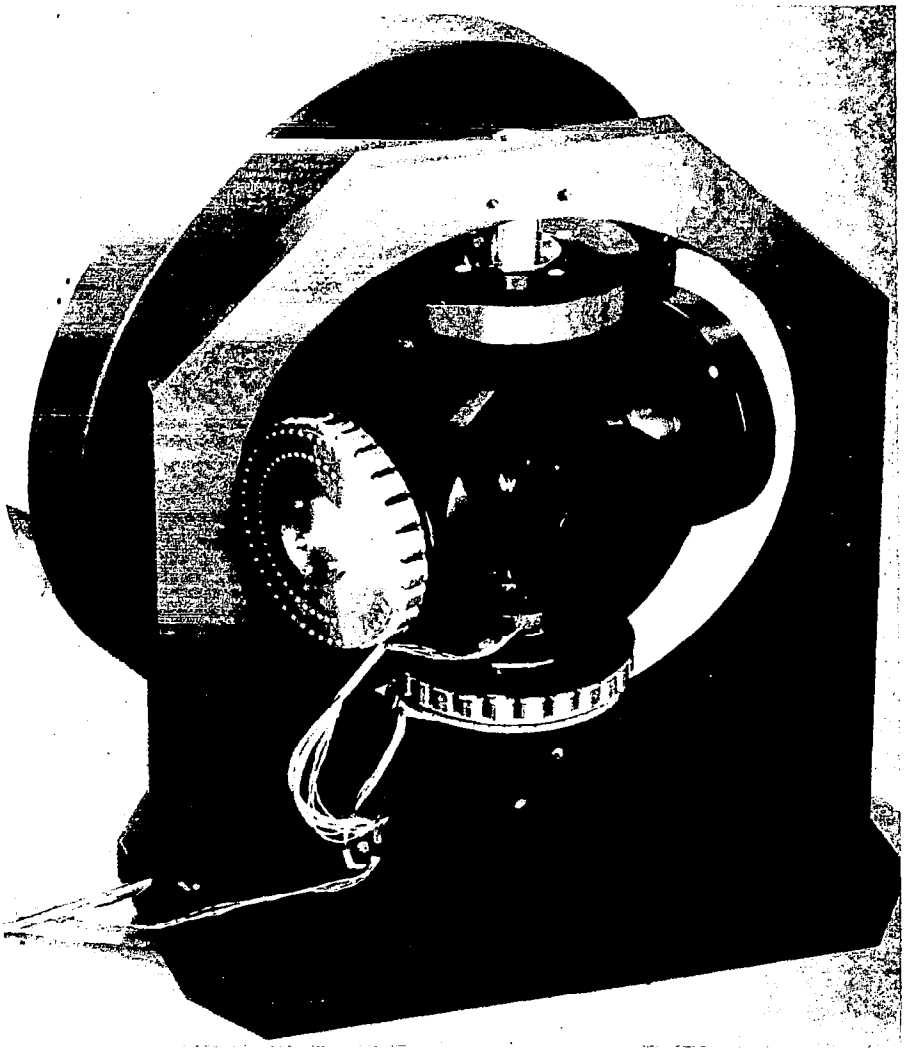

Figure 5 Inner gimbal system with stepper motors for two momentum wheel, one wheel removed

THE DESIGN AND DEVELOPMENT OF A SELF-COMMUTATING STEPPER MOTOR

By K.R. Dalley M.Sc.

Marconi Space & Defence Systems Ltd., Frimley, Surrey, U.K.

ABSTRACT

This paper is the result of a M.Sc. Project ref. 1 carried out by the author in co-operation with Marconi Space and Defence Systems Ltd (MSDS) and the University of Surrey. The Project established that a self-commutating (s.c.) stepper motor could be used as a high speed d.c. brushless motor. The system discussed adopts a well established and space proven motor, the 'stepper-motor' and shows that with simple commutation techniques it can be operated as a Brushless d.c. motor at high speeds (>10,000 rpm).

1.0 INTRODUCTION

The design of this particular motor has been developing over the past 5 years and was successfully put into practice during a system study of a Temperature Sounding Radiometer for a Geostationary Meteorological Satellite ref 2. The motor was controlled by LED/Photodiodes pulsed by a shutter attached to the rotor and maintained 2000 rpm with speed control of 0.06%. Recently another system was developed where the stepper motor was controlled by reed-switches. These were activated by static magnets shunted by an iron shutter attached to the motor shaft. However, both these applications were at relatively low speeds. The M.Sc. project undertaken by the author extended the knowledge of the reed-switch concept and concluded with the development of a self-commutating motor capable of 20,000 rpm. During the development program two unique stepper motor concepts were introduced. These were to operate a 'stepper' with continuous voltages greater than the recommended drive voltage and at speeds in excess of the 'drop-out' pulse rate. The final design comprised a Moore Reed Co. Ltd, size 15, 4-phase permanent magnet*(p.m.) stepper motor incorporating Hall Effect elements for its commutation.

2.0 PRINCIPLE OF THE SELF-COMMUTATING STEPPER

Although the stepper is essentially a position control device, the ability to rotate a load rapidly through large angles requiring many incremental steps is a common requirement. Previously the conventional method of driving a stepper motor at high speeds was to increase the drive frequency, until the step rate is in synchronism with the drive frequency. However, there are two operational limitations when adopting this drive technique. The motor will only start if the drive frequency is within the 'response range'. Then if greater step rates are required the drive frequency must be increased as a ramp function. The motor is now said to be in its 'slew range', but a further limit is then imposed as the motor eventually losses synchronism at the 'drop-out' rate

* The p.m. motor discussed within the context of this paper is as defined by British motor manufacturers; in that the rotor consists of a 2 pole magnet and is not toothed.

(typically 5000 rpm). However in the s.c. stepper, the motor is not frequency driven but like the d.c. motor the speed is proportional to the voltage applied across the motor winding. The motion of the rotor with respect to the stator is controlled by self-generated switching of the stator windings. If one of the stator windings is energised then the rotor will step to its magnetic equilibrium point. If now on immediately acquiring this equilibrium point the next winding is energised then the rotor will continue to the next equilibrium point. If now again the next winding is immediately energised the process will continue and the rotor will rotate as if a velocity drive. The switching is controlled by encoding the position of the rotor and is therefore described as 'self-commutating'. An important feature of this drive technique is that the self-commutated stepper operated at speeds greater than the 'drop-out' rate.

3.0 THE SELF-COMMUTATING STEPPER

3.1 Commutation: Brushless motors can be driven in either a switching or a proportional mode. The principle advantage of the proportional drive is the elimination of generated torque ripple. However, as the stepper motor has been optimally designed to drive in a switched mode, this mode was adopted for the self-commutating stepper. Early experiments were carried out upon the stepper to establish an optimum drive mode. The performance of the stepper was found to be significantly dependant upon which of the 3 principle energisation modes A, B or AB were adopted. Mode A is when only one phase at a time is energised, whereas mode B is when two phases are energised at any one time. In both cases the motor executes one basic step for each input pulse. A combination of A and B in which the motor phases are energised sequentially in mode A followed by B is known as AB. In this mode, the motor will execute half of the basic step. The number preceding the mode letter defines the number of motor phases to which the mode applies. As a 4 phase, size 15 stepper was readily available for the author's M.Sc. project, the investigation was only concerned with the 4A, 4B and 4AB modes. The tests were carried out using a reed-switch system having an inertial load of 1×10^{-5} Kgm^2. Measurements were made at various speeds between 2000 and 12000 rpm. A summary of the results from these tests is presented in figures 1 and 2. It can be seen that the 4A mode required the least input power and that a phase advance of 45° further improved the overall performance. A study of various torque waveforms demonstrated that the value of the mean torques predicted the above experimental results.

3.2 Rotor position sensors: There are a variety of devices commercially available as rotor position sensors. However, only non-contacting sensors were considered as only these ensured long operational life and reliability. The principle types reviewed were (a) capacitive; (b) inductive; (c) optical and (d) Hall effect elements. Capacitive devices although having low power were considered unreliable for satellite applications. Inductive sensors such as proximity switches, variable electronics devices and variable transformers were eliminated as they either required complex circuitry for excitation and demodulation, or because they required a moving magnetic field were therefore not self-starting. An exception to this was the magnetic relay (reed-switch) see fig. 3. This concept comprises 4 equally spaced reed-switches, each activated by 4 static magnets which are shunted by a rotating iron shutter attached to the rotor. If the gap in the shunt is 90 degrees then at any

instant of time only one relay is energised and this constitutes a 4A mode. The advantages of the reed-switch is that it acts as both sensor and commutator and therefore requires no additional components. Unfortunately because of low contact operation life, the reed-switch concept is only suitable for low speed or short life applications (≤ 2000 rpm). The Optical sensor, in its simplest form is a disc attached to the rotor. The disc carries a reflective track that provides the same function as the shunt gap in the reed switch system. A fixed light source is reflected by the track onto a photo-sensitive device whose output is used to generate the switching signal. However the reliability of optical devices in a space environment is again doubtful. Two Hall effect transducers were investigated, the magneto-resistor and the Hall Effect Element. Both are semiconductor devices capable of detecting a magnetic field similar to the reed-switch concept. However, the Hall effect element has one unique property, it can distinguish between north and south poles of a magnet. This property means that only two sensors are required to provide the necessary commutation. The shape of the Moore Reed rotor magnet is particularly appropriate as it provides the 90 degree commutation angle required for a 4A energisation mode. The Hall Effect Element commutator fig. 4 was chosen for the optimum design because of its reliability, low power consumption, and that it did not require an additional commutation disc.

3.3 Drive Techniques: The emphasis during the design of the drive amplifiers was to keep the complexity of the electronics to a minimum. Ideally the reed-switch technique achieved this design aim, but because of unreliability at high speeds a transistor drive had to be adopted. The s.c-drive amplifiers can be divided into two basic types, (a) the Unipolar, and (b) the Bipolar amplifier. The Unipolar drive is defined as an amplifier were the drive voltage is from a single polarity supply. The motor windings are usually arranged such that the centre-taps form a 'star point' and each of the remaining winding terminals are then energised in the appropriate sequence depending on the drive mode. The Bipolar technique is here defined as an amplifier which adopts both positive and negative voltage supplies. The motor winding centre-tap is not required in this technique, but the current reversal requires the use of a bridge amplifier. The use of a dual voltage level amplifier sometimes referred to as Bipolar was not considered a suitable technique in velocity control applications. Although during the comparison it was found that the Bipolar amplifier was the more efficient it required twice the number of components and therefore the Unipolar drive was chosen for the optimum circuit. The drive circuit is shown in fig. 5. As the motor was tested up to a maximum voltage of 60 volts a current limit was necessary to prevent over-current drive causing demagnetisation of the p.m. magnet. It is usual to have a protection diode across the output transistor collector/emitter junctions to prevent the back-emf spike damaging the output transistor. However in the case of the s.c-stepper this diode would also suppress the back-emf voltage of the unenergised coils. The requirement to protect the output transistors and still maintain the back-emf was achieved by connecting Zenar Diodes in series with the diode. The value of the Zenar being determined by the output transistor Vce max. As the requirements for the output transistors was that the Vce max must be twice the drive voltage only NPN transistors were found available. The required motor drive voltage was only applied to the output transistor and the rest of the circuit operated from a low voltage rail.

3.4 Feedback Techniques: The design criteria for the feedback transducer was to keep the concept simple. Traditional methods such as commercially available tachometers were not considered for this application as they would introduce a further inertial load to the motor shaft. Two feedback techniques were studied during the project, both of which utilised existing waveforms within the self-commutating motor and therefore required no additional hardware. The first method used the output from any one of the position sensors. A frequency to analogue converter would then produce a dc voltage proportional to either speed or error. The second method utilised the internal back-emf voltage developed in the unenergised windings of the stepper. The generated back-emf is sensed in all four windings by four diodes. These diodes provide a low impedance path for the induced reverse currents. The currents are then summed in a resistor. The voltage drop across this resistor, when suitably smoothed, provides a d.c. signal proportional to the rotor angular velocity. This latter method proved to be the most effective and simpler of the techniques.

3.5 Motor Performance: Several performance tests were carried out on an unloaded motor shown in Fig. 6 using a standard manufacturers test jig (courtesy of the Moore Reed Co. Ltd.) The measurements of Torque against speed and input current mode are presented in figures 7 and 8. Other measurements made included back-e.m.f., efficiency, performance in vacuum and motor friction. A summary of the motor parameters measured is given in the table below.

Motor type		Size 15, 4 phase p.m. stepper
Drive mode		4A self-commutating
Peak torque		140 gm cm.
Volts at peak torque		28 volts
Amps at peak torque		0.4 amp
Torque sensitivity		0.034 Nm. amp^{-1}
Motor Friction torque		6.4×10^{-5} Nm.
No-Load speed in air	V = 28V	7000 rpm
	V = 60V	12500 rpm
No-Load speed in vacuum	V = 60V	31600 rpm
Power consumption in vacuum	1.7 watts at 20,000 rpm	
	0.1 watt at 5,000 rpm	
Efficiency	>70%	

During these tests it was noticed that a phase shift of 45 degrees did not provide the maximum motor speed for a fixed voltage. Further investigations showed that the no-load speed could be increased if the phase advance was increased to 90 degrees, at a cost of increased input power and loss of efficiency. This improved speed was attributed to the relationship between the drive pulse and the peak of preceeding motor winding's back-emf waveform. Further increases in no-load speed were later achieved by operating the motor in a pseudo-4AB mode. This was achieved by adjusting the Hall Effect Element control current. Again the increase in speed was at a cost of increased power consumption of both the drive circuit and motor. A No-load speed of 31,600 rpm was recorded when operating in this pseudo-4AB drive mode.

4. SIMULATION MODEL

During the project a mathematical model was developed to describe the dynamic characteristics of the s.c-motor. The objective was to obtain a system of differential equations which represented the motor under high speed operations. The dynamic behaviour of the step motor is in general non-linear. Consequently it was inadequate to approximate its performance by linear models. The solutions to these equations were therefore achieved by a computer simulation. In the past, analogue computer simulations have been attempted, however these have proven only practical for single step performance studies and for multiple stepping would prove to be extremely tedious. On the other hand a digital computer overcomes this problem and offers a great deal of flexibility. The Model represented the winding voltage equations, expressions for the developed torque, and the dynamic equations. Hysteresis and eddy currents were neglected as a linear magnetic circuit could be assumed for the particular motor under test. The equations used were those derived by Hughes and Lawenson ref 3 and Ellis ref 4 with the exception of the motion dynamics which were modified to include windage torque. Deriving the model constants from basic principles was found to be impracticable as the motor parameters required for such analysis were commercially confidential and therefore any such constants were found experimentally. Figure 9 shows the basic structure of the computer program which consists of six main blocks; torque; current; load dynamics; back-emf; phase equations and winding logic. Although the model represented only a 4 - phase stepper the program had been written to enable the investigation of the various drive modes (4A, 4B, or 4AB) and the introduction of a phase shift to obtain the minimum current condition. Details of the program and the derivations of the equations are presented in ref 1. Both the Back-emf and current equations are controlled by the phase equations which were fed into the forward loop by multipliers. The winding logic block determined which phase, or pair of phases are energised depending on the rotor magnet position, any phase advance and the selected drive mode. Each winding voltage is derived from the sum of the controlled voltage and the appropriate Back-emf voltage. The corresponding winding current is then calculated and depending on the winding logic and phase equations produced the total instantaneous current. From the instantaneous current the developed torque was computed, and hence the output speed. The Dynamic Equation Block included windage torque and load constraints and was given by

$$Td = J\ddot{\Theta} + Kw\dot{\Theta} + Tm$$

where Td is the developed torque.

J is the total inertia of the rotor and load

Tm the motor friction torque, which includes all decelerating torques, other than rotor windage.

Kw is a constant obtained experimentally and expresses the relationship between windage torque and motor speed for a given set of load dimensions.

The viscous damping terms were neglected as they are small compared with the motor friction.

The simulation model predicted that at high speeds there would be a high power consumption due to the windage. However under vacuum conditions the windage would be dramatically reduced and as confirmed by experiments at 1 torr the running torque was reduced to only that due to the motor friction torque.

5.0 THE GEMS CHOPPER MECHANISM

In 1971-72 a preliminary system study of a temperature sounding radiometer for a Geostationary Environmental Meteorological Satellite (GEMS) was performed for the UK Meteorological Office. The radiometer was to determine the temperature profile of the troposhere and low stratosphere over partially clouded as well as clear areas. In addition the instrument could determine water vapour in the lower troposhere and the total ozone concentration both for temperature sounding correction and for the purpose of ozone detection alone. The radiometer measured radiance in eleven spectral channels, six in the CO_2 absorption band, two in atmospheric window region, two in atmospheric water absorption regions and one in the ozone absorption band. Cadmium Mercury Telluride detectors were specified with passive radiation cooling. The optical arrangement is based on a 20 cm aperture Cassegrain telescope with a large moveable plane mirror to perform the required scanning. The field of view of the instrument was 113 km diameter for the high altitude channels and 34 km for each sub-field of the remaining channels. Modulation being achieved by a reflecting chopper blade giving alternate space/earth views. The chopper mechanism as shown in fig. 10 comprises a 14 cm diameter disc with 30 slots. The chopper was to rotate at a uniform speed of 2000 rpm over a 5 year period in space. As the motor requirement was that it must be small, light, efficient, reliable and easily driven, the self-commutating stepper motor was chosen as the optimum drive. The drive motor assembly would incorporate dry lubricated bearings and if required, additional reliability would be assured by the inclusion of redundant bearings and stepper motor. Work carried out by the MSDS Tribology Group on lead lubricated bearings (ref. 3) predict single bearing reliability of 0.935 for a 5 year mission at 2000 rpm. This result being extrapolated from bearings having completed 10 years life at 3000 rpm at pressures of 10^{-10} torr.

CONCLUSION

The M.Sc. Project demonstrated that a self-commutating permanent magnet stepper motor could be adapted to operate as a brushless d.c. motor. Several motor drive techniques were investigated and the development of several commutating and tachometer techniques established two final brushless designs. A low speed motor ($<$ 2000 rpm) using reed-switches and a magnetic shunt and a high speed motor using Hall Effect elements. Both these motors used an inertialess tacho utilising the motor back-e.m.f.. The experimental results verified that the self-commutating stepper motor has the same output performance as a d.c. motor, and demonstrated that the final design provided a very high speed d.c. motor with an efficiency of better than 70%. The study of the torque and back-e.m.f. performance and the establishment of enhancing the motor performance by a phase advance technique contributed to the success of this motor design. Also although the aim of the project was to achieve a speed of 20,000 rpm, a no-load speed of 32000 rpm was recorded during the performance test. The most significant advantage that this self-commutating motor has over other commercially available brushless motor is that it is fabricated from a motor available from many manufacturing sources. The simplicity of the drive, commutation and tacho ensures reliability, and the high speed and efficiency capability makes this motor a low cost rotary device, suitable for high speed applications in a space environment. Apart from the development of a novel brushless motor it is believed that the operation of a stepper motor at speeds in excess of the 'drop-out' rate is an important contribution to the knowledge of stepper motor technolog

ACKNOWLEDGEMENTS

The author would like to thank Dr. L. Mansi University of Surrey, Mr. D. Steward MSDS whom originally inspired the self-commutating stepper motor and L. Kozuchowski of Moore Reed whose knowledge and test equipment provided invaluable assistance. Thanks are also due to the Technical Director of GEC - Marconi Electronics Ltd. for permission to publish this paper.

REFERENCES

ref 1 Design and Performance of a self-commutating High Speed Stepper Motor. K. Dalley, M.Sc. Thesis, University of Surrey. Sept. 77.

ref 2 A Preliminary System Study of a Temp. Sounding Radiometer for a Geostationary Met. Sat. Marconi Report reference 28053 Dec. 72.

ref 3 Electromagnetic damping in stepping motors.
A Hughes and P.J Lawrenson.
Proc. IEE Vol. 122 No. 8 August 1975.

ref 4 Analysis and Control of Permanent-Magnet Stepper Motor.
P.J Ellis.
The Radio and Elec. Eng. Vol. 41 No. 7 July 1971.

ref 5 Lubrication by Lead Films. A survey of existing and proposed applications.
P.J. O'Donnell ESA SP111 1st Space Tribology Symp. Oct. 75.

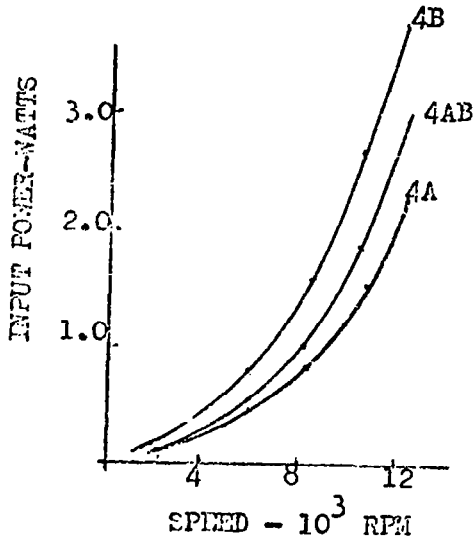

FIG. 1 DRIVE MODE CHARACTERISTICS

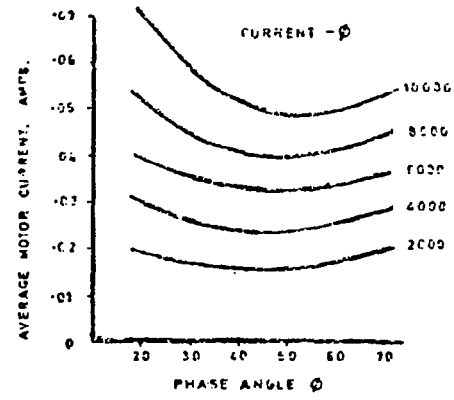

FIG. 2 PHASE SHIFT CHARACTERISTICS

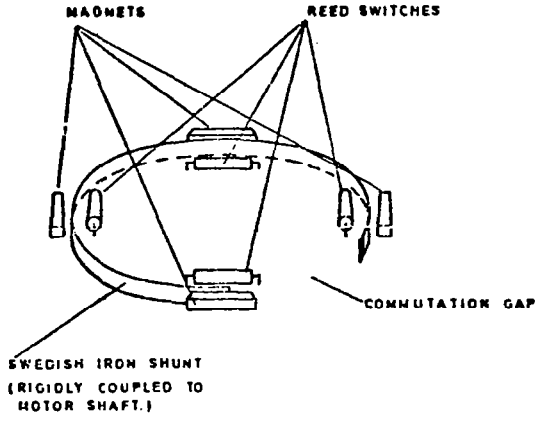

FIG. 3 REED SWITCH POSITION SENSOR

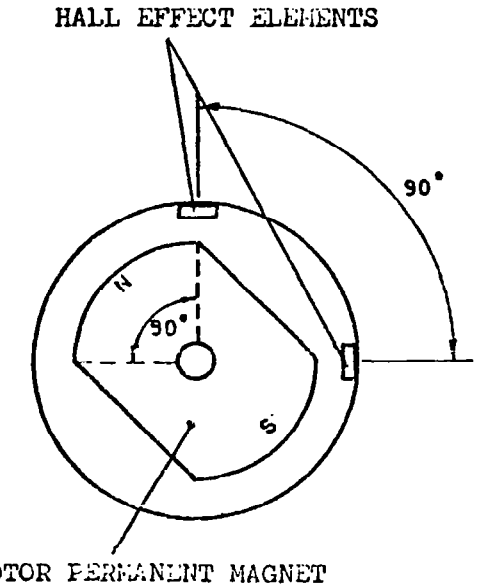

FIG. 4 THE HALL EFFECT SENSOR

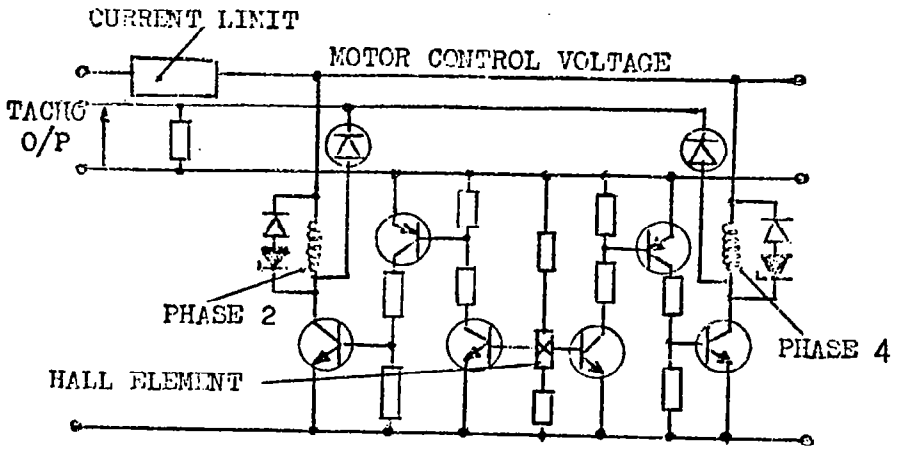

FIG. 5

BASIC DRIVE CIRCUIT

(PHASE 2 & 4 ONLY)

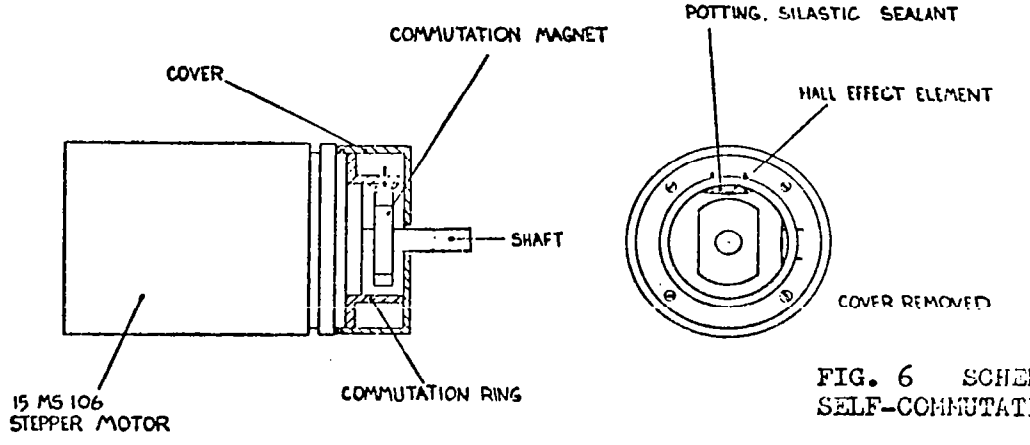

FIG. 6 SCHEMATIC OF THE SELF-COMMUTATING STEPPER *

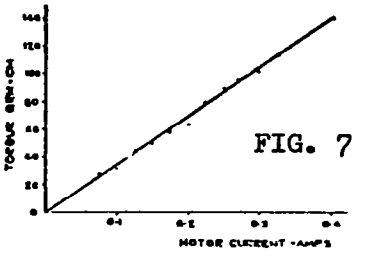

FIG. 7

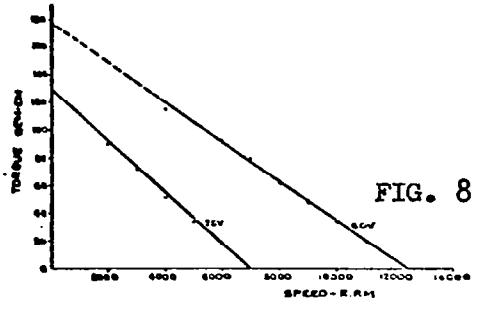

FIG. 8

MOTOR TORQUE PERFORMANCE

* For the M.Sc. project the Hall Elements were externally mounted.

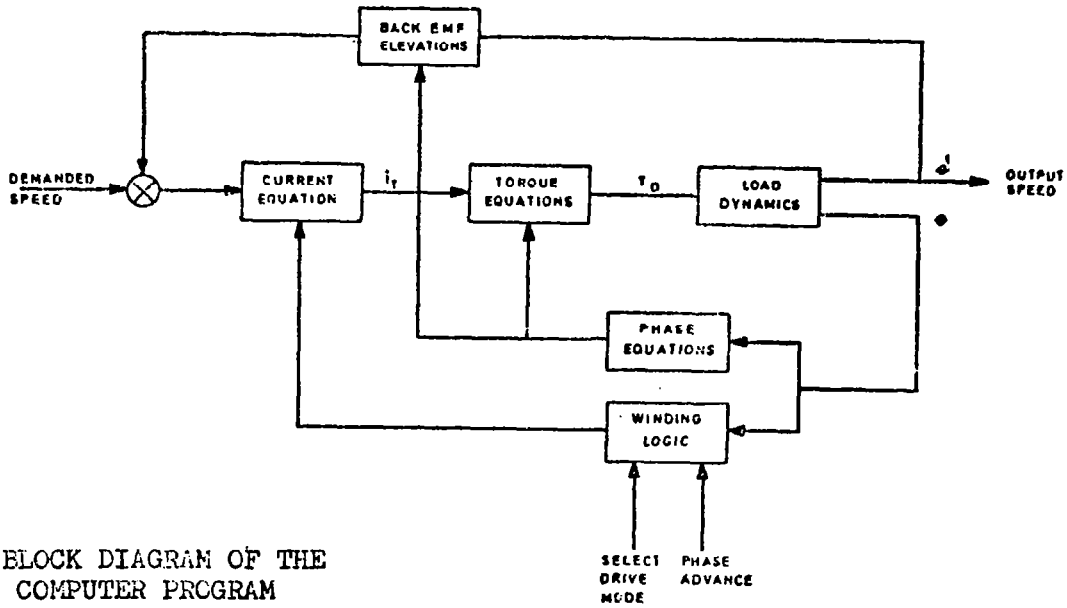

FIG. 9 BLOCK DIAGRAM OF THE COMPUTER PROGRAM

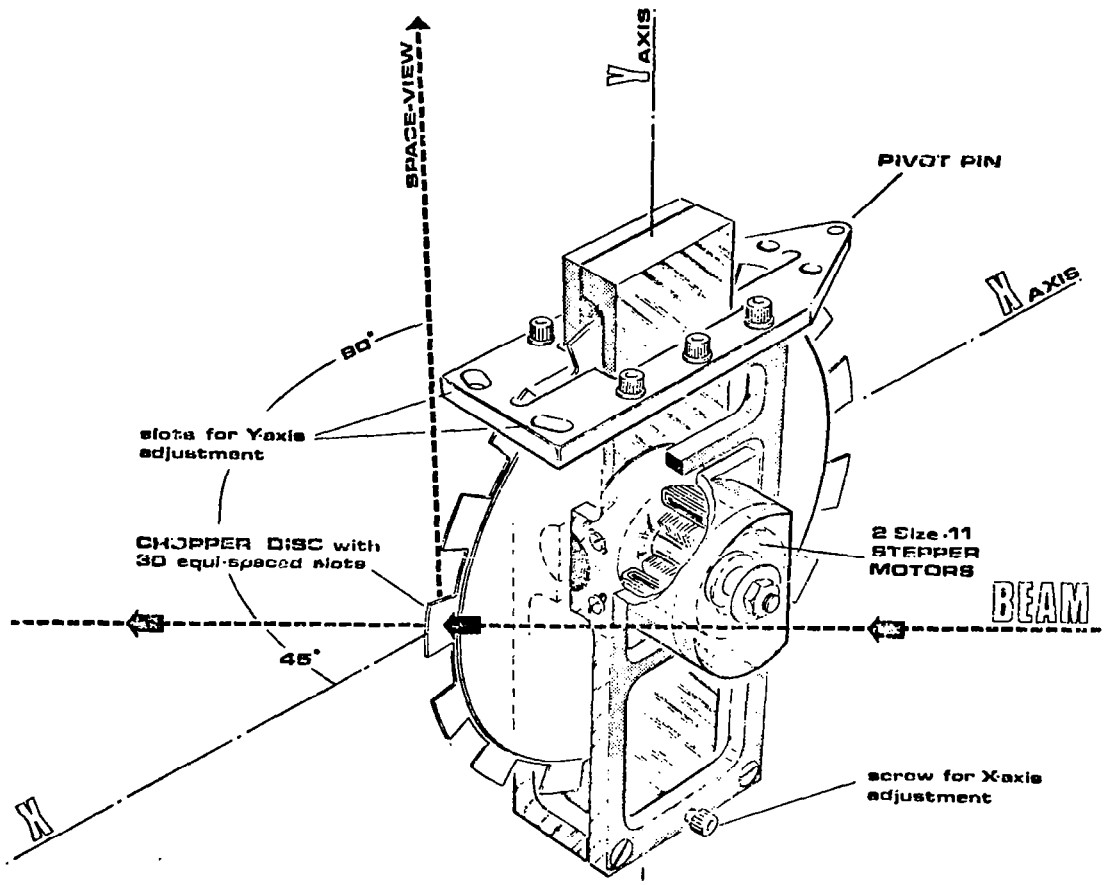

FIG. 10 GEMS CHOPPER MECHANISM

A DEPLOYABLE .015 INCH DIAMETER WIRE ANTENNA

Lamont DiBiasi

Fairchild Space and Electronics Company

ABSTRACT

This mechanism has been developed to dispense a small diameter wire which serves as a receiving antenna for electric field measurements on an Earth orbiting satellite. The antenna is deployed radially from a spinning satellite. A brushless DC motor drives a storage spool to dispense the wire at a controlled rate. Centrifugal force, acting on a mass attached to the end of the wire, keeps the wire in the radial position. The mechanism design, testing and performance characteristics are discussed. Finally, operational data of the mechanism while in orbit is presented.

INTRODUCTION

The International Sun Earth Explorer (ISEE)-A is a spin stabilized satellite in a 22 Earth radii apogee by 278 KM perigee Earth orbit. One of its missions is to study the characteristics of the electric fields in this region of space. On board are two Deployable Wire Antennas, positioned 180° apart, which function as receiving antennas for these electric field measurements.

Approximately one week after launch, both antennas were successfully deployed to their full length. Each antenna is a beryllium-copper stranded wire conductor measuring 106.7 meters (350 feet) in length. The outboard 36 meters is bare wire while the remaining 70.7 meters has an insulation coating of Stilan*. The mechanism is both extendible and retractable and is driven by a brushless DC motor using Hall effect commutation. The mechanism weight is 2.5 Kg (5.5 pounds) and occupies an envelope of 25 cm x 14 cm x 18.5 cm (9.88 in. x 5.5 in. x 7.3 in.).

Because the antennas are deployed radially, they act as a despin system. Therefore, the mechanism must be capable of intermittent starts and stops so that the satellite can be spun-up when required. In addition, in order to deploy the long wire (106.7 meters)

*Trademark of Raychem Corporation

at the desired rate of 3 cm per second (.1 feet per second) the motor had to be capable of long running times in a vacuum. The total deployment time is approximately one hour.

DESIGN REQUIREMENTS

In order to gather meaningful low frequency data from the electric fields in space it is necessary to deploy a system of receiving antennas at a great distance from the spacecraft to preclude interference from on-board equipment. The following requirements were imposed by either experimental needs or spacecraft capabilities.

MECHANICAL

- Extendible and retractable
- No extension under vibration
- Positive stop at full extension
- Self-lubricating bearings
- 25 cycle life capability
- Non-magnetic materials wherever possible

ELECTRICAL

- 14 watts peak power
- Cutoff switches at full extension and retraction
- Deployed length indicator
- Motor life cycle of 100 continuous hours' operation between -15° C and +40° C

ANTENNA CHARACTERISTICS

- 106.7 meters (350 ft) long
- 30pf to case ground deployed over 100 Hz to 200KHz
- Non-magnetic wire
- 150 ohms resistance
- Insulation on inboard 70.7 meters (235 ft)

MECHANISM DESCRIPTION

The mechanism consists of two fiberglass side plates separated by aluminum posts. These side plates also support aluminum shafts to which are mounted the mechanism drive components. In the extend mode a motor, through a gear train, drives a spool containing the wire antenna element. As the wire is unwound from the spool it passes around a drive roller, under a backup roller and through an exit guide assembly. Centrifugal force acting on a tip mass attached to the end of the wire, maintains tension on where to keep it straight. The drive roller is also driven by the gear train but an integral slip clutch allows it to be driven at a slightly faster rate. This arrangement maintains a slight tension on the wire between the drive roller and the storage spool. This prevents any slack in the wire which could result in backwrapping, mistracking or looping of loose wire. The moving wire drives the backup rollers which is geared to a potentiometer to give an electrical readout of deployed length. At full extension, a microswitch is tripped which cuts power to the motor. In the event of switch failure, a positive mechanical stop is incorporated. In the retract mode, the spool is again driven to pull in the wire. The drive roller is on a one-way clutch and in this mode it is free-running. The centrifugal force acting on the wire provides the tension required to ensure even wrapping on the storage spool. At full retraction, microswitches again cut power to the motor.

To meet the weight requirements, all large gears were drilled out; alternate gears were dry-lubed using Electrofilm #2306. Aluminum was used wherever possible for weight considerations and to keep the unit magnetically clean. The bearings used were beryllium-copper with self-lubricating retainers. (A drag brake was designed into the system to prevent deployment of the antenna during vibration.)

The motor is a 28-volt DC brushless motor using the Hall effect electronics for commutation; it has an integral gearhead with a 17.76:1 reduction ratio. The motor/gearhead housing was machined steel for magnetic cleanliness purposes. The motor/gearhead was required to operate, under load, for 100 continuous hours under a thermal vacuum environment of 10^{-6} torr between -15° C and +40° C while being cycled in the forward and reverse direction without any failure or abnormal operating parameters.

The antenna element is a conductor of seven strands of wire. For magnetic cleanliness, the conductor material chosen was beryllium-copper. The base conductor is .015 inches in diameter and .019 inches in diameter over the insulation. The breaking strength of the wire is 23 pounds, which is more than three times the maximum flight induced loads. The full length of 106.7 meters (350 ft) is partially base (outboard 35 meters) and partially insulated. The insulation is Stilan, a product of Raychem Corporation.

TEST RESULTS

A thorough qualification and acceptance test program was completed on the protoflight and flight models, respectively. The life cycle test on the protoflight model was performed to verify the ability of all components to withstand repeated operation without failure. At the conclusion of the tests, the unit was disassembled and all parts checked for damage or signs of excessive wear. The only parts that showed wear although not excessive were the gear on the drive motor, a gear which drives the spool and the one-way clutch housings. Reviews of the parts and the amount of wear were initialed. Results were that the wear, after 25 cycles, was not significant enough to warrant design changes since the flight units would only get about 5 cycles at most prior to flight.

The qualification of the motor was one of the most successful tests of the program. The 100 continuous hours cycle test showed no dropoff in performance. The disassembly after resulted in no refurbishment of any part. The motor was reassembled and installed in the protoflight mechanism. This same motor went through all tests of the protoflight without any problems and is still operating without specifications. The total running time on this motor is now in excess of 175 hours.

Another test result which was well within specifications is the power required for the mechanism. The allotted power was 14 watts. Test result proved that the actual power required was 7 watts maximum with only about 4.5 watts nominal. Under both ambient and thermal vacuum conditions the motor case showed only a 10° F rise in temperature during an operational time of approximately one hour. This allowed the elimination of the motor heat sink in future mechanisms. (Test results and corresponding specifications are presented in Table 1.)

PROBLEM AREAS

There were a few problem areas which became evident during testing. The first concerned the drag brake setting. Under initial vibration the brake was set to provide no drag on the mechanism. During vibration the wire self-deployed approximately 1/2 inch. The brake was then adjusted until no deployment was noted. At this setting the motor current was observed and this was the criteria used for each mechanism. Further testing verified that this was a feasible method to set the drag. It did, however, put a small additional current drain but the power required was still well within specification. In addition, as the mechanism runs, the drag surface wears and current drain is reduced.

The second problem arose during the thermal vacuum testing of the first flight unit. One requirement during all tests is to monitor continuity of the antenna. This was accomplished by applying a voltage to the wire. During operation, a loop formed on the spool and as the spool was turning the loop of wire touched a shaft and shorted causing the wire to burn through. Although the failure occurred during thermal vacuum testing, it was evident that the problem was not associated with this environment. Continuity was then checked by means of an ohm-meter and no further problems arose. The looping was caused by random wrapping of wire on the spool whereby a large loop could form. It was then decided to level wind on each retraction when possible to avoid this problem.

The third failure also occurred under thermal vacuum but again the environment was not at fault. This was evident by a complete loss of power to the mechanism. Upon opening the chamber, investigation revealed a loose piece of solder in the test harness connector which, under the right conditions, could short out the power supply. This was then corrected and testing completed.

The last problem occurred during deployment in orbit. The potentiometer output indicated full deployment but the motor did not cut off. The deployment was stopped and an investigation begun into probable causes. The antenna was sending data. The spacecraft spin rate indicated that the wire was not fully deployed. It was finally determined that the telemetry supply voltage from the spacecraft was unregulated and was probably supplying 12.45 to 12.6 volts rather than the 12.0 volts used for calibration. The mechanisms were restarted and allowed to run to automatic cutoff. When this was done both mechanisms cut off within 1/2 meter of the recalculated values.

TABLE 1

TEST		DATA	UNITS	ENVIRONMENT
Operational		Actual - (Spec)		Ambient
a) Rate	Ext	1.8-2.7 (1.5-427)	cm/sec	
	Ret	2.4-3.0 (1.5-4.27)		
b) Motor Power	Ext	6.9-7.8 (14.0)	Watts	
	Ret	4.2-4.5 (14.0)		
c) Pot. Output	Ext	Per pre-calibration		
	Ret	Per pre-calibration		
d) Continuity	Ext	Yes		
	Ret	Yes		
e) Auto Shutoff	Ext	Yes		
	Ret	Yes (Manual Actuation due to test fixture)		
Vibration		All axis passed		Ambient
Spin		Extent 2 meters @ 60 RPM Retract 2 meters @ 60 RPM		
Thermal Vacuum				
a) Rate	Ext	2.4	cm/sec	-20° C
	Ret	2.4		-20° C
	Ext	2.4		+20° C
	Ret	2.4		+20° C
	Ext	2.1		+40° C
	Ret	3.4		+40° C
b) Power	Ext	8.0	Watts	-20° C
	Ret	5.0		-20° C
	Ext	8.0		+20° C
	Ret	4.8	+20° C	
	Ext	7.0		+40° C
	Ret	4.8		+40° C

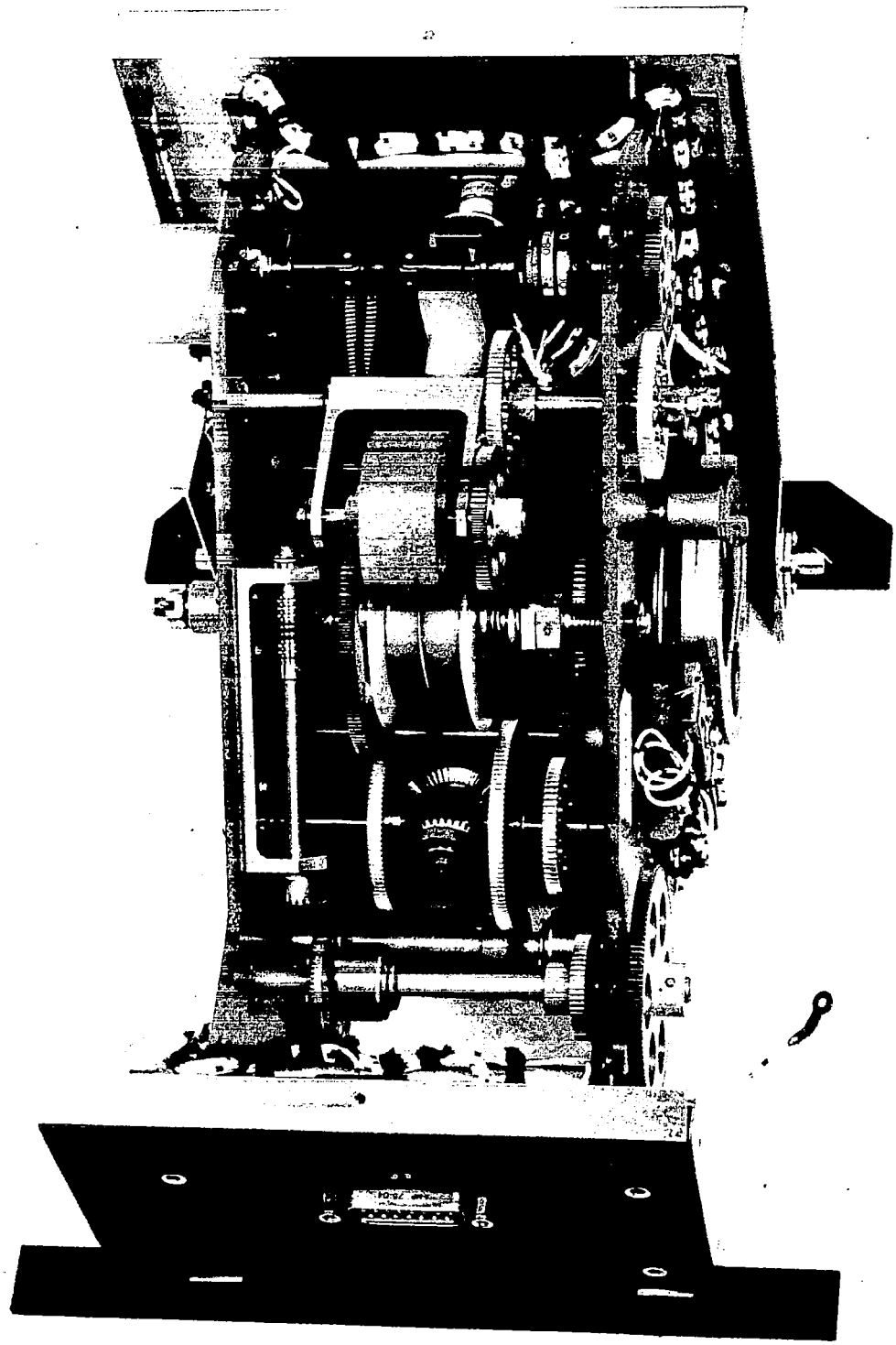

Antenna deployment mechanism.

MARS PENETRATOR UMBILICAL

By Christopher E. Barns
NASA-Ames Research Center

ABSTRACT

To obtain data on certain geophysical properties of the planet Mars, it is desirable to implant sensors below the Martian surface. The device proposed to gather this sub surface data is a ballistic probe which penetrates the soil after a free fall through the Martian atmosphere. Highlights of the design, development, and testing of several features of the Mars Surface Penetration Probe (MSPP) are outlined in this paper.

INTRODUCTION

A typical mission using the MSPP would commence with a launch from Earth aboard the Shuttle Space Transportation System (STS). The MSPP would be one of several experiments carried by a Mars Orbiter Vehicle. The orbiter would proceed under its own power after separation from the STS. Once in position near Mars, as many as 12 MSPP units could be jettisoned from the orbiter on command for impact on designated target areas.

As the MSPP falls through the Martian atmosphere, heat shields will protect its instruments and aerodynamic braking devices will control the rate of descent to limit the impact velocity to 150 m/s (492 fps) (Fig. 1). Upon impact the tail section separates from the forward body and remains at the surface. The forward body penetrates the Martian crust to a depth of 12m (39 ft.) or less depending upon the local soil properties. The two parts of the MSPP remain connected by a coiled umbilical cable carried in the foreward section and deployed through the penetration shaft.

The instruments in the forward section of the MSPP include accelerometers, seismometers, a thermal conductivity probe and a soil chemical analyzer. Data gathered by these instruments is carried through the umbilical cable to a transmitter in the tail section. In addition to the transmitter, the tail section houses an antenna and various meteorological sensors. Two advantages of this design are that: (1) instruments for measuring soil and crust characteristics are firmly imbedded in the Martian landscape where they are protected from temperature fluctuations and wind loads; (2) instruments for transmitting data and measuring atmospheric properties remain at the surface. Penetration devices similar to the MSPP have been used by the Army and Coast Guard. Umbilical cable breakage during deployment has plagued all previous designs. Development of a reliable cable and cable deployment method has been a major consideration in the testing of the MSPP experimental model.

DESIGN

The umbilical cable must meet severe demands imposed on it by the MSPP mode of operation. It must remain intact while being uncoiled at 150 m/s (492 fps). It must withstand the impact deceleration estimated at 20,000 G's. About 30 conductors are needed to meet the projected requirements of the instruments for

data channels. The conductors must be 12m (39ft) long with less than 10 ohms resistance. The entire cable package must be compact and fit within a cylindrical volume approximately 7.62cm(3 in) in diameter and 15.24 cm (6 in) long.

With the foregoing constraints in mind, a model was built for testing design concepts. The important features were fabricated half-size. The four components of the experimental penetration model are the forebody, the umbilical cable, the funnel and the afterbody (Fig. 2). All were designed to enhance the survivability of the umbilical cable.

The forebody provides the fuselage for the experimental penetration model. Its interior features include a mandrel with cylindrical and hemispherical portions, plus sufficient space for housing the umbilical cable and funnel. A blunt nose and several stabilizing fins form the exterior. The umbilical cable is coiled about the cylindrical part of the mandrel until impact separation, then the cable is guided smoothly by the hemispherical section as it unwinds. The mandrel is designed to minimize the friction experienced by the cable during deployment.

Space constraints and performance tests indicate that forming the umbilical cable into a coil provides certain advantages over other configurations. Stress fluctuations in the cable (thought to be a major cause of cable breakage) are minimized by uniformly accelerating the cable as it leaves the mandrel. Photographic data shows that high velocity waves traveling along the cable also contribute to cable failure. Experiments seem to indicate that the dynamics of a cable as it unwinds from a cylindrical mandrel promote uniform acceleration, minimize stress fluctuations and control wave velocity.

A beryllium-copper alloy was found to be the most suitable conductor material. It combines the desirable mechanical properties of high tensile strength and acceptable elongation with good electrical conductivity. The individual wires are insulated with an enamel-like coating of Formvar which is tough and lightweight. The cables used for testing are fabricated by twisting six conductors around a seventh in the center (1-7 construction). The resulting bundle is 0.079 cm in diameter. Seven such bundles are then combined into a cable with 7-7 construction. This forms a 49-conductor umbilical cable which is flexible yet strong because tensile stresses are borne equally among the individual wires.

As the coiled cable unwinds, it acquires a large rotational velocity which causes twisting and torsional failure (Fig. 3). A funnel is incorporated as a cable-guide to reduce the magnitude of the cable spin velocity through friction. As the funnel diameter decreases, the umbilical cable scrubs the funnel wall and yields its rotational energy to friction-produced heat. The geometry and frictional properties of this device have been chosen to optimize the energy exchange without inducing excessive cable tension along the projectile's line-of-flight.

The after body, which serves as the anchor for the umbilical cable, also uses a bell-shaped surface similar in function to the funnel. Cable rotational energy is dissipated through a scrubbing action between the cable and the afterbody surface. The design also reduces stress concentrations in the cable at the attachment point.

TESTING

The testing was conducted in the ballistic ranges at NASA-Ames Research Center. The MSPP experimental models were fired from a 57 mm smooth bore gun, to the target velocity of 150 m/s (492 fps). From the muzzle the model flies through the stripper which is constructed to simulate ground impact and arrests the afterbody at a deceleration level of approximately 20,000 G's (Fig. 4). A hole which exists in the stripper has a profile that allows the forebody, with its fins, to slip through untouched while the afterbody is abruptly arrested. The stripper contains layers of plywood and aluminum which retain the afterbody and prevent bouncing.

Other equipment used during testing includes break wires to measure velocity and trigger shadowgraphs, double exposure shadowgraphs that show detailed deployment at two stations during flight and high speed movie cameras which show the dynamic and after effects (such as continued twisting). At the end of the flight the forebody is stopped by a plywood box filled with layers of Celotex and particle board.

CONCLUSION

The analyses of many tests have yielded these important results: (1) the initial acceleration of 20,000 G's is not a problem if the suspended free length of cable is short; (2) the rotational velocity which induces twisting of the cable must be controlled; and (3) no sharp corners may exist in the mechanism. Two major differences between these tests of the umbilical's motions and the actual MSPP operating conditions are reduced aerodynamic damping resulting from the lower air density in the Martian atmosphere, and greater rotational energy dissipation of the umbilical during deployment through contact with the shaft wall formed by the penetrator. Additional tests are planned to determine the effects of these conditions, although at this time neither appears to present problems. Further testing and minor optimization will complete the design of a reliable umbilical system for the MSPP.

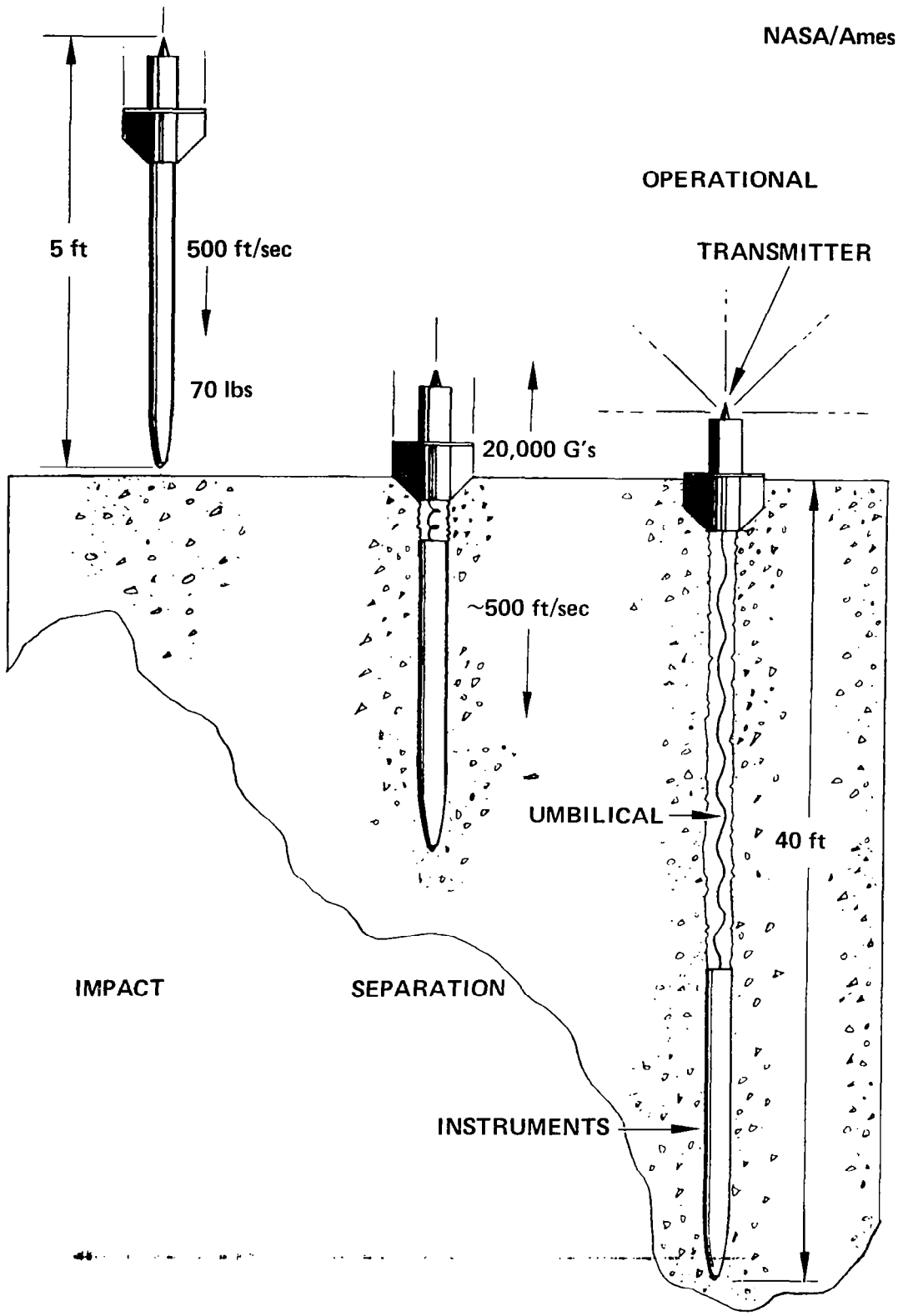

Figure 1 Penetration Sequence

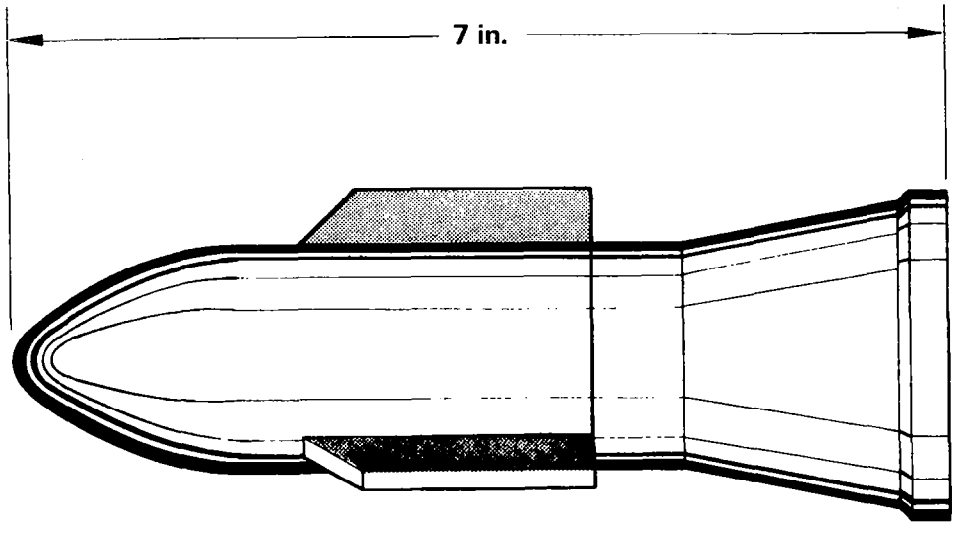

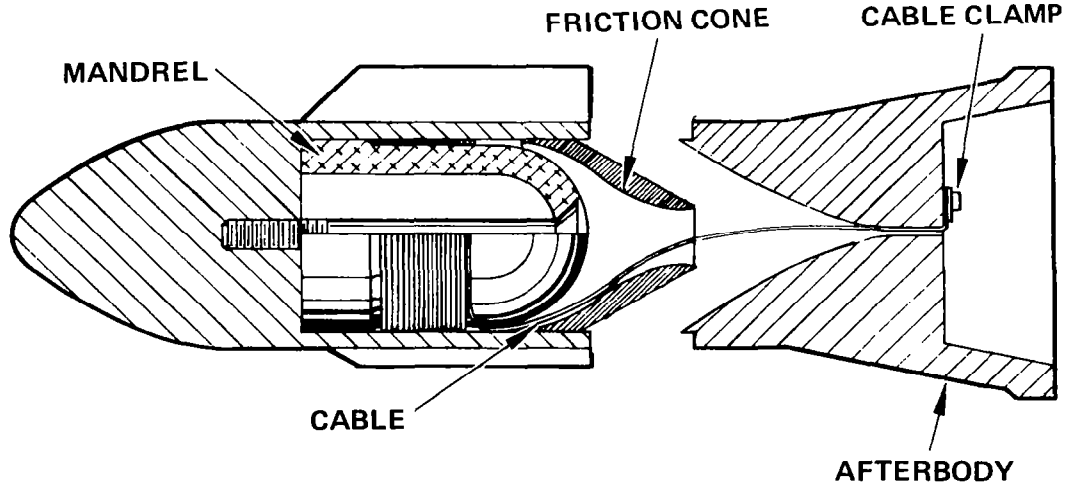

Figure 2 Umbilical Test Model

NASA/Ames

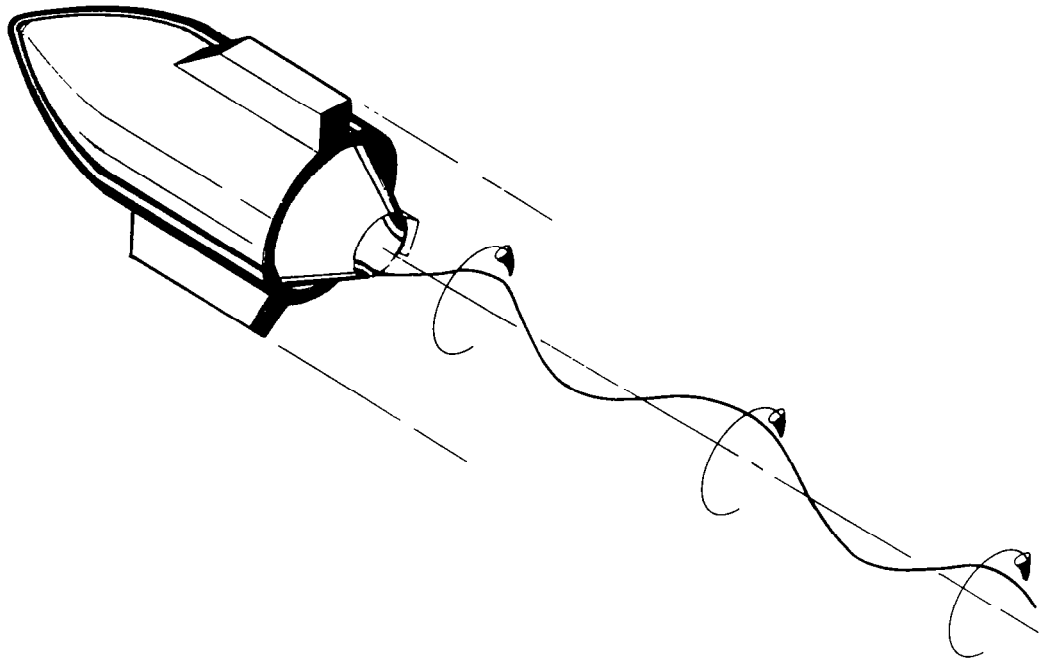

Figure 3 Umbilical Deployment (Note Rotation)

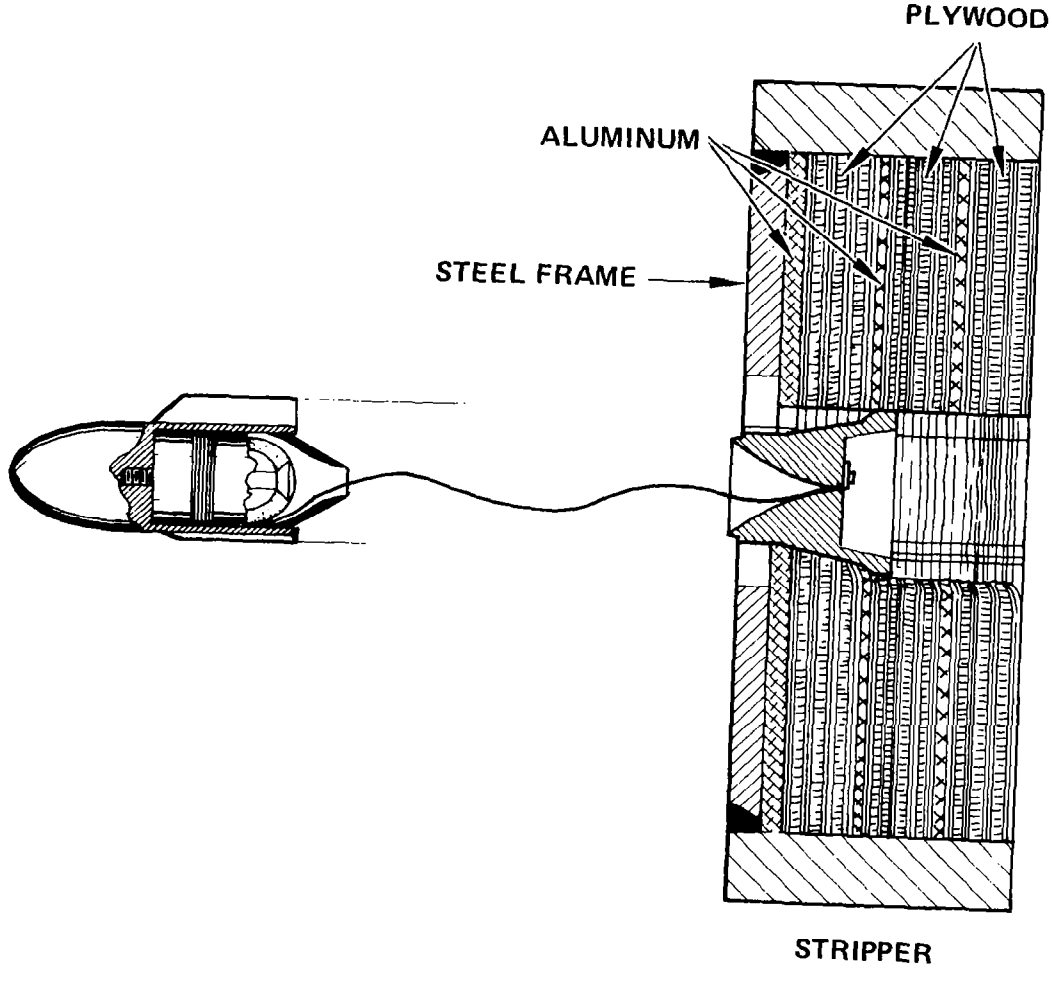

Figure 4 Ballistics Test Rig

THE VOYAGER MAGNETOMETER BOOM*

David C. Miller
Jet Propulsion Laboratory

ABSTRACT

The Voyager spacecraft magnetometer experiment utilizes two sensors on a deployable boom. The boom is an Astromast (Ref. 1), which has been described in the literature. This paper describes the implementation of the Astromast into the Voyager design. The hardware used to hold, latch and deploy the mast is described. The tests to demonstrate damping, deployment and alignments are described. Several problems encountered are discussed and their solutions are given. Flight deployment and preliminary alignment results are presented. Finally, the design is evaluated in retrospect.

HARDWARE DESCRIPTION

The magnetometer boom provides the attachment for the two magnetometer sensors to the spacecraft. One sensor is mounted seven meters from the boom base; the other is thirteen meters. The sensors are to be nominally aligned with the spacecraft axes. Alignment knowledge is to be $\pm 1°$ relative to the spacecraft and $\pm 0.4°$ relative to each other. Boom and spacecraft combined must produce a magnetic field no greater than 0.2 nT at the outboard sensor. All surfaces of the boom assembly must be electrically conductive.

The magnetometer boom and canister assembly is a part of the Voyager spacecraft as shown in Figure 1. It is made up of the following major elements: (a) the deployable structure itself is a 9" dia by 512" long (13m) Astromast (Refs. 2, 3, 4, 5), which is shown in Figure 2; (b) two deployable magnetometer sensors are attached, one near the middle of the boom and one at the end of the boom as shown in Figure 3; (c) the magnetometer sensor electrical cables are attached to the boom as shown in Figure 4, as is the canister which supports the boom during launch; (d) the baseplate and damper location are shown in Figure 5, which also shows the installation on the spacecraft; (e) the latch for the end plate is shown in Figure 6 and for the mid-sensor in Figure 7; (f) the retracting supports are shown in Figures 8 and 9. The fixed supports are shown in Figure 8; (g) the rate limiter is shown in Figure 13.

During launch, the boom is not completely stowed, but is in the configuration shown in the lower portion of Figure 2. The fully stowed portion or "stack" is 12 inches long and the transition region from the stack to the base is 14 inches long. The outboard end of the stack is supported by the boom end plate, whose latch and release is described below. The inboard end of the

*This paper respresents one phase of research conducted at the Jet Propulsion Laboratory, California Institute of Technology, under Contract No. NAS 7-100, sponsored by the National Aeronautics and Space Administration.

stack is supported by three retracting supports equally spaced (Figs. 8, 9). Torsion springs pivot them out of the way to provide an unobstructed canister ID as soon as the stack moves outboard, permitting the transition longeron to pass. The transition longeron is supported in its curved shape by the fixed supports (Fig. 8) to prevent the "stack" from rotating during vibration, thus tightening the transition longeron and causing it to bend sharply over its retracting support.

The outboard end plate carries the boom loads and the magnetometer loads to the canister. The three latch pins which do this are held into holes (elongated holes) in the corners of the end plate by two wire ropes (Fig. 6) which are in turn restrained by a pinpuller. The same pinpuller holds a third wire rope which keeps a latch pin in a clevis and holds the mid-sensor support snug against two conical pins (Fig. 7). All these latch pins are spring loaded to release the latched items. Operation of the pinpuller releases the wire ropes which release the latch pins and allow the boom and instruments to deploy. The deployment force is provided by its mast itself, which tends to self-deploy with a constant force of 8.5 lb. Achievement of this force is the reason the base of the mast is erected during launch. The mast is capable of stowing completely, but then the extension force goes to nearly zero. Without restraint, the boom would deploy with ever increasing speed, possibly damaging itself or the sensors when they stop abruptly at full deployment. Therefore, the rate of deployment is controlled by a rate limiter. This is a reel which contains a nylon lanyard that is attached to the boom structure at the outboard end. Connected to the reel shaft is a rotor that rotates in a silicone fluid filled housing. Once extended in flight, the boom is never retracted.

The mast assembly is unidirection S-glass epoxy composite with 6061-T6 aluminum fittings bonded to it with EA 934 A/B epoxy adhesive. The supports for the boom-mounted sensors are epoxy-glass layups. The sensor cables are wrapped with conductive black teflon ribbon. The end plate and sensor support brackets are painted white for thermal reasons over conductive black for static charge bleed reasons. The longerons have a 34-gauge beryllium-copper wire taped to them every few inches by means of copper foil tape. The lanyard has conductive ribbon sewn to it. All these are required to insure that no portion of the boom can accumulate a static charge large enough to arc to ground and damage the spacecraft electronics. All these items are non-magnetic to very low levels.

The canister is 7075-T73 aluminum, .016 inches thick. The rings riveted to it are also 7075-T73. The spacecraft attachment is made through three quadrupod trusses. Each of these is made up of 6061-T6 aluminum tubes riveted to 6061-T6 aluminum fittings. The base support truss is made of epoxy glass tubes (thermal isolation) bonded to 6061-T6 aluminum fittings. The baseplate is a 6061-T6 aluminum machining. The dampers (Fig. 10) which bridge between the baseplate and the base support truss fittings (Fig. 5) are a polyurethane elastomer ("Dyad 606", Ref. 6) bonded to 6061-T6 aluminum bushings.

DAMPING TESTS

So that oscillations during picture-taking sequences won't cause image smear, 4% damping of the boom was required. Boom tests showed less than 1%

inherent damping, so it was clear that dampers were required. A detailed structural analysis of the spacecraft showed that the critical vibration mode for the boom was equivalent to a 12 lb simple pendulum on a 375-inch arm pivoted at the boom base.

In order to test one damper rather than a set of three, it is necessary to determine the appropriate inertia. For the flight condition, the inertia is 12 lb x $(375 \text{ in})^2 = 1.69 \times 10^6$ lb-in.^{2}. This is damped by three dampers equally spaced on a 5 in radius. The appropriate inertia for one damper is $I = 1.69 \times 10^6 \div [1 + \sin^2(30) + \sin^2(30)] = 1.12 \times 10^6$ lb-in^2, also acting on a 5 inch arm. This was provided by a damper test fixture (Fig. 11) consisting of a beam pivoted in the center with 200-lb weights at 50 in from the pivot: $I = 2\,ml^2 = 2 \times 200 \times (50)^2 = 1.0 \times 10^6$. (The 12% discrepancy was due to a geometry error - the original calculation erroneously arrived at 353 inches instead of 375.)

The test was set up as shown in Figure 12. The U-shaped spring was adjusted to provide .30 Hz with the damper replaced by a rigid block. This motion simulates the undamped boom attached to a rigid base. When the rigid block is replaced by the damper, the motion properly simulates the flight design condition. Amplitude is measured by a proximity sensor and recorded on a strip chart at the end of the beam. The beam tip amplitude is started at .025 in., which gives the damper arm a .0025 in. displacement. Some of this absorbed by the adjustable spring, which simulates the flexing of the boom; the remainder is absorbed by the damper, and matches the flight displacement.

The damper design is shown in Figure 10. To size the washer, a dummy damper was made with a large area damping washer. It was installed in the fixture and tested. The dummy was removed and machined to a smaller size and the test was repeated. This was continued until the size providing optimum performance was obtained. The flight dampers were made to this size, and were all tested in the fixture to verify they performed as required. Tests were conducted over temperature-the white box is a foam insulating box in Figure 11.

DEPLOYMENT TESTS

Two types of deployment tests were conducted. A full-length test at low temperature was done one time only as a design verification test. A two-foot deployment test was conducted on each assembly at low and high temperatures as a flight qualification test to verify proper unlatching and exiting from the canister.

The two-foot deployment test was done vertically upward, with a counterweight. The stack was tied together except for the six feet nearest the base. This permitted only a few feet of deployment, but it was adequate to demonstrate proper unlatching and exiting of the canister. Typically, the force margin was 5 or 6 pounds, indicating the drag against the canister was about 3 pounds (compares to the deploy force of 8.5 pounds).

There was concern that the electrical cables might prevent boom deployment, especially because they could be as cold as -20°C at deployment. A test was conducted in which the boom assembly was attached to a stand so the mast could deploy full length downward. A chain counterweight whose weight per foot

matched the boom (and cabling) was wrapped up on a drum during mast extension, as shown in Figure 13. This simulated zero-g by counterweighting the stack. The entire assembly was precooled in foam box, the bottom of the box was removed, and the latches were released with a pneumatically powered pinpuller. The test was successful. Note than an upward deployment with the chain allowed to collapse into the floor will not work because this will pull the boom out of the canister tip end first (much as fish line spools off a spinning reel) instead of whole stack coming out.

ALIGNMENT TESTS

To obtain the alignment of the Magnetometer sensor mounting surfaces in zero-g, the following system was devised. The boom was initially deployed down putting it in tension (+1 g). The boom was then deployed upward placing it in compression (-1 g). The boom was also counterweighted in both modes to obtain fractions of g's in both tension and compression. The angles obtained were then plotted (g's vs misalignment angle), and a zero-g value was obtained by interpolation. Misalignment angles were obtained, before and after assembly level vibration at each sensor location relative to the mounting points of the canister to the spacecraft. A worst case tolerance build-up from this interface to the spacecraft axes was then calculated and introduced into the results as part of the uncertainty. Measurements were obtained using mirrors at each sensor location and at the canister for bending and a porro prism for twist. A laser mounted on a three axis rotating head was used to find the angles by autocollimation.

A basic problem was discovered in the test. With the boom in tension the angles measured at a sensor location for each counterweight value were plotted and found to be nearly linear, as expected. This was also true in the compression mode. When the two curves were extrapolated to zero-g, however, a significant offset occurred between the tension and compression curves as shown in Figure 14 (approximately two degrees in twist and less than one degree in bending). This anomaly was never resolved.

The predictions of the sensor mounting surfaces in zero-g with respect to spacecraft X, Y, and Z axes and each other for each boom are given in Table 1, along with a total uncertainty comprised of the boom repeatability (from deployment to deployment), boom thermal distortion, sensor removal and reinstallation, allowable sensor bracket thermal distortion, S/C bus and RTG outrigger worse case tolerance build-up, boom dampers, and alignment test measurement error. Because of these large uncertainties, a magnetometer calibration coil was constructed around the high-gain antenna reflector. This permitted an in-flight measurement of two axes of sensor alignment.

PROBLEMS

There were many problems with the development of this hardware. Those judged to be of interest to a future use of this type of boom are given here.

Canister Diameter. The canister diameter is a compromise between a snug fit around the boom to provide good support in launch vibration and a loose fit to provide low drag on the boom during deployment. The geometry is illustrated in Figure 15. The problem was that the tie-strap locks did not nest between the cables as intended, resulting in their rubbing against the canister. In addition,

one deployment was stopped by a lock which became caught in one of the retracting support cut-outs. The solution was to replace the tie-straps with string ties. This was a much more tedious installation, but the knots in the string ties were significantly smaller and they caused no significant problems.

Inboard Sensor Slot. As the boom deploys, a point on the stack traces a helix. However, the helix is not uniform because of end effects. The actual path traced by a point on a longeron is shown qualitatively in Figure 16. The first motion of a fully stowed mast is axial; once the base is fully deployed (approximately 30 inches for this mast), the helix angle is 45°; there is a smooth transition between them. This curve, from the 14-inch point outward (our mast is 14 inches from fully stowed) is the curve that should be cut in the canister to allow for deployment of the inboard sensor. (An adjustment has to be made because the canister diameter is greater than the mast.) The design, however, failed to take this into account, and the slot was at the angle appropriate for 30 inches and beyond. The result was that the inboard sensor support moved more nearly axial than the slot and hit the edge of the slot. This was sufficient to stop deployment, under some test conditions. Two changes were made. First, a low-friction pad (teflon) was attached to the inboard sensor support to rub on the canister. Second, the edge of the canister was cut away to provide more clearance.

Handling. A problem which persisted throughout the program was handling damage. This was largely because the mast is a new item and is delicate due to the many slender members. About a dozen diagonals were kinked or significantly nicked such that they were replaced. A handling procedure was generated and revised twice as more handling information became available.

Inspection. The mast is an inspector's nightmare. The boom assembly is made up of 91 bays, each with approximately 20 visual inspections for nicks, splits, chips, etc. in longeron, diagonal and batten elements, tears in the conductive ribbon on the sensor cables, tears or unwrapping of the copper tabs, and ground wire out of place or broken. The electrical checks are simple continuity tests with a multimeter on each pivot fitting and each foil tab. The visual checks are not quickies, especially scanning the diagonals for damage, which requires good lighting and a view from two directions. Initially, these inspection points and methods were not known. Damage was discovered, especially to the diagonals, and when it occurred could not be pinpointed because the inspections made earlier were not in enough detail to have detected them. All this came to light only during rework of the booms for late changes. From that point on, good inspections were performed and in fact verified that vibration and deployment operations were not the cause of these diagonal damage incidents. It takes two people approximately 6 hours to inspect a boom properly.

FLIGHT PERFORMANCE

Final mast stowage and installation on the spacecraft for launch occurred after many problems had been resolved and tests developed to give us confidence that the mast would deploy properly. Nevertheless, the signal confirming full extension of the mast was a most welcome event. The magnetometer sensors were recording data during mast deployment, and the output from each axis was a sinusoid as it rotated in the earth's magnetic field. Figure 17 shows the data from

one axis of the sensor at the end of the Voyager 2 boom.

A 12 foot diameter 20 amp-turn coil is attached to the spacecraft antenna for the purpose of making certain alignment measurements in flight. However, two such coils perpendicular to each other would be needed for a complete verification. The experimenter is using the one coil and the interplanetary field to make such measurements as are possible. The work involves developing some new techniques and is not complete at this time. However, we have the preliminary results shown in Table 2. The discrepancies between predicts and actuals are not resolved, and are most disappointing. However, the use of two independent measurements (tension and compression) was most important. Their disagreement identified the problem so that an alignment coil could be implemented to make an in-flight measurement.

DESIGN IN RETROSPECT

The Astromast appears to have been the right choice for the magnetometer boom; it was superior to any of the alternates, including a graphite-epoxy 4-member boom with hinges. Keeping the base erected in the launch configuration was also a good decision. Dampers at baseplate corners worked well. Use of a rigid batten for the mid sensor was good. The pretwisted boom was correct for this application, to preclude thermal twist distortions. The rate limiter works extremely well. Attachment of sensor cabling to the longerons, rather than reeling from a separate spool, worked well but some details should be reexamined. The latch concept of spring-loaded pins held engaged by a cable which is released by a pinpuller was good choice. The outboard sensor latch details were fine but the inboard latch needs reexamination. In fact, the inboard sensor mounting and latching scheme is the only design concept that is really poor, due to operational problems and temperature sensitivity as described below. The alignment concept was most difficult to implement, gave some inconsistent results, and needs to be reexamined. However, alternate approaches appear to have their difficulties also.

The inboard sensor latch has been a source of concern ever since it was designed. The existing hardware meets the requirements, but possesses two troublesome features: temperature changes cause preload on the latch pin, and latch engagement with sensor attached is difficult. The temperature characteristic is resolved by performing an unlatching test over the expected temperature range. The engagement difficulty is largely muddled through with much grunting and groaning of technicians. Another problem with this area is that the boom must be deployed to install the sensor.

The following list of potential changes is offered for consideration. (a) order three lengths of diagonals instead of one to provide twist angle adjustment capability; (b) make the longerons, battens and diagonals electrically conductive inherently instead of as an add-on. (Carbon-filled resin, graphite epoxy, wires imbedded in the material, use titanium instead of fiberglass, etc?); (c) use as large a diameter mast as practical. This minimizes the number of bays, the number of parts (to be reworked perhaps) and the cost. It maximizes the deployment force and accessiblity; (d) the instrument supports (end plate, outboard support bracket, rigid batten) should be redesigned. Present designs are intricate and a little heavy. Consider metal machining with fiberglass insulators. (Voyager eddy current fears resulted in a requirement for nonconductive parts);

(e) pursue a completely stowed boom. If conditions permit full stowage, the result is a shorter package and the elimination of both the retracting and fixed supports.

REFERENCES

1. Product of Astro Research Corporation, Santa Barbara, California.
2. "Astromasts for Space Applications", available from Astro Research Corporation, P.O. Box 4128, Santa Barbara, California, 93103.
3. "Automatically Deployable Booms", available from ABLE Engineering Company, P.O. Box C, Goleta, California, 93017.
4. "Ball Brothers Research Corp. Design Data for a Coilable Lattice Boom", available from Ball Brothers Research Corporation, P.O. Box 1602, Boulder, Colorado, 80302, Attn: Mr. Nelan Peterson.
5. R. F. Crawford, "Strength and Efficiency of Deployable Booms for Space Applications", AAS/ASAA Variable Geometry and Expandable Structures Conference, Anaheim, California, April 21-23, 1971 (AIAA Paper No. 71-396).
6. Product of the Soundcoat Company, Inc., Brooklyn, N.Y.

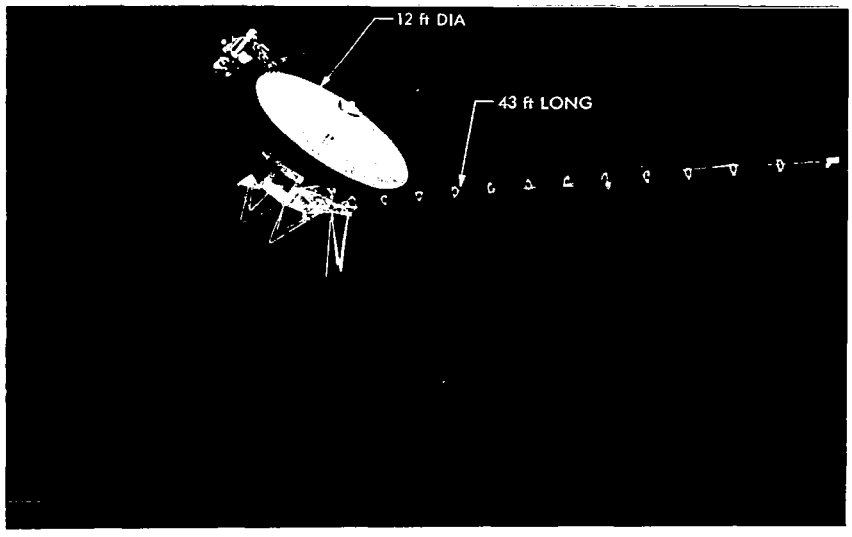

Figure 1. Voyager Spacecraft

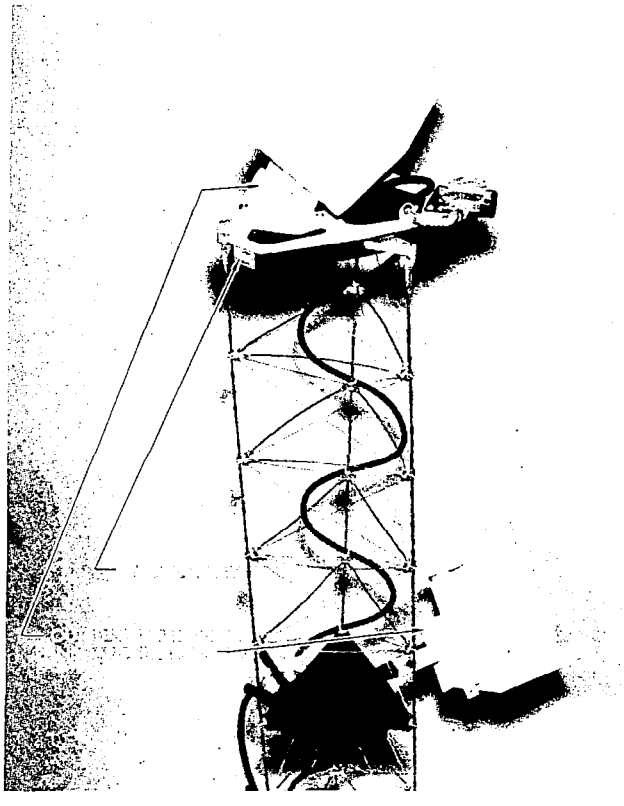

Figure 3. Sensor Attachments

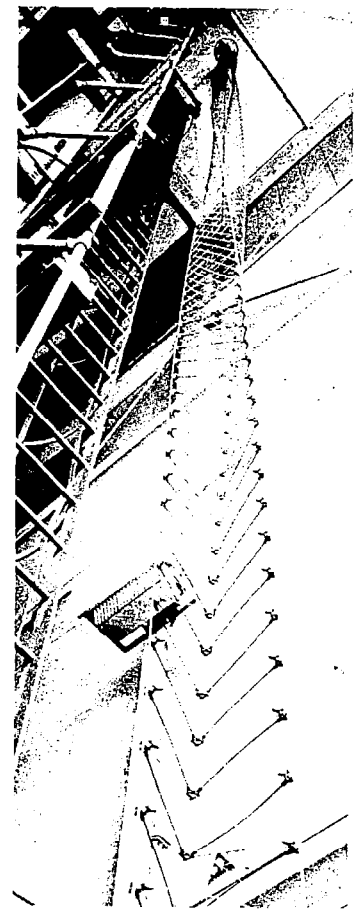

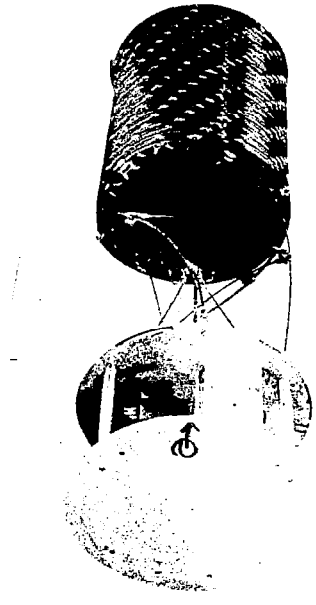

Figure 2. Astromast

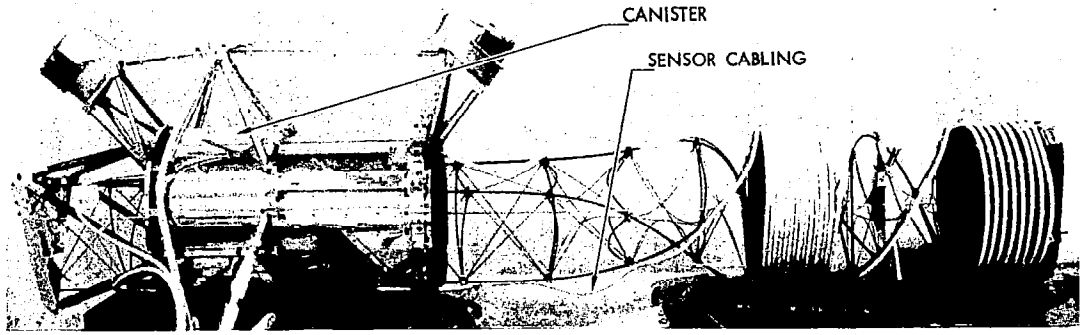

Figure 4. Sensor Cabling Attachment

Figure 5. Spacecraft Installation

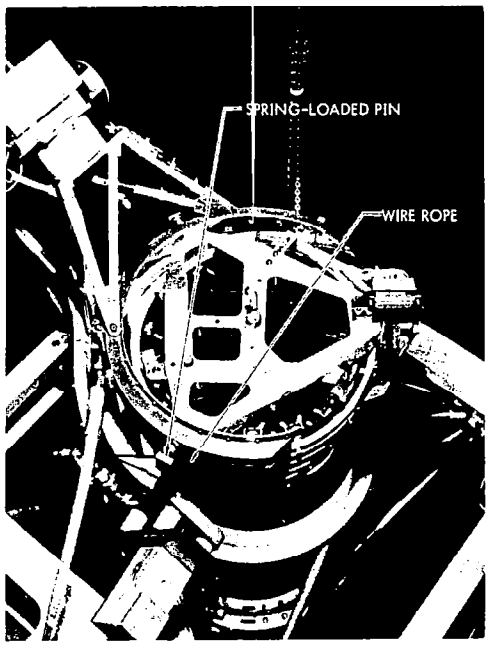

Figure 6. Outboard Latch

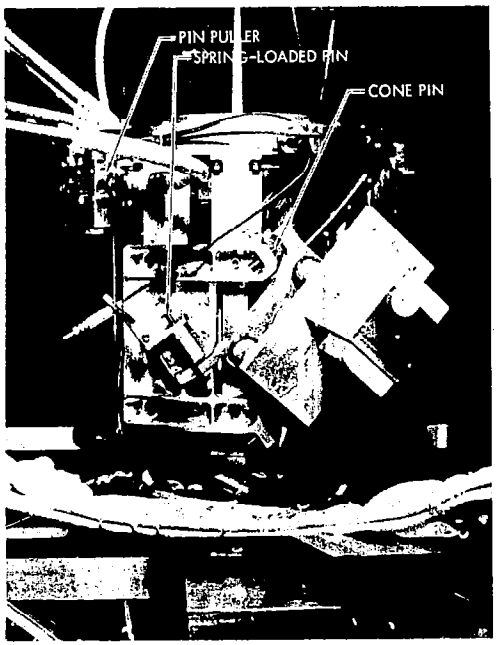

Figure 7. Inboard Latch

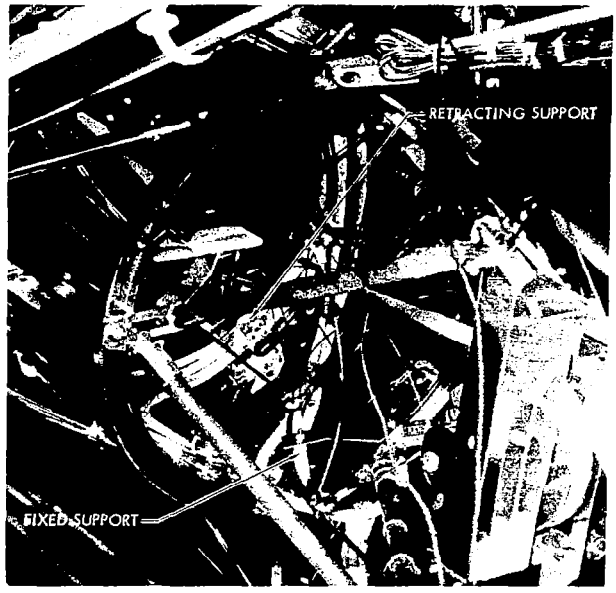

Figure 8. Retracting & Fixed Supports

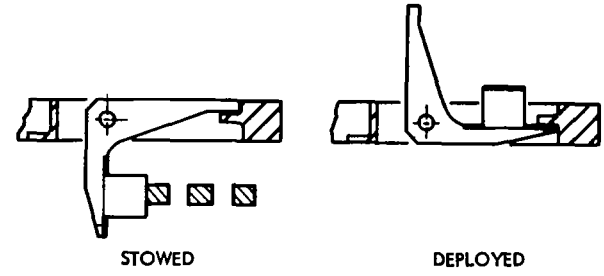

Figure 9. Retracting Support

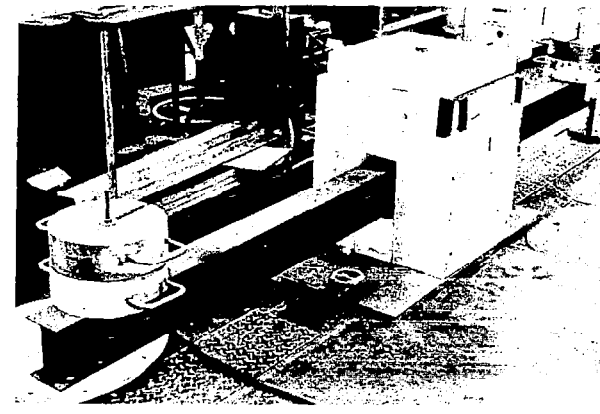

Figure 11. Damper Tester

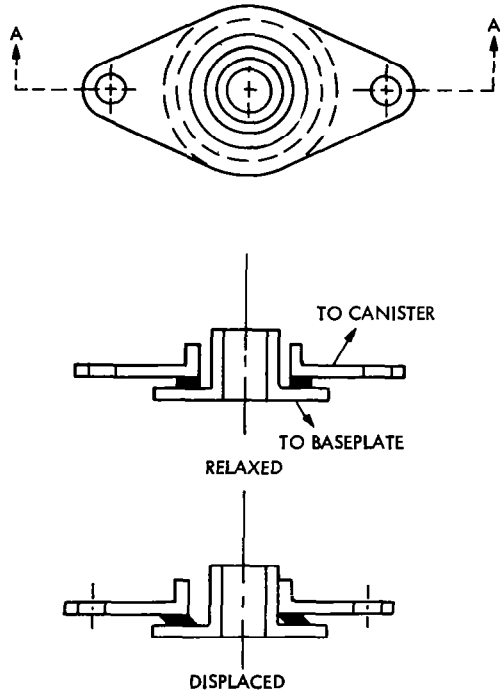

Figure 10. Damper

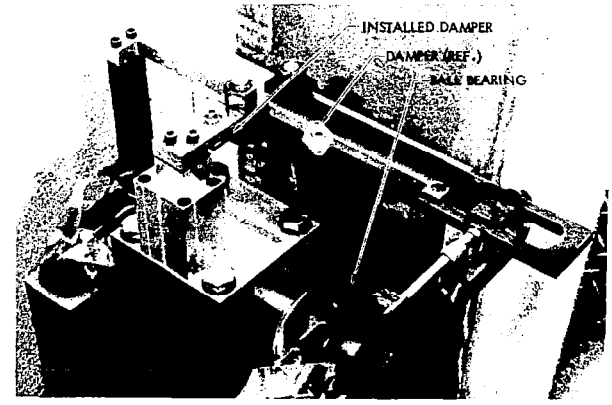

Figure 12. Damper Tester Details

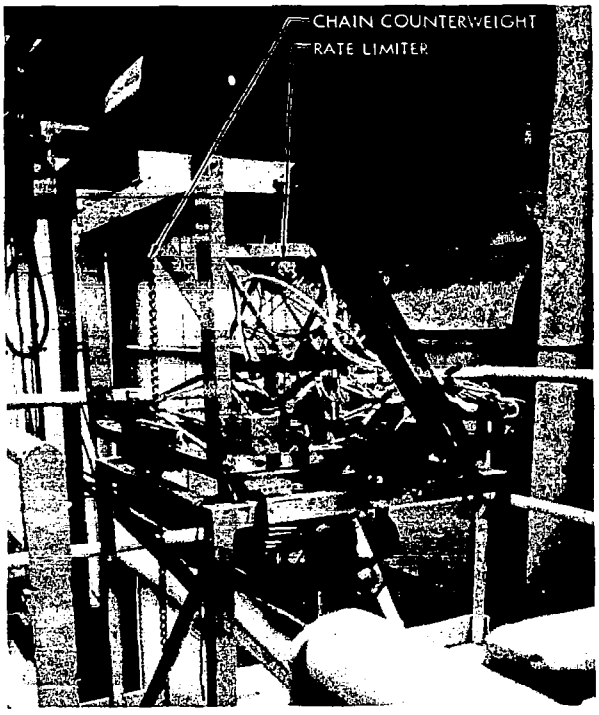

Figure 13. Full Length Deployment Test

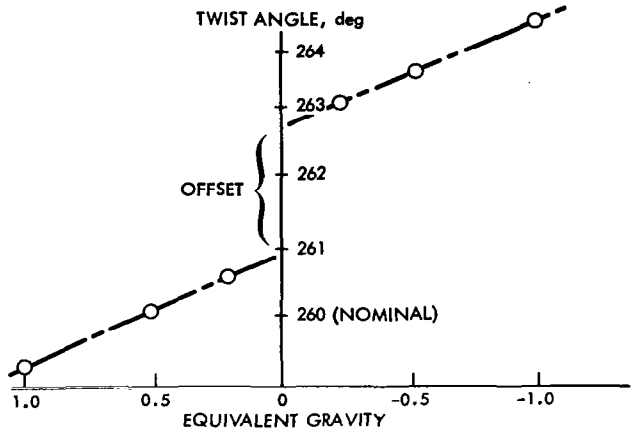

Figure 14. Twist Angle vs Gravity

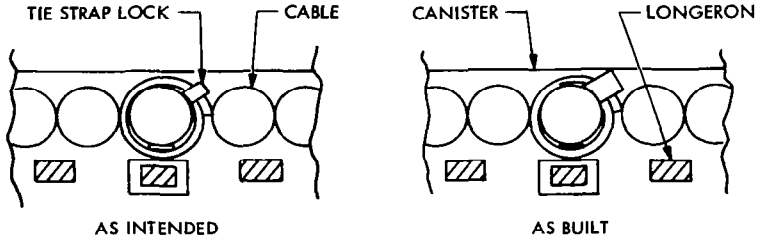

Figure 15. Tie Strap Problem

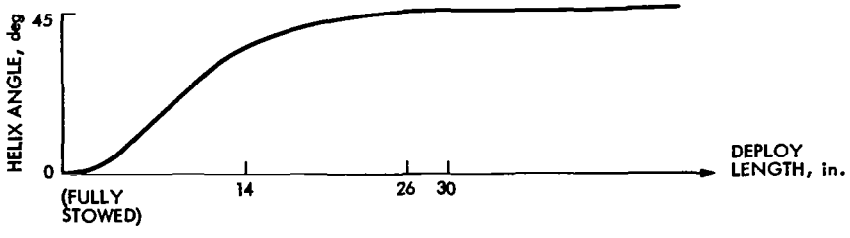

Figure 16. Helix Angle vs Transition Length

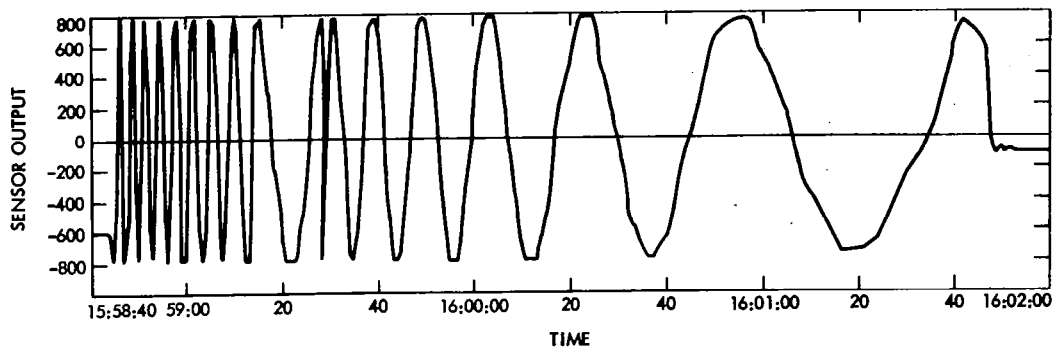

Figure 17. Voyager 2 Flight Deployment

Table 1. Predicted Flight Alignments*

		X-AXIS	Y-AXIS	Z-AXIS
VOYAGER 1	INBOARD SENSOR TO S/C	+1.59 ± 0.39	+1.51 ± 2.21	-1.49 ± 1.95
	OUTBOARD SENSOR TO S/C	-0.20 ± 0.87	+0.17 ± 1.35	-0.17 ± 1.14
	INBOARD TO OUTBOARD SENSOR	+1.40 ± 1.16	+1.37 ± 1.70	-1.35 ± 1.95
VOYAGER 2	INBOARD SENSOR TO S/C	+2.40 ± 0.67	+1.80 ± 2.82	-1.73 ± 2.42
	OUTBOARD SENSOR TO S/C	+0.79 ± 0.71	-0.76 ± 2.26	+0.76 ± 1.94
	INBOARD TO OUTBOARD SENSOR	+1.62 ± 0.67	+2.27 ± 4.06	-2.25 ± 3.45
SPARE	INBOARD SENSOR TO S/C	+1.27 ± 0.67	+1.70 ± 2.17	-1.69 ± 1.90
	OUTBOARD SENSOR TO S/C	+1.09 ± 1.03	+0.96 ± 1.15	-0.95 ± 1.02
	INBOARD TO OUTBOARD SENSOR	-0.45 ± 0.64	+0.68 ± 1.56	-0.68 ± 1.34

Table 2. Actual Flight Alignments (Preliminary)*

		X-AXIS	Y-AXIS	Z-AXIS
VOYAGER 1	INBOARD SENSOR TO S/C	0	0	+1.9
VOYAGER 2	INBOARD SENSOR TO S/C	-1.6	0	+1.4
	OUTBOARD SENSOR TO S/C	0	0	0

*Values are deviations from nominal (in degrees) about spacecraft axes, with 3-sigma uncertainties given for the predictions.

FOCAL PLANE TRANSPORT ASSEMBLY

FOR THE HEAO-B X-RAY TELESCOPE

By

R. Brissette

P.D. Allard, F. Keller, E. Strizhak, E. Wester

AMERICAN SCIENCE AND ENGINEERING, INC.

Cambridge, Massachusetts

ABSTRACT

The High Energy Astronomy Observatory - Mission B (HEAO-B) is an earth orbiting X-ray telescope facility capable of locating and imaging celestial X-ray sources within one second of arc in the celestial sphere. (1)

The Focal Plane Transport Assembly is one of the basic structural elements of the three thousand pound HEAO-B experiment payload. The FPTA is a multi-functional assembly which supports seven imaging X-ray detectors circumferentially about a central shaft and accurately positions any particular one into the focus of a high resolution mirror assembly. A drive system, position sensor, rotary coupler and detent alignment system are all an integral part of the rotatable portion which in turn is supported by main bearings to the stationary focal plane housing.

INTRODUCTION

The High Energy Astronomy Observatory X-Ray Telescope is shown in Figure 2. Major components are the High Resolution Mirror Assembly, Optical Bench, and Focal Plane Transport Assembly (FPTA). On the left hand side appears the FPTA in its fully assembled state attached to the optical bench. The Focal Plane Transport Assembly has been designed and fabricated to satisfy a wide variety of structural, scientific, and environmental requirements. Among these are chiefly:

- To physically maintain each detector focal plane within prescribed limits as defined by the high resolution mirror focus criteria.

- To withstand launch environments induced by Atlas-Centaur launch vehicle.

- To maintain alignment during on-orbit temperature excursions.

- To rotate one of many detectors into and out of the telescope field-of-view upon ground command, and maintain the detectors in position.

- To maintain structural factors of safety of two on yield and three on ultimate strength.

- To provide complete redundancy in all moving systems including drive system, position sensing and detent alignment system.

The major constituents of the (FPTA) are delineated in Figure 1 and those appearing in solid lines will be discussed individually.

DRIVE SHAFT ASSEMBLY

The Drive Shaft Assembly is the central most feature of the FPTA. It provides support to all X-ray detecting instruments by way of an Instrument Support Structure, which is hard mounted to the drive shaft at four circumferential locations. Both the Drive Shaft itself and the Instrument Support Structure are made from Invar LR-36. This material possesses a low coefficient of thermal expansion ($\sim 1.0 \times 10^{-6}$ in/in/$^{\circ}$F) which is a near perfect match to the remaining structures that control the mirror focus, namely the High Resolution Mirror itself, made from quartz primarily, and the Optical Bench which is made from a graphite/epoxy composite.

The Drive Shaft Assembly also houses (centrally within itself) the Position Sensor Assembly, Rotary Coupler, and Harmonic Drive Assembly, all of which are statically connected to the shaft. The shaft mounts to the main support bearings on which the whole FPTA rotates.

Some of the imaging X-ray detectors which are mounted to the FPTA use a special gas, in order to function properly, which is also stored on the rotating assembly. This gas is stored in 3000 psi titanium spheres which contain enough gas for two years consumption in orbit. However, the gas does flow through the detectors and therefore, must be vented to space. To accomplish this, the FPTA provides several separate rotary plenum chambers whereby gas lines can be plumbed directly to the rotating portion of each plenum chamber and likewise from the static portion where it can then be directly connected to the spacecraft vent panel. This method allows for five continuous separate vent paths across the main support bearings, handling one of three gases or gas mixtures, without

the use of cumbersome flexible vent lines since available volume is a real premium in this area. In addition to the aforementioned gas usage, another instrument contains solid ammonia and methane which are used to cool detectors for proper operation. These solids have a finite life at certain low pressures resulting from sublimation. This sublimation also needs to be vented across the main support bearings; however, interface pressures must not exceed 8.0 Torr for CH_4 nor 0.065 Torr for NH_3. The calculated interface pressures resulting from the actual hardware configuration are 0.76 torr for CH_4 and 0.054 torr for NH_3, well below the triple point of the substances.

A variety of O-rings are used to seal the integral plenum chambers, VITON which is compatible with methane, argon, CO_2 and xenon, NITRILE which is compatible with both methane and ammonia, and BUTYL which is compatible with ammonia. All seals are liberally lubricated with Braycote (2) 3L-38 RP, an inert, low vapor pressure perflourinated polyether stable grease. Life tests have been conducted on all these seal materials with grease in the design configuration and found to have a margin of 4.9 over the intended usage. Figure 3 shows the completed drive shaft with the welded Invar Instrument Support Structure attached. The ISS is painted while the drive shaft is nickel-plated, thus the difference in appearance for the same material.

FOCAL PLANE HOUSING

This member is that static portion which houses the fixed halves of the main support bearings. Additionally, it provides the static connection for the Harmonic Drive Assembly as well as a reference for the Position Sensor Assembly. The FPH is made from two materials. On the forward portion where the interface is made to the graphite epoxy optical bench (a low coefficient of thermal expansion material) Invar is used. This provides good lateral control of thermal growth of detector positions with respect to the optical axis, as well as a good α match to the bench. The completed FPH is shown in Figure 5 while the integration of the circumferential shear tie between the forward bulkhead of the FPH and the optical bench is shown in Figure 4. The remainder of the housing is made of aluminum which is a riveted-and-epoxied construction, thereby reducing the overall weight, increasing the specific stiffness and minimizing thermal gradients.

The axial positioning of all detectors mounted to the FPTA, as well as the structural support during launch, is maintained through the forward main bearings. These bearings are preloaded back-to-back as a duplex pair capable of taking both radial and thrust loading. The aft main bearings provide support in the radial direction only. The FPH also provides a mounting interface for two of the four telescope mounting points to the Spacecraft.

HARMONIC DRIVE ASSEMBLY

The Harmonic Drive Assembly (HDA) is used to rotate the entire array of X-ray detectors along with the associated support equipment and structure. The rotating mass is approximately 800 pounds and volumetrically occupies approximately 60 ft.^{3} The HDA is packaged within the central main shaft at the aft end. This is also where the static connection is made to the Focal Plane Housing through the center of the rear support bearings. The connection extends radially outward and attaches to the stationary aft bearing support.

Two redundant drive systems are so arranged in a single assembly such that one drive relies on the other to complete the drive path from static connection to output shaft. Both drives are completely independent of one another for functional operation. The basic arrangement of each functional section is a Brushless DC Gearmotor(3) which drives a Harmonic Drive Transmission(4) and is shown in Figure 6. The purpose of this arrangement is to develop substantial torque through a large mechanical advantage using relatively little power. The brushless DC motor operates at approximately 8500 rpm and drives the input stage of a three stage planetary gear box resulting in a speed reduction of 170:1 and a torque multiplication of 144:1. The planetary is then the input to the single stage Harmonic Drive Transmission.

The Harmonic Drive is a constant ratio mechanical drive system used for power transmission, angular positioning or other motion conversion. It is comprised basically of three components namely the wave generator which in this case is the input member, the flex spline which is the output member, and the circular spline which is the fixed member. A continuous deflection wave generated in a flexing spline element achieves high mechanical leverage between concentric parts. That is, rotation of the wave generator produces radial deflection and tangential motion of the flexible spline. Essentially, the circular spline (fixed member) is a fine toothed internal gear while the flexible spline is a fine toothed external gear which meshes with the circular spline at two regions diametrically opposite on the major axis of the ellipsoid when radially deflected. Teeth of the two splines clear at the minor axis. The wave generator creates this elliptical shape inside the flexible spline. Without the radial deflection of the flexible spline, there would be no effective gear mesh since there are slightly fewer teeth on the flexible spline than on the circular, however, teeth on both splines are cut to the same circular pitch. To allow engagement at two diametrically opposite regions, the tooth arrangement must be symmetrical. In this case, the system has two regions of tooth engagement, therefore the difference in the number of teeth is an integral multiple of two regions. The calculation for mechanical advantage is then:

$$R = \frac{N_f}{N_f - N_c}$$

where R = gear ratio
N_f = number of teeth on flex spline
N_c = number of teeth on circular spline

A negative value for R indicates output is in opposite direction from input.

The Harmonic Drive used here has a speed reduction of 200:1, in series with the 170:1 of the planetary resulting in a 200 x 170 or 34,000:1 speed reduction. The FPTA then rotates 8500/34,000 or 0.25 rpm.

The drive system torque summary is shown in Figure 8 while the primary and redundant drive components are shown in Figure 9.

Several unique advantages are derived from using the Harmonic Drive. Among those include:

- A high-ratio speed reduction in a single stage.
- Many spline teeth are in simultaneous engagement to carry high torque loads. Teeth adjacent to load-bearing teeth are in near engagement and provide reserve capacity to accommodate shock overloads.
- Low tooth friction losses due to almost pure radial motion at contact.
- Regions of tooth engagement and application of load torque are diametrically opposed, and result in a force couple that is symmetrical and balanced.
- In-line relationship of input and output elements where space is limited, resulting from concentric orientation and minimum diameters provides a desirable package.

A cross section through this assembly is shown in Figure 6. It becomes obvious how the primary drive and the redundant drive interact. Figure 7 describes the torque vs. various failure modes associated with this model of the Harmonic Drive, as well as the FPTA operating points.

BRUSHLESS DC GEARMOTOR

The brushless DC gearmotors used in this application drive the input stage of both the primary and redundant drive. This is shown in Figure 6 also in two respective places. The brushless aspect was chosen for a number of reasons. Primarily, the operating lifetime of a conventional brush motor in hard vacuum of space is very limited. The requirement for our application is $\sim$760 hours operation over a mission life of one year in-orbit, plus much ground operation, checkout, and margin. Nowhere was it obvious that there was a brush motor to perform reliably under these conditions. The drawbacks of conventional brush type

motors are well-known. The brushless DC Motor has three basic components: housing, rotor shaft and electronics assembly, including magneto-resistors and solid state logic. All switching circuits are handled external to the motor assembly.

The housing contains the stator windings where any heat generated passes directly to the housing unlike conventional motors where heat generated in the rotor windings must pass through an air gap to the housing, a relatively high resistance thermal path. The rotor shaft then contains the permanent magnet as well as the targets necessary to change the sensor magnetic field. Essentially, this sensed change in magnetic field causes a level change in the input signal to the logic circuit. What we have basically is a motor shaft proximity sensor which indicates when to energize each stator winding. The rotor position sensors are speed independent and non-contacting. There is no physical contact between rotor and stator except through the bearings.

POSITION SENSOR ASSEMBLY

Knowledge of the angular position of the FPTA is important in that the drive electronics needs positional information for CW and CCW sequencing. In order to accomplish this, there is mounted to the stationary member two types of potentiometers, a ten turn and a single continuous turn giving 3600° and 360° electrical degrees respectively. The pot shafts are driven through an anti-backlash gear set whereby the follower gear is pot mounted and the driver gear is FPTA mounted in a 9:1 speed increasing arrangement. That is, the potentiometer shafts are rotating 9 times the speed of the FPTA thereby maximizing the resolution. Effectively, we are using the large majority of the 3600° electrical degrees for one equivalent revolution of the FPTA while the single turn potentimeter provides a vernier reading to the less accurate 10 turn. This arrangement is located just behind the Harmonic Drive Assembly and can be seen in Figure 6.

ROTARY COUPLER ASSEMBLY

In order to provide the necessary signal and power leads to the X-ray detecting instruments on the rotating FPTA, it became obvious that the best route would be directly down the shaft center of the FPTA at the opposite end from the harmonic drive and position sensor. Since the FPTA rotates through only approximately 300° absolute, moving CW and CCW, the wire bundle need only twist plus and minus through half that angle. Approximately 750 wires are serviced through this Rotary Coupler. They are so arranged relative to one another such that they provide minimal torque resistance when rotated as well as minimize routing problems at either end.

Figures 10 and 11 show the life test set up and also the rotary coupler in the revolved state respectively. One can readily see from the wire twist

variations, that emphasis was placed on axial separation of potted ends, surface friction coefficient of inside guide tube and wire orientation to produce a satisfactory operating rotary coupler. A mock-up of this design was fabricated and life-tested for an equivalent of 5 years of normal operation.

DETENT ALIGNMENT SYSTEM

In order to locate each detector in the focal plane properly, a simple over center toggle mechanism is employed. On the rotating portion exists several position detents which are dedicated to each instrument viewing position. They are complimented by the over-center toggle assembly which is located on the stationary Focal Plane Housing. The symbolic arrangement of the Detent Alignment System is shown in Figure 12. When a viewing position is desired (instrument in the telescope focus) the FPTA is driven in a CW and/or CCW specific sequence and the rotating position detents physically drive up against the toggle mechanism and reach a physical stall condition. Meanwhile, the brushless DC gearmotor is current limited to a predetermined value (1.5A) which effectively limits the torque applied. In order to reconfigure to any other instrument viewing position, the sequence must start by rotating CW away from the toggle previously positioned against.

The design of the toggle mechanism itself is such that it is equally stable in the full open or full closed position but not so half way. If a position detent on the CW rotating FPTA moves by the toggle, the geometry is such that the toggle will spring return to its original location ready to provide the necessary location for the next viewing position. In order to rotate substantially (more than one viewing position) in the CCW direction, one must first rotate CW to the end position where reset cams move the toggle into the full-open position where it will stay until reset at the opposite end of rotation. The need for rotational position sensing becomes more obvious at this point since the drive electronics is so designed to handle this rather complex CW/CCW driving logic automatically. That is, the logic is "built-in" to reconfigure from any one of 11 detent positions to any one of the other remaining positions. Several different sequences are necessary depending on what position is current in the viewing position and what position is desired. Figure 13 shows the electronics block diagram describing the aforementioned interaction.

TEST AND INTEGRATION ACTIVITY

The entire FPTA with its support electronics in the fully integrated condition has been functionally tested at AS&E. The HEAO-B X-ray telescope was successfully tested in vacuum for 41 days at Marshall Space Flight Center during the summer of 1977. The FPTA performance was satisfactory over a range of temperatures from $-10^{\circ}C$ to $30^{\circ}C$. The entire X-ray telescope has since been shipped to TRW in Redondo Beach, Ca., integrated with the spacecraft, and awaiting

further environmental testing. The entire spacecraft and experiment payload will then undergo vibration testing, acoustic testing and a thermal balance test in vacuum in preparation for launch in late 1978.

ACKNOWLEDGEMENTS

The authors would like to express their sincere thanks to many people who participated at various stages of this program. In the engineering area, thanks go out to W. Antrim, R. Miller, T. DeFuria, R. Sawicki, V. Davulis, T. Hebert, C. Bejtlich, G. Austin, R. Madelung, D. Wheinstone, R. Larson, M. Pitasi, D. Boyd, H. Langner all from Mechanical Engineering at one time or another; K. Kubierschky, J. Morris, and M. Mintz from Electronics Engineering; R.B. Dias, D. Dennis, R. Marrone, R. Goddard, R. Carroll, F. Madden and the many machinists and technicians from Manufacturing; V. Trovato from Reliability; D. Cipolle and E. Powers from Quality Assurance; T. Kirchner and M. Russell from the Program Office.

The authors acknowledge the scientific direction and technical support provided by many at SAO, including: L. VanSpeybroeck, H. Tananbaum, and of course, the Principal Investigator, Dr. Riccardo Giacconi.

In addition to the many contributions at AS&E and SAO, thanks also go out to both Marty Arnold and Mike Schwartz of Aeroflex Laboratories, who were largely responsible for the success of the "Brushless DC Motor".

Last but not least, our thanks go to Marie LaRosa for the fine job she has done in the typing of this paper.

REFERENCES

(1) HEAO-B is a NASA program managed by the Marshall Space Flight Center. Scientific requirements were established by a consortium consisting of Smithsonian Astrophysical Observatory, Massachusetts Institute of Technology, Columbia University, and NASA Goddard Space Flight Center. Dr. Riccardo Giacconi of SAO is Principal Investigator. TRW, Inc. is the Spacecraft prime contractor and AS&E is the X-Ray Telescope prime contractor under contract NAS8-30750;

(2) Product of Bray Oil Co., Los Angeles, Ca.

(3) Provided by Aeroflex Laboratories, Inc., Plainview, L.I., N.Y. under contract to AS&E.

(4) Component parts provided by USM Corporation, Woburn, Ma. under contract to AS&E.

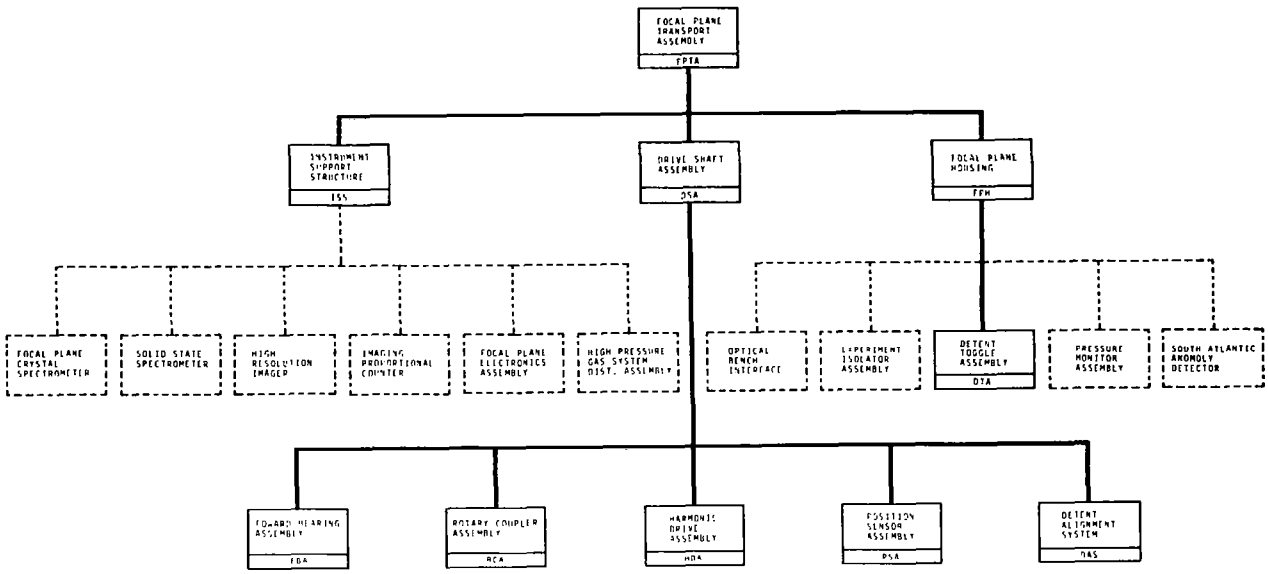

FOCAL PLANE TRANSPORT ASSEMBLY BREAKDOWN

Figure 1

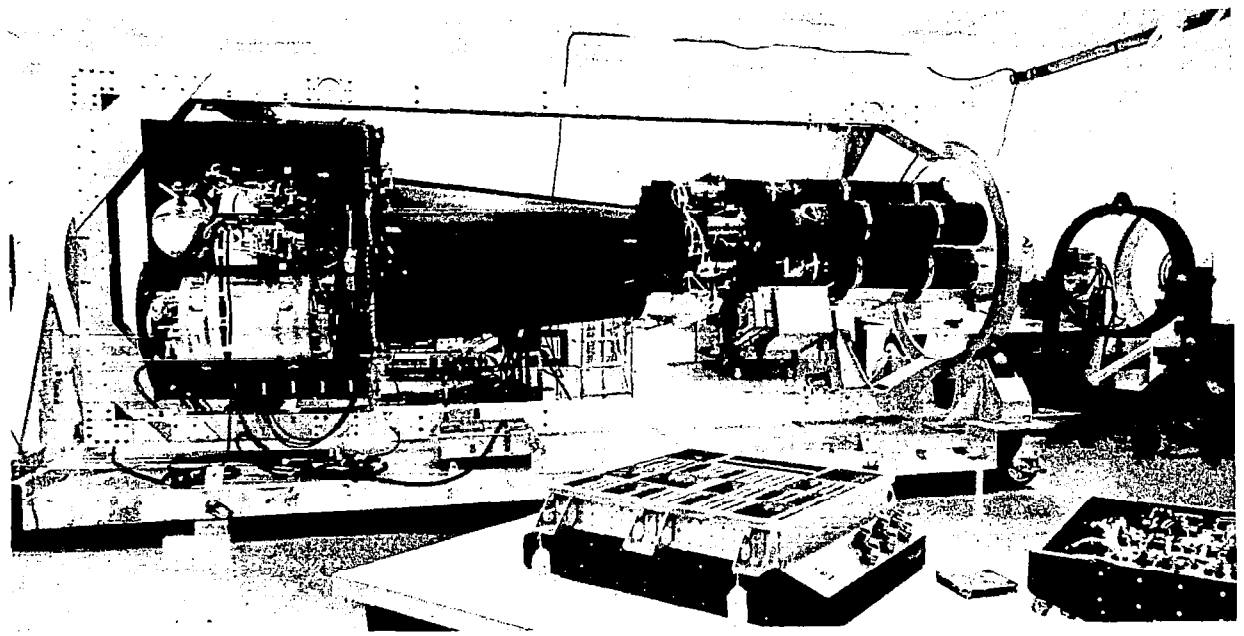

HEAO-B X-RAY TELESCOPE

Figure 2

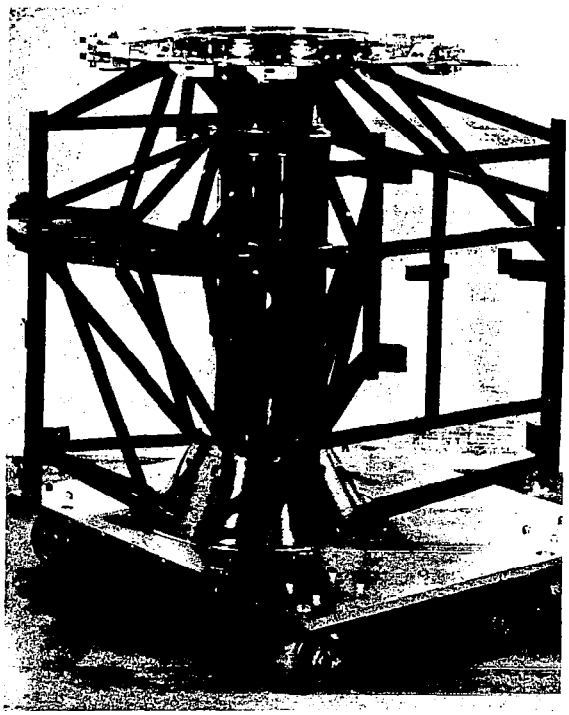

INSTRUMENT SUPPORT STRUCTURE

Figure 3

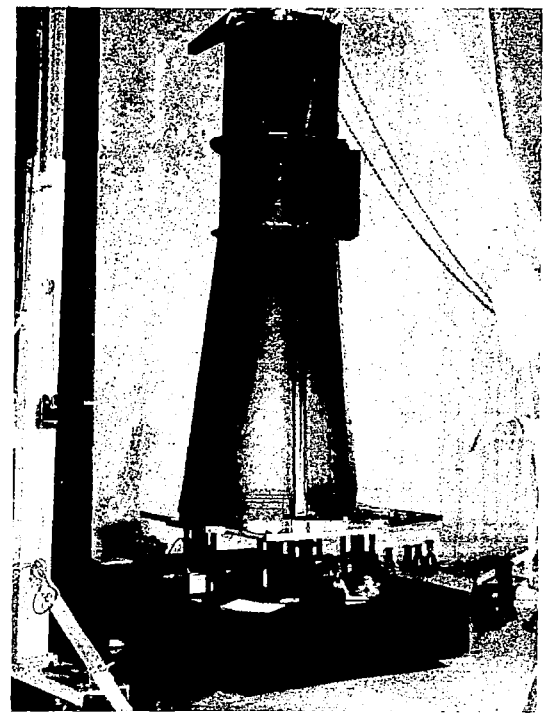

OPTICAL BENCH/FOCAL PLANE HSG.
BULKHEAD INTEGRATION

Figure 4

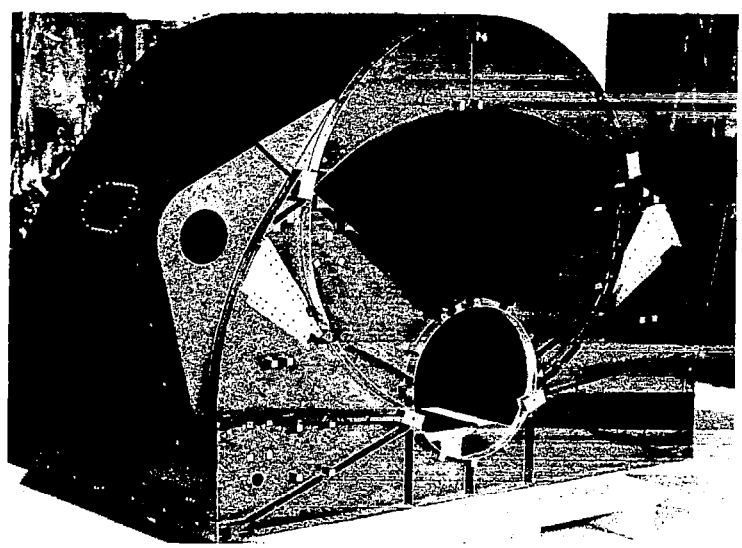

FOCAL PLANE HOUSING

Figure 5

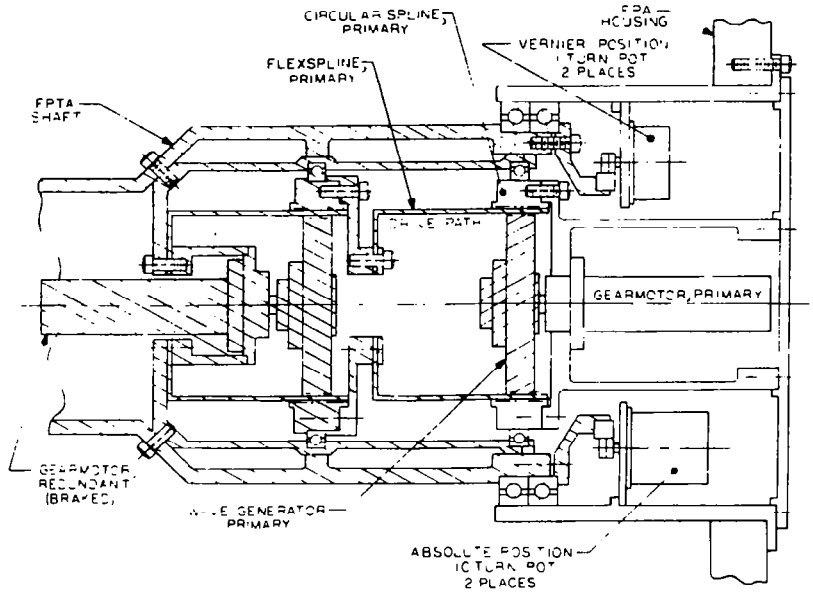

HARMONIC DRIVE PRIMARY

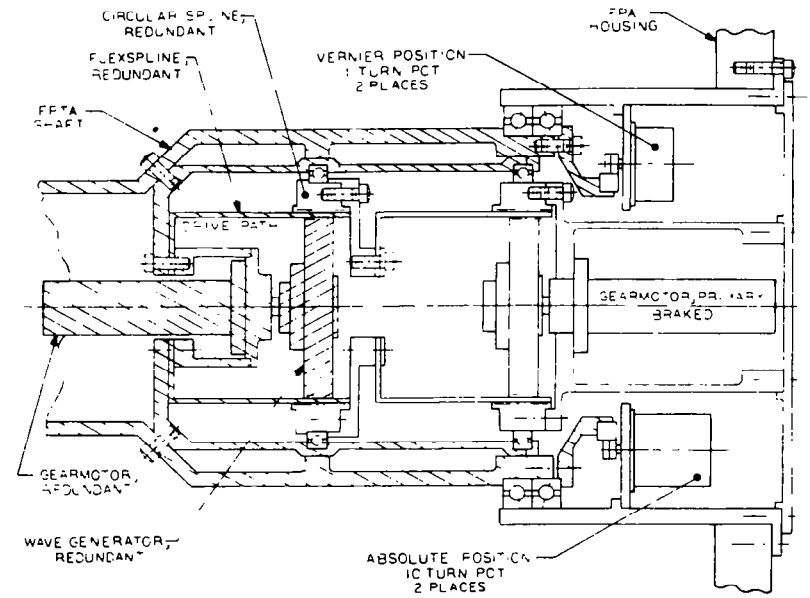

HARMONIC DRIVE REDUNDANT

HARMONIC DRIVE ASSEMBLY CROSS SECTION

Figure 6

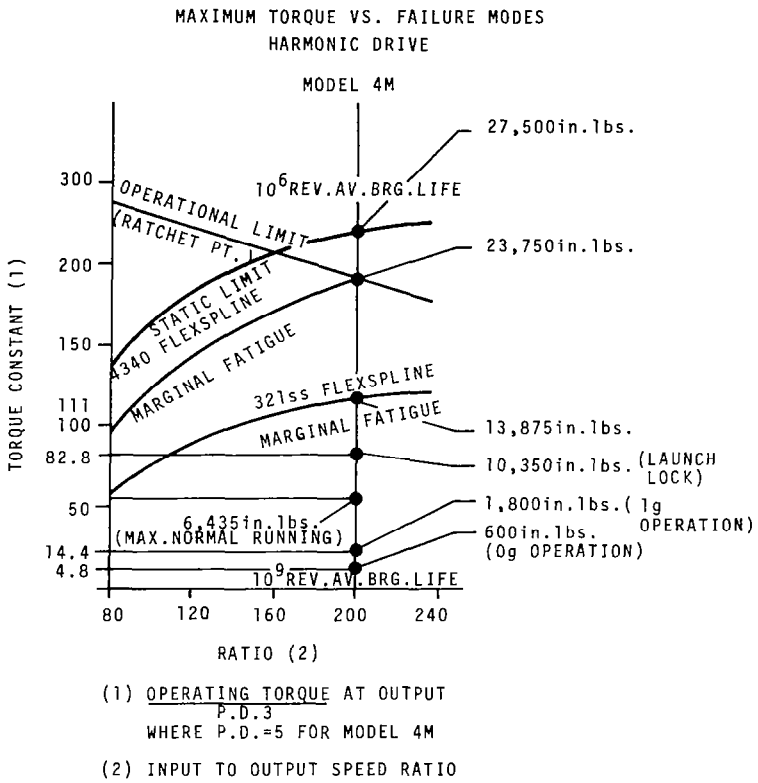

Figure 7

1g OPERATION

APPLIED:	unbalance moment	=	1,200	in. lbs.
	system friction	=	600	in. lbs.
	total:	=	1,800	in. lbs.
AVAILABLE:	DC gearmotor current limit condition			
@1.5A	715 oz in x 200 x .72 / 16	=	6,435	in. lbs.
@2.0A	975 " "	=	8,531	in. lbs.
TORQUE MARGIN (Normal):				
	6435/1800	=	3.6	
TORQUE MARGIN (Max):				
	8531/1800	=	4.7	

0g OPERATION

APPLIED:	system friction	=	600	in. lbs.
AVAILABLE:	DC gearmotor @ 1.5A current limit condition	=	6,435	in. lbs.
TORQUE MARGIN (Normal)		=	10.7	
TORQUE MARGIN (Max)		=	14.2	

LAUNCH LOCK CONDITION

TORQUE PRELOAD:	1150 in. oz. 200 x .72 / 16	=	10,350	in. lbs.
	System Friction	=	600	in. lbs.
	System resisting torque	=	10,950	in. lbs.
MECO INDUCED TORQUE		=	8,563	in. lbs.
TORQUE MARGIN:	10,950/8563 design goal 1.25	=	1.28	

DRIVE SYSTEM TORQUE SUMMARY

Figure 8

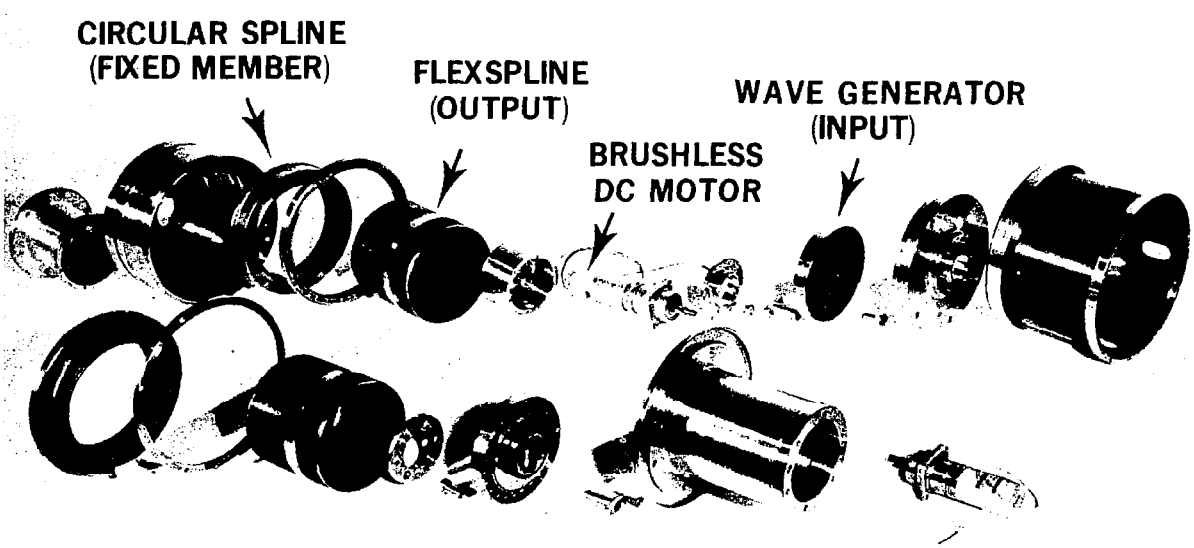

PRIMARY AND REDUNDANT DRIVE COMPONENTS

Figure 9

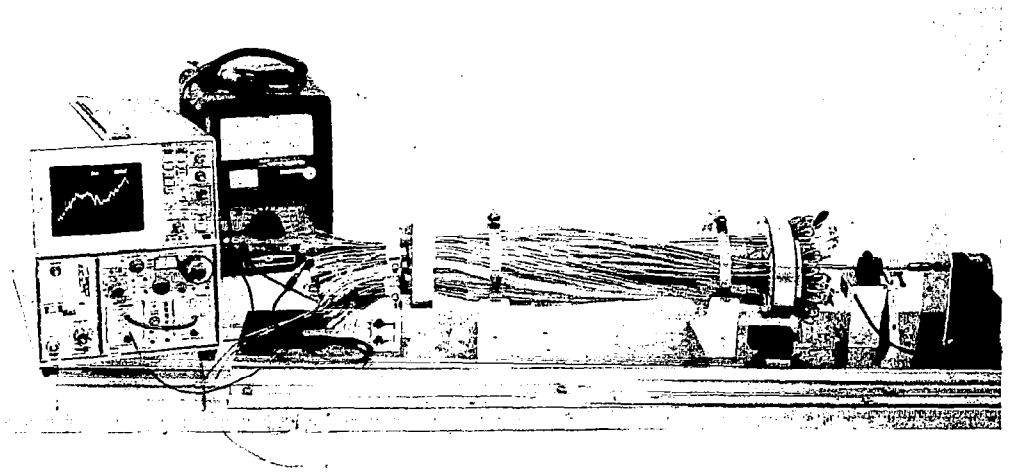

ROTARY COUPLER LIFE TEST

Figure 10

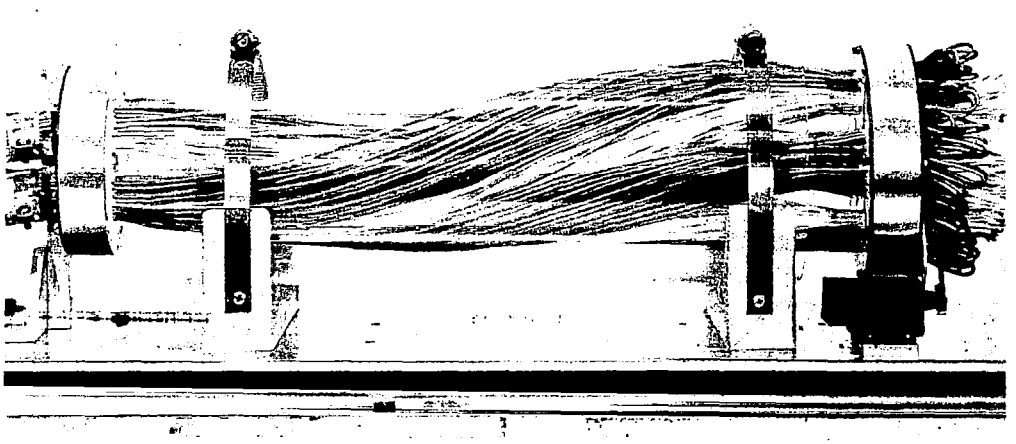

ROTARY COUPLER REVOLVED

Figure 11

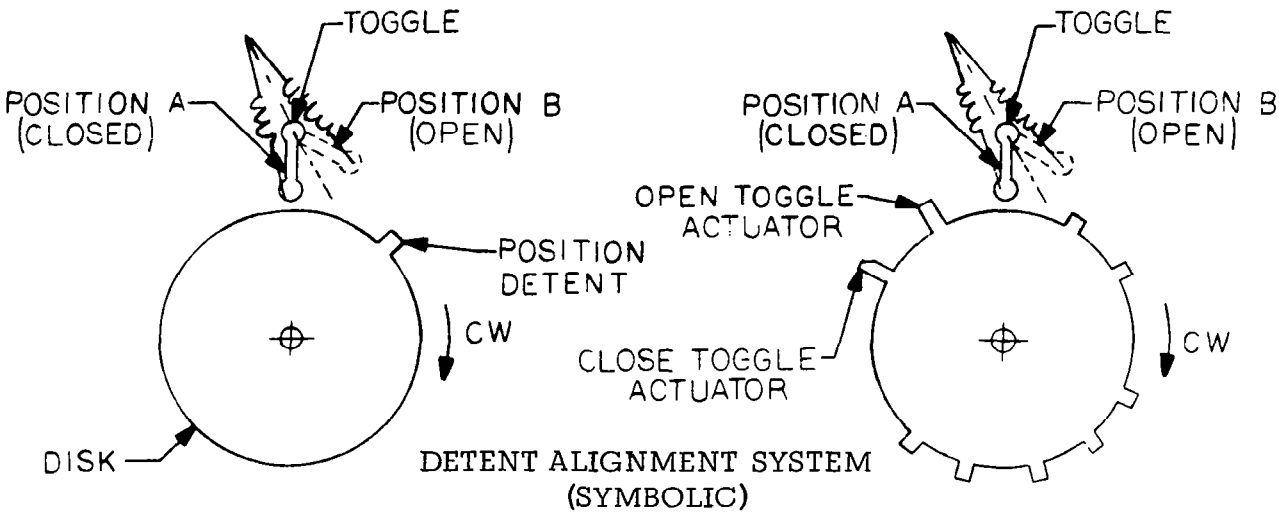

DETENT ALIGNMENT SYSTEM
(SYMBOLIC)

Figure 12

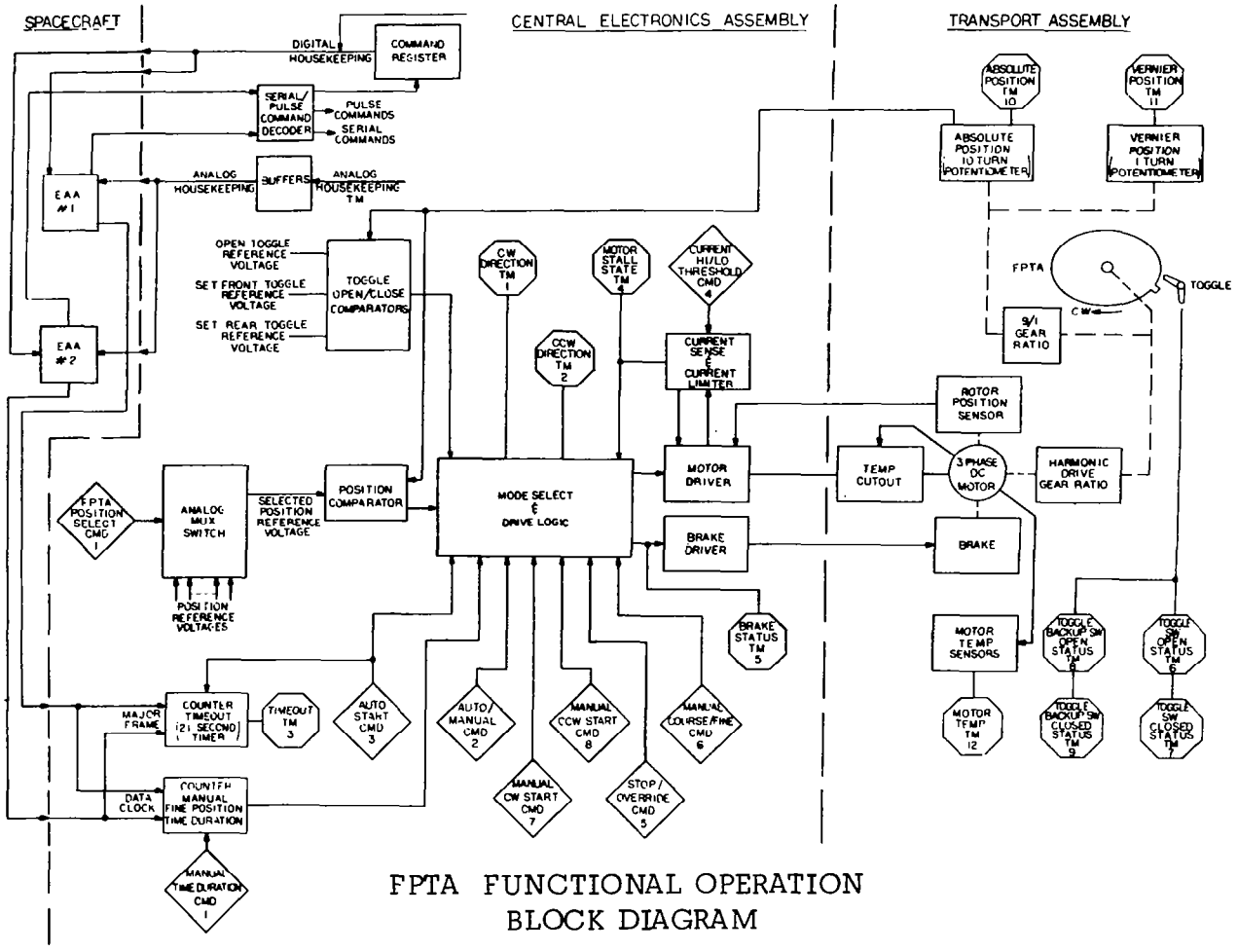

FPTA FUNCTIONAL OPERATION
BLOCK DIAGRAM

Figure 13

AN 11-METER DEPLOYABLE TRUSS FOR THE SEASAT RADAR ANTENNA

by

Bruce E. Campbell
Astro Research Corporation

and

Wesley Hawkins
Ball Brothers Research Corporation

ABSTRACT

The recently developed Extendable Support Structure is a folding three-dimensional truss and tripod assembly which deploys the SEASAT Synthetic Aperture Radar Antenna. The folding structure with the antenna panels and rf components stows in an 8.5-inch-thick package. Upon deployment, the structure produced is a flat and rigid support for the antenna.

INTRODUCTION

The Extendable Support Structure (ESS) is a 35-foot (10.7-meter) deployable truss developed by Astro Research Corporation, Santa Barbara, California. The structure provides launch packaging and on-orbit extension for the Synthetic Aperture Radar (SAR) Antenna developed by Ball Brothers Research Corporation, Boulder, Colorado, for the SEASAT Global Ocean-Survey Satellite.

Scheduled to be launched during the spring of 1978 from Vandenberg Air Force Base, California, the SEASAT Satellite will be inserted into a circular 430-mile near-polar orbit by an Atlas/Agena Booster system. The satellite will continuously circle the globe, covering 95 percent of the earth's ocean area, every 36 hours.

After ascent to orbit, upon command, the folded and stowed SAR Antenna will be deployed from the SEASAT Satellite and extended, via the ESS, into a planar array 35 by 7 feet. The array will provide valuable and precise realtime all-weather radar imagery of ocean topography such as wave patterns, ice heads, icebergs, coastal erosion and environmental management features. The on-orbit configuration of the SAR Antenna and Satellite is shown in Figure 1.

The ESS furnishes a mounting bed for the eight honeycomb panels, which upon extension becomes the planar array of the SAR Antenna.

The ESS provides the strength and rigidity necessary to withstand the launch vehicle environments. Upon extension, it supports the antenna panels to maintain precise flatness, including mechanical alignments and thermal distortions, throughout the mission-orbit environment.

DESIGN REQUIREMENTS

The ESS was challenged by several major design requirements:

1. pointing of the array's planar surface to ±0.2 degree,
2. repeatability of the array's pointing to ±0.1 degree,
3. fundamental resonant frequency (stowed ≥10 Hz and extended ≥0.5 Hz),
4. weight less than 77 pounds,
5. planar flatness within ±0.25 inch over the orbit temperature ranges of 200 to -250°F, and
6. fourteen-month program from start of development to delivery of the flight ESS, which meant the development unit was to become the qualified flight unit.

Envelope

The envelope for packaging the SAR Antenna was defined by the volumetric availability of the SEASAT Satellite sensor module. The dimensions of this envelope are 101.5 by 64.0 inches with a packaged thickness of 8.5 inches. Thus, the planar array length of 35 feet was required to be folded and restrained for launch within the 8.5-inch dimension. This alone was a major design parameter, in that the total thickness of the eight antenna panels accounted for 3.66 inches, leaving only 4.84 inches for the development of a three-dimensional rigid and stable folding truss and launch fittings.

Truss

The ESS has to support the 130-pound weight of the eight antenna panels and associated rf system for launch. To achieve this goal, the truss work of the ESS provided mounting hardware for the panels. To withstand the 8-g axial launch-vehicle acceleration, the truss incorporated nesting and interlocking structural features so that panel and truss loads could be transferred to the spacecraft

structure by three launch restraint-arm mechanisms. The interlocking features of the truss consists of cups and cones and key-type fittings which engage each other in the folded configuration and release one another during the truss extension. The stacks of cups and cones are clamped and preloaded by the launch restraint-arm mechanisms. Three load paths are employed, one at the apex of the truss and two at the hinge line of the truss (Figure 2). Thus upon the satellite's obtaining a ready-for-SAR deployment status, the launch restraint arms are pyrotechnically released and the ESS freed for deployment maneuvers and extension.

Deployment

The envelope allocation also required the folded and stowed package to be rotated out-board of the spacecraft in two 90-degree maneuvers. These maneuvers were required to achieve a position for array extension which would result in the long axis of the planar array being aligned with the velocity vector of the spacecraft. In addition, the normal of the array's planar surface was to be pointed 20 degrees up from nadir, thus requiring the ESS to pitch-up the antenna plane during extension of the array.

This deployment sequence was efficiently implemented by a BIAX mechanism, developed by Lockheed Missiles and Space Company, which performed the two 90-degree maneuvers (Figure 3). The ESS performs the array extension concurrent with the 20-degree pitch-up rotation.

Upon completion of the 7-minute powered extension, the ESS truss forms a three-dimensional structure providing a flat array surface (within ±0.090 inch to a least square best-fit plane).

DETAILED DESIGN DESCRIPTION

The ESS consists of a tripod assembly and a truss assembly. They are discussed separately in the following. Also, the design of important joints in the structure is described.

Tripod Assembly

The tripod is the single mounting of the deployed antenna to the spacecraft and controls the orientation of the truss during and upon extension. The tripod consists of two folding arms and a fixed brace mounted to a short box structure (Figure 4). The location of the pivots of the arms and the single pivot at the tip of the brace

direct the motion of the truss from its flat package to its extended position. As the ESS unfolds, the orientation of the truss is rotated to the position 20 degrees from its initial packaged angle.

Deployment is controlled by the extension of a dc-motor-driven linear actuator. The actuator drives a central lever which has two ball-ended connecting rods joining it to the tripod arms. The arms are pulled to full deployment where spherical stops seat and provide support to the arms.

The arms and the nonrotating brace are titanium members with aluminum fittings in the arms. Titanium is used to minimize the effect of temperature changes on the pointing angle of the antenna.

Truss Assembly

The truss is made up of repeating frames and members which connect in seven types of joints. Along its long dimension are three longerons; two are tubular and the third is a flat bar (Figure 5). With the exception of the control linkage, each of the other members is tubular and connects the longerons. The control linkage is the second flat-bar linkage which mounts to the flat-bar longeron in seven places. The frames which lie in the plane on which the antenna panels are mounted consist of a section of the two tubular longerons, a perpendicular cross bar connecting them, and a diagonal. A vee-shaped, two-member frame connects the two tubular longerons to the single flat longeron, and two other straight members complete the truss.

The joints are designed such that the member axes intersect in the deployed truss. Each of the joints is pin-connected with dual tangs in each titanium fitting through which the pin passes. Special fittings were also bonded into the tubes where they cross, in the stowed position, to permit the flat package to be obtained.

The tubes and the flat bar are all graphite/epoxy composite. The fittings are bonded to the members with graphite/epoxy outside on the tube members and inside on the solid flat bar. The graphite/epoxy composite was chosen primarily for its low thermal-expansion properties. The composite members also provide a beneficial stiffness-to-weight ratio, but require the use of the titanium fittings to reduce thermally generated stresses in their attachment bond joints.

To synchronize the extension of the truss and assure full extension, two special types of joints were designed. These joints function to assist extension by torsion springs which drive to straighten the flat-bar longeron.

The synchronized joint connects two vee-shaped frames to the flat-bar longeron and control linkage (Figure 6). This joint utilizes a toggle linkage to control the spread of the vee-shaped frame in accordance with unfolding of the flat-bar longeron. The rotation of the central shaft of the joint drives opposing ball-ended linkages to deploy the frames. The stud which protrudes upward in the upper view of Figure 6 is located in two places along the apex of the truss where the tripod arms join the truss.

A spring-loaded toggle-type joint was designed into the flat-bar longeron hinges. To permit the longeron to fold 180 degrees, the hinge centerline is placed on the edge of the longeron as shown in Figure 7. The torsion spring on the hinge axis is greatly assisted toward the end of deployment by an "almost-over-center" latch which acts on the opposite edge of the hinge. The latch consists of two levers and a torsion spring and contributes approximately 12 in.-lbs of torque to close the longeron hinge at full deployment. This lever action multiplies the torque from the torsion spring so as to assure that the hinge will remain closed, even with 1-g loads, without requiring a lock.

FABRICATION AND TEST

The ESS has been integrated into the SAR System as shown in Figures 8 through 10. In these photographs, the thermal blankets and rf components are being installed and the assembly is mounted on a gravity-compensation fixture.

The weight of the ESS, consisting of the tripod and truss assembly, is 64 pounds. This is less than one-third the total antenna weight.

The deployed ESS produces a panel mounting surface which measures to be flat within ±0.09 inch peak from the least square best-fit plane. Extension of the structure and measurements of flatness were made with the ESS mounted on the gravity-compensation fixture.

The stowed natural frequency was tested with the panels, rf components, and launch restraint. The fundamental frequency was greater than 10 Hz. The deployed frequency was determined to be 0.9 Hz.

SEASAT PAPER NOTE

This work was performed for JPL, sponsored by NASA under contract NAS7-100. The folding truss concept was developed by Astro Research Corp. during internal proposal funding.

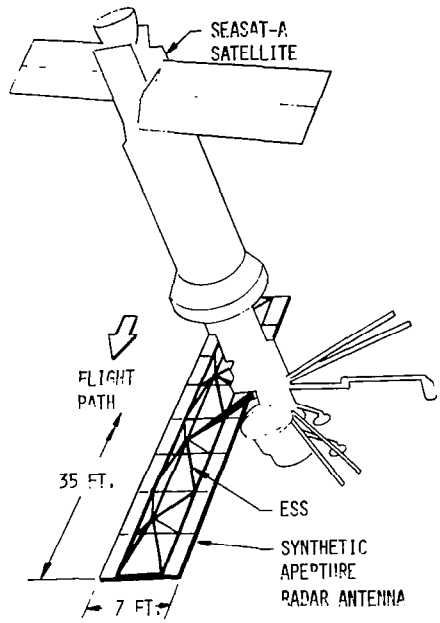

Fig. 1. Satellite Configuration.

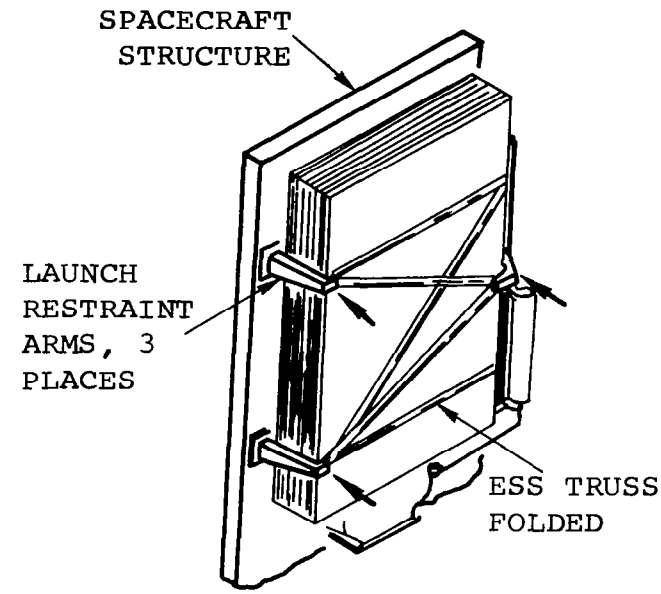

Fig. 2. Stowed Truss Load Paths.

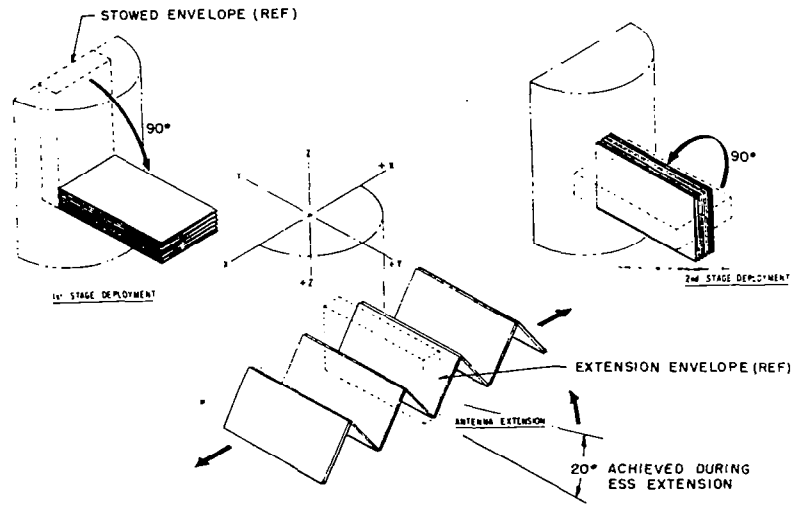

Fig. 3. Envelope Deployment Sequence.

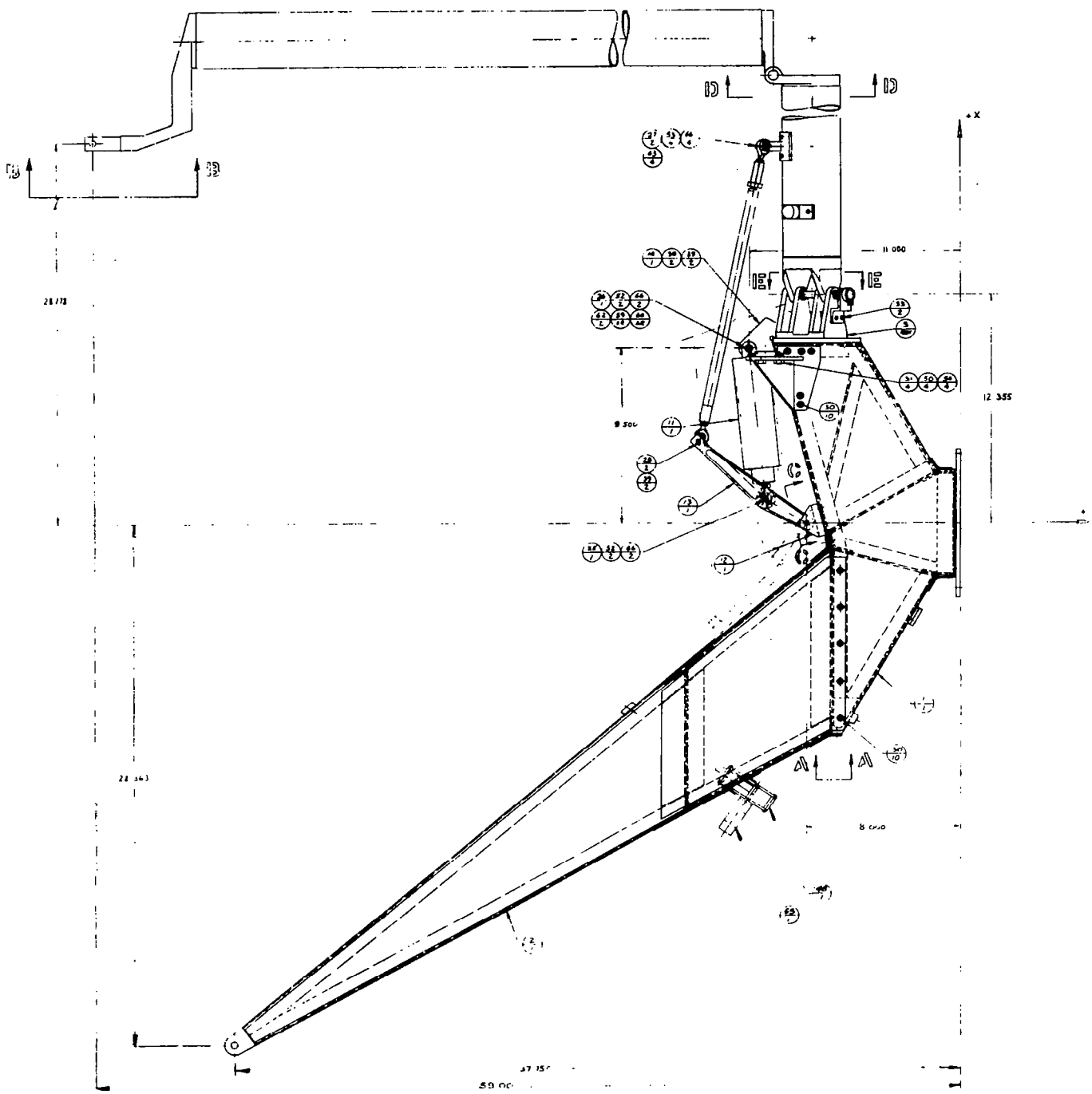

Fig. 4. Tripod Assembly.

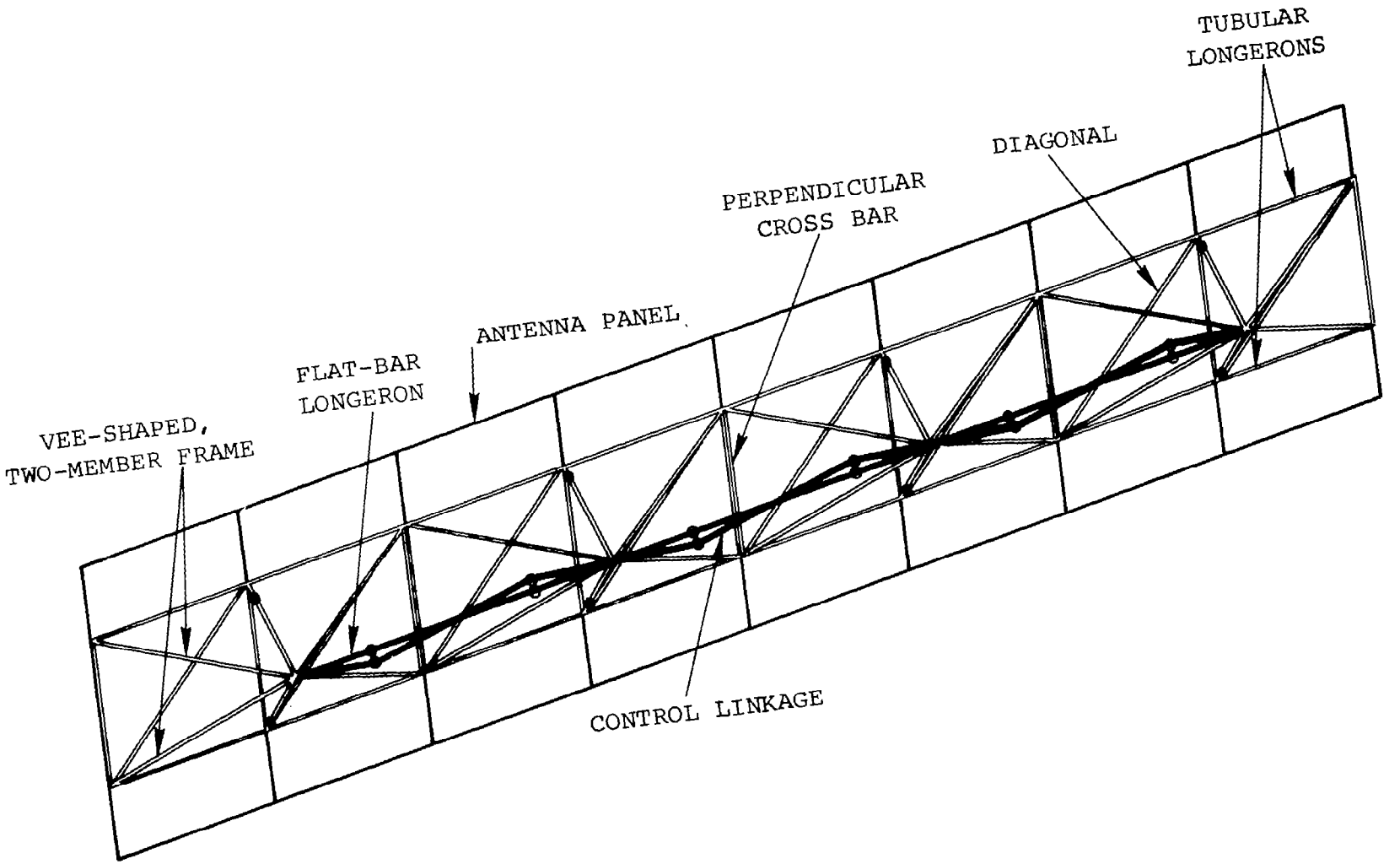

Fig. 5. Deployed ESS.

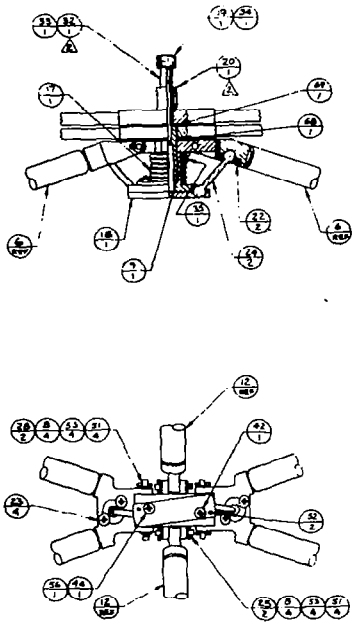

Fig. 6. Synchronized Joint.

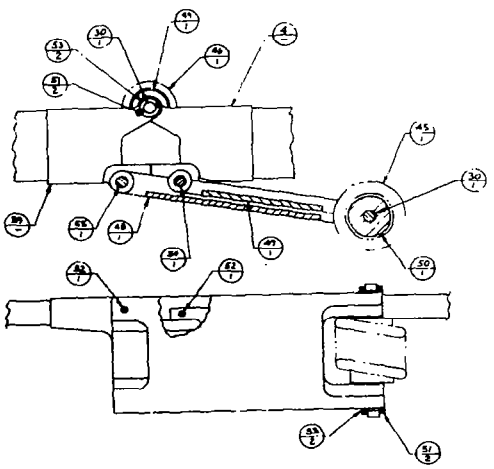

Fig. 7. Longeron Hinge.

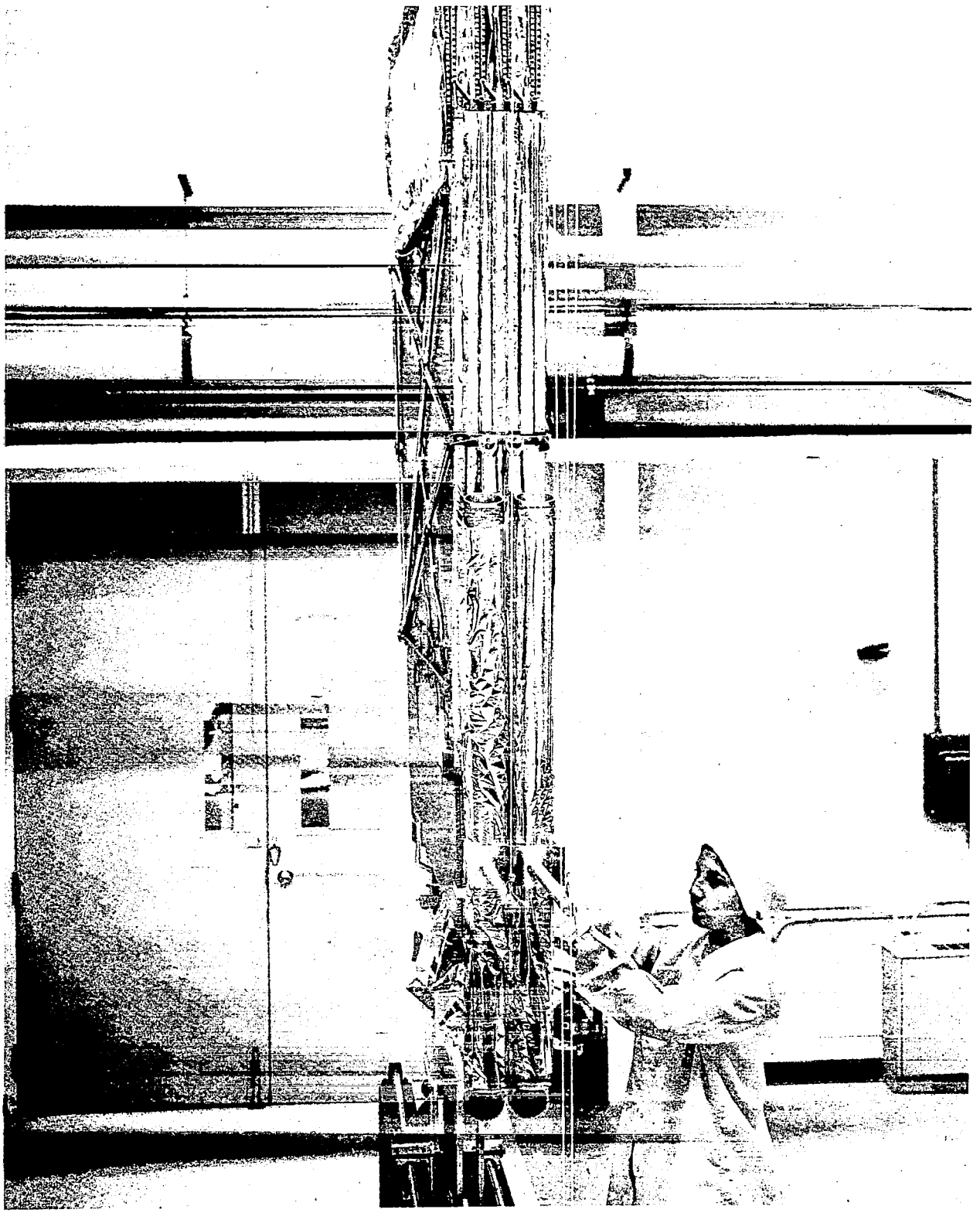

Fig. 8. SAR Stowed.

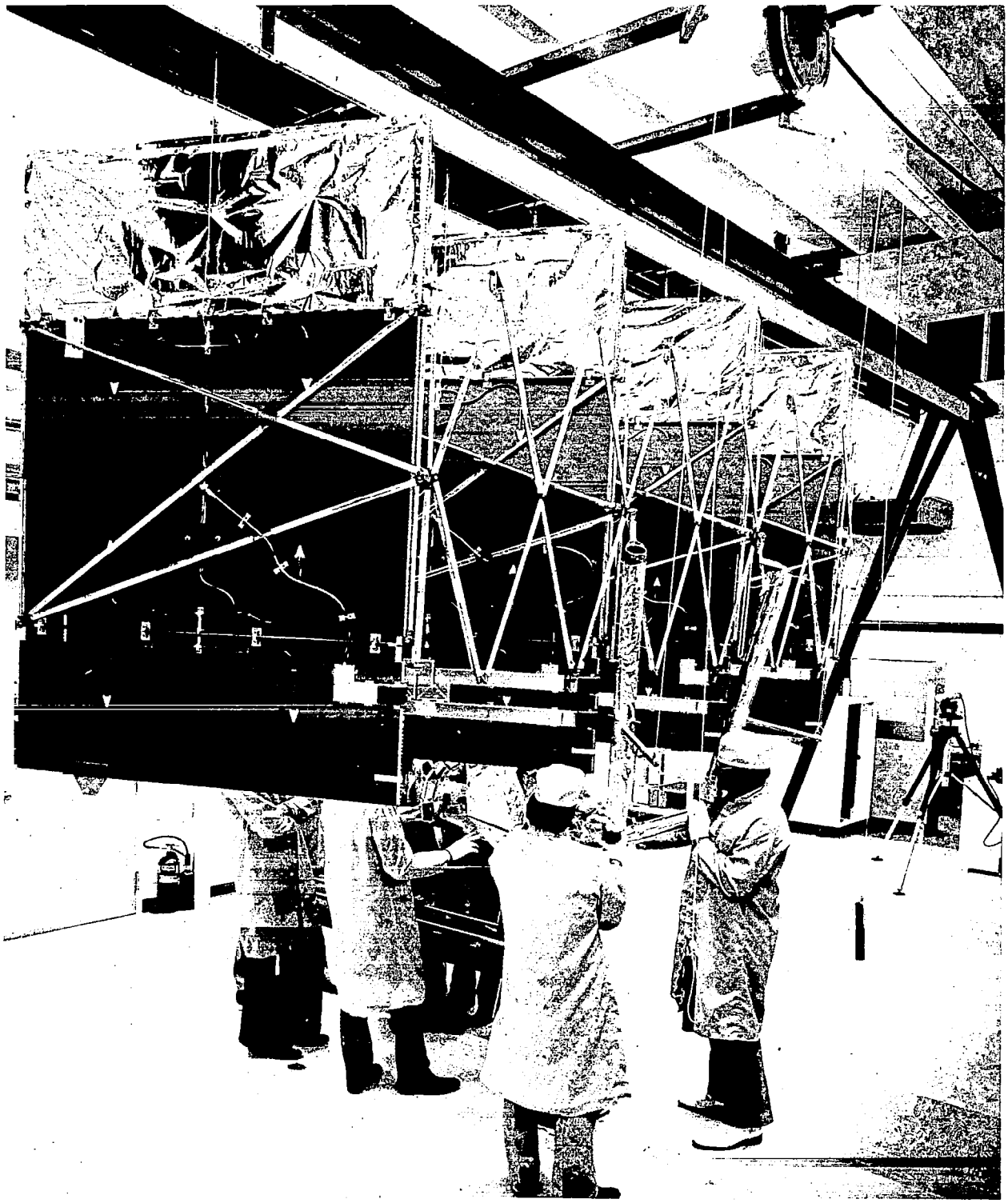

Fig. 9. SAR Partially Deployed.

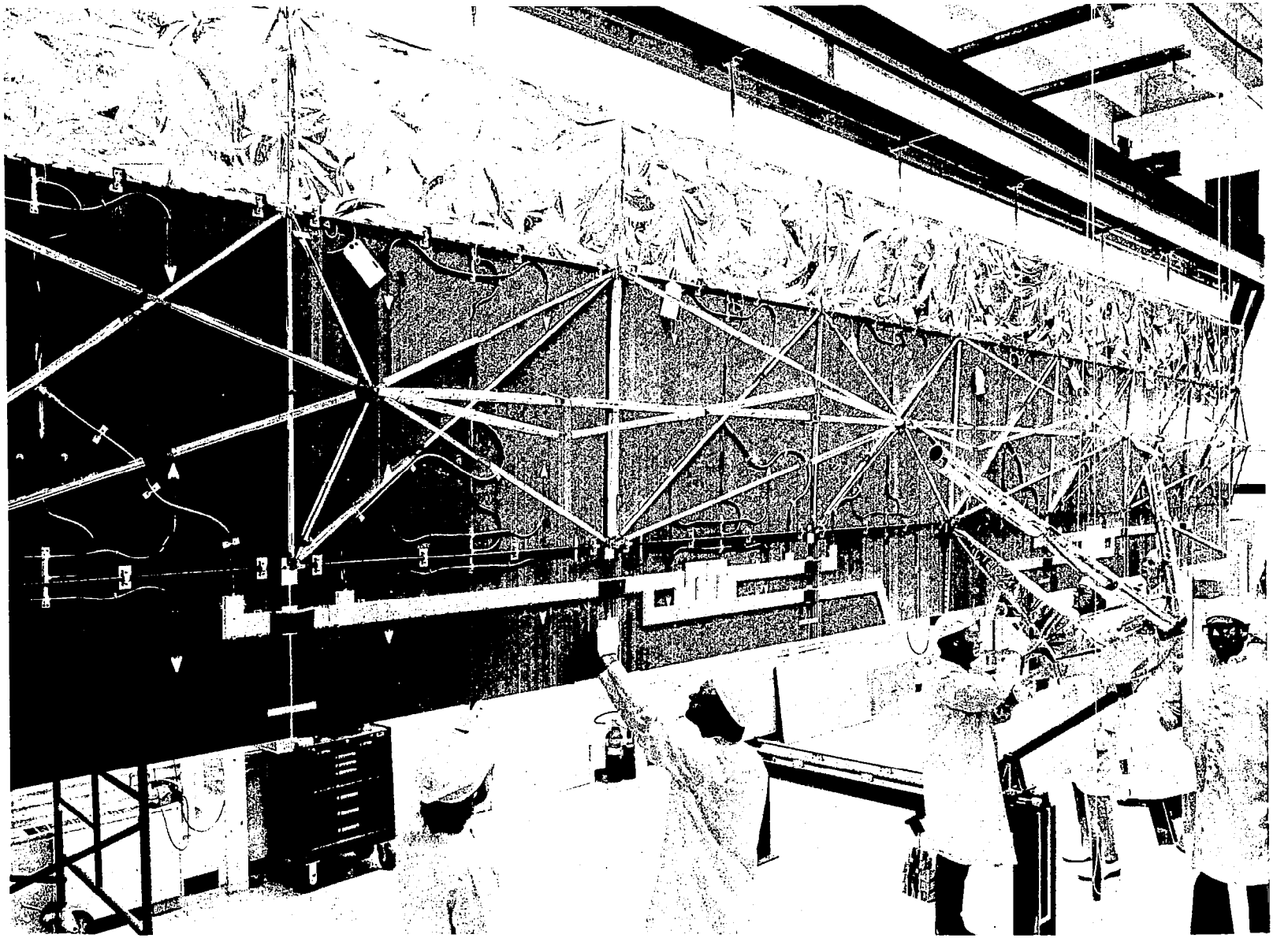

Fig. 10. SAR Deployed.

HATCH LATCH MECHANISM FOR SPACELAB SCIENTIFIC AIRLOCK

by Ir. G.R. ter Haar

Fokker-VFW Space Division

ABSTRACT

This paper describes the requirements, design trade-off, design and performance of the Spacelab scientific airlock hatch latching mechanisms.
At space side the hatch is closed and holded against internal airlock/module pressure by 12 tangential overcentre hooks driven by a drivering. At module side the hatch is holded by 4 hooks driven by rollers running on a cammed drivering. Both mechanisms behaved well in tests.

INTRODUCTION

The Spacelab Scientific Airlock (see fig. 1) will be mounted in the top of the Spacelab module as shown in figure 2. The main parts forming the airlock are:

- A 1 meter diameter and 1 meter long cylindrical shell with sealing and mounting flange
- A flat hatch on space side (Outer Hatch) with conical sealing flange, hinging as shown in fig. 2.
- A completely removable flat hatch on module side (Inner Hatch) with a flat sealing flange.
- A latticed table consisting of 3 parts moving an experiment upto 150 kg either into space or into the module. The airlock provides power and data lines to the experiment.
- Manually operated mechanical controls to move, latch, lock and interlock the various mechanisms
- Housekeeping, signals, heating, etc.

Most of above parts are rather specific for this airlock. Therefore only the more general latch mechanism for both the inner and outer hatch will be described here.

OUTER HATCH LATCHING MECHANISM

REQUIREMENTS

The main requirements which had to be fulfilled for the outer hatch latching mechanism are:

- Latching and holding of outer hatch against pressures up to 1.1. bar as limit and 2.2 bar as ultimate
- Allowable leakage over seal < 1 gram/day
- No drive failure allowed when 400 N is applied on the drive handle at any jam of the system
- Unlatching has to be performed with only 1 operation

DESIGN TRADE-OFF

To meet above requirements several design solutions have been studied. Mechanisms compressing an O-seal represent state of the art techniques, with hardly any need for qualification. However, due to the high forces needed to compress the seal, and maintain the seal compression against the airlock pressure, the mechanisms will be relatively heavy and high transmission ratios will be needed. This especially results in jamming behind the transmission becoming a considerable design case, furthermore, the feeling for a jam is negligible which might cause undesired damage. When different types of seals are used qualification of the seals is deemed to be necessary with a relatively high development risk. Sliding of the hatch over a compressed seal is impossible without a separate mechanism because of the long moment arms involved and undesirable because of increased wear.
Table 1 shows the different mechanisms studied and a summary of the main advantages and disadvantages. The tangential hook design was chosen for the outer hatch latch mechanism because of its straight forward and state of the art sealing technique,

but also its flexibility for thermal and mechanical distortions and the possibility for opening the outer hatch at relative high pressure differences.

DESCRIPTION OF CHOSEN DESIGN

The latch mechanism consists of 12 latches on overcentre cranks driven via pushrods by a drive ring at the bottom of the airlock flange as shown in fig. 3. The drivering is activated by a manually operated handle at module side driving a pinion running on a rack on the drivering. Wrong operations are prevented by interlocks. The hooks catch directly onto spherical bearings attached to the hatch. The seal flange is 60^{o} conical to keep vertical seal compression forces and variations in gap size as low as possible. The outer hatch is guided by guidepins and leveled by spring-loaded seats just above seal contact to provide proper hatch alignment. To allow for misalignments up to 1 mm in lateral directions the hooks are supported in teflon lined spherical bearings, and stabilized by two springs pushing the hook towards the hatch grippoint. During latching the latch hooks rotate forward until they touch the ball bearings on the outer hatch and then they pull the hatch downward until nominally 2 mm overcentring in the cranks is reached. At pressurization overcentring can increase until the hooks reach their individual stops in the hook brackets. Therefore the drivering position is not very critical and ample clearances can be allowed. such preventing jamming cases. Overloading of the mechanism inherent to overcentring devices is prevented by the curved shape of the hooks.

TEST RESULTS

During tests the mechanism behaved well. The characteristic force curve at the handle is shown in fig. 4. The peak value depends on seal hardness and system adjustments; at nominal adjustment and a seal hardness of 75 shore a 100 N handle load was measured
The only disadvantage of the current system is the fact that jamming behind the transmission can hardly be felt on the handle with the risk of causing damage.
Leakage was always found to be far within the 1 gram/day requirement, even with 1 hook failed. With 2 mating hooks failed an intermittent bleed-off at 600 millibars was found. Furthermore it was shown that the outer hatch can even be opened at 100 mBar

pressure difference without any chance for personnel injury, which reduces venting times tremendously. In practice opening will be allowed at about 30 mBar.

INNER HATCH LATCHING MECHANISMS

REQUIREMENTS

The main requirements which are applicable to the inner hatch latching mechanism are:

- Keeping the inner hatch in place and providing initial sealing against shell until module pressure seals the hatch firmly against seal and shell flange when the airlock is evacuated.
- Keeping inner hatch in place at repressurization, but allowing bleed-off when pressure difference airlock/module exceeds 30 mBar and preventing a pressure difference above 80 mBar at maximum supply (5 grams/sec).
- At release under zero G the latches shall free the hatch without the possibility that the hatch starts flying around.
- At release under 1G conditions the latches shall retain the 18 kg hatch
- Release shall be effected by a single operation

DESIGN TRADE-OFF

To obtain initial sealing at least 4 hooks are required to keep the hatch edge member within reasonable dimensions. A single release operation can only be obtained when the 4 hooks are interconnected by a drive ring. Because of the relative low loads required during latching a cam roller design was chosen because of its simplicity and resulting low mass.

DESIGN DESCRIPTION

Fig. 5 shows the current design for the latch mechanism. The hooks have a roller, fitting in the hatch rim and enabling mounting of the hatch in every rotational position. The rollers which are running, springloaded downwards, on a cam of the drivering, move the hooks up and down. The hooks are guided by the two side-walls of the brackets and two guiding pins in a slot on the hooks. During release the hooks move downwards on the cam until the guide pins touch the end of slot, which starts rotation of the hooks away from the hatch. However, under 1 g conditions the hatch mass keeps the hookroller in the rim until the hatch is slightly lifted. In space the hooks only rotate so far away that some force is needed to pull the hatch out of the hookrollers. The best method of replacing the hatch is to push the hatch through the rollers onto its seat. Under 1g conditions the hatch has to be hooked in into the rollers to avoid drop down. When latching, the hooks first move inwards and then upwards, giving enough pretension in the seal to obtain initial sealing.
The tubular drivering, running all the way around the cylinder and supported by rollers, is driven by a crank handle system. Its rotational accuracy is kept to a minimum by a flat upper surface of the cam. Overloading of the system is prevented by the curved shape of the hook.

TEST RESULTS

During tests the mechanism behaved well. However, on some points minor deviations were found:

- At airlock overpressure bleed off via the hatch sealing did not occur at the required 30 mBar but already at 20 mBar. It seemed possible to meet the 30 mBar requirement by change of adjustments, however, then the required handle forces became too high.
- When, under 1g conditions, release is performed too quickly, the hatch might drop down due to slight sticking effects of the hatch to the seal, which allow the hooks to swing out during the unlatching operation
- Sometimes the hookrollers remained at the edge of the rim of the hatch, which might cause high hookstresses when the airlock has some overpressure.

CONCLUSIONS

Both latching mechanisms described here were tested on detail models and recently on the first airlock model. Their functioning has proven to fulfill the requirements. In a few months time qualification of the mechanisms will be performed on the airlock qualification model.

REFERENCE

"Functional description of Scientific Airlock"
Spacelab Program Technical Report TN-FO-11-063-77 d.d. 19-09-77
Authors : Benes/ter Haar/Setz

Some copies will be available during the presentation.

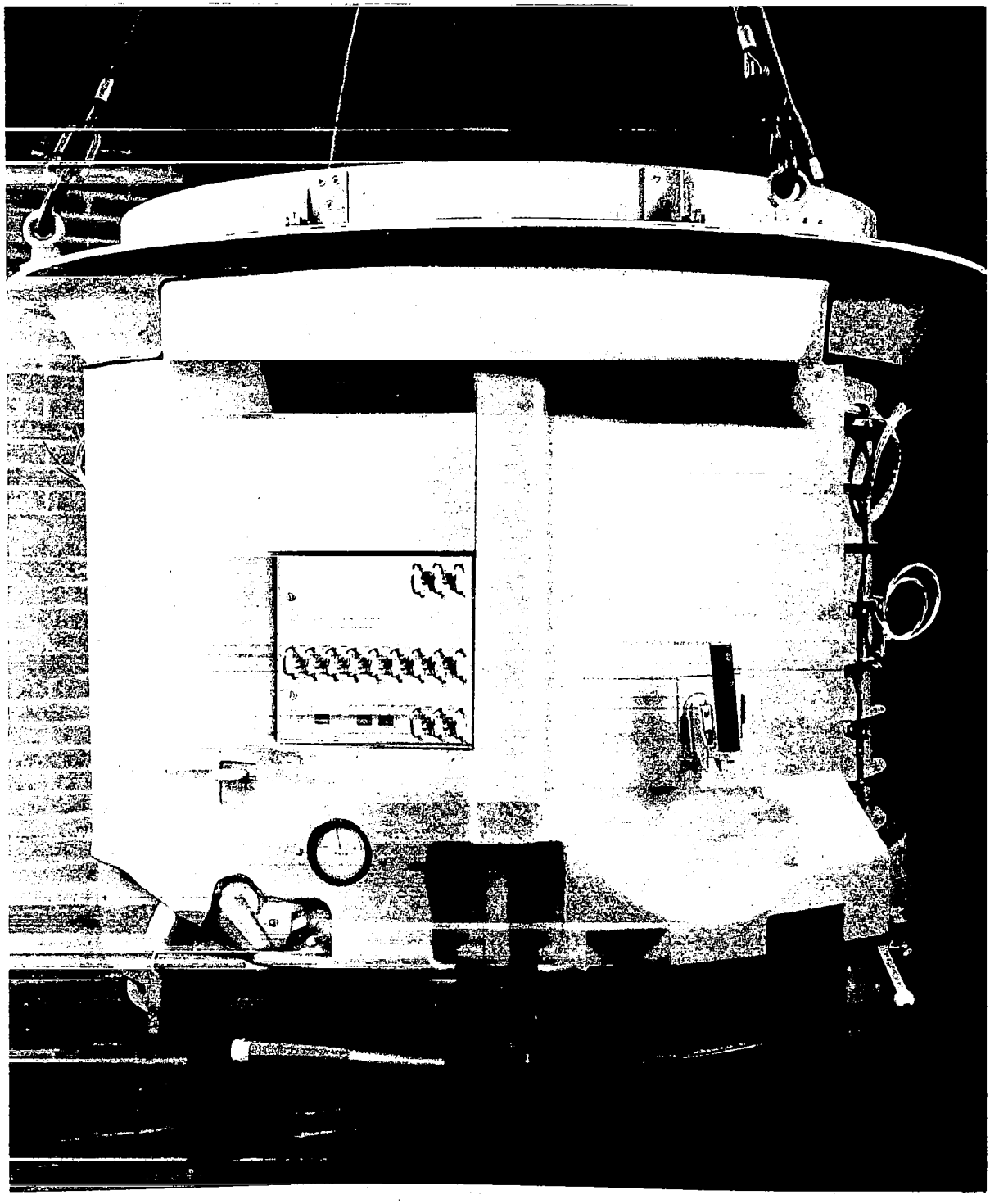

Fig. 1. Hard Mock-up model of Spacelab Scientific Airlock

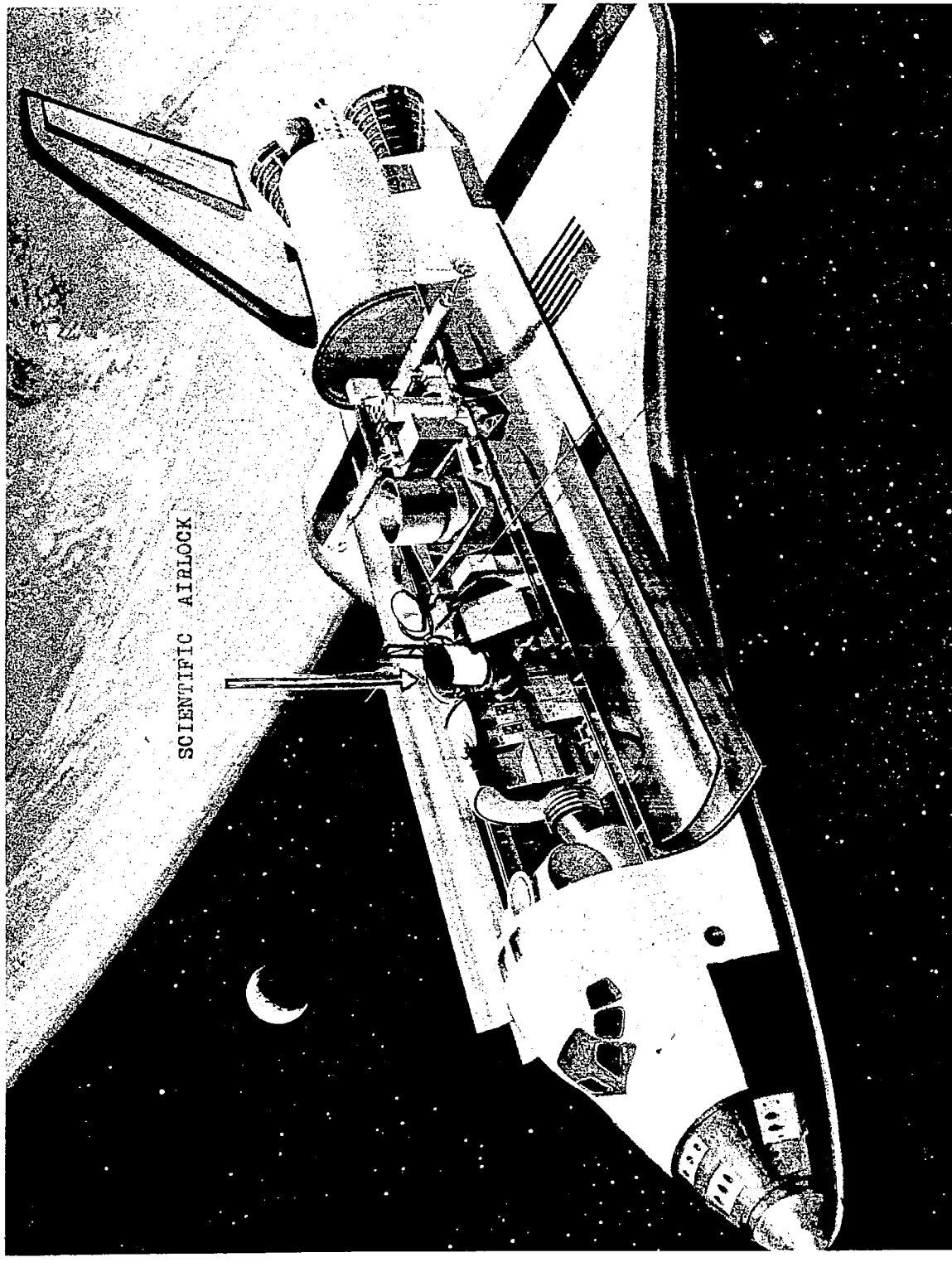

Fig. 2. Scientific Airlock mounted in Spacelab

	Type of mechanism	Characteristics
MECHANICALLY COMPRESSED SEALS	1. Tangential hooks 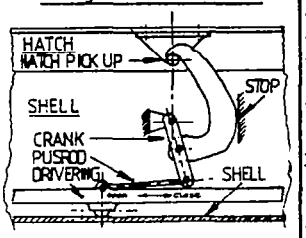	Main advantages: - Short load path - Simple adjustability - Relative long travel allowing great mechanical and thermal distortions - Controlled unlatching at internal over-pressure Main disadvantages: - Many parts causing high weight - Seal compression requires high strength - No feeling for jams
	2. Radial hooks 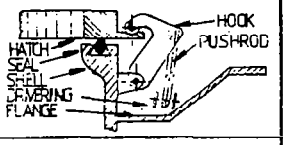	As 1. Additional disadvantages: - Critical lateral hatch positioning - Difficult shape hatch rim - Roller cold welding - Critical for mechanical and thermal distortions of hatch
	3. Marman clamp principle 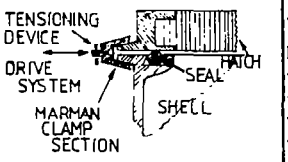	Main advantages: - Slight weight reduction possible w.r.t. 1 - Direct load path - Simple design Disadvantages: - Well known operational problems - Many possible coldwelding areas - Reliability clamp release - Complex drive - Opening at higher ΔP questionable
	4. Cam-roller system 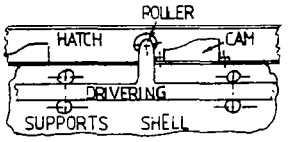	As 1. Additional disadvantages: - System cannot apply high compression loads so alternative sealing technqiue required - Very sensitive for debris - Required accuracy and similarity of cams - Loose of function at jam of 1 roller - Coldwelding problems
PRESS. COMPR. SEALS	5. Pressure cooker principle 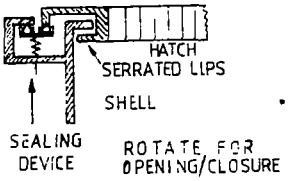	Main advantages: - Relative high weight reduction possible w.r.t. 1 to 4 - Simple design - Direct structural load support Main disadvantages: - Drive power required to slide over seal → soft seal design - Alignment sealing - Redundancy sealing - Qualification sealing technique - No unlatching possible at overpressures
	6. "Sliding" lip 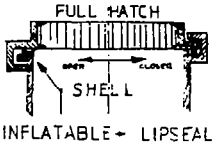	As 5. Additionally: - Sealing design (inflatable seal + lipseal) requires additional pressure system - Sealing design needs development and qualification

Table 1 Design trade-off Outer Hatch latching mechanism

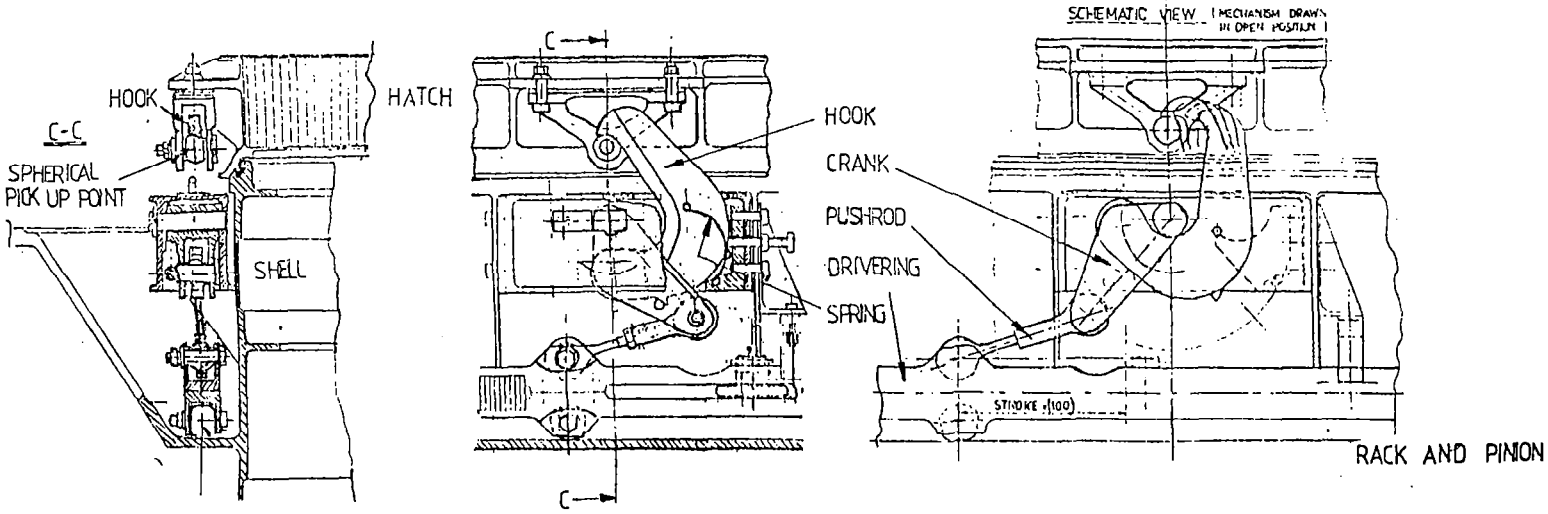

FIGURE 3 **Outer hatch latch mechanism**

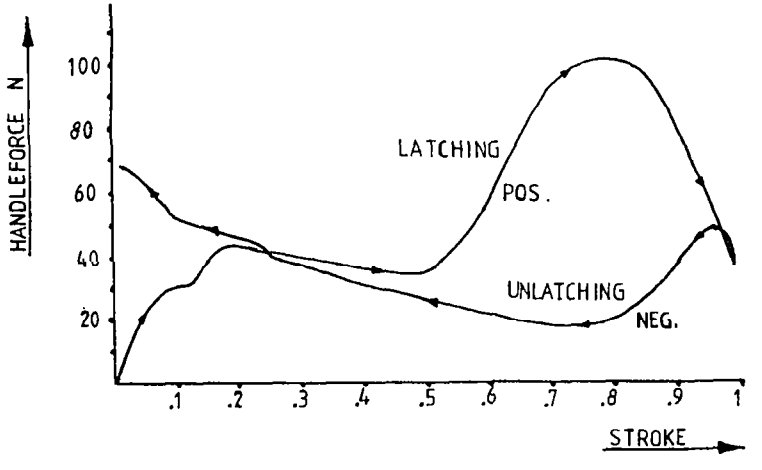

FIGURE 4 **Operational force curve**

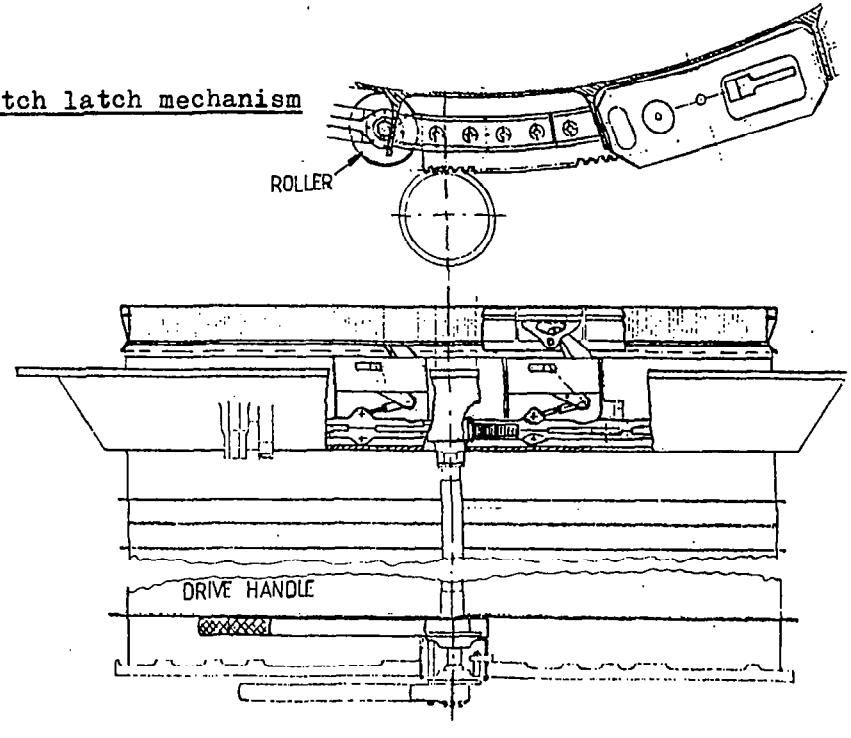

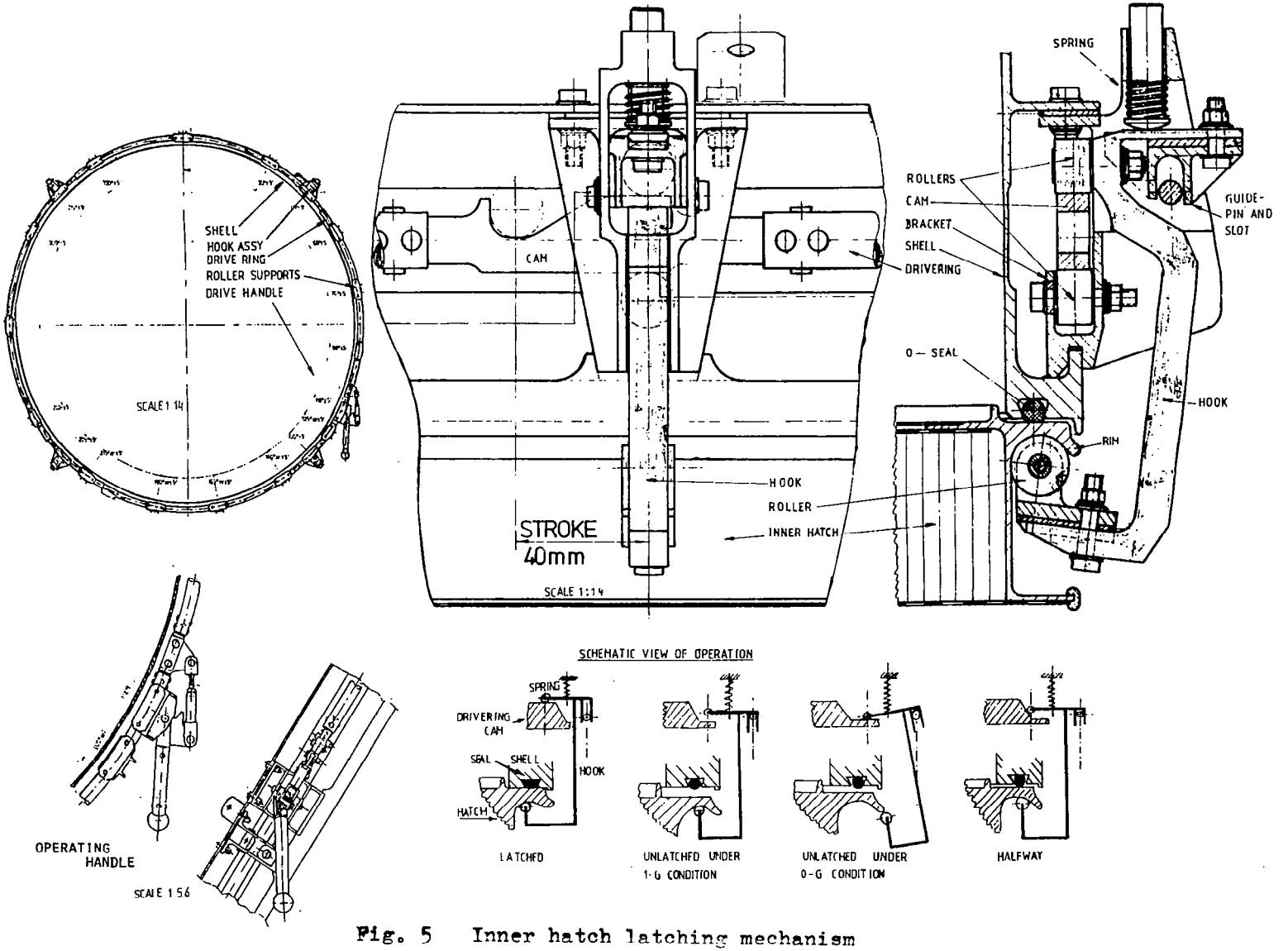

Fig. 5 Inner hatch latching mechanism

DESIGN FEATURES OF SELECTED MECHANISMS DEVELOPED FOR USE IN SPACELAB

by Dipl. - Ing. W. Inden

ERNO Raumfahrtechnik Gmbh
Hunfeldstrasse 1-5
2800 BREMEN, West Germany.

ABSTRACT

The paper introduces the Spacelab and selected mechanisms developed for this program. It addresses a typical interface of a flight hardware to mechanical ground support equipment. Then one of the most attractive MGSE mechanism, the "roller rail", is described being used to install/remove the Spacelab floor loaded with racks carrying experiments. The details of the design and criteria are explained.

The next two mechanisms are related to the astronaut crew operations. The foot restraint is a special Spacelab development allowing the use of Orbiter common suction cap shoes. The design requirements as well as the design features are presented. The last element is the Lithiumhydroxide canister. In view of the multiple usage on orbit simplicity was the prime driver.

INTRODUCTION

Spacelab (Fig. 1), Europe's contribution to the Shuttle Program, stimulated the design of a number of mechanisms departing from standard industrial engineering design.

Depending on the usage, on ground or in space, different design drivers became predominant, although low cost, low mass, easy and safe operation are common requirements to all of them.

One of the most sophisticated mechanism assemblies of Spacelab is the Scientific Airlock and is therefore discussed in a separate paper.

This paper explains the design features of other elements selected against the following considerations:

- Related to the modularity of the Spacelab concept
- Astronaut operations

The MGSE to Spacelab Interface, as well as the "roll-in roll-out" concept for the quick replacement of payloads mounted in rack/floor assemblies of the habitable area of Spacelab, belong into the first category. Typical for the second one is the foot restraint mechanism in combination with handrails and the lithiumhydroxyde canister replacement on orbit.

SYMBOLS / ACRONYMS

SL	Spacelab
MGSE	Mechanical Ground Support Equipment
LIOH	Lithiumhydroxyde
mm	Millimeter(s)
Kg	Kilogram(s)
m	Meter(s)
g	Earth Gravity
N	Newton(s)
s	Second(s)

THE SPACELAB TO MGSE INTERFACE

One of the prime interfaces is the support of the entire Spacelab. In order to avoid degrading/damage of the Spacelab to Orbiter interface, a different interface was selected for MGSE. The MGSE to Pallet interface is essentially conventional with a statically determinant fixation. The Module interface on the other hand is statically indeterminant.

Figure 2 shows the integrated pallet on the assembly stand and Fig. 3 the details "1" and "4". Support "1" is a bearing which allows presetting in all directions. The support strut "2" allows movement in lateral direction and strut "3" gives the freedom in axial direction. Detail "4" shows the support frame bolted to the pallet. This MGSE had to accommodate quite important tolerances and deflections resulting from the pallet.

The tolerances between two trunnions (item 5) in axial direction, (vertical to the plane shown in Figure 2), for a three pallet train (three pallets bolted together) are

$\pm$ 13mm pallet manufacturing

+ 9mm) for thermal distortion
- 5mm) (-10° to $+ 55^{\circ}$C)

$\pm$ 4mm MGSE manufacturing

resulting in + 26 / - 22mm tolerance range.

THE "ROLL-IN" - "ROLL-OUT" CONCEPT OF THE RACK/ FLOOR ASSEMBLIES

The concept was conceived to allow fast removal and installation of SL payloads installed in racks or on the floor as illustrated in Fig. 4. Initially (1973) standard aircraft design was looked at but turned out not to be useable mainly because of

- the multiple/heavy fixation points required to accommodate a great number of possible rack locations
- high mass of the roller assembly (about 60Kg/m on each side)
- considerable reinforcement of rack structures violating the minimum mass criterion

incompatibility of plastic materials or lubricants with the stringent requirements concerning outgassing and flammability of parts and materials.

Therefore new design solutions were developed without losing the feature of fast ground operation.

Figure 5 shows the rack/floor assembly mounted on the MGSE stand.

An MGSE rail (see Fig. 5, 7) is inserted in between the primary structure and the floor. Then the floor and rack attachment bolts are removed and the rolls moved up. The clearance between the racks and primary structure is such that the rack/floor assembly can be rolled out on the MGSE stand.

The concept of the removable non flyable roll device allowed a decoupling of "1g" operations with its negligible load conditions from the flight load condition seen by Spacelab during ascent/descent. The design driver in the latter case is the crash landing within a 20° half cone angle in flight direction with 9,0 g's.

Thus low mass and lower costs could be achieved than making the typical aircraft design work for Spacelab. In addition, this solution avoided the anticipated problems of tolerances and additional loads due to deflections.

The design of the roller rail assembly (Fig. 7) represents sophisticated engineering concept driven by extraordinary design requirements. These resulted from the philosophy - less complexity on the flight articel but on the MGSE where mass is not a driver.

The nominal design load was 7,5 tons for the long experiment rack/floor assembly of 4,4m. The safety factor of 2 was applied for limit load.

Specific difficulties resulted out of the Module floor displacements schematically shown in figure 6.

In addition a lateral tolerance of $\pm$ 3mm of the mainfloor had to be compensated. Figure 7 illustrates the main features of the roller rail assembly:

- vertical movement of upto 12mm by Rollers "1" together with the upper housing "2", lifting the rack/floor assembly sitting on this plate. This is achieved by spreading the levers "3". Since these elements are arranged in a mirror fashion, no movement in axial direction occurs (requirement from flight hardware). The activation of the levers "3" is achieved by a remotely operated spindle "4", operated by a worm gear.

- For installation/removal of the unladen roller rail assemblies, the bottom rollers (7) are used, they will be retracted when moving the rack and floor assembly.

- lateral track misalignment compensation by means of springloaded rollers 5.

- compensation of lateral mainfloor tolerances (between roller rail assembly and Module primary structure) by means of adjustable eccentrically driven rollers (see detail "6").

- the axial movement of rack and floor assembly is achieved by a driving mechanism using a tooth gear "8" along the roller rail assembly in combination with a driving trolley manually operated.

The capabilities of the design have already been demonstrated through successful usage during Spacelab Engineering Model System Integration.

ASTRONAUT FOOT RESTRAINTS

The design features developed for Skylab were considered in the initial design phase but could not be used because the mainfloor could not be made from triangular grid structure (structural and noise reasons). This lead to the "suction cap shoes" used on the flat surfaces of honeycomb panels.

Due to the severe mass constraints and the multiple location requirements, a versatile design concept was found using the handrails as attachment, see Figure 8.

The specific design requirements are

- rotable in 15^{o} increments
- fully adjustable along double rack handrails and aft end cone handrails
- loads:
  - 589N each direction
  - torsion moment normal to attachment plane: 200Nm
  - kick loads: 9 Kgm/s at a max. velocity of 1,5m/s

The kick load requirement is being verified by a drop test of 6Kg with a 5mm radius point from a height of 100mm.

The design has passed the qualification program successfully. Flight unit production drawings are almost ready.

LIOH STORAGE CONTAINERS

LIOH is used for decontaminating the air exhausted by the crew. The cartridges are identical to those used in the Shuttle Orbiter but the containers are different.

One of the main considerations of the storage containers design was the location of the cartridges. The replacement of the cartridges in use by the environmental control and life support system (in the sub-floor area) had to be optimised for easy crew operation on orbit. Figure 9 shows study details of the crew systems analysis and Figure 10 further details of the cartridge container design, where simplicity was the main driver.

The design has passed its qualification successfully. Flight unit production drawings are in final preparation.

REFERENCES

1. Spacelab Critical Design Review data package 1978

2. Spacelab System Support Specification SR-ER-0008

3. SENER drawing 612.011 0301.000.03

4. Unger, Burnell:

   TN-ER-37-005-76 Verification of Work-bench and Central Console Architecture, incorporating foot restraint utilization.

5. T. Ward, U. Munkelt:

   TN-ER-37-004-76 LIOH Task Analysis.

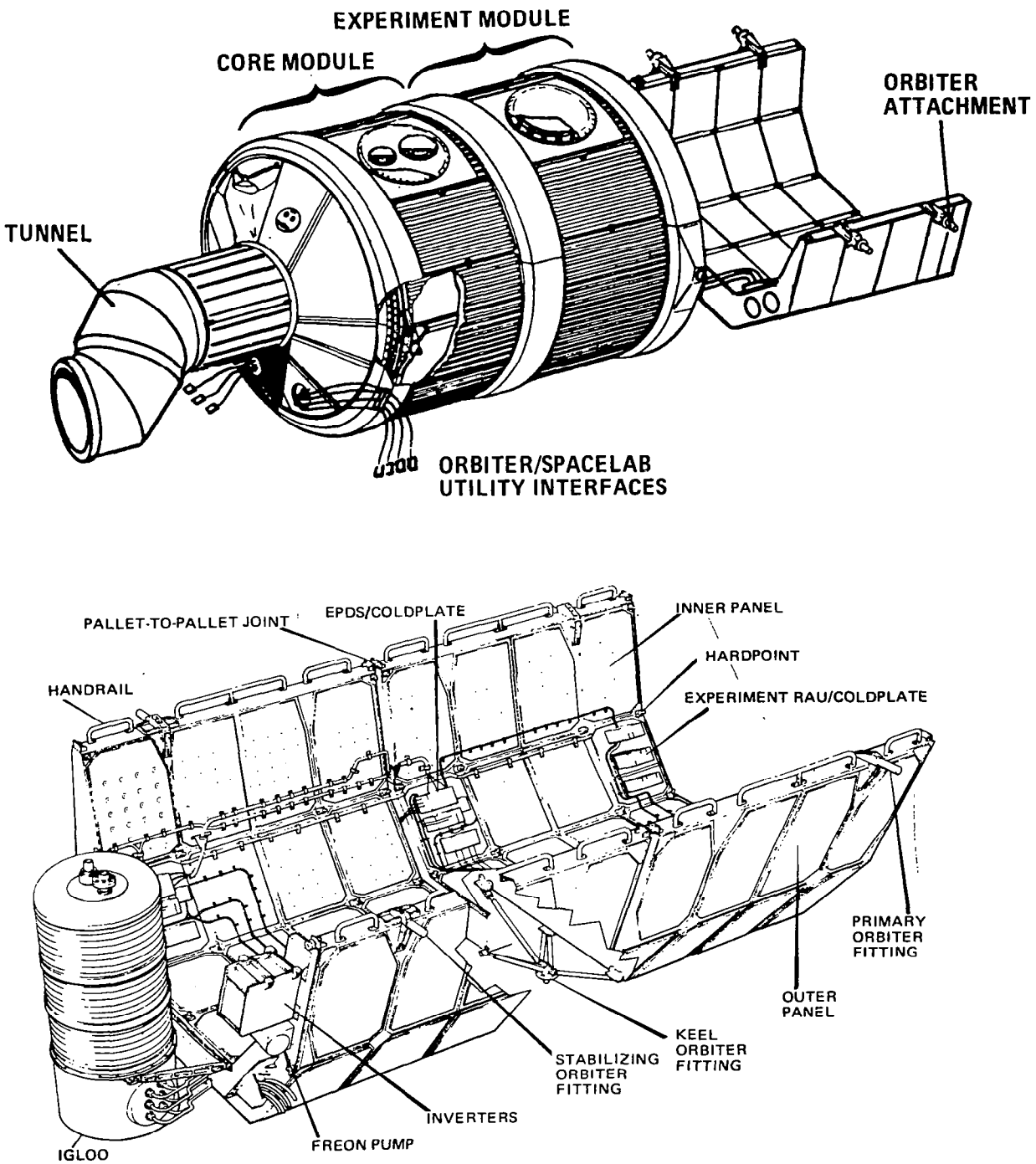

FIG. 1 SPACELAB CONFIGURATIONS

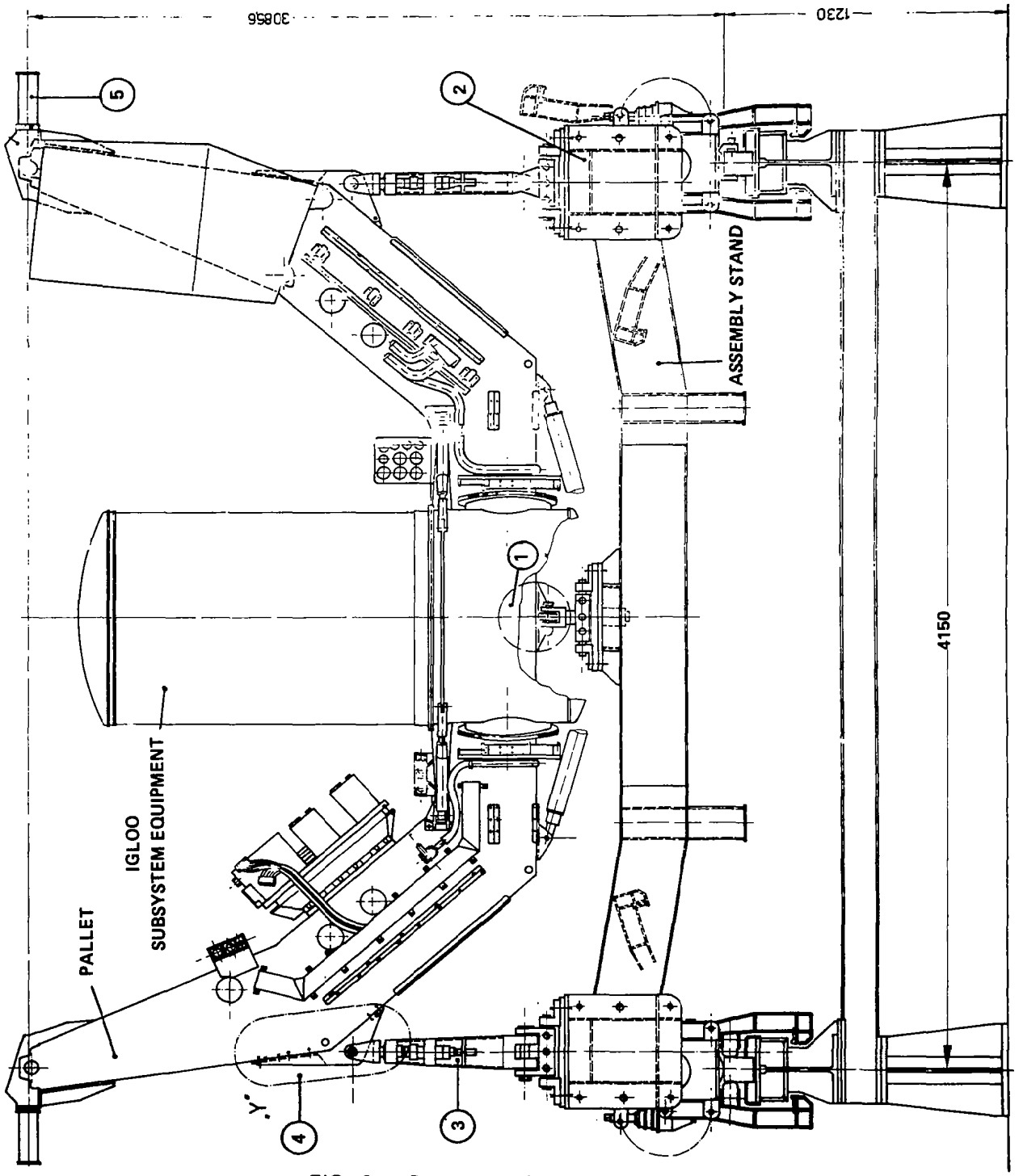

FIG. 2 PALLET & IGLOO CONFIGURATION ON THE ASSEMBLY STAND

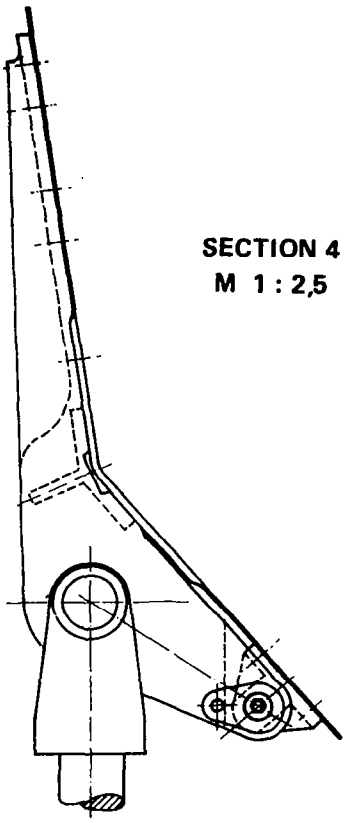

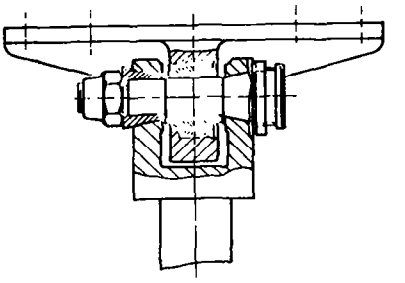

FIG. 3 DETAILS 1 AND 4 OF PALLET SUPPORT MGSE

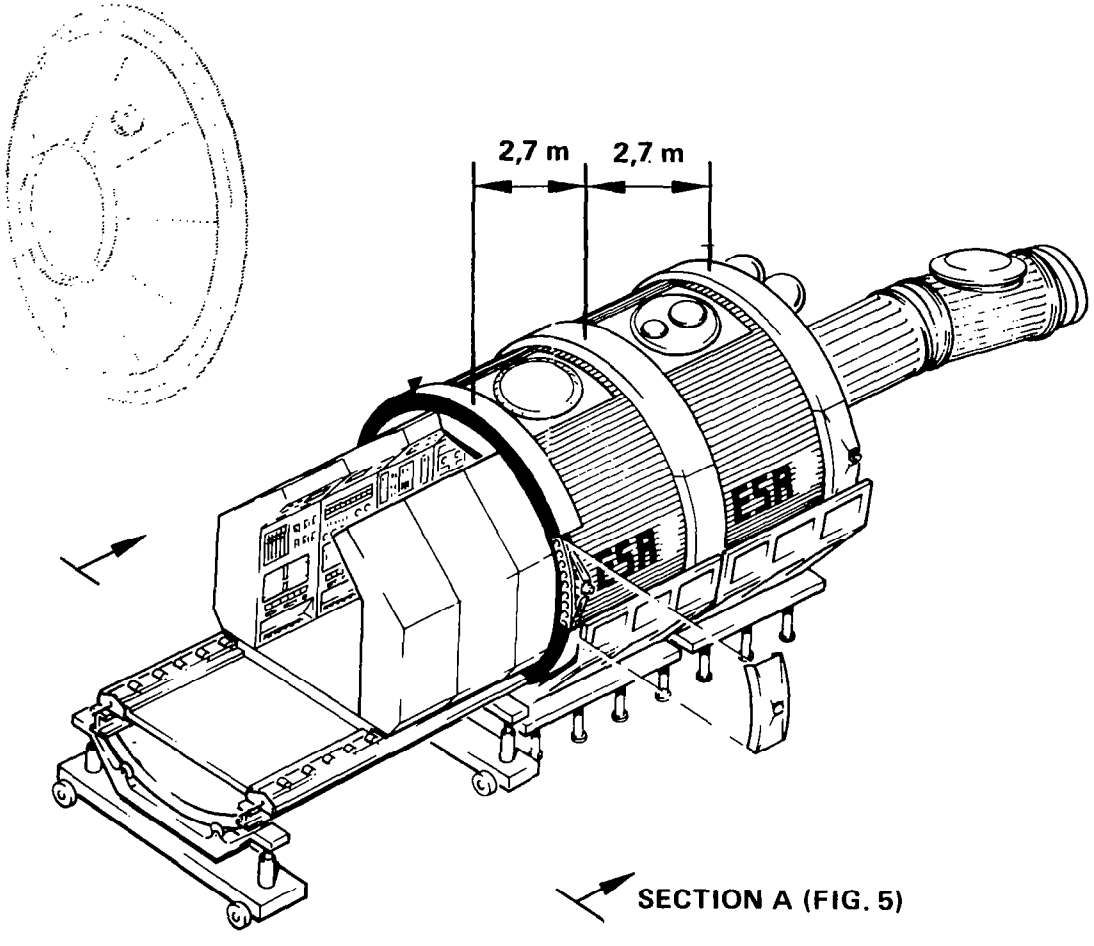

FIG. 4 "ROLL–IN – ROLL–OUT" CONCEPT FOR SPACELAB RACK/FLOOR ASSEMBLIES

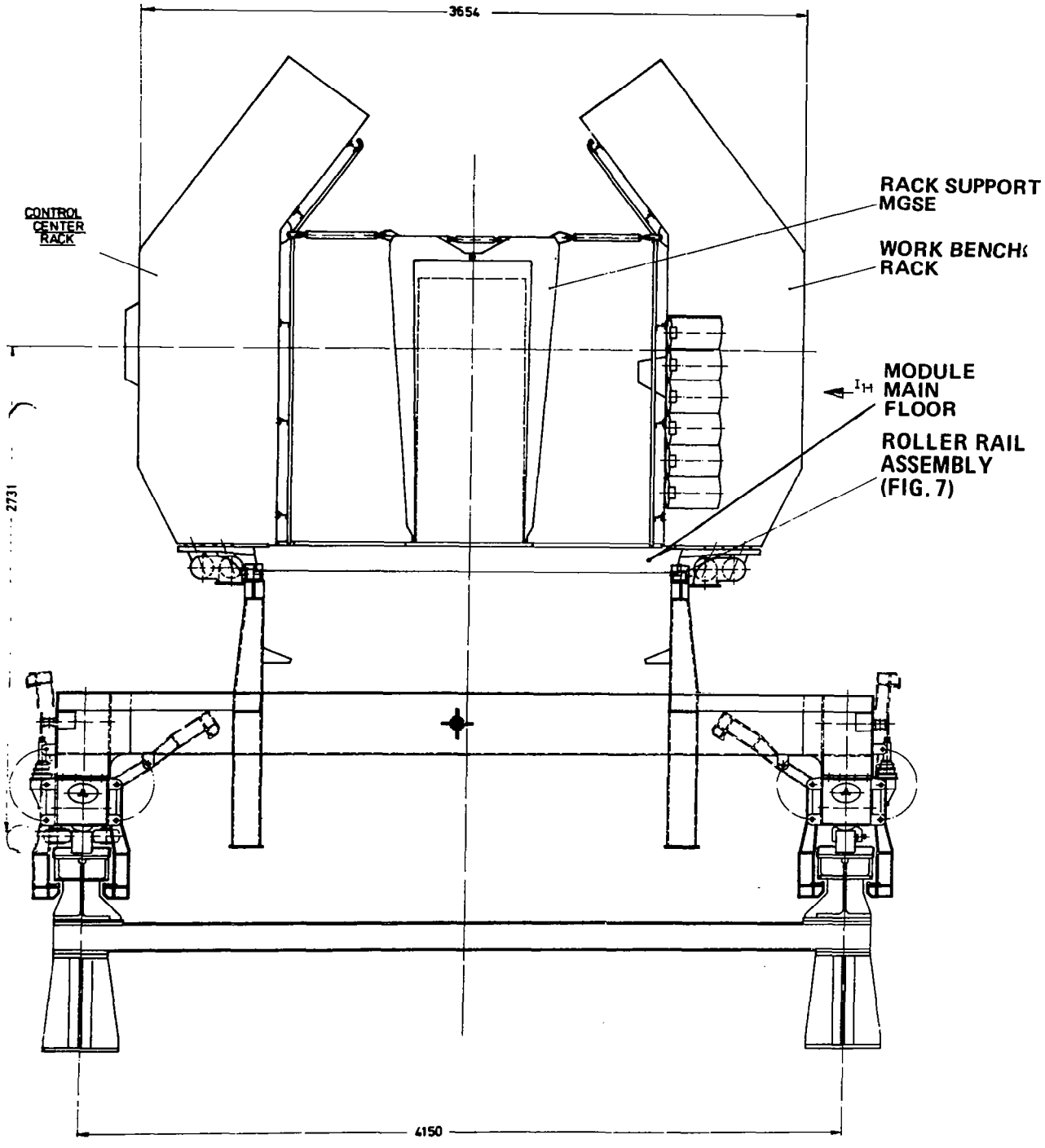

FIG. 5
RACK AND FLOOR ASSEMBLY AND STAND
(SECTION A OF FIG. 4)

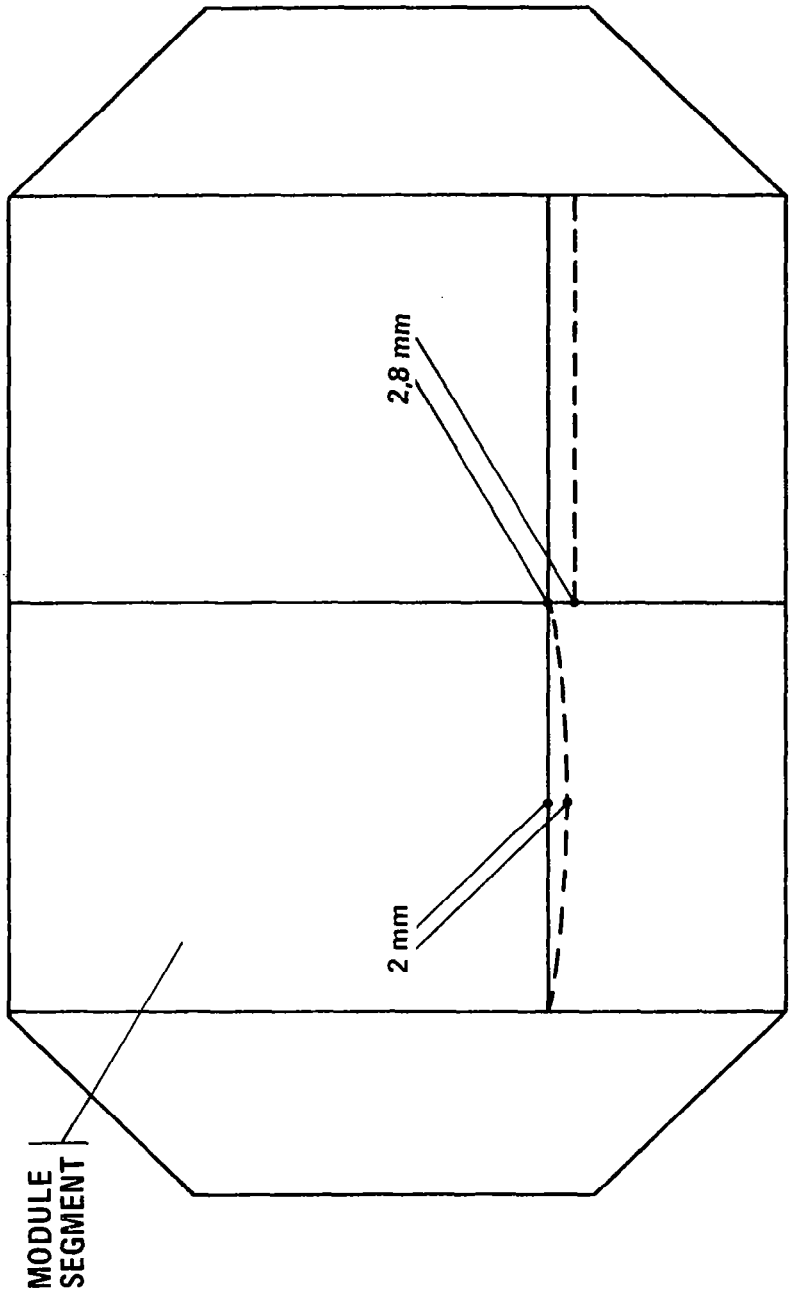

FIG. 6 MAINFLOOR DISPLACEMENTS TO BE COMPERATED BY ROLLER RAIL MGSE

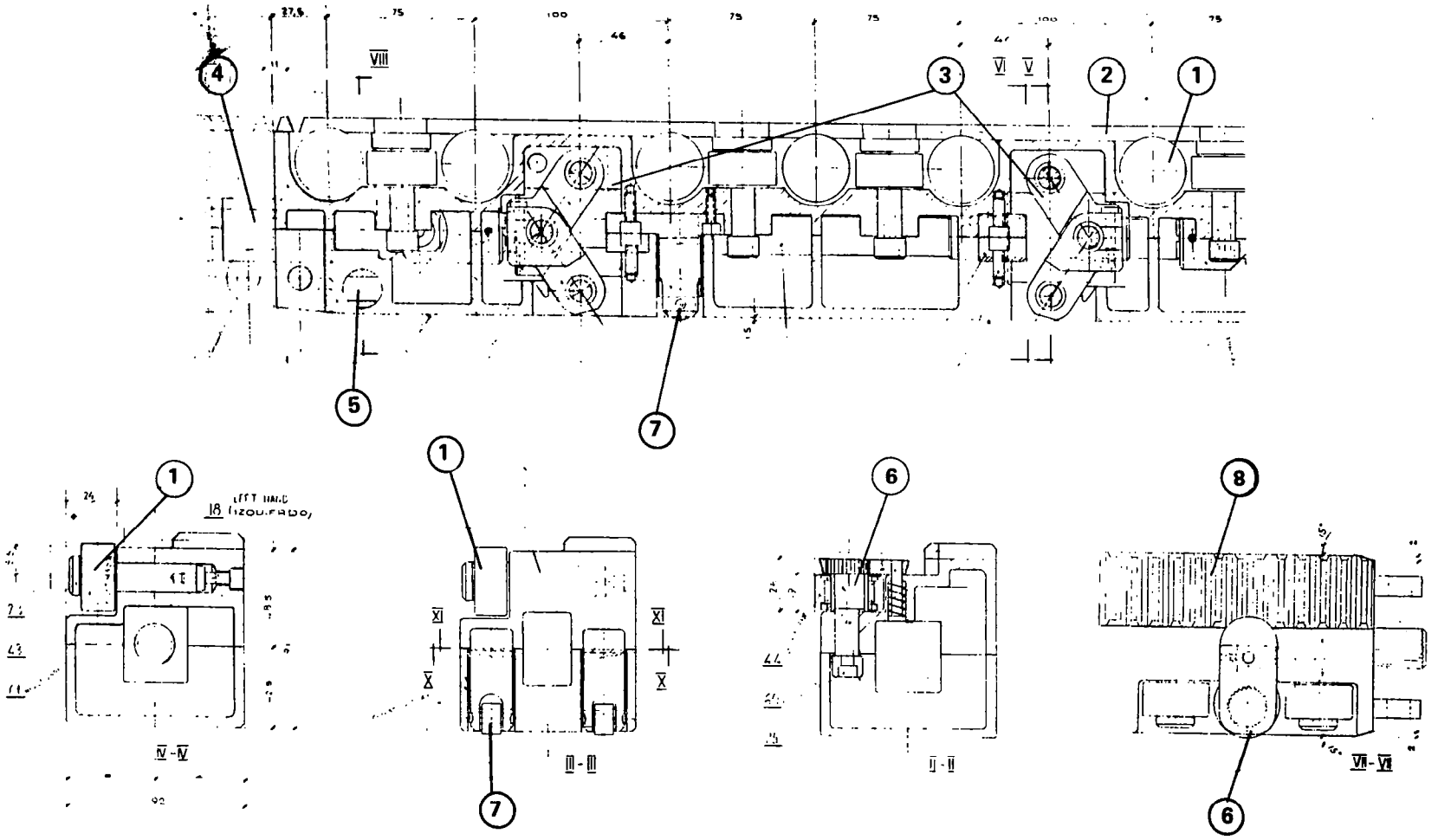

FIG. 7 ROLLER RAIL ASSEMBLY AND VARIOUS SECTION VIEWS

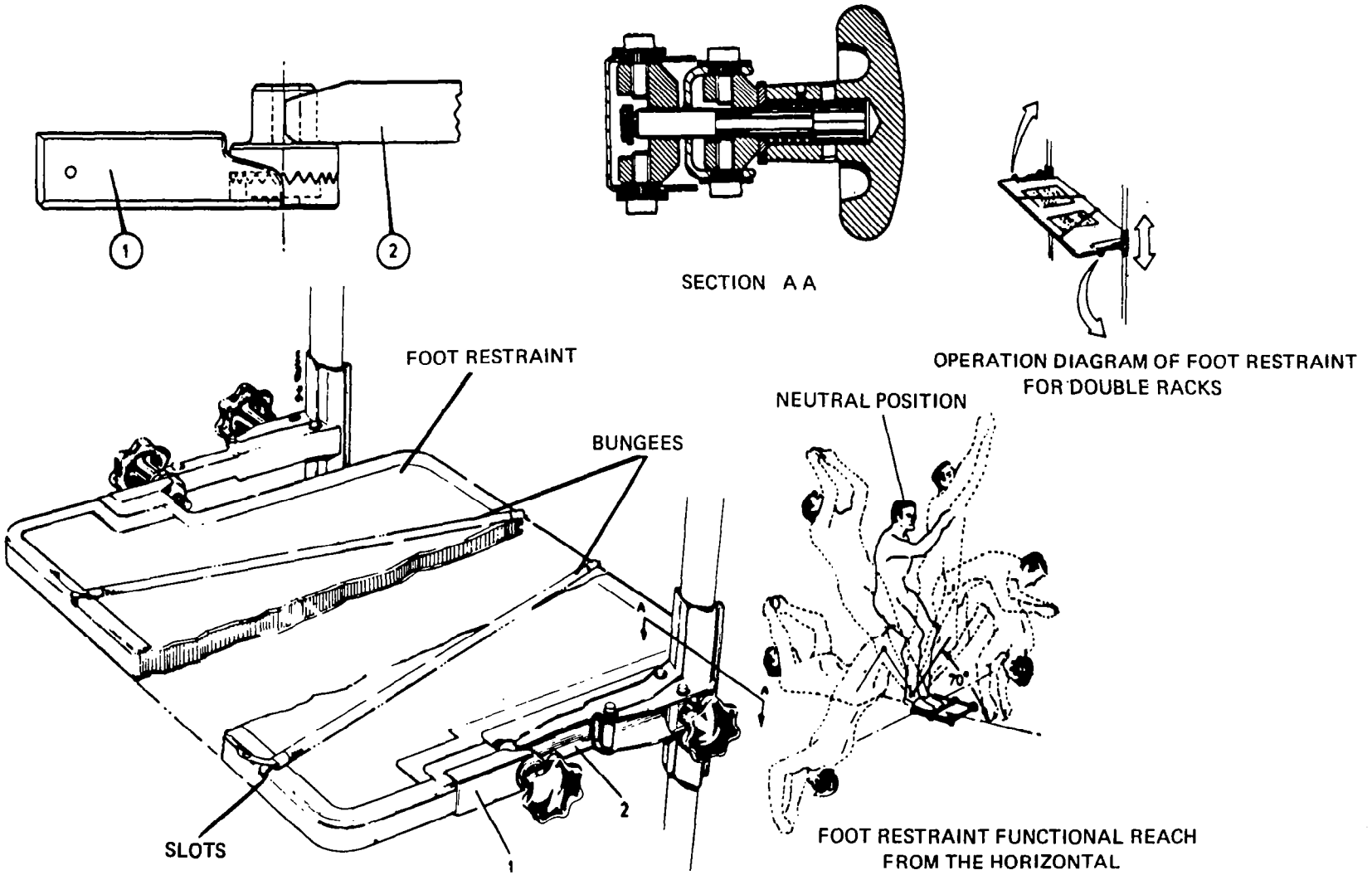

FIG. 8 DOUBLE RACK FOOT RESTRAINT WITH TEMPORARY RESTRAINT

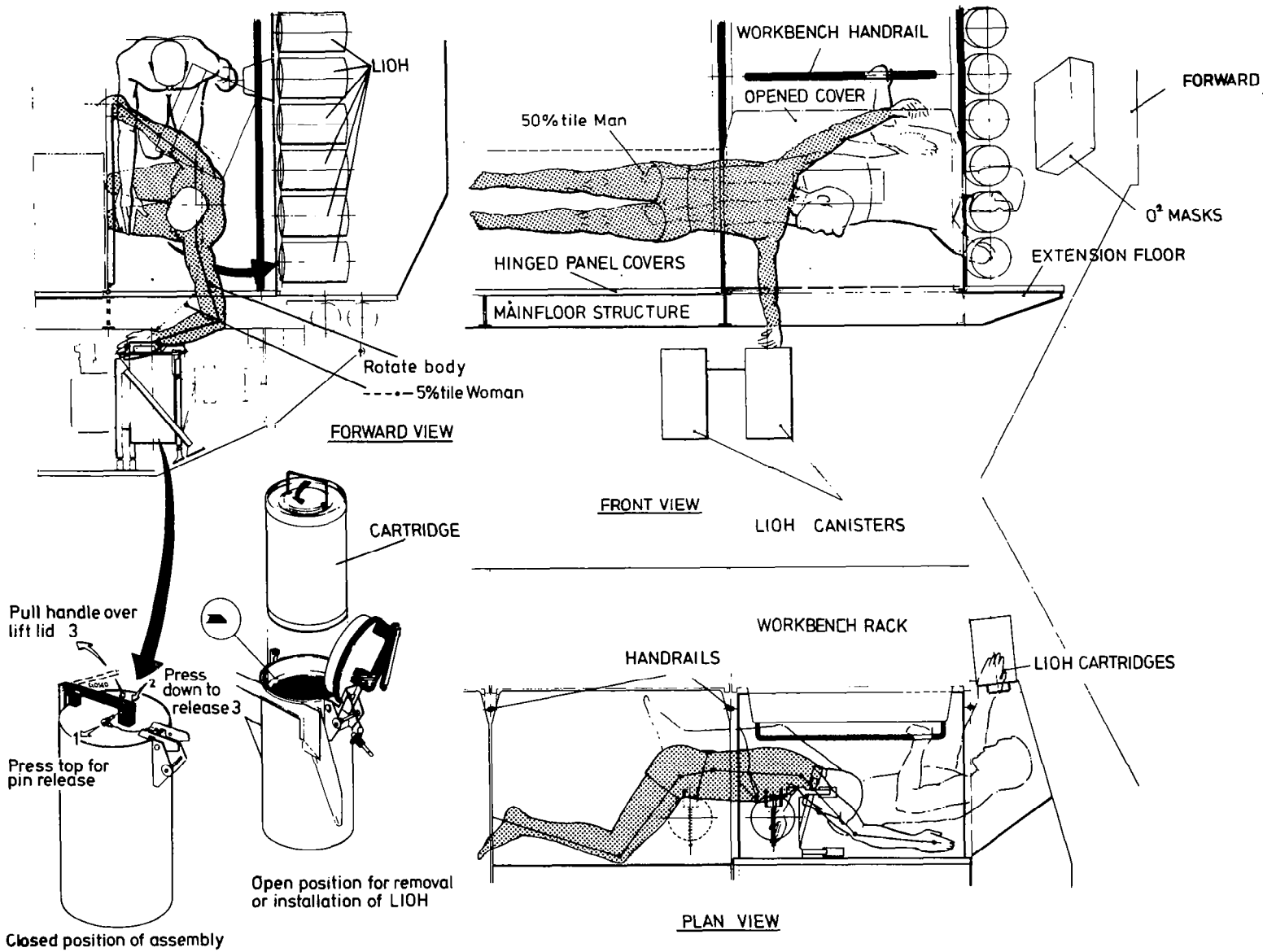

FIG. 9 LIOH OPERATION AND REMOVAL

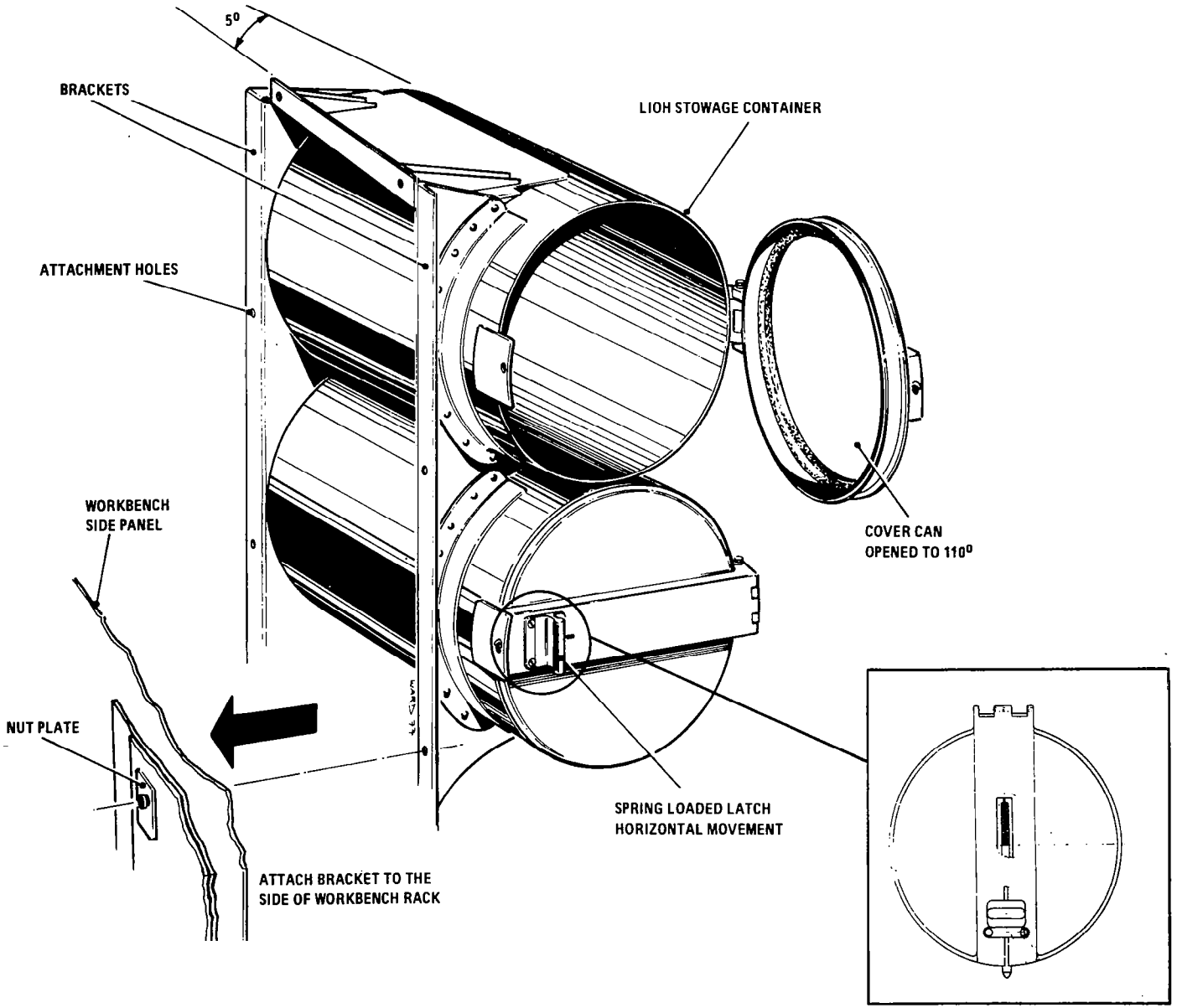

FIG. 10 STOWAGE OF THE LIOH CARTRIDGES

THE DESIGN AND TESTING OF A MEMORY METAL ACTUATED BOOM RELEASE MECHANISM

by

D.G. Powley : British Aircraft Corporation Ltd.
G.B. Brook : Fulmer Research Institute Ltd.

ABSTRACT

Shape memory metals are used commercially in a number of gripping mechanisms such as tube connectors. A boom latch and release mechanism has been designed, manufactured and tested, based on a specification for the ISEE-B satellite mechanism in order to demonstrate and gain experience of shape memory alloys to do useful work by operating a useful mechanism.

From experimental results obtained, it is now possible to calculate the energy available and the operating torques which can be achieved from a torsional shape memory element in terms of the reversible strain induced by prior working. Some guidelines to be followed when designing mechanisms actuated by shape memory elements are included.

INTRODUCTION

Shape memory metals can be deformed into a new shape below a critical transformation temperature. On heating above this temperature the shape changes back to the original shape. If this change of shape on reheating is restrained, the shape memory alloy can be used to generate a force capable of doing work or of gripping a rigid body. The work done can provide the primary energy in a mechanism or activate the released energy stored in another way e.g. by a spring.

This mechanism is designed to enable three hinge booms to be latched for launch, and deployed by the spinning satellite once it is in orbit (Figure I). It utilizes the recovery of a nickel-titanium alloy torsion element to effect the high speed release of two spring laoded ball bolts. These release two of the booms, the mechanism itself remaining attached to the third boom when deployed.

In order to understand the reasons for the design of the mechanism, it is necessary to look at some of the properties of memory metals.

PHYSICAL PROPERTIES OF MEMORY METALS

The specific alloy used for this application is a solid solution based on the intermetallic compound TiNi, using a composition exhibiting a martensitic transformation close to ambient temperature.

In its high temperature state, TiNi demonstrates high strength and ductility, impact resistance and high creep and fatigue resistance. As the temperature is lowered through the Ms temperature (that at which the martensitic transformation begins on cooling with zero stress) a stress induced plasticity can be obtained at progressively lower stresses until at the Ms temperature, stresses as low as 27 MNm^{-2} (4000 p.s.i.) are sufficient to cause deformation (Figure 2). On release of the stress, at temperatures above the Ms temperature, all or substantially all of the stress induced strain is recovered in an apparently elastic manner.

On deformation below the martensitic transformation temperature, Ms, only part of the stress induced strain is recovered on unloading (Figure 3, upper region). However, if the material is heated above the temperature at which the reverse transformation takes placed, (As temperature) the high temperature structure is progressively reformed, the apparently plastic strain is reversed and the original shape restored (Figure 3, lower region). Thus the shape memory material can be put into the required shape at a high temperature and retained in such a state during cooling to a lower temperature, (below the Ms temperature in the absence of an applied stress). It can then be deformed to a new shape at the low temperature. On reheating above the As temperature, the material recovers to its original shape, or if the change in shape is restrained, will exert a force up to the yield stress of the material at that temperature. If the alloy is then cooled again it will normally retain that shape unless the restoration of the original shape is not complete, when some reversion to the deformed shape will occur. If a stress is applied during cooling, the shape will change so as to relieve the applied stress.

Two modes of use are thus possible:-

a) The material is deformed and is normally in a low temperature (below As) state. On heating above the As temperature the original shape is recovered and this activates the mechanism.

b) The material restrains a high stress, and is normally in a high temperature (above Ms) state. On cooling to below the Ms temperature, the material progressively deforms under the applied stress and allows the mechanism to operate.

In the heating mode (a), there is a disadvantage that the yield stress of the material in its normal (low) temperature state is low, and thus cannot be used to react any significant load. Whilst this situation does not occur in the cooling mode (b), the obvious difficulties of cooling the material in a spacecraft in order to activate the release mechanism lead to the selection of the heating mode for the design.

BOOM RELEASE MECHANISM DESIGN

Design Requirements

The main requirements for the mechanism are:-

(i) it must release within 30 seconds of the release command being given;

(ii) the booms must be released within 20 milliseconds of each other (necessary to maintain spin stability);

(iii) the power available for heating is 15 Watts from a 28 volt power source;

(iv) the latch must withstand thermal cycling in the range $-30^{\circ}C$ to $+30^{\circ}C$ without loss of ability to operate on command;

(v) the booms must be latched with a pre-load of at least 800 N (180 lbs).

Design Details

The constraints of power and release time fix the maximum mass of material that may be used at 3.2 grams (assuming a heating efficiency of 50 per cent) i.e. just under 0.5 cc. In its low temperature state, this amount of material is too weak to operate the mechanism directly, and is used as a trigger to release two spring operated ball bolts (Figure 4). The spools in the bolts are joined to a crank by a connecting rod (Figure 5). In the latched position this crank tries to turn counter-clockwise and is prevented from doing so by a fixed stop, so that no load is transmitted to the element. The bolts are pre-loaded by tightening the nuts and thus pulling the fixtures attached to the two booms firmly onto the conical seatings.

The NiTi memory metal element takes the form of a short torsion cylinder, (Figure 6) having square ends and a cartridge heater located in the central bore. This form was chosen to minimise the amount of redundant material and enables efficient utilisation of heat from the cartridge heater located in the cavity. The ends were made from TiNi as a matter of convenience but could be any low conductivity material. The element is twisted by 20° after immersion in liquid nitrogen in a simple jig, and retains this shape at all temperatures below about $35^{\circ}C$ (the As temperature). One end of the element fits in a square hole in the housing (Figure 5), and the other fits into a small drive dog, which just contacts one of the pivot pins in the crank. The housing has slotted fixing holes to allow it to be rotated until the drive dog comes into contact with the pivot pin, whereupon the housing is fixed.

When the element is heated the strain is gradually recovered and the element rotates the drive dog by up to 20°. The slow recovery rotates the crank up to, and over, the top dead centre position, when the crank rotates rapidly clockwise under the influence of the spring loaded spools in the ball bolts.

Since both spools are connected to the common crank both release rapidly and simultaneously. Because the drive dog only pushes against the pivot pin, the crank is not restrained in any way by the remaining slow recovery of the element and can rotate clockwise very rapidly. At the end of their travel the spools strike the cap nuts at the inner end of the ball bolts, the balls drop inwards, and the booms are released.

The spools are a Ti6Al4V alloy, and are lubricated where the balls contact with a buffed-on film of molybdenum disulphide. All the bushes in the connecting rods and trigger mechanism are of a proprietary dry-lubricated type.

TEST RESULTS

Tests on TiNi Alloy

Extensive testing was carried out to determine the properties of the NiTi alloy in tension, compression and torsion. The performance of the torsion element was preferred and an element was manufactured and tested. The performance characteristics are recorded in Table 1. It should be noted that the strain occurs largely in the circular cross-section part of the element and that the deformation of the square ends is minimal. The "active volume" of the material is therefore less than the overall volume of the element and amounts to 0.5 cc (3.2 g).

Tests on Release Mechanism

Tests were carried out on the mechanism to assess its performance under nominal conditions, and also to investigate the effect of altering parameters such as bolt pre-load, angular movement of the crank to achieve top dead centre position (over-centre angle) etc.

The main performance characteristics measured were the time taken for deployment to occur after the command was given, and the temperature attained by the element at release (this was corrected for fluctuations in ambient temperature from a knowledge of the temperature rise characteristics of the element). The longer the time taken to operate and the higher the temperature, the more stress and/or angular recovery is being developed by the element. The results are summarised in Table 2.

Two failure modes were anticipated:-

(i) The pre-load on the bolts may be too high (due to errors in torque tightening), pushing the balls onto the spool so hard as to prevent it withdrawing, even though the crank has rotated over-centre. However, pre-loads of 5000 N (3 times the nominal value) did not prevent operation. Calculations showed that the friction coefficient between the steel balls and the spool was about 0.13. The molybdenum disulphide coating lasted for about 40 operations before the spools failed to release, necessitating re-application of the molybdenum sulphide.

(ii) The over-centre angle could be increased to such a degree as to prevent the trigger mechanism from operating. A higher torque and a larger angular movement are necessary to overcome this defect. Testing showed that the element had the capability to release the mechanism with an over-centre angle of 13^{o} (normal value 8^{o}). As expected, both time-to-release and temperature at release were increased as more recovery and higher torque is necessary.

DESIGN GUIDELINES

Where input power is limited, as is often the case with satellite mechanisms, only small volumes of material may be used. Because of the correspondingly small amount of energy available, the material may best be used to trigger the release of other stored energy, as in this design.

The low yield stress when in the low temperature (quiescent) state points to the selection of designs in which the memory metal is unloaded.

Whilst other forms of the material are useful in specific applications, torsion elements are particularly useful in offering a significant amount of movement with a moderate force, while maintaining a compact form easily heated and integrated into a mechanism.

Although pyrotechnic devices may perform some functions as well if not better, there may be applications in which memory metals offer considerable advantages. For instance, in a satellite operating in an electrically noisy environment, a pyrotechnic device may be prematurely triggered by spurious command signals, where as a memory metal device needs a 'fire' command of at least several seconds, so making it much more resistant to electrical interference.

CONCLUSIONS

High speed operation can be obtained by a suitable design, even though the shape recovery process itself is relatively slow. Memory metals can be used to meet real engineering requirements, as an alternative to electric motors, pyrotechnic or electric actuators, which are often larger and heavier. Sufficient data now exists to enable a designer to select a NiTi alloy for a mechanism with a high degree of confidence that it will perform as predicted.

REFERENCES

Brook, G.B. and Powley, D.G., 'Development of a Memory Metal Boom Latch and Release Mechanism'. Final Report R662/4/Jan 1977, held at the European Space Technology Centre, Noordwijk, Netherlands.

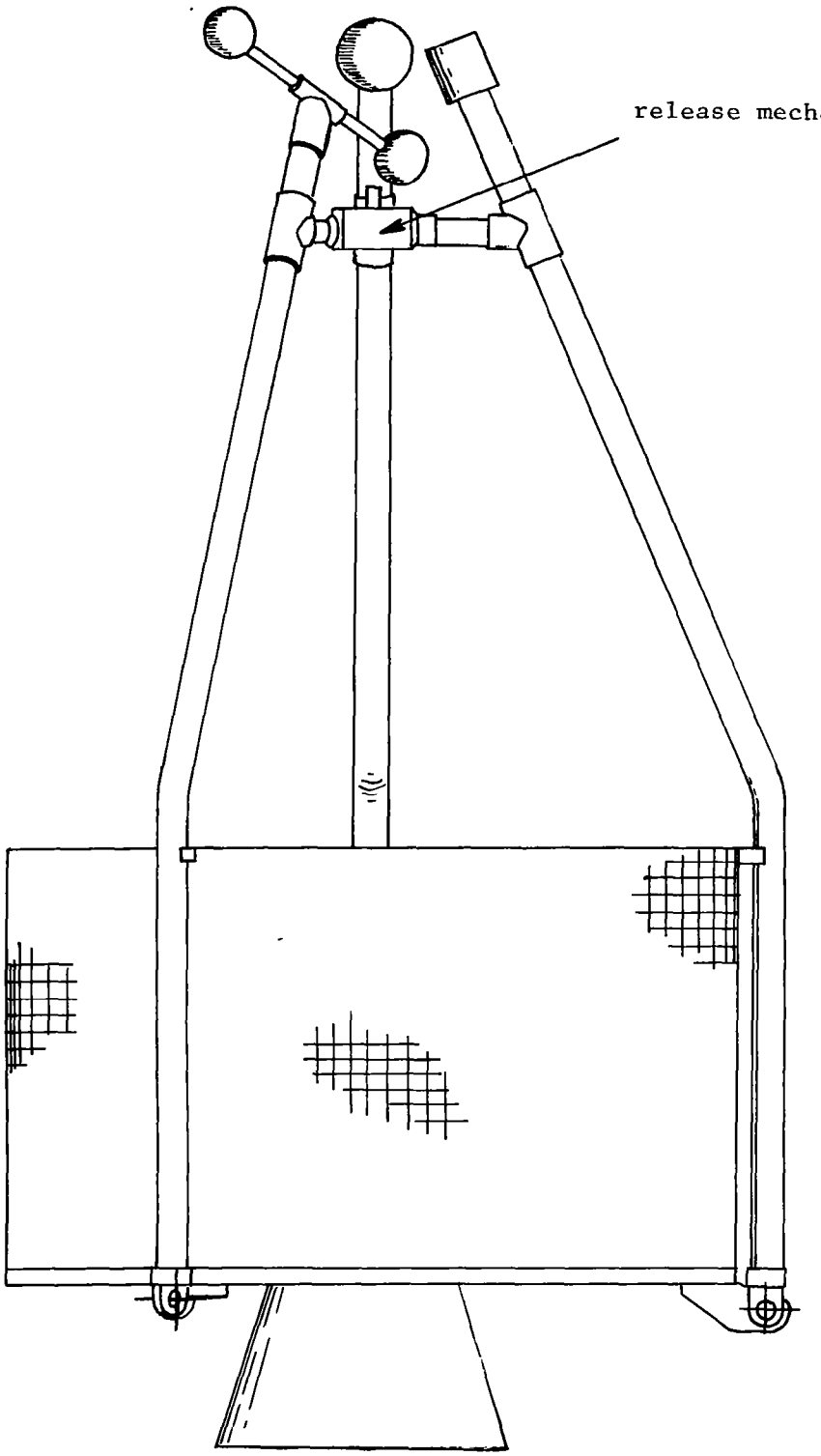

HINGE BOOMS IN LATCHED CONFIGURATION Fig. 1

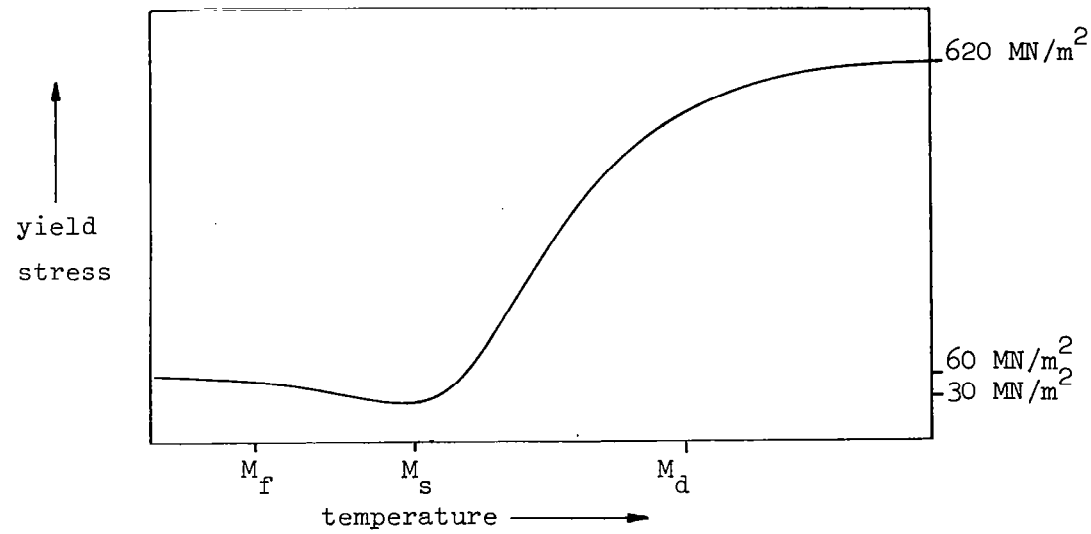

Relationship between yield stress and temperature for a typical shape memory alloy. M_d and M_s temperatures are the maximum temperatures for the start of the transformation under stress and at zero stress respectively. M_f is the temperature at which the transformation ends under zero stress.

Fig.2

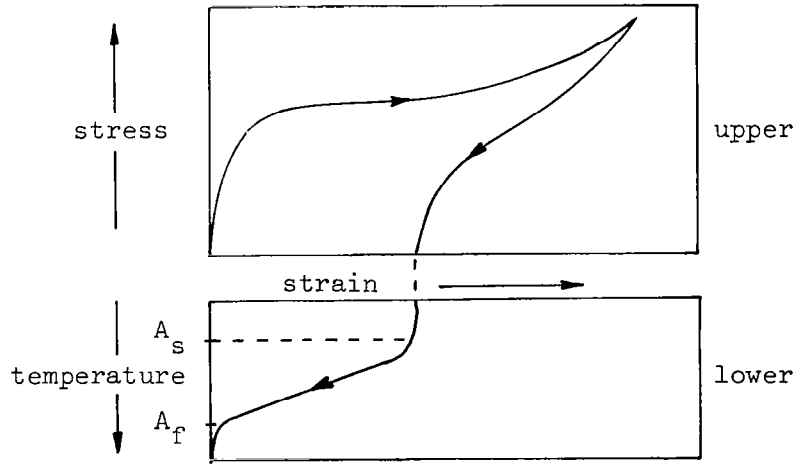

(upper) Stress-strain curve of memory metal at constant temperature below M_s temperature.

(lower) Temperature-strain curve of deformed shape memory metal at zero stress on heating to above A_f temperature.

Fig.3

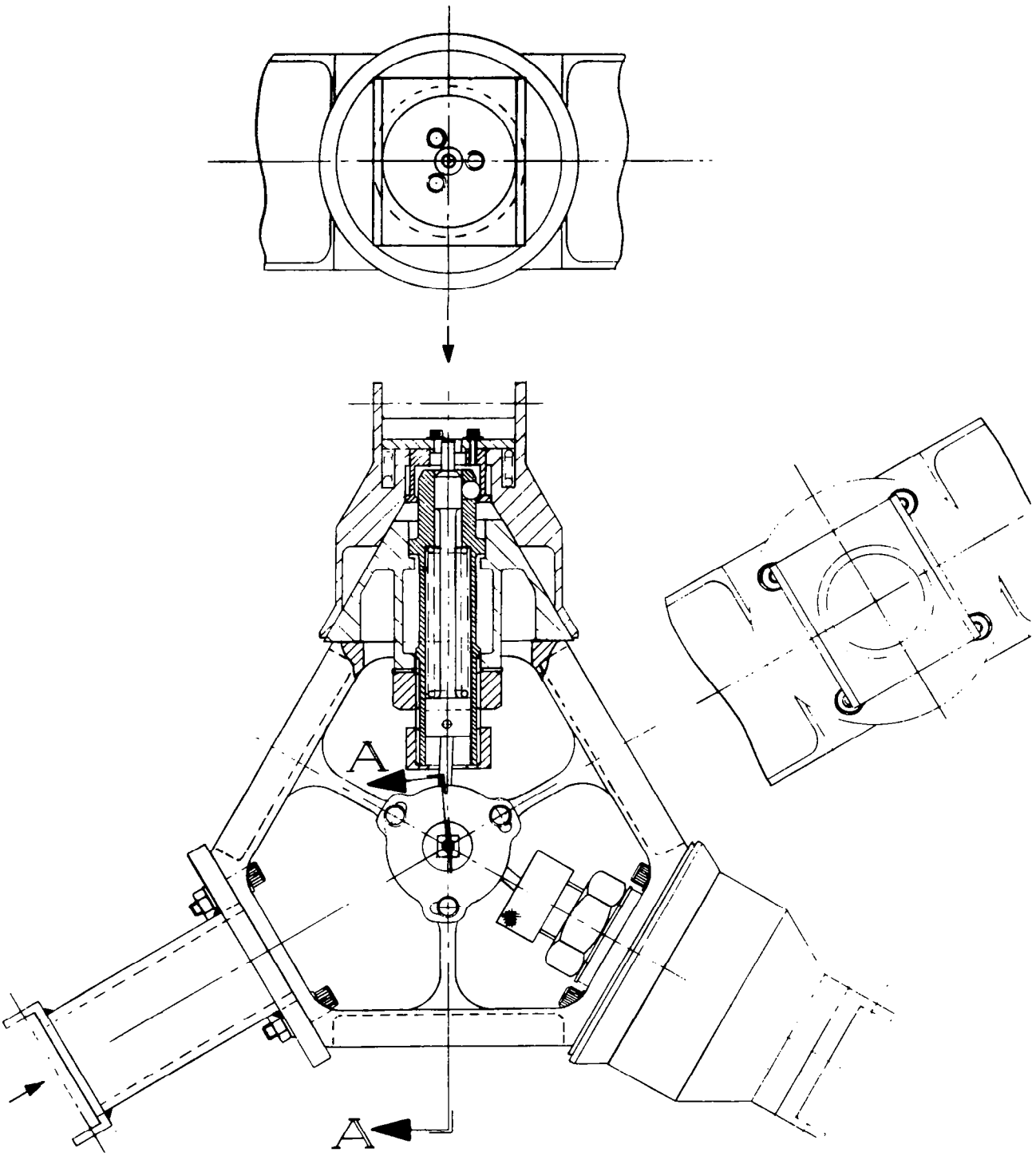

RELEASE MECHANISM

Fig.4

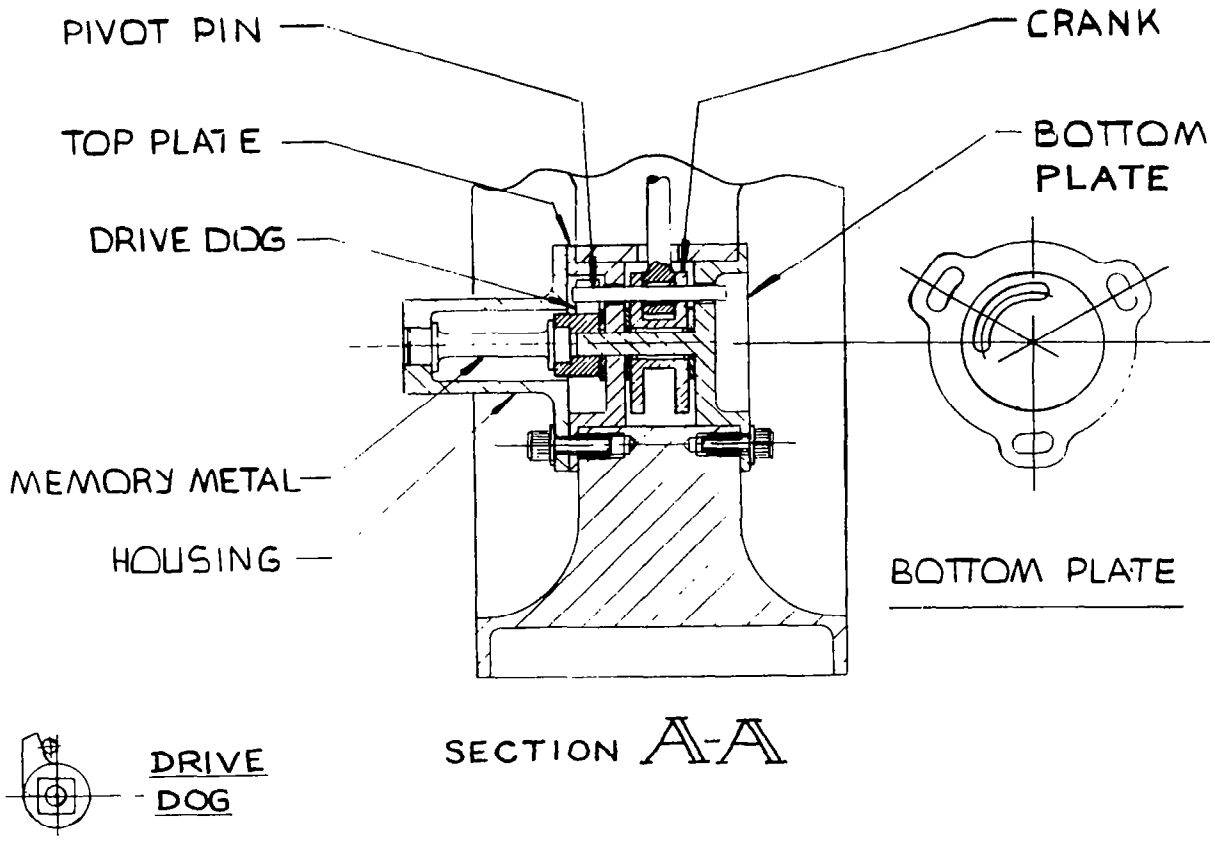

TRIGGER MECHANISM DETAILS

Fig.5

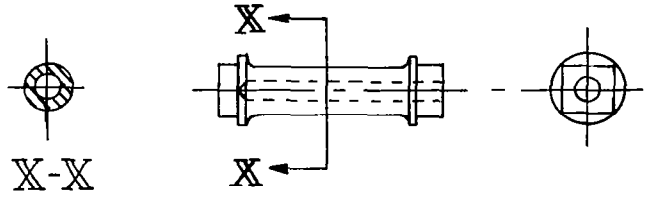

Circular cross-section:-	
Outside dia.	7.0mm
Bore dia.	3.5mm
Length	22.0mm

SHAPE MEMORY METAL TORQUE ELEMENT DIMENSIONS

Fig.6

Angular rotation	20^{o} (0.35 rads.)
Torque available	16 Nm (11.8 ft.lbf.)
Energy available	6.78 Joules
Surface shear strain	0.097 rads.
Start of shape recovery	$35^{o}C$
50% recovery	$47^{o}C$
Specific energy	13.7×10^{-3} J.mm^{-3}

TABLE 1

CHARACTERISTICS OF THE TORQUE ELEMENT

Test description	Release time (secs)		Release temp. ^{o}C	
	Mean	Standard deviation (No. tests)	Mean	Standard deviation (No. tests)
Nominal parameters	15.6	1.63 (8)	48.0	3.00 (3)
13^{o} over-centre angle	24.9	2.28 (5)	62.4	3.13 (5)
5000 N bolt preload	16.0	1.16 (4)	46.0	2.16 (4)
Ambient temp. $-30^{o}C$	28.0	1.58 (5)	42.8	3.11 (5)
Ambient temp. $0^{o}C$	23.6	2.30 (5)	46.8	12.87 (5)
Ambient temp. $+30^{o}C$	12.3	2.20 (5)	36.4	1.14 (5)

Nominal parameters:-

Tension in booms — 600 N

Preload ———— 1100 N

Over-centre angle —— 8^{o}

Power input ———— 11 Watts

TABLE 2

CHARACTERISTICS OF THE RELEASE MECHANISM

ACKNOWLEDGEMENTS

The work was supported by an E.S.A. contract and the authors gladly acknowledge the permission of the Director of E.S.A. to publish this paper.

They also wish to acknowledge the contribution of their colleagues, Dr. W. H. Bowyer and Mr. J. M. Cook to the experimental work.

ADVANCED VEHICLE SEPARATION APPARATUS

By Michael J. Ospring and Ronald E. Mancini

NASA-Ames Research Center

ABSTRACT

An advanced Vehicle Separation Apparatus is presented as a method of obtaining test data from two independent models or bodies in a conventional wind tunnel. The system makes efficient use of wind tunnel test time with computer control performing complex coordinate transformations necessary for model positioning. The new apparatus is designed to be used in any of the three Unitary Wind Tunnels at NASA-Ames Research Center. This paper will present mechanical design details and a brief description of the control system for the new separation apparatus.

INTRODUCTION

Within NASA there is a strong interest in wind tunnel studies involving separation of aerodynamic shapes in flight including vehicle-from-vehicle, stores-from-vehicle, pilot escape capsules and staging of large vehicles. A model support apparatus designed to perform such testing could be extended for use in many other important areas. Component interference studies to provide optimum location of nacelles, canards, tail surfaces and ventral fins could be accomplished quickly and efficiently. In addition, rake surveys could be performed on engine inlets, wing wakes and boundary layers. An effort was directed at the NASA-Ames Research Center into the design of an Advanced Vehicle Separation Apparatus which would enable aerodynamic data to be obtained from two computer controlled model supports operating simultaneously in close proximity within the same wind tunnel test section.

BASIC OPERATION

Figure 1 shows the Advanced Vehicle Separation Apparatus in the Ames Research Center 11-by 11-Foot Wind Tunnel. This is a closed return, variable density tunnel capable of continuously varying Mach numbers from .4 to 1.4. Maximum Reynolds number for this facility is 9.4×10^6 per foot. The new apparatus will be capable of automatically positioning a pair of models at preselected locations and orientations for specified time periods. This will provide efficient force or pressure data sampling at a large number of sample points. For maximum positioning capability, independent pitch, roll and yaw are required at each model while relative translation in all three directions is required between the models. The new system will provide X and Y translations between models in addition to three rotations of the secondary model. Z translation and rotations of the primary model are provided by the existing main centerbody/strut and a separate roll mechanism. The Axial Extender Mechanism is to be mounted in front of the existing main centerbody to provide 30 inch relative X translation between the models along the tunnel centerline. The Secondary Centerbody Mechanism is mounted cantilever fashion from a new blade entering through the tunnel side wall. The blade bearings and horizontal Y translation drive motor are mounted outside the test section wall and provide 30 inches of

secondary model movement across the test section while the Secondary Centerbody provides all rotations of the model.

The servo control system will be responsible for model path selection to reach desired individual points as well as collision prevention between models and support systems. Coordinate transformation equations will be used by a mini-computer to convert desired model movements into a proper combination of motor rotation outputs. Analog signals from precision multi-speed resolvers will be digitized and sent to the computer for position feedback.

The user will be able to select an automatic or manual control mode. Automatic control will cause the computer to step through preselected model positions. Manual control will allow the user the freedom of selecting random positions and time steps subject only to limit stop and collision prevention restraints imposed by the computer.

Axial Extender Mechanism. The axial or X-direction translation is provided by an Axial Extender Mechanism shown in Figure 2. The design requirements for X-direction movement include a 30 inch minimum relative translation between models at a rate of 2 inches per second. Positioning accuracy is $\pm$ .03 inches with readout at $\pm$ .005 inches. Design loads are 2,000 pounds normal force, 500 pounds side force and 2,000 inch-pounds rolling moment at the model added to a maximum 300 pounds per square foot starting load on the entire assembly (model, sting and axial extender mechanism) in the supersonic tunnels.

This mechanism was conceived as an addition to the existing wind tunnel centerbody and strut. In this manner, the primary model would be capable of existing motion in pitch, yaw and Z-translation with a new capability to translate up to 30 inches in the X direction. The concept of giving the X translation to the primary model is good for two reasons. First, tunnel blockage is not increased by the relatively large diameter (14 inches O.D.) of the new mechanism because the existing centerbody is larger. Second, the primary model is pushed forward in the test section by the length of the new mechanism to a point which coincides with possible secondary model placements.

Translation is accomplished using a direct current motor coupled to a ball screw. Ball bearings support the ball screw at each end of the stationary housing. The ball nut pushes a collar connected to the moving housing. 1/4 inch lead on the ball screw requires only 480 rpm at the motor for a 2 inch/second rate of translation. Sliding is done on linear bearings and roll is carried between housings with cam followers. A feedback resolver is mounted at the rear of the motor. This design provides infinite positioning capability with near zero backlash and low friction.

Secondary Centerbody Mechanism. Pitch, yaw and roll rotations for the secondary model are provided by a Secondary Centerbody Mechanism shown in Figure 3. The design requirements for these rotations include a maximum of 20 degrees pitch or yaw (not simultaneously) and $\pm$ 180 degrees roll. Angle change rates are 5 degrees per second on all rotations. Angle positioning requirements are $\pm$ .05 degrees with readout accuracy at $\pm$ .01 degrees. Design loads on the Secondary Centerbody are 750 pounds normal force, 500 pounds side force and 1,000 in-pounds rolling moment at the model added to a maximum

300 pounds per square foot starting load on the model and centerbody assembly. Overall size of the centerbody was to be kept at an absolute minimum to reduce tunnel blockage.

The new centerbody was conceived from spacesuit technology and operates in exactly the same fashion as an elbow joint in a hard spacesuit. Figure 4 shows the four basic cylindrical housings of the mechanism. The fixed housing is grounded to the blade and the three forward housings are free to rotate independently. The middle rotating housing actually revolves on an axis offset by 10 degrees (called the bisector angle) from the centerbody centerline. With this geometry, the model is capable of sweeping out a cone with a 10 degree half-angle by rotation of this housing alone. Rotation of the rear rotating housing then moves the model anywhere within a $\pm$ 20 degree cone. Figure 5 illustrates some typical pitch and yaw combinations including the worst combined loading case for the drive motors.

The detail design of the secondary centerbody (reference Figure 3) includes three rotating housings driven by direct current motors with varying horsepowers of .25, .75 and 1.25 from front to rear. Each motor contains a tachometer and fail-safe brake capable of resisting all motion due to aerodynamic loading in the event of power loss. The motors are custom designed units only 4.5 inches in diameter to keep overall centerbody diameter as low as possible. In order to keep centerbody length down, harmonic drive units with 200 to 1 reduction are used behind each motor. This 200 to 1 reduction coupled with a maximum motor speed of 1400 rpm gives a housing rotation speed of 7 rpm, necessary to achieve the design requirements of 5 degrees/second rate change of model angle. Feedback resolvers are referenced to harmonic drive output so that motor and brake backlash do not affect position readout. Motor, resolver and model wires pass through hollow motor shafts and finally exit at the rear. Protective tubes surround the wires inside of each motor and are fixed to motor housings to prevent contact with the high speed shaft. Needle roller bearings are used at each housing to resist high moment loads while small section thrust bearings are used to hold the housings together and resist axial loads.

In a pure pitch or yaw mode, the Secondary Centerbody Mechanism is capable of the desired 5 degrees/second rate change of model angle only up to around 15 degrees. This is because the model rate change of pitching or yawing angle approaches zero near 180 degrees of bisector rotation. In order to provide a unique set of model positions, all housings are mechanically restrained to $\pm$ 178 degrees. This limits actual maximum pitch and yaw to $\pm$ 19.95 degrees.

This centerbody design gives maximum versatility in the minimum size possible.

Support Structure for Secondary Centerbody. Y translation for the secondary model is provided by the support structure shown in Figure 6. Design requirements of travel, rate and accuracy are identical to those previously listed for the Axial Extender Mechanism.

The cantilever blade concept is used to provide greater mobility between models and reduce tunnel blockage. Translation is provided by a direct current

motor operating a ball screw as before in the Axial Extender Mechanism. Linear bearings are used to resist moments in all directions and force loads in X and Z directions. Forces in the Y direction are reacted by large thrust bearings at the end of the ball screw.

Wall penetration into the test section at the Ames 11-Foot Wind Tunnel is through an existing window frame with the glass removed. Figure 7 shows a different mounting scheme used at the Ames 9- by 7-Foot Supersonic Wind Tunnel with blade penetration through the roof for the secondary model. A new pressure can is shown which houses the extended blade, motor and bearing assembly.

CONCLUDING REMARKS

The Advanced Vehicle Separation Apparatus is designed to simultaneously position two aerodynamic models or bodies in a single wind tunnel test section through use of a computer control system. Separation testing will be used to optimize location of aircraft components and investigate flow patterns and problems associated with two aerodynamic shapes in close proximity. This paper has described the design of a system to be used for efficient wind tunnel testing in this area.

ADVANCED VEHICLE SEPARATION APPARATUS
ELEVEN FOOT WIND TUNNEL INSTALLATION

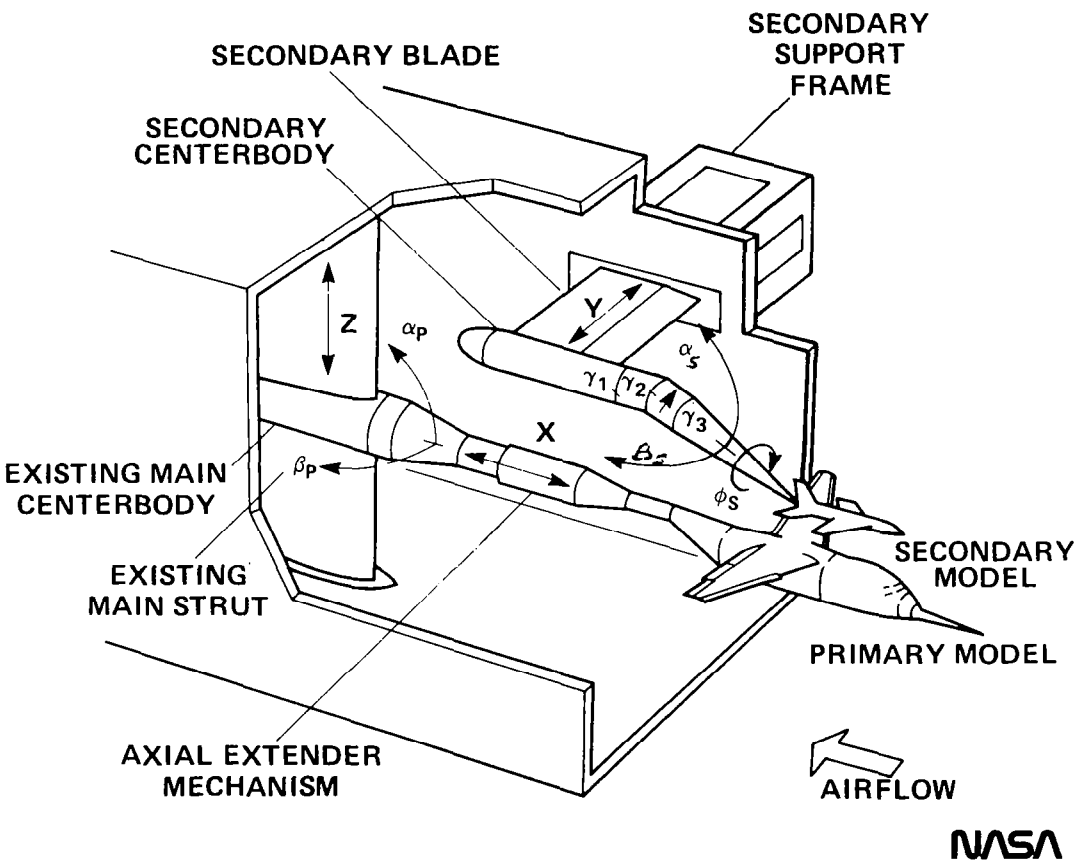

Figure 1

ADVANCED VEHICLE SEPARATION APPARATUS
AXIAL EXTENDER MECHANISM

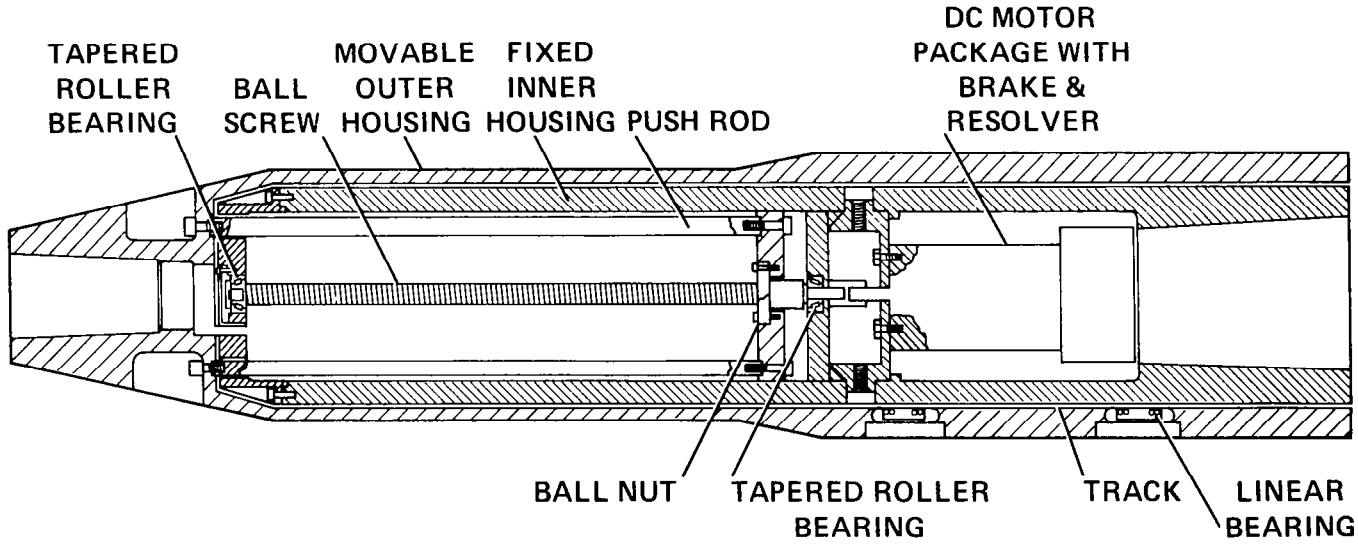

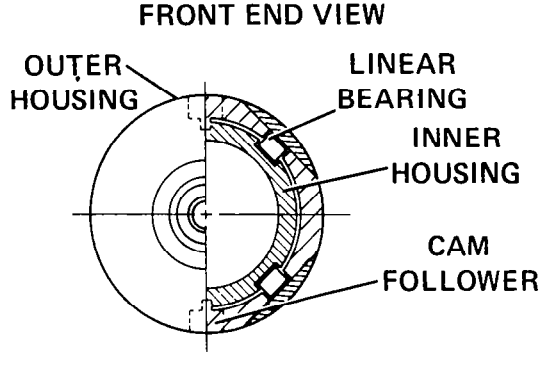

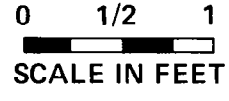

NASA

Figure 2

ADVANCED VEHICLE SEPARATION APPARATUS
SECONDARY CENTERBODY

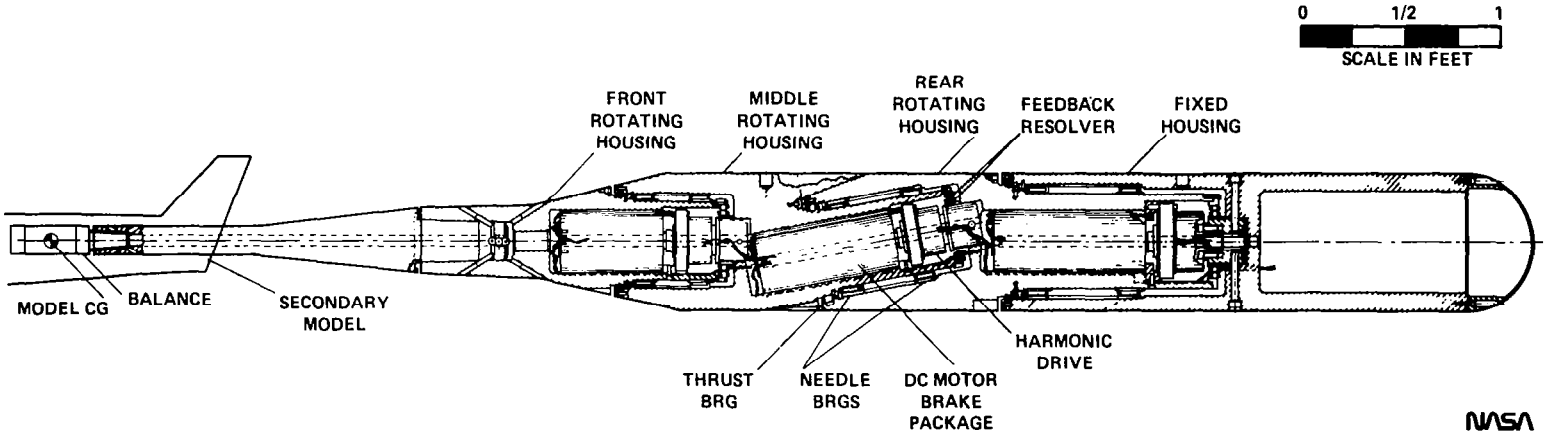

Figure 3

ADVANCED VEHICLE SEPARATION APPARATUS
SECONDARY CENTERBODY JOINT GEOMETRY

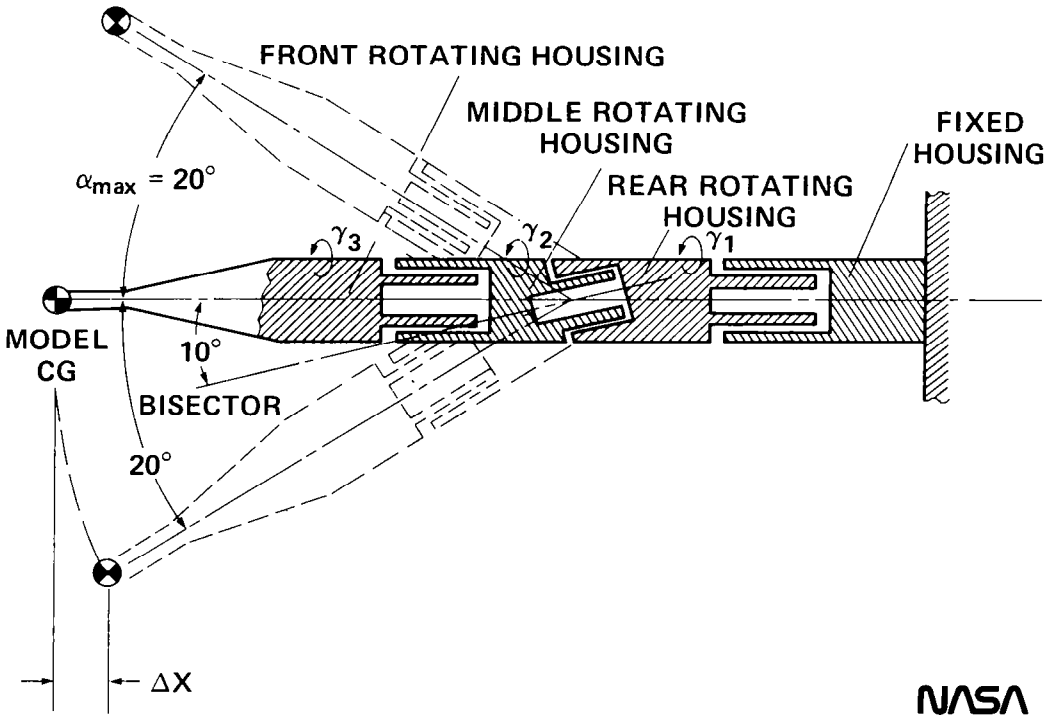

Figure 4

ADVANCED VEHICLE SEPARATION APPARATUS
SECONDARY MODEL POSITION ENVELOPE

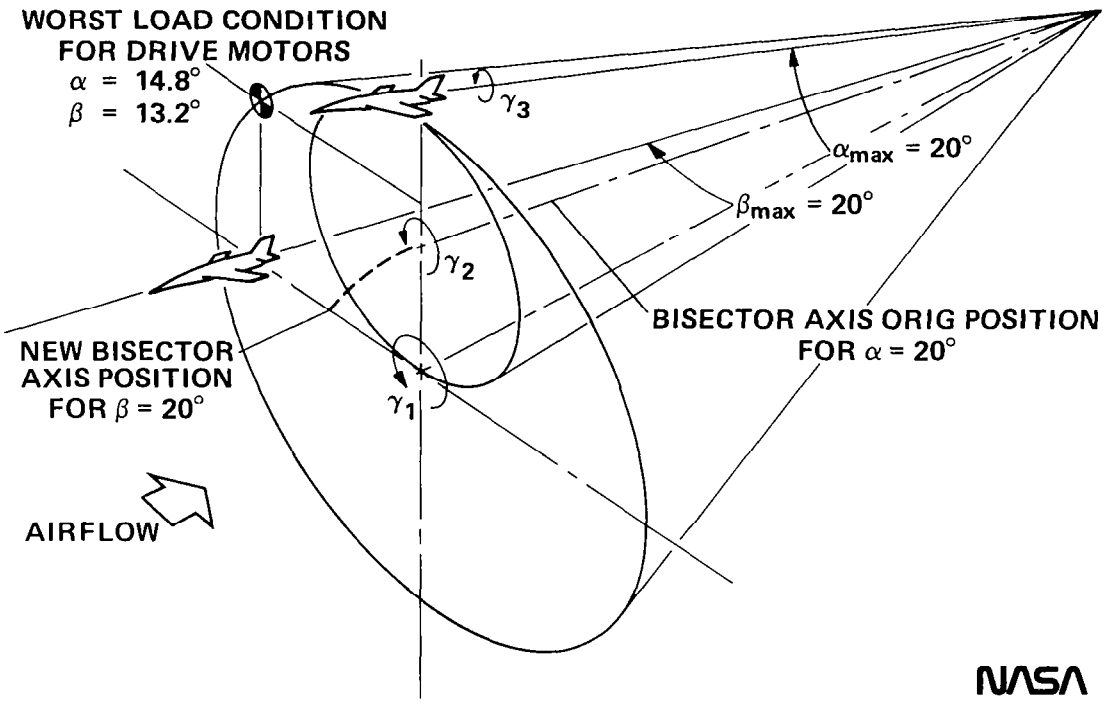

Figure 5

ADVANCED VEHICLE SEPARATION APPARATUS
BLADE SUPPORT STRUCTURE FOR 11 FT. WIND TUNNEL

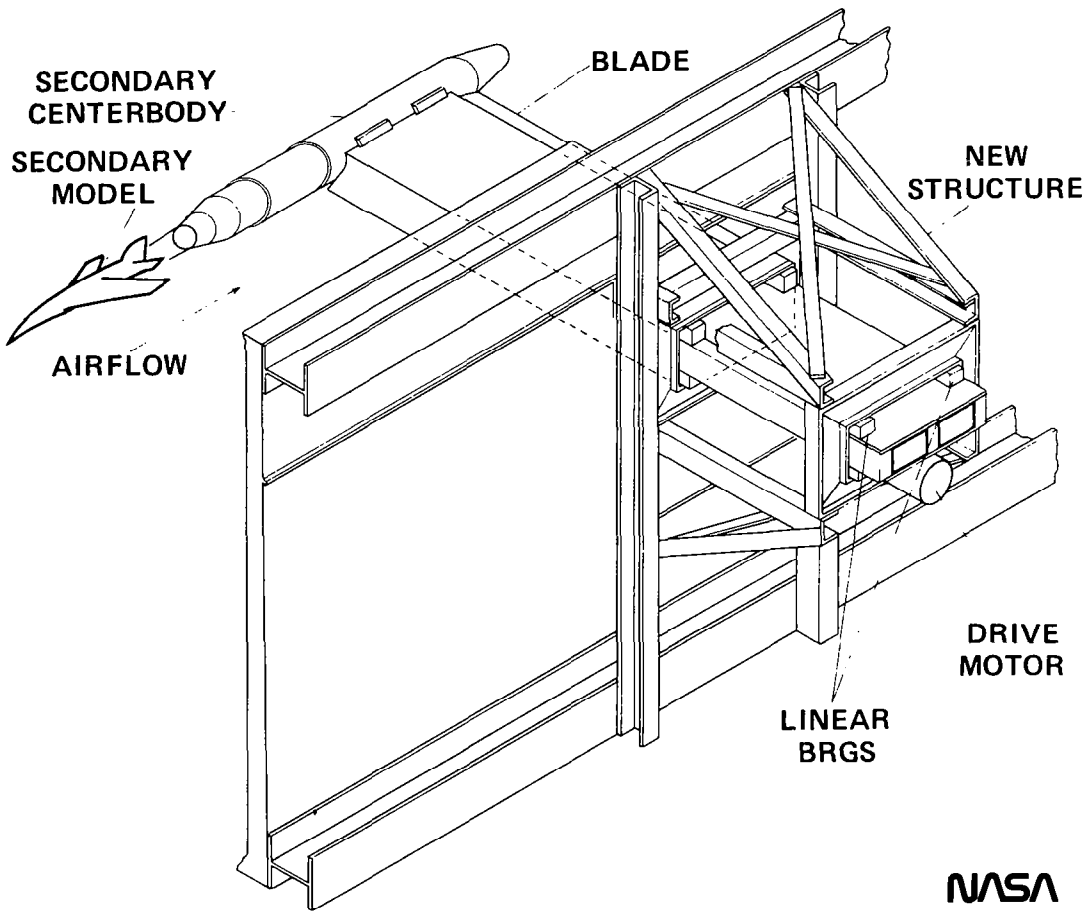

Figure 6

ADVANCED VEHICLE SEPARATION APPARATUS
9 x 7 FOOT WIND TUNNEL INSTALLATION

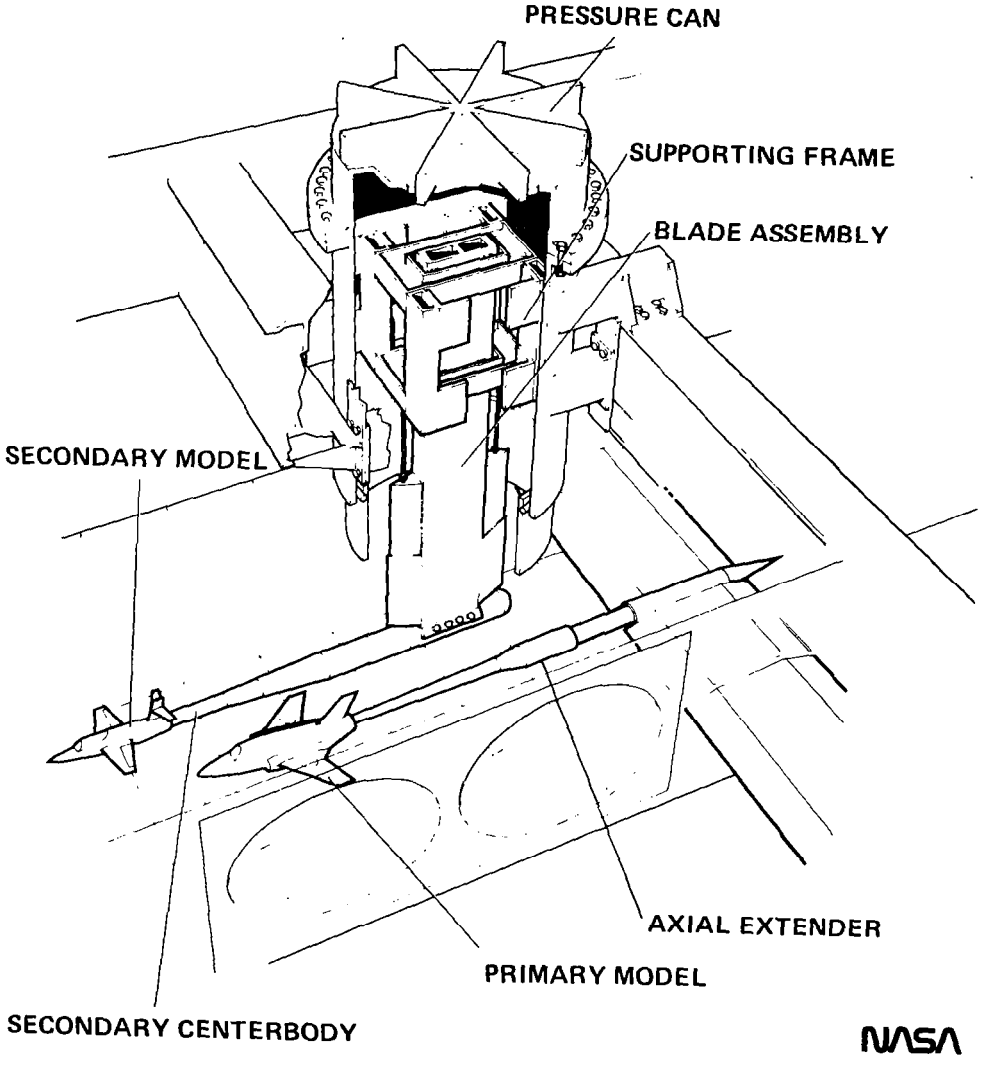

Figure 7

DEPLOYMENT MECHANISMS ON PIONEER VENUS PROBES*

By W. L. Townsend, R. H. Miyakawa,
and F. R. Meadows

Hughes Aircraft Company

ABSTRACT

Deployment mechanisms were developed to position scientific instruments during probe descent into the Venus atmosphere. Each mechanism includes a provision for pyrotechnic release of the enclosure door, negator springs for positive deployment torque, and an active damper using a shunted d-c motor. The deployment time requirement is under 2 seconds, and the deployment shock must be less than 100 g's. The mechanism is completely dry lubricated and constructed mainly of titanium for high strength and high temperature stability. The mechanism has been qualified for descent decelerations up to 565 g's and for instrument alignment up to 940°F. The paper describes the mechanism requirements, the hardware design details, the analytical simulations, and the qualification testing.

INTRODUCTION

The Pioneer Venus mission includes a Probe Bus that carries three small probes and one large probe to Venus for release and descent into the Venus atmosphere. Each of the three small probes, as shown on Figure 1, has two deployment mechanisms designed to stow scientific measurement instruments during the 565-g deceleration of descent. When the Probe has reached 65 Km altitude from the surface, the enclosure doors are pyrotechnically released to allow rapid deployment of the Small Probe Net Flux Radiometer (SNFR) and the Small Probe Atmospheric Structure Experiment (SAS) instruments. Atmospheric data are taken for the last 65 Km of descent until the Probe lands. The Venus atmosphere is very dense, reaching 1400 psia at the surface, and aerodynamic heating causes a maximum temperature of 940°F on the mechanism.

The generation of the mechanism design requirements has covered many variables such as entry angles, spin speed and direction, Probe nutation and aerodynamic turbulance torques. For instance, the lumped environmental torques could either aid the SAS deployment as much as 3.0 in-lbs or possibly retard SAS deployment as much as 8.5 in-lbs. This extreme variation in environmentally applied torques meant that a large spring force must be applied to ensure deployment, but damping provisions must also be made to prevent instrument damage should these environmental extreme forces not be present.

*This work was conducted under NASA-Ames Contract 2-8300.

In addition to the deployment requirements, the instruments have to be protected structurally and thermally during the deceleration prior to deployment. The SAS and SNFR instruments are stowed aft of the conical heat shield to avoid temperatures of several thousand degrees during initial entry. A full enclosure, which is covered with silicone rubber ablative material, is still required for mechanism protection.

The six mechanisms are now installed on the small probes and are undergoing system testing. The launch of the Pioneer Venus multiprobe mission is planned for August 1978.

REQUIREMENTS

The mechanism design requirements can be divided into three basic modes of operation as listed below. Table 1 lists the specific parameters required of each mode.

1. Stowed Mode. The instruments are kept folded into a retracted position by the enclosure door. While in the folded condition, the mechanism is subjected to vibration and entry deceleration simulations up to 706 g's for qualification.

2. Deployment Mode. The enclosure door is pyrotechnically released by a bolt cutter. As the door is sprung open, the instruments must be deployed in less than 2.0 seconds. However, if the deployment is too rapid, the stopping shock must not exceed 100 g's at the instrument tip.

3. Descent Mode. The mechanism must withstand the high pressure and temperatures up to 940^{o}F while maintaining alignment of the instruments within $\pm$ 1 degree.

MECHANISM TRADEOFFS

The deployment time requirement of less than 2.0 seconds along with the deployment shock restriction made the possible mechanism approaches very limited. An undamped spring deployment design showed impact shocks above 400 to 500 g's. In addition, the rebound problems with the undamped spring approach could only be solved with a deployed latch which had difficult dynamic and strength requirements.

An active d-c brush motor could be sized to drive the mechanism but requires active rate feedback to fall within the impact requirement. The rate feedback closed-loop electronics for each of six mechanisms makes the cost and weight penalties much higher than the baseline. The more simplified stepper motor driver electronics are more attractive for rate control than the d-c

motor system, but the stepper motor would be much heavier. A heavier stepper motor is required because the 2.0 second deployment time means a small gear ratio and high motor torque for control.

The damped spring approach could use viscous fluid, rubbing friction, or electromagnetic damping. The nearby science payloads along with the wide temperature excursion ruled out the viscous damper because of concern for outgassing. The electromagnetic damper was selected over the friction damper due to the fine tuning capability and consistency of the d-c motor. The d-c motor can be fine tuned using a shunt resistor to allow for changes in requirements or variations from unit to unit.

DESIGN DESCRIPTION

The deployment mechanisms and protective housings are designed to accommodate both the SNFR and SAS instruments interchangeably. There are differences in instrument attachment, interconnections, and instrument aerodynamic shapes. The mechanism has different deployment springs, different stop angles, and damper settings for each type of instrument. The diagram of Figure 2 describes the mechanism with the SAS in the deployed position.

The mechanism includes a machined structural base that supports both the mechanism and the protective housing. The protective cover is deployed 90 degrees by a torsional spring after the tie-down bolt is cut by a pyrotechnically driven device. The squibs and squib drivers are redundant. The instruments are deployed by a negator spring once the door motion has started. The door is deployed in 0.1 to 0.2 seconds which is more rapid than the instrument motion. As a backup, there is a mechanical finger on the instrument platform to safely push the cover ahead in case of interference. The cover support is captured by the wedging action of a C-shaped clamp to absorb excess energy and to prevent rebound.

The instrument deployment is driven by a 301 CRES negator spring selected for its constant torque properties. The damping is provided by a d-c brush motor geared to a higher speed by a 38.3:1 ratio. The motor is mounted on ball bearings to preserve the air gap, but dry-lubricated journal bearings are used elsewhere. The titanium gears have Vitrolube 1220 MoS_2 dry lubricant which was selected for the binder cure temperature of 950^{o}F to minimize further outgassing during descent. There is no latch in the deployed position. A cantilevered beam provides a spring action stop that is rigid enough to maintain alignment after a short settling time.

The photographs of Figures 3 and 4 show the mechanisms in the deployed condition with the housings removed. The instrument deployment negator spring and the cantilevered beam stop are depicted in Figure 3. The base structure is machined 6AL4V titanium because of the high strength requirements during entry and thermal expansion compatibility with the mating probe structure. Beryllium copper is the shaft material selected to act as a journal bearing and for shock absorbing properties, since it has a low modulus of elasticity

compared to steel. The mechanisms' physical characteristics are shown in Table 2.

ANALYTICAL MODEL

The flight loading environment at the time of deployment, as depicted in Figure 1, is severe and difficult to predict. Trajectory dependent and hence time varying aerodynamic conditions are primarily within the transonic region characterized by bow shocks and complex local flow fields. Attitude motion of the probe generates time varying inertial loads in addition to axial deceleration. Asymmetric ablation on the aeroshell can induce vehicle spin of up to 100 rpm resulting in centrifugal force fields. In addition, the mechanism performance is dependent on design parameters such as friction, spring tolerances, cable bending effects, and motor damping which are all in varying degrees environmentally dependent.

The time sequencing and complex interaction of both environmental effects and dispersed design parameters necessitates the development of analytical models in order to assess mechanism performance and structural integrity. A computer program was written incorporating both probe and mechanism dynamics for time simulation of the rigid body aspects of the deployment process. A finite element model and standard modal analysis techniques are employed to determine structural response at impact. Parametric studies are utilized to establish the combination of extreme conditions which result in worst case fast and slow performance as summarized for the SAS in Table 3.

The level of torque for the negator deployment spring is selected to ensure positive torque margin throughout deployment without benefit of momentum. In other words, should the instrument momentarily stall at any intermediate angle, the negator must have sufficient torque to restart. The significant torque variables are displayed on Figure 5 for conditions influencing the SAS deployment. The static torque margin shown on Figure 5 never falls below zero. The resulting fast and slow deployment times are graphically shown on Figure 6. The computer results are shown in Table 4 depicting the wide spread in all parameters between fast and slow deployment conditions.

The cantilevered beam used as a spring stop is necessary because the tip accelerations during stopping exceed 100 g's even with an active damper. A key contributor to the stopping acceleration is the shock produced by ongoing motor rotor energy after the instrument reaches the end of travel. Therefore, the use of higher damping coefficients cannot directly solve the problem without far exceeding the 2.0 second limit in slow deployment cases. Figure 7 describes the relationship between stop spring stiffness and tip acceleration for the fast deployment case. The figure also shows the overtravel tradeoff which is an important consideration for enclosure clearance.

TEST PROGRAM

A comprehensive test program was conducted on a prototype unit to cover all aspects of environments, including high-g, vibration, deployments under many environmental simulations, and descent temperatures. Two of the six flight units were tested to qualification levels of acceleration, temperature and vibration. The remaining four units were subjected to acceptance levels of acceleration, temperature, and vibration. The acceptance criteria were in terms of deployment time, deployment shock, and deployed alignment measurements. The pyrotechnic bolt cutter release was done once in development and four times in qualification to ensure compatibility with the mechanism. In order to save on the cost of the non-reusable bolt cutters, manual releases were done for most deployment tests.

The high-g testing turned out to be most revealing in discovering design deficiencies. Several cases occurred where structural distortion at 706 g's caused mechanical contacting of delicate parts not designed to carry loads. These areas had to be reinforced with structural stiffeners along with better supports for electrical wiring. During the first high-g test, the free end of the negator spring was driven off its support post so that subsequent deployment could not occur. A special hook was designed to prevent this unacceptable negator motion during high-g forces and to spring away during normal deployment.

The probe descent simulation of the high pressure and 940^{o}F temperature was conducted on the development model only because of permanent damage to some parts of the system. Since it would be very difficult to measure instrument angle change during exposure, measurements were made on a fixture before and after exposure. Unfortunately, the instrument angle changed about 1.5 degrees as a result of this test. Subsequent testing was conducted to isolate the problem to permanent set of the beryllium copper cantilever stop spring shown on Figure 3. It was discovered that beryllium copper creeps to a new permanent set when exposed to 940^{o}F under the residual preload of the negator deployment spring (approximately 15 in-lbs). The cantilever stop spring was then changed to a 17-4 PH CRES design with the same spring rate. The mechanism exposure was rerun with a small acceptable change in alignment of only 0.035 degree.

The deployment tests were conducted at high and low temperatures, but most data were collected at room ambient conditions. A loading fixture was designed to apply either aiding or restricting torques to simulate the extremes of the environment. Provision was made to add a shunt resistor to the motor to trim the extent of damping of each unit. As it turns out, a 5 ohm resistor was suitable for all units. The results are summarized in Table 5. It should be noted that the data show results that are less than one-half the allowable specification limits in time and g-loading. The analytical results showed a much wider dispersion predicted at Venus because the aerodynamic induced torques as shown on Figure 5 have a more severe effect than the linear simulation used in test. The computer simulations were rerun using the laboratory induced torques and verified this difference.

CONCLUDING REMARKS

The development of these mechanisms shows a high degree of sophistication and confidence in performance predictions compared to just a few years ago. For instance, the use of dry lubrication on gears, ball bearings, journal bearings, and motor brushes is now well enough defined to predict friction and life instead of just survival in space. The use of the computer simulations of mechanism behavior now allows all variables to be studied so that the testing matrix can be very much reduced. However, it continues to be important to touch on each test environment to check the level of accuracy of the computer simulations and be sure that some critical condition has not been overlooked.

Table 1. Requirements summary for qualification

Launch Mode (Stowed)	
Sine vibration - lateral	45 g 45-60 Hz
thrust	30 g 25.5-100 Hz
Random vibration	12 g rms overall
Acceleration	706g
Temperature	-98°F to $+170^{\circ}$F
Deployment Mode	
Deployed angle - SAS	$160^{\circ} \pm 1^{\circ}$
SNFR	$120^{\circ} \pm 1^{\circ}$
Peak tip acceleration	100 g
Deployment time (including door opening)	2.0 seconds
Overtravel allowance	5°
Temperature	-98°F to $+123^{\circ}$F
Acceleration	5.5 g
External torques - SAS	13.0 in-lbs peak
(lumped) SNFR	8.5 in-lbs peak
Deployed Mode	
Deployed angle error	$\pm 1^{\circ}$
Temperature	-98°F to $+940^{\circ}$F

Table 2. Mechanism physical characteristics

Enclosure structure	6AL 4V titanium with silicone rubber ablative material	
Enclosure size (inches)	4.2 W x 9.4 L x 5.8 H	
Weight summary (lbs)	SAS	SNFR
Enclosure	2.01	2.01
Base structure	1.04	1.04
Mechanism parts	1.71	1.74
Instruments	0.29	0.80
Total	5.05	5.59
Instrument connections		
SAS	6 electrical wires 1 bellows	
SNFR	9 electrical wires	
Damper motor		
Weight (lbs)	0.15	
Static torque (in-lbs)	0.94	
Damping (in-lb-sec/rad)	1.10	
Motor resistance (ohms)	6.5	
Negator spring torque		
SAS (in-lbs)	19 $\pm$ 1	
SNFR (in-lbs)	16 $\pm$ 1	

Table 3. Definition of worst-case deployment conditions

	SAS	
	FAST	SLOW
Trajectory and aerodynamics	$\gamma_E = -20^o$ (1) Maximum aiding aero.	$\gamma_E = -75^o$ Maximum retarding aero.
Angle of attack	-12^o	$+12^o$
Attitude dynamics	Outboard = +0.3 g Inboard = -1 g	Outboard = -0.3 g Inboard = -1 g
Negator spring	20 in-lbs	18 in-lbs
Motor damping	1.5 in-lb-sec/rad	5.2 in-lb-sec/rad
Temperature	123^oF	-103^oF

(1) γ_E is the probe trajectory entry angle relative to zenith.

(2) Aiding and retarding aerodynamic torques have 30% dispersion margin.

Table 4. Performance results of the computer simulation

CONDITIONS		DEPLOYMENT PARAMETERS			
		Peak Accel. (g's)	Elapsed Time (sec)	Tip Overtravel (deg)	Alignment Error (deg)
SAS	Fast	51	0.24	2.8	-0.005
	Slow	6	1.52	0.3	+0.14
SNFR	Fast	75	0.23	3.0	-0.05
	Slow	8	1.29	0.3	+0.1
Specification maximum		100	2.0	5.0	1.0

TABLE 5. Deployment data

Configuration	Temperature	Average External Torque (in-lbs)*	Deployment Time (sec)	Deployment Shock (g)	Deployed Angle Error (deg)
SAS	Ambient	0	0.34	42	0.45
	Ambient	+ 4.5	0.29	43	0.70
	Ambient	-10.0	0.80	13	-0.05
	Ambient	0	0.34	40	-0.08
	High	+ 4.5	0.29	45	-0.05
	Low	-10.0	0.83	10	-0.73
	Ambient	0	0.35	35	-0.22
SNFR	Ambient	0	0.37	48	0.11
	Ambient	+ 5.2	0.27	60	0.26
	Ambient	- 6.3	0.80	12	-0.02
	Ambient	0	0.35	51	-0.01
	High	5.2	0.22	65	+0.06
	Low	6.7	0.88	11	-0.39
	Ambient	0	0.31	42	-0.06

*Aiding torques are positive and restricting torques are negative.

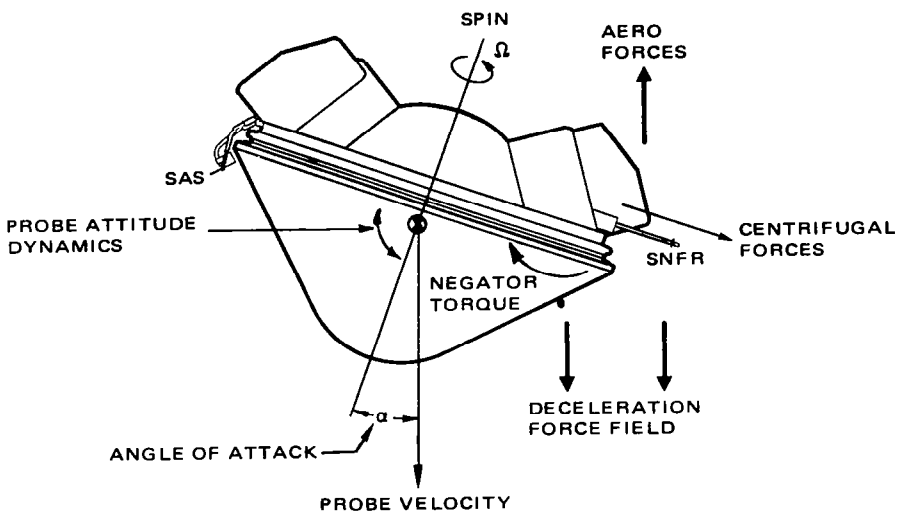

Figure 1. Pioneer Venus Small Probe

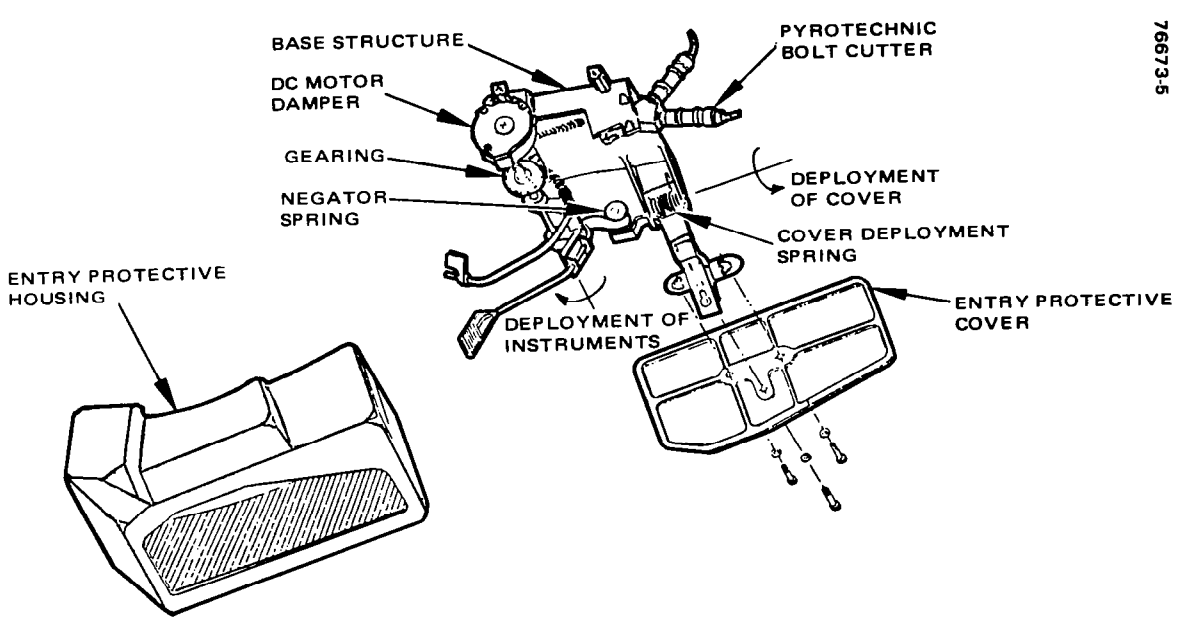

Figure 2. SAS Deployment Mechanism and Cover

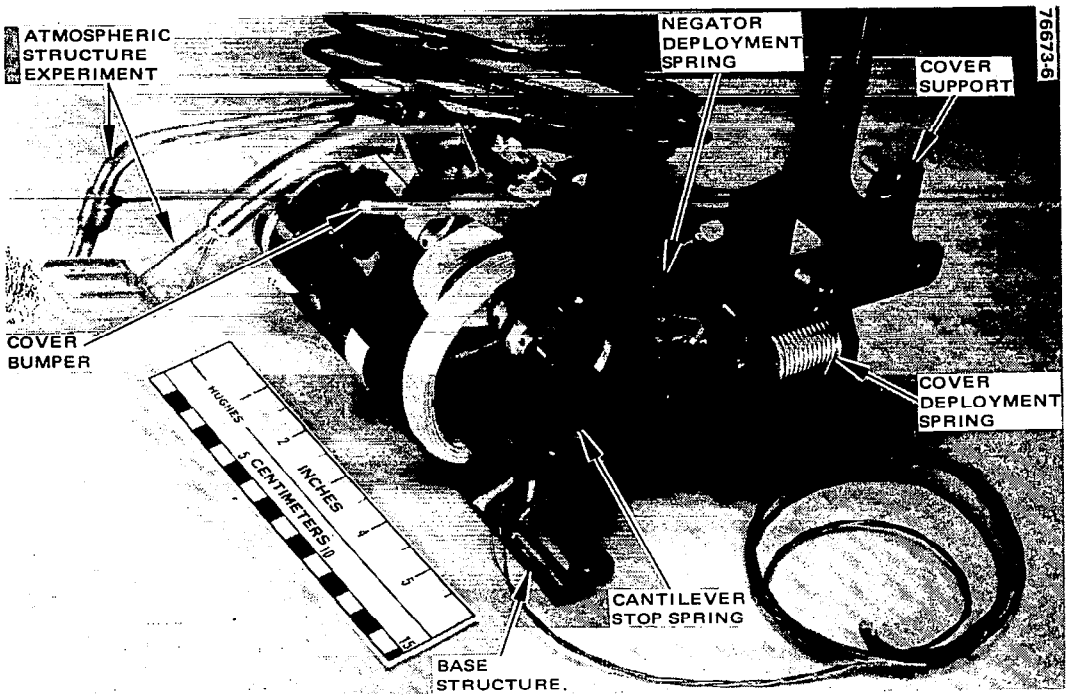

Figure 3. SAS Deployment Mechanism

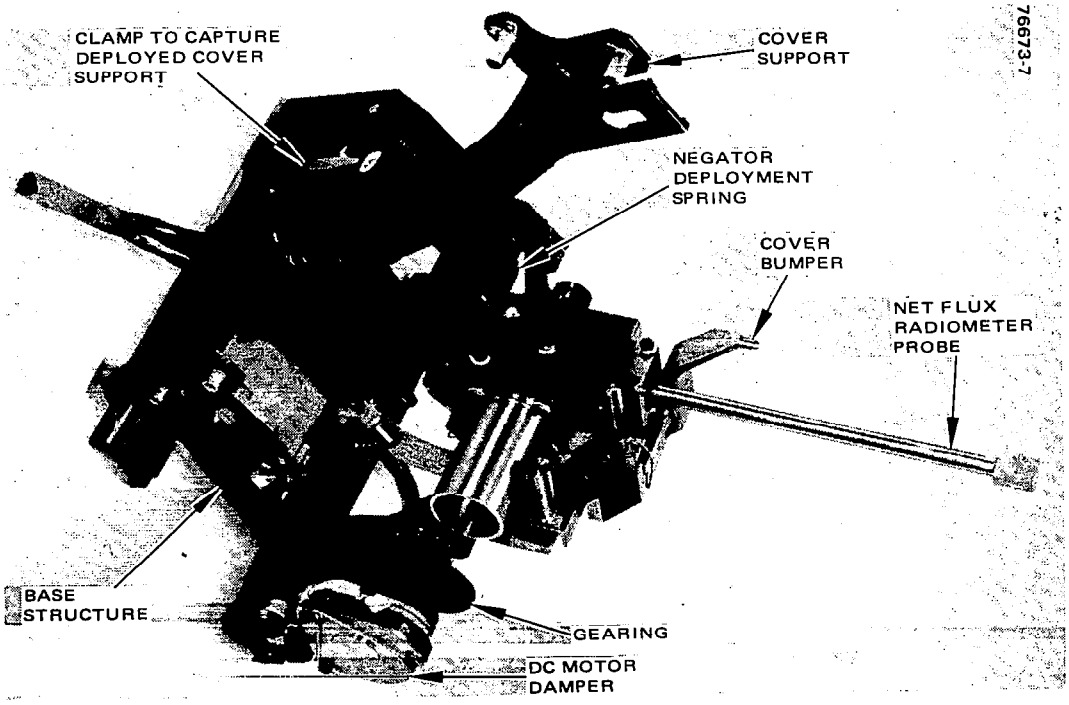

Figure 4. SNFR Deployment Mechanism

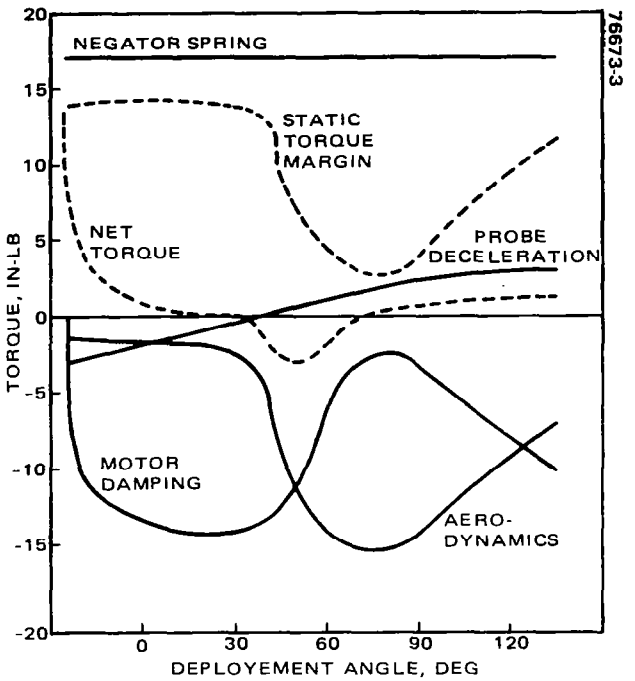

Figure 5. SAS Minimum Deployment Torques

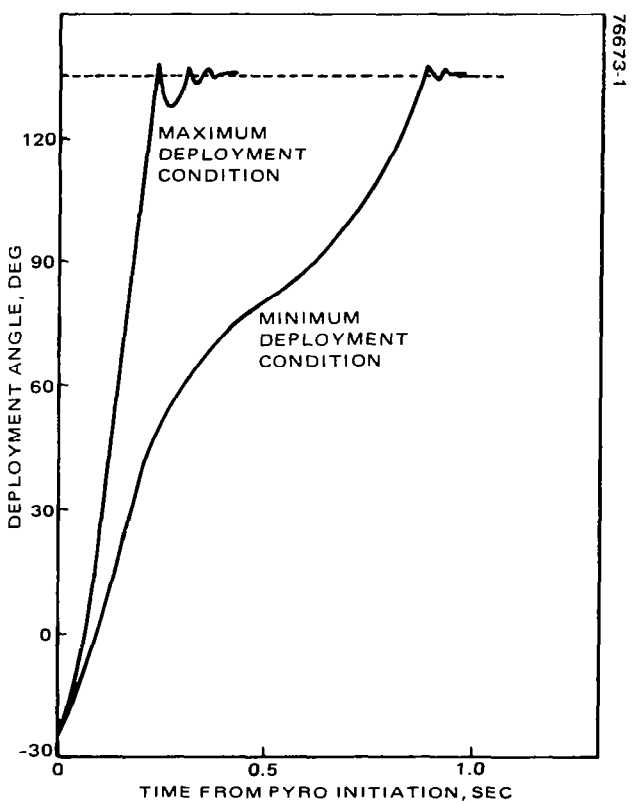

Figure 6. SAS Deployment Time History

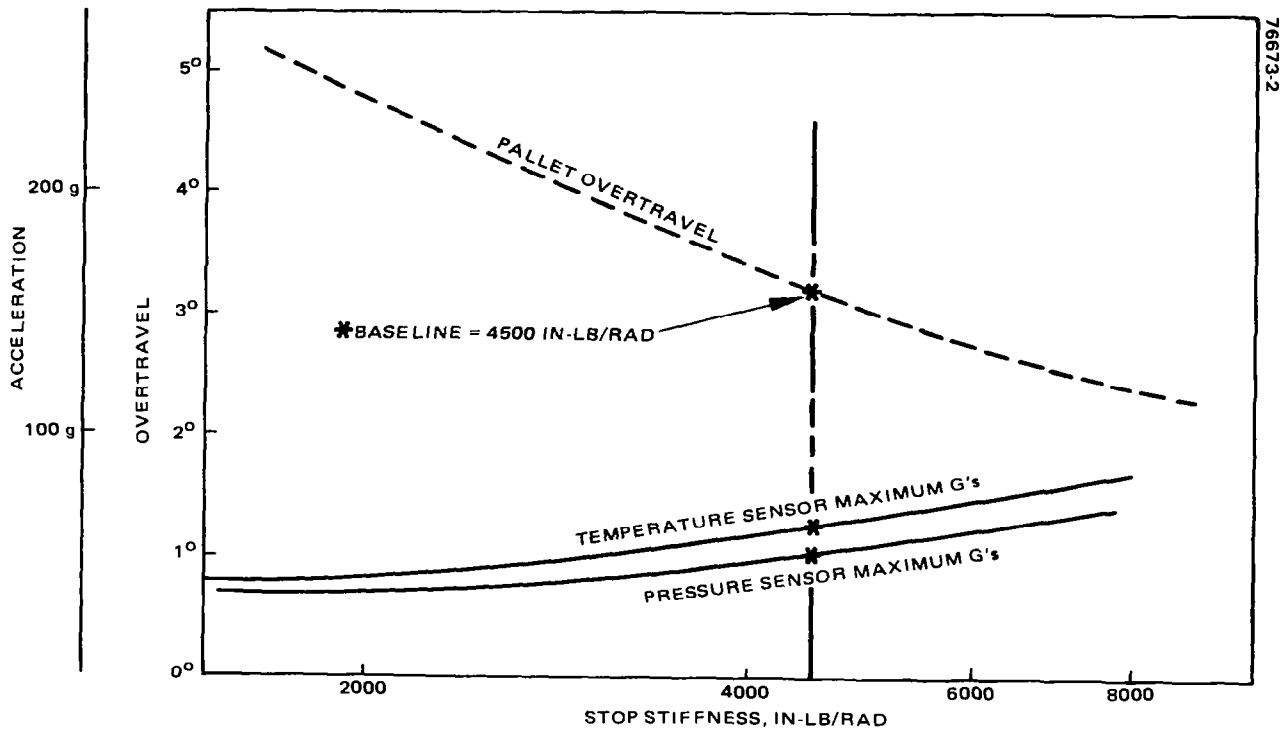

Figure 7. SAS Impact and Overtravel Response

SPACE SHUTTLE SEPARATION MECHANISMS

By William F. Rogers

NASA Johnson Space Center

ABSTRACT

The development of Space Shuttle separation devices is reviewed to illustrate the mechanisms involved in separating the Orbiter from the Boeing 747 carrier aircraft and from the externally mounted propellant tank. Other aspects of the separation device development to be discussed include design evolution, operational experience during the Orbiter approach and landing tests, and the work to be accomplished before an operational system becomes a reality.

INTRODUCTION

The separation of the Space Shuttle Orbiter from the Boeing 747 carrier aircraft and from the external tank (ET) will be reviewed in this presentation; however, several other crucial separation events occur during a typical Shuttle mission. These include the separation of the Shuttle vehicle from the launch platform at lift-off and separation of the two solid rocket boosters attached to the ET approximately 2 minutes into the flight (fig. 1). Actual structural separation of the Orbiter from the ET is preceded by the separation and retraction of the fuel and oxidizer lines and of the electrical connections between the Orbiter and the ET.

The Orbiter and the Boeing 747 carrier aircraft are shown before release in figure 2. The first separation occurred in 1977 during a series of test flights. The purpose of these test flights was to verify Orbiter handling capabilities and to verify the adequacy of all systems used in the approach and landing procedures. For both the earlier test flights and the actual orbital flights, the separation hardware provides structural attachment of the Orbiter until the time of release and then mechanical release within the system design constraints.

The purpose of this paper is to summarize the development of the structural separation system of the Orbiter for (1) launching the Orbiter from the 747 aircraft during flight tests and (2) releasing the Orbiter from the ET during orbital flight operations.

Two particular developmental problems are discussed for the Orbiter/747 aircraft separation system: (1) the development of the separation device, a pyrotechnic-actuated bolt, and (2) the requirement for lateral as well as fore and aft motion capability at separation. For the orbital flight separation system, a significant developmental problem is that of obtaining a sufficiently

smooth surface on the Orbiter after release. The purpose of this requirement is to control the aerothermal heating on the spacecraft to prevent excessive structural temperatures during entry.

DESIGN REQUIREMENTS

The separation system design requirements may be divided into two general categories: structural and mechanical. The separation hardware is the primary structural load path between the Orbiter and the 747 and between the Orbiter and the ET; hence, the hardware must satisfy the spacecraft overall structural design requirements. For the separation event, the system acts as a mechanical device and must satisfy the design requirements to assure a safe separation. The importance of this system is evident. A structural failure before separation, a failure to separate, or an improper separation could be catastrophic.

The structural design requirement for the Orbiter/747 separation is to provide structural support of Orbiter/747 interfaces for flight environments. The mechanical design requirements for the Orbiter/747 separation are the following.

1. To accommodate unrestrained horizontal motion at release
2. To accommodate the load measurement system
3. To accommodate ground adjustment of the Orbiter incidence angle
4. To provide redundancy in the release device and initiation
5. To separate without fragmenting

The structural design requirement for the Orbiter/ET separation is to provide structural support at Orbiter/ET interfaces for prelaunch, launch, and boost environments. The mechanical design requirements for the Orbiter/ET tank are the following.

1. To provide release of the Orbiter from the external tank for normal and abort separation
2. To preclude degradation of Orbiter functional systems after operation
3. To satisfy aerothermal smoothness criteria after separation
4. To provide redundancy in the release device and initiation
5. To separate without fragmenting

The requirements for the Orbiter/747 and Orbiter/ET design systems are similar; however, the Orbiter/747 system requires the capability to accommodate horizontal relative motion at release in addition to the obvious requirement

for unrestrained vertical motion. The purpose of this requirement is to allow the Orbiter to move relative to the 747 at release without inducing additional forces or impulses that would complicate the separation dynamics. The horizontal motion capability would allow the Orbiter to move forward and aft because of differences in drag between the two vehicles.

The requirement to measure interface attachments loads had a twofold purpose: to confirm the flight conditions for release and to monitor the structural loads during the various phases of mated flight. Representative design flight loads for the two separation systems are summarized as follows.

1. Orbiter/747

   a. Forward attachment (combined loads)

      Tension = 154.8 kN (34 800 lbf)
      Radial = 90.3 kN (20 300 lbf)

   b. Aft attachment (combined loads)

      Tension = 425.7 kN (95 700 lbf)
      Forward = 206.0 kN (46 300 lbf)
      Side = 147.0 kN (33 000 lbf)

2. Orbiter/ET

   a. Forward attachment

      Tension = 529.3 kN (119 100 lbf)
      Radial = 404.8 kN (91 000 lbf)

   b. Aft attachment

      Bolt tension = 1579.1 kN (355 000 lbf)

The incidence angle between the Orbiter and the 747 was preset based on aerodynamic and separation dynamic analyses. However, the ability to change this angle based on updated analyses and flight test data was required for separation as well as for ferrying the Orbiter. For the approach and landing test (ALT) system, the design was also influenced by the goal of minimizing the development of different release devices for this specialized application.

As previously mentioned, a very stringent requirement for aerothermal smoothness at the outer moldline has resulted in a difficult developmental problem for the release device at the Orbiter/ET forward attachment. Redundancy in the release system and separation without fragmentation are required for both systems.

CONFIGURATION DESCRIPTION

Orbiter/747 Separation

Figure 2 shows the Orbiter spacecraft attached to the 747 aircraft before release and figure 3 shows the combination just after separation. The one forward and the two aft structural attachments are represented in figure 4. At each attachment, a load cell measures the vertical and horizontal interface loads. To avoid the development of several different separation mechanisms for this very specialized test program, a single pyrotechnic bolt design (fig. 5) was selected for the three attachments. One separation bolt is used at the forward attachment and three bolts are used at each of the two aft attachments to carry the interface loads before separation. At each aft attachment, three electrical connectors carry pyrotechnic and communications wires and are designed to part immediately after structural release.

It should be noted that the separation bolt (fig. 5) fractures in tension at the separation plane - an ideal situation for the Orbiter/747 system. However, this device does not satisfy the stringent outer moldline smoothness criteria for entry from orbital flight, so a similar device, which fractures in shear internally, is being developed for that application.

Orbiter/ET Separation

Figure 6, illustrating the major components for separation of the Orbiter from the ET shows details of the forward and aft structural attachments. At the forward attachment, release is accomplished by the shear-type separation bolt previously mentioned. Figure 7 shows in detail the shear section of the bolt before and after separation. After the piston shears the bolt shank, it pushes the lower section of the shank free of the spherical bearing, and the bottom of the piston stops flush with the outer surface of the bearing.

At the two aft attachments, a frangible nut is used as the release device. Once the Orbiter is safely separated from the ET, doors close over the cavities left at the point of structural, feedline, and electrical umbilical attachments.

SEPARATION SYSTEM DEVELOPMENTAL PROBLEMS

Of the problems encountered during the development of the separation system, the following examples illustrate a variety of mechanical design problems and their solutions.

ALT Separation Bolt

The pyrotechnic-actuated separation bolt used for the ALT flights failed to separate during a functional test of a production bolt, just before the

start of qualification testing. This failure occurred after several successful development tests of nearly the same configuration. The functional failure occurred using one production cartridge in the lower chamber at a temperature of 219 K (-65° F). Several additional tests incorporating various changes were attempted before a successful separation was achieved with a modified bolt. The failure could not be definitely attributed to any specific inadequacy in design, construction, or material during these additional structural and functional tests. However, a series of cartridge tests indicated that output pressure was dependent on cartridge propellant loading pressures. In effect, the bolt was redesigned, resized, and underwent a new series of development tests. The principal modification consisted of reducing the fracture area to increase the ease of fracture, thereby reducing the structural margin. The pyrotechnic cartridge loading pressures were also modified to obtain more uniform chamber pressures. This particular hardware failure, which is discussed in more detail in reference 1, was never fully duplicated during the failure investigation. However, a combination of design changes and the additional developmental work resulted in the bolt successfully passing qualification tests and interface certification tests before the Orbiter/747 mated flight tests. This particular hardware problem illustrates a design compromise by decreasing the hardware structural margin to increase overall functional reliability.

ALT Aft Attachment Redesign

The original design concept for the Orbiter/747 aft attachments used linear-shaped charge explosive devices to sever the attachment structure at the separation plane (fig. 8(a)) to satisfy the design requirement for possible lateral motion at release.

Two additional concepts are illustrated in figures 8(b) and 8(c). These concepts involve the use of frangible nuts like that used at the Orbiter/ET aft structural attachments (fig. 6). Although these concepts did incorporate a pyrotechnic device already under development, neither concept provided the degree of horizontal motion at release as that in the final design. Both concepts were undesirable in that bolt withdrawal was required for a clean separation and a momentary hangup could occur. However, because of the massive structure involved at the aft attachment to satisfy the Orbiter/747 load requirements and because of the additional pyrotechnic device that would have to be developed for this concept, it was decided that a separation concept using the existing separation bolt design was desirable and would be cost-effective. The baseline design that resulted (fig. 4) incorporates three separation bolts at each aft attachment. These bolts react the tensile loads at the interface, and a shear surface approximately 1.3 cm (0.5 in.) deep reacts the forward and side loads. It was judged that this shear surface would not significantly affect the vehicle dynamics at release. Interface certification tests and flight tests have confirmed this to be the case. This design was a logical approach to satisfy the design requirements as well as to minimize the development of pyrotechnic devices.

Orbiter Outer Moldline Criteria

For the Orbiter/ET forward structural attachment, a stringent design requirement exists to maintain a smooth outer surface after separation to minimize the aerodynamic heating on the lower surface of the Orbiter during entry. The aerothermal requirement is a maximum step of ±0.043 cm (±0.017 in.) and a gap no greater than 0.089 cm (0.035 in.). Many developmental approaches have been considered, including various combinations of release devices, close-out mechanisms, and doors.

Early design concepts for the Orbiter/ET structural attachments used electrical/mechanical release devices (fig. 9). These devices were soon discarded in favor of pyrotechnic-actuated release devices because of the positive structural attachment before release and the highly reliable pyrotechnic function at release. A preliminary design goal during the early phases of the Space Shuttle Program was to use completely reusable separation devices (primarily because of the Orbiter's quick-turnaround requirement) rather than pyrotechnic devices that had to be replaced after each flight. Figure 10 shows the initial pyrotechnic devices chosen for the forward attachment. Because of the smoothness requirement for the outer moldline, the reusable devices were soon replaced by the pyrotechnic separation bolt design.

The tension-type separation bolt was originally intended for this application; however, because the fracture plane was not within the aerothermal requirement and because of increased loads at this attachment, the shear-type separation bolt (fig. 7) was adopted. The shear bolt has the advantage of an internal fracture surface and a slight disadvantage in that the sheared bolt shank must be ejected from the monoball fitting for separation to be complete. It should be noted that the shear bolt has one pressure chamber with two pyrotechnic cartridges to satisfy the Space Shuttle redundancy requirements. This developmental problem illustrates a very difficult detail design challenge because of a combination of specific design requirements.

FLIGHT PERFORMANCE RESULTS

Before the first flight of the Orbiter/747 combination, the structural adequacy and functional operation of the separation system were demonstrated by analysis and by extensive ground tests. To date, the ALT separation system has been used for five Orbiter free flight tests and it has also served as an emergency system for Orbiter jettison on mated flight tests, both manned and unmanned. The ALT system operated successfully during the first free flight test on August 12, 1977, and has performed well during all other flight tests. In all tests, the pyrotechnics have functioned and the bolts have broken cleanly. The Orbiter and 747 crews have reported only a moderate "thump" as the bolts have separated. In all cases, onboard and chase plane photography have verified a normal release and separation.

After each flight test, the separation interfaces were thoroughly inspected during buildup of hardware for the next flight. Only minor problems associated with the pyrotechnic and umbilical electrical connectors were encountered. Because pyrotechnic connectors have a tendency to gall at the initiator interface (presumably because of pyrotechnic shock), they have had to be replaced periodically. These connectors were lockwired to the initiator bodies during the later flights to preclude any possibility of the connectors becoming disengaged.

The load measurement system functioned well during flight tests. Before the free flight tests, the system provided data to verify loads and aerodynamic predictions. During the free flight tests, the system provided backup data to verify the Orbiter/747 separation conditions for Orbiter launch.

CONCLUDING REMARKS

The approach and landing test phase of the Space Shuttle Orbiter flight test program has been successfully concluded. The developmental problems have been solved in a variety of ways without compromising the operational capabilities of the vehicle. A significant amount of testing and analysis remains to be accomplished before the actual orbital flight separation system is operational. However, developmental testing has already confirmed the adequacy of the basic design approach for these separation devices. For orbital flight separation, other types of pyrotechnic devices could be used and may be adopted in the future. Changes may occur to increase the Orbiter operational capabilities, to reduce operational costs by using refurbishable components, or to minimize the pyrotechnic mechanical shock by devices that operate at lower energy levels.

REFERENCE

1. Ritchie, Robert S.: Space Shuttle Orbiter Separation Bolts. Paper presented at the 12th Aerospace Mechanisms Symposium, April 27-28, 1978.

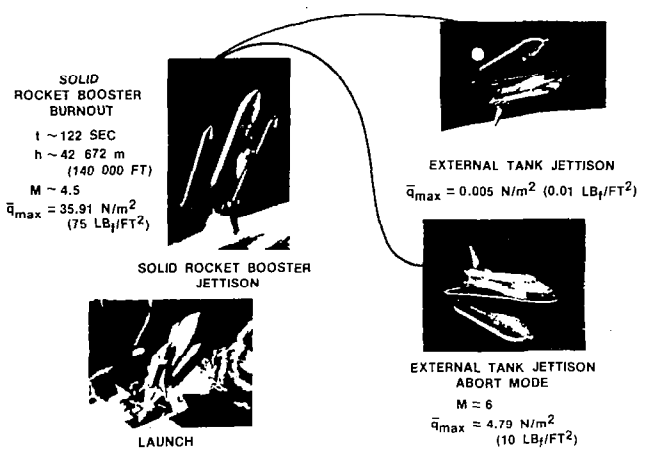

Figure 1. - Orbital flight separation mission profile.

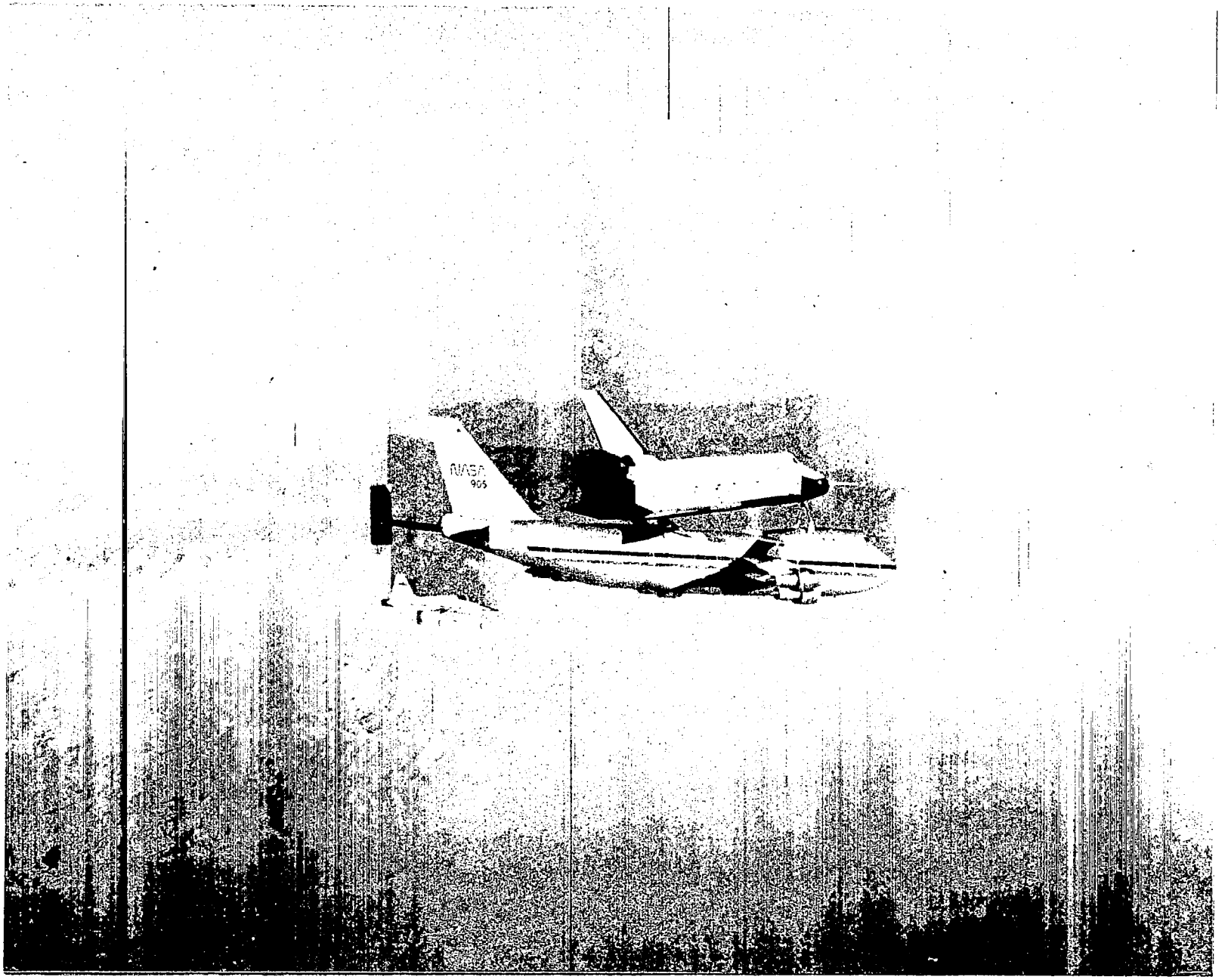

Figure 2 - Orbiter/747 configuration before release

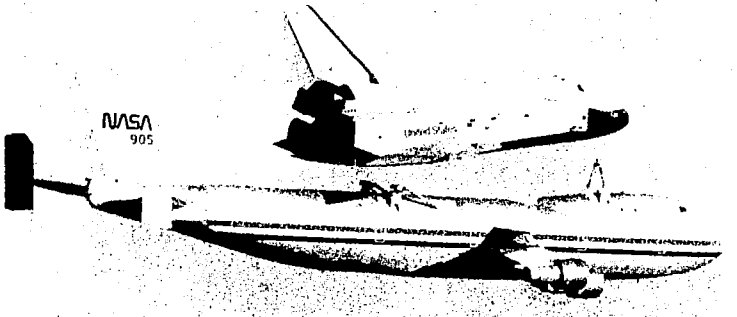

Figure 3a - View of the Orbiter/747 after release

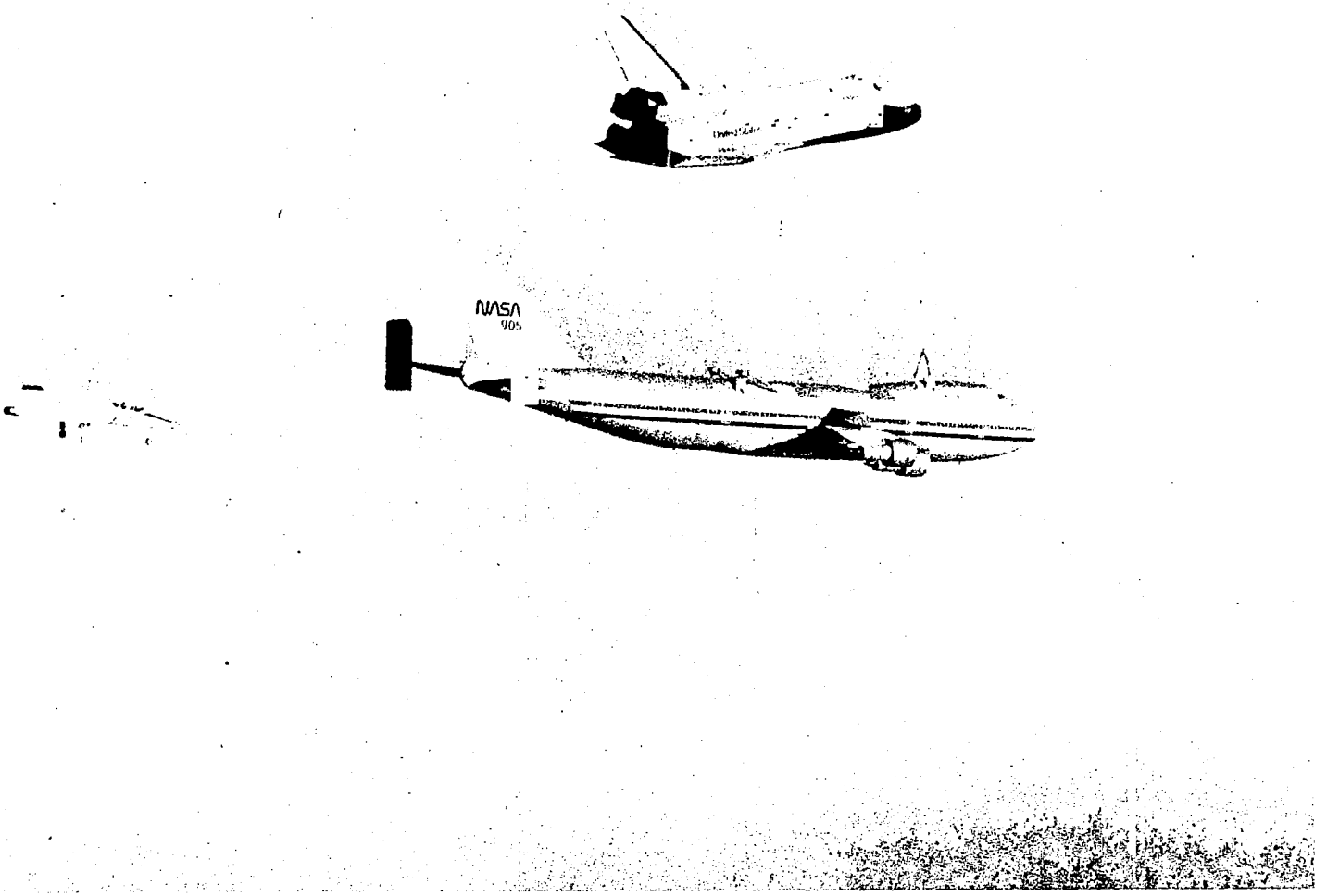

Figure 3b - View of the Orbiter/747 after release

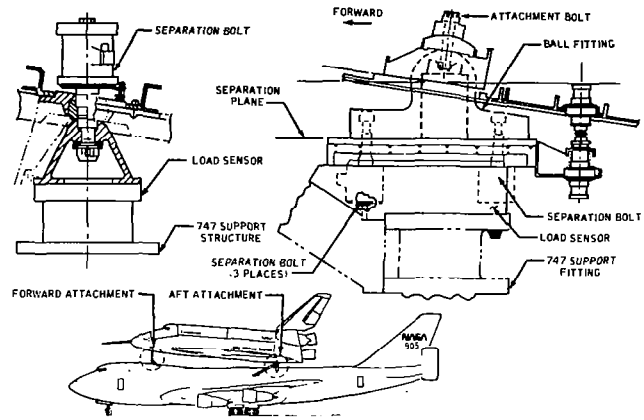

Figure 4 - Orbiter/747 separation system

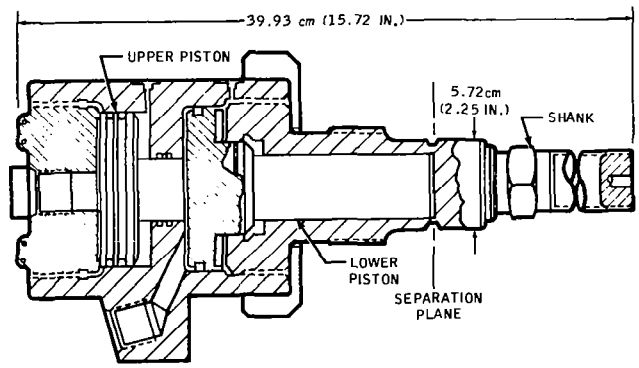

Figure 5 - Orbiter/747 separation bolts

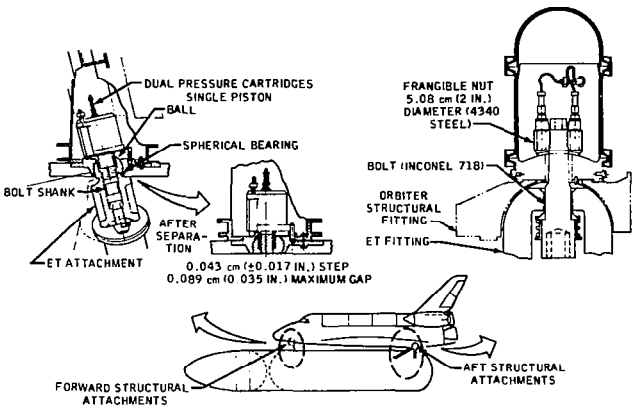

Figure 6.- Orbiter/ET separation system.

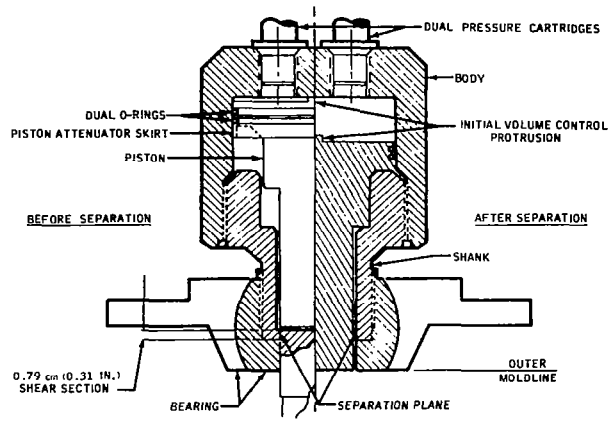

Figure 7.- Shear flange separation bolt.

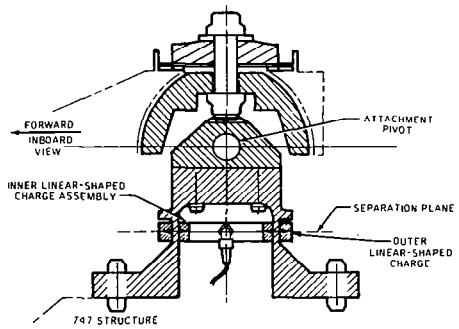

(a) Linear-shaped charge separation device.

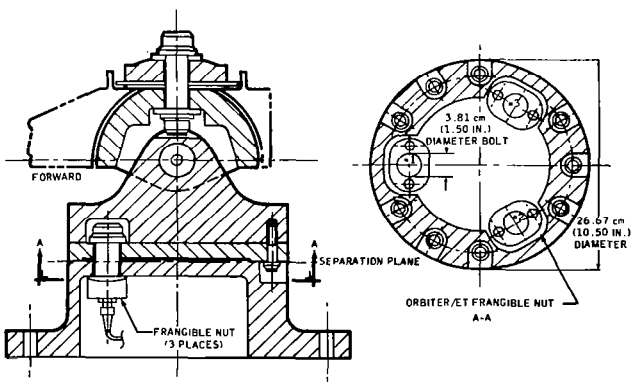

(b) Multiple frangible nut configuration.

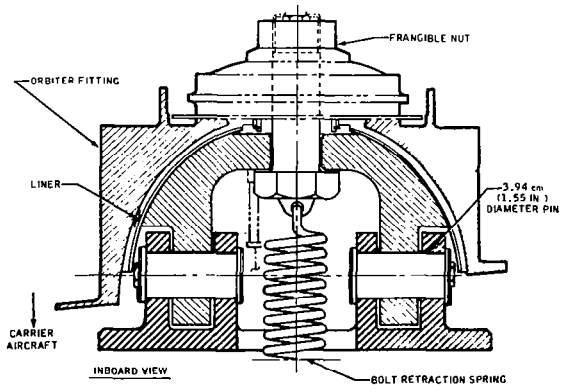

(c) Single frangible nut configuration

Figure 8.- ALT aft attachment.

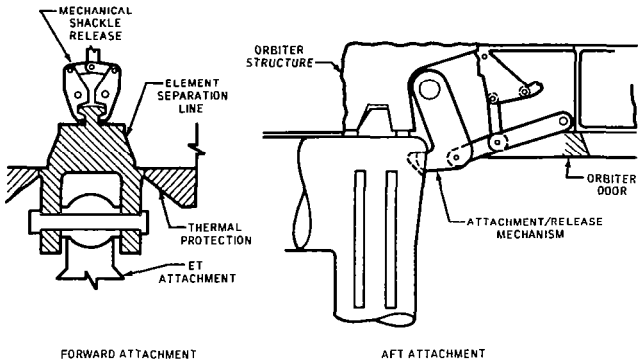

Figure 9.- Orbiter/ET structural attachments (ET request for proposal configuration).

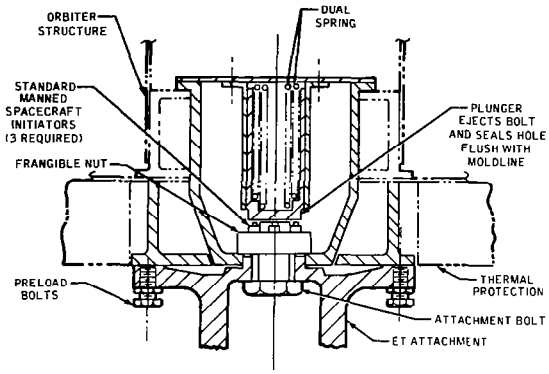

Figure 10.- Orbiter/ET forward attachment (frangible nut configuration).

SPACE SHUTTLE ORBITER SEPARATION BOLTS

By Robert S. Ritchie

Space Ordnance Systems Division
TransTechnology Corporation

ABSTRACT

Evolution of the Space Shuttle from previous spacecraft systems dictated growth and innovative design of previously standard ordnance devices. Initially, one bolt design was programmed for both 747 and External Tank application. However, during development and subsequent analyses, two distinct design evolved. The unique requirements of both bolts include: high combined loading, redundant initiation, flush separation plane, self-righting and shank attenuation. Of particular interest are the test methods, problem areas and use of subscale models which demonstrated feasibility at an early phase in the program. The techniques incorporated in the shuttle orbiter bolts are applicable to other mechanisms.

INTRODUCTION

The Space Shuttle Orbiter Separation Bolts are located as shown in Figure 1. The Orbiter/747 attachment system used for Approach and Landing Tests (ALT Bolt) has one bolt forward, three each side aft, and the Orbiter/External Tank (Shear Bolt) uses one bolt forward and one frangible nut each side aft. Development of both bolts followed similar sequences with much of the experience gained during ALT Bolt development and testing applied to the Shear Bolt.

The sequence of development testing for both bolts consisted of the following:

Cartridge Load Sizing
Separation Section Sizing
Margins Demonstration
Piston Flushness Verification
Centering Mechanism Operation
Environmental Exposure

After development, the bolts are subjected to a rigorous qualification program prior to flight certification.

ALT BOLT

The ALT Bolt, illustrated in Figure 2, has mechanical and pyrotechnic redundancy. Either cartridge will cause separation of the shank at the separation plane. The housing adapter and secondary piston are 4340 steel, nickel plated; the primary piston and shank were specified to be Inconel 718, all components are heat treated to 180 - 200 KSI. Load capacity is 141,630 lbs. tension, 11,168 lbs shear and 85,757 in-lb. in bending. The two pressure chambers are isolated such that either piston will cause the shank to separate in a tensile failure.

Separation was not a problem with the upper cartridge due to direct impengement of the cartridge output on the head of the secondary piston. The side cartridge port design initially offered sufficient gas flow restriction and pressure decay to not permit separation. The side port was subsequently enlarged to an eliptical shaped hole. Because the new shape and location of the port did not permit conventional machining, proting was accomplished using electro-discharge machining.

The second problem which casued a failure to separate was traced to the pressure cartridge. The cartridge load and subsequent consolidation pressure had been increased after several development tests. Closed bomb tests revealed that the additional loading pressure increased the pyrotechnic density such that the burn rate was reduced. The loading pressure was reduced and successfully verified by functioning the bolt with a single lower 80% loaded cartridge at low temperature.

The third corrective action was the use of a shrink fit collar at the base of the bolt housing. When the bolt was functioned with dual simultaneous cartridges, the residual energy of the primary piston slamming against the shank caused the shank and housing threads to yield. As deliverable hardware was complete at this time, a shrink fit collar was added on the outside of the housing which increased the hoop strength eliminating any yield of the housing.

A total of 35 ALT Bolts were expended during the five Shuttle Approach and Landing Tests recently completed. Thirty-four bolts were successfully tested in qualification and seventeen were consumed in development.

SHEAR BOLT

Analysis of the post-separation plane interface indicated that the .1 inch wide by .2 inch deep groove of the ALT Bolt was not tolerable due to aerodynamic boundry layer disturbance Additionally, to enhance reliability, a single piston, dual cartridge bolt was configured as shown in Figure 3. Shearing of the bolt with a punch and die technique allows the piston to fill the hole made by the separated end of the shank. Several sub-scale and full-scale specimens were sheared under static and dynamic loading conditions to confirm repeatability of a straight cylindrical shear plane.

The Shear Bolt components are fabricated from Inconel 718 forgings. The primary piston and shank material was specified due to flight environments, and the housing for compatibility and to eliminate the need for additional processing. Sizing of the break section and ultimate load testing was accomplished on a specially designed test fixture which applied tension and shear loads simultaneously. Load capability of the Shear Bolt is 166,740 lbs. tension and 127,400 lbs. shear applied simultaneously.

Initial concerns for the Shear Bolt were the spread of margins, (single 85%, dual 120% loaded cartridges) and piston flushness (plus/minus .010 inch). After several successful development tests, a failure to separate occurred. Investigation revealed a possible mechanical interference of the bolt housing and shank which increased the initial free volume. The design interference was corrected and the free volume reduced. The design change was verified by successful separations with single 80% and dual 130% loaded cartridges.

Experience from the shank/housing thread problem on the ALT Bolt was utilized in the Shear Bolt by increasing the cross section of the piston attenuation skirt and incorporating a buttress thread to minimize radial loads.

Primary piston attenuation and flushness within .020 inch at end of stroke was a difficult requirement. Due to the margin requirement with a single cartridge, the piston has considerable energy after separation with dual cartridges. The piston has a skirt which flanges outward upon inpact with the shank, slowing the piston and absorbing residual energy. Final piston position is determined by deformation of the mating surfaces. Final dimensions were determined by emperically tuning each shot until acceptable and repeatable flushness was achieved.

PRESSURE CARTRIDGES

The pressure cartridge for the two bolts are almost identical (See Figure 4), except for overall size to accommodate different pyrotechnic loads. The cartridges are of modular design utilizing the NASA STANDARD INITIATOR (NSI-1). Construction and materials are standard for spacecraft applications. The output charge is SOS 109, selected for its stability and previous experience. The cartridges produce pressures up to 50,000 PSI in the bolt initial volume. The pressure cartridges are fabricated from homogeneous lots of materials and subjected to hydrostatic, electrical, leakage, X and N-Ray inspection. Approximately 10% of each lot is functioned in a closed bomb for acceptable and uniform pressure/time characteristics.

CENTERING MECHANISM

The forward Separation Bolts are installed in a spherical bearing, Figure 5, which provides angular displacement while installed. After separation the centering mechanism must re-align the bolt, making the piston end flush with the external surface of the spacecraft. The envelope for the centering mechanism made the use of high strength alloys mandatory.

In order to achieve forces in the plungers which prevent displacement under accelerations, Cobalt Alloy was selected for the spring wire. This material has a tensile strength of 300,000 psi.

SHANK ATTENUATOR

The separated bolt shank has considerable residual energy when the bolt is functioned with two cartridges. In the Orbiter/747 configuration the bolt shanks had to be easily removable and cause no permanent damage to the structure. A ring of 6061-T651 aluminum was designed to be extruded between the shank and the mating structure. The deformation of the ring absorbed most of the energy and the difference in materials permitted easy removal of the shank. Although not required for the External Tank, the attenuator was retained in the design to eliminate the possibility of any re-bound of the shank. The attenuator is shown in Figure 6.

CONCLUDING REMARKS

Although the principle of cartridge actuated piston type bolts has been used for spacecraft applications for some time, the Space Shuttle Orbiter Separation Bolts represent a growth in loads, operating pressures, material strengths and mechanical features which have never previously been combined into operational devices.

To ensure continued reliability, in addition to testing conducted during development and qualification of the initial flight lots; subsequent hardware will maintain stringent process control, extensive use of non-destructive test techniques and destructive sample testing.

ACKNOWLEDGEMENTS

Acknowledgements are given to NASA, who conceived the Space Shuttle concept which originated the need for the Orbiter Separation Bolts and Rockwell International/Space Division, who generated the detailed bolt functional requirements.

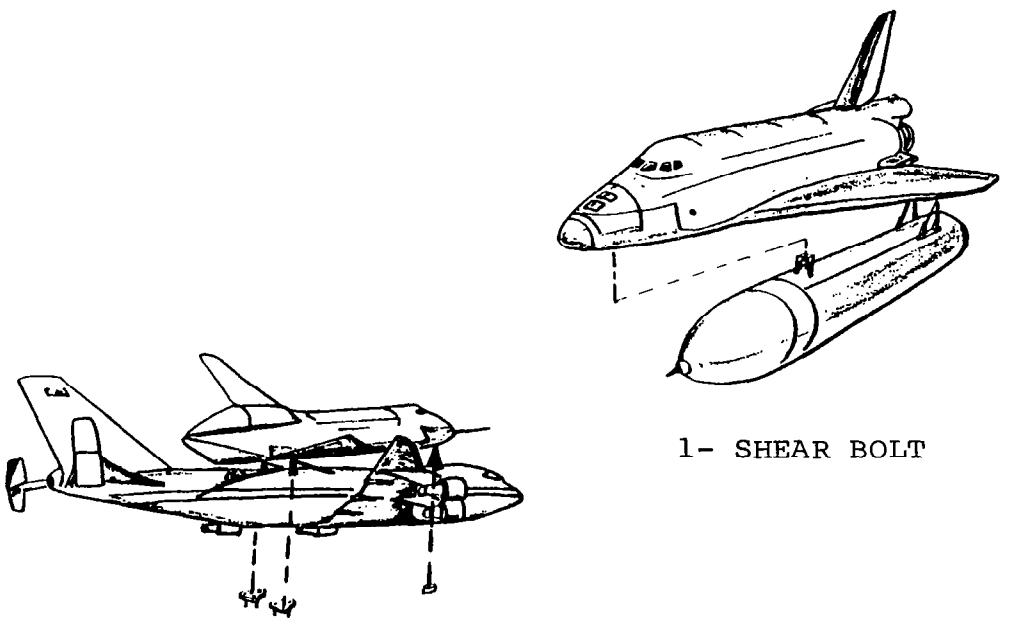

FIGURE 1
ORBITER ATTACHMENTS

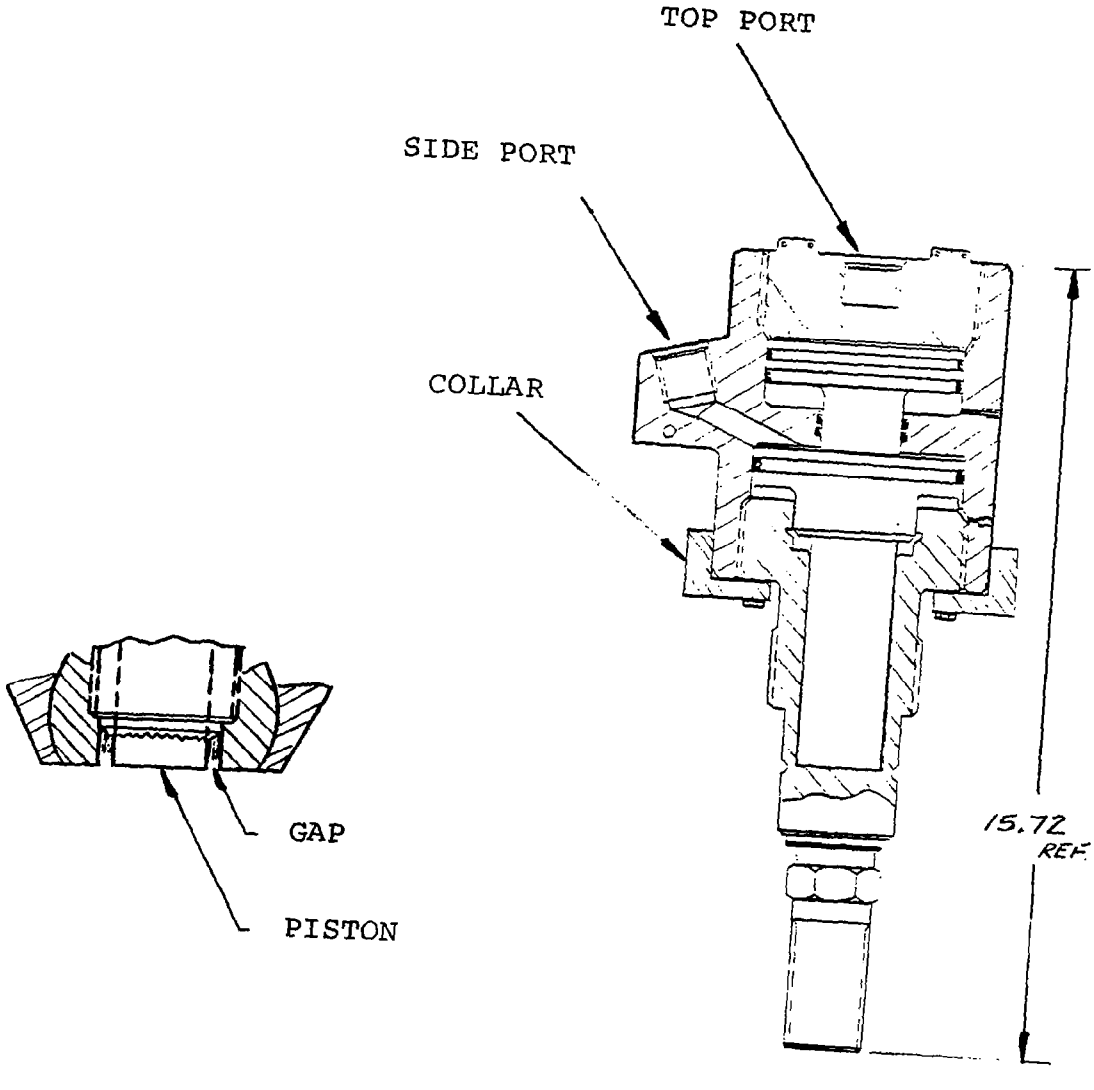

FIGURE 2

ALT BOLT

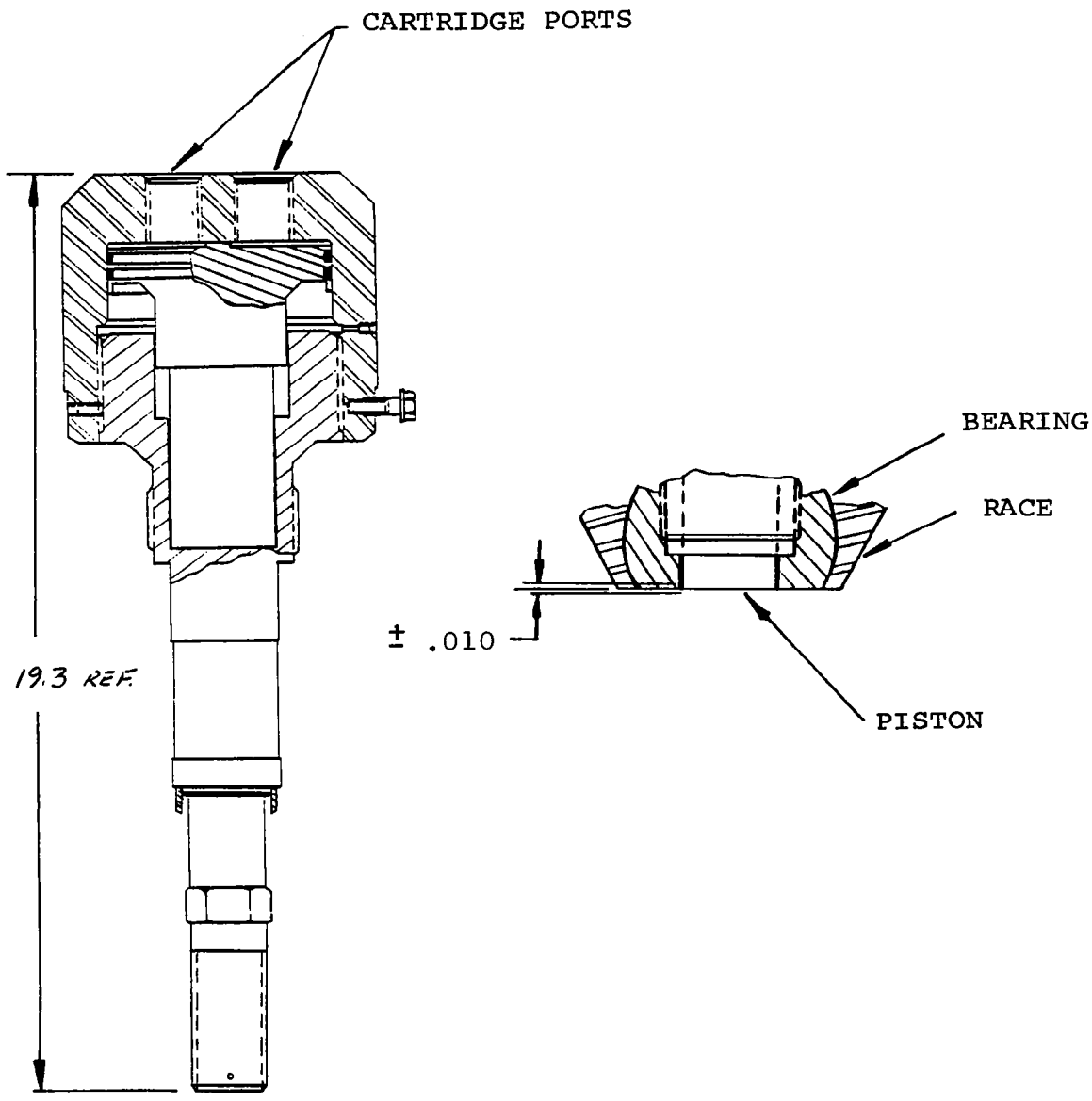

FIGURE 3

SHEAR BOLT

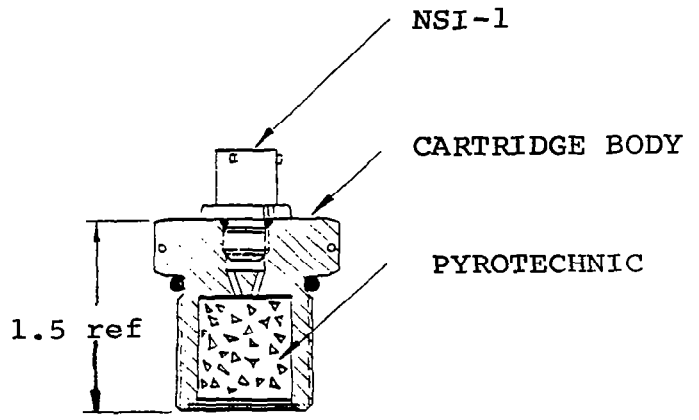

FIGURE 4 - PRESSURE CARTRIDGE

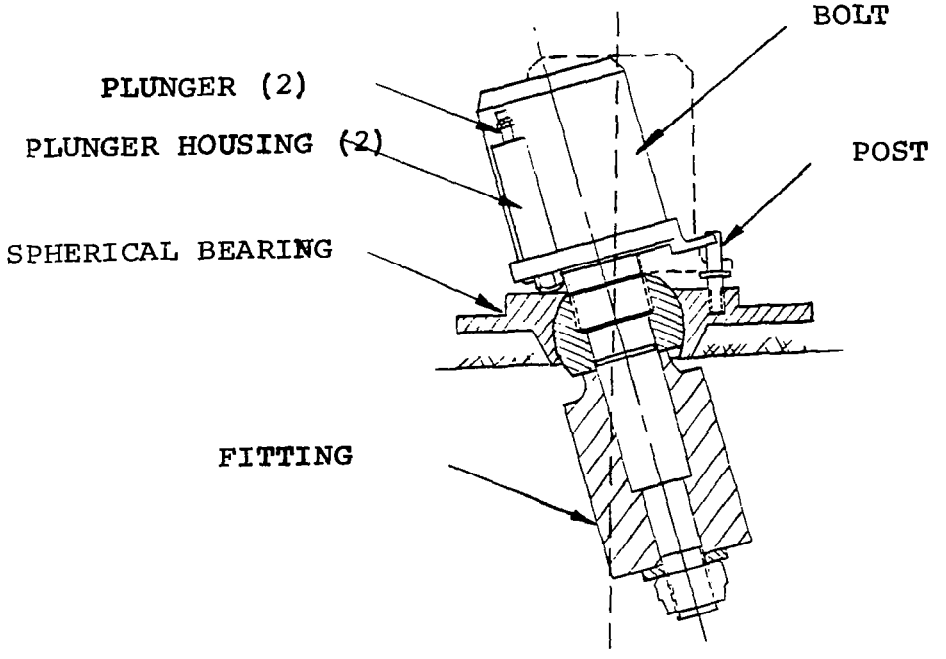

FIGURE 5 - CENTERING MECHANISM

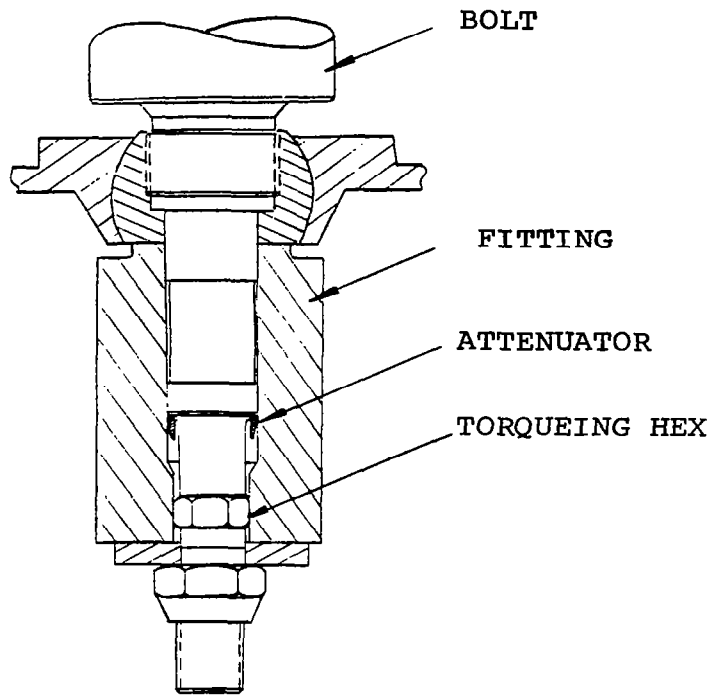

FIGURE 6 - ATTENUATOR

PNEUMATIC PRELOADED SCANNING SCIENCE LAUNCH LATCH SYSTEM*

By J. C. Kievit

NASA Jet Propulsion Laboratory

ABSTRACT

Sophisticated spacecraft science payloads mounted to scanning or pointable platforms required preloaded platform launch latches with a low shock release. Brainstorming and trade studies conducted by JPL and Northrop Aerospace resulted in a relatively simple system using a preloaded pneumatic piston latch with a pyrotechnic valve release. The system was the only candidate that met all the imposed requirements utilizing reliable state-of-the-art components. This paper traces the development of the latch system from its first use on JPL's Mariner '69 Mars Flyby Spacecraft through its most recent use on the Voyager Spacecraft that will fly to Jupiter and Saturn.

INTRODUCTION

A pneumatic preloading latch system has successfully met the need for a high-reliability, low-shock launch latch for science instrument scanning platforms on JPL spacecraft for all missions since Mariner '69. The increasing size, weight and complexity of scanning payloads on interplanetary spacecraft demands special attention to launch load transfer to stationary structures. The load transfer must consider the control of instrument launch environment and releases the platform on command after the boost phase of the mission. Special problems were preloading of joints, control of pyro shock, cleanliness of release, reliability and testing of the system. Studies conducted during the first design of the pneumatic latch showed non-preloaded joints, rapid release of strain energy and close coupled structure borne pyro shock were the contributors of environmental conditions that needed to be eliminated in a science latch. Several devices, such as pyro actuated release nuts, explosive bolts and pinpullers, failed to meet at least one of the criteria established for an acceptable system. A gas pressurized preloading cylinder type of latch met all launch load requirements. The release event using a pyrotechnically actuated valve to bleed off the nitrogen gas resulted in a soft release with low shock levels at the instruments.

---

*This paper presents the results of one phase of research carried out at the Jet Propulsion Laboratory, California Institute of Technology, under Contract No. NAS 7-100, sponsored by the National Aeronautics and Space Administration.

This paper presents the history and evolution of the pneumatic latch system. Some of the testing and flight application information are also presented. Several test problems and pieces of information relative to challenges of the design are also discussed.

BACKGROUND INFORMATION

Scanning science platforms in excess of 50kg have been flown on several JPL spacecraft. The normal boost vehicle induced environment on such a platform is usually in excess of the load carrying capability of the support bearings or structure needed for other phases of the mission. A structural mount in parallel to cruise load path is required for launch. The device used to latch the platform to the structure must meet a long list of constraints and desirable traits to be selected for use. The specific requirement used in selection of a pneumatic latch were:

1. ability to carry the launch loads to the latch points;
2. latch joints must be linear through the load range;
3. release should be slow to minimize shock from stored energy;
4. electrical power for latch release should conform to pyro-type pulse;
5. contamination and release effects on spacecraft should be minimized;
6. device should have a relatively long shelf life;
7. maintenance should be simple for successive uses;
8. latch up and monitoring of preload should be simple and continuous;
9. reliability and failure modes should be understood;
10. flight telemetry should be built-in and simple;
11. weight and cost should be compatible with aerospace technology.

Initial studies and a later reevaluation of available release deivces considered four devices as prime candidates for the job. They were: 1) pyro release nuts; 2) pyro pinpullers; 3) ball detent locks (Quantic Industries type); and 4) preloading pneumatic latch devices. All of these devices are used in todays spacecraft for various functions and a strong case can be made to use each one as a platform latch. Trade studies determined that the pneumatic latch was able to meet all requirements and was definitely superior to other latches in two major areas. First, the pneumatic latch gave the best controlled release with little or no pyro shock effects. Second, the pneumatic latch had better reuse capability. The only drawback seemed to be in the area of weight required to make a personnel safe pressure vessel for the preloading cylinder. In summary, the pneumatic latch was chosen and has been used in various configurations on scan platforms on all JPL interplanetary spacecraft since 1969.

DETAIL DESCRIPTION

Stress related details of the design of the pressure vessel and latch components is all state-of-the-art technology and will not be discussed except

in relation to philosophy of the configuration. The first pneumatic scan platform latch designed at JPL contained a single acting piston and return spring, a torsion spring pivoted tee-bar latch, interconnecting plumbing, pyro release valve, pressure transducer and various load and tie-down hardware. The cross-section of a typical Mariner spacecraft cylinder and the pneumatic schematic are shown in Figure 1.

This unit was used satisfactorily on Mariner '69, '71 and '73. System tests performed during the development program proved that the performance was exceptional. Leakage of nitrogen gas past the viton piston seals was so small that it could not be measured in a 30-day pressure monitoring test. Two items of interest showed up in the test program that caused further development effort. First, the restrictor used to release the gas to control the unlatch rate would have to be dual function; one, trap debris from blow-by of the pyro valve piston without clogging; two, control flow. This was accomplished by using a sintered porous plug of 25-50 micron filter material in the line in front of the 5-10 micron plug used to produce a controlled pressure drop. This approach was successfully tested and has been used in all the systems to date. The second item of interest was the pressure fill valve, shown as part of the pyrotechnic valve in Figure 2, did not seal reliably if torqued to specification on successive uses. To cure the problem, the ball valve seat was lapped to renew the sealing surface and an O-ring sealed cap was added to the fill port. These measures combined with a procedure to reduce the torque on the ball valve any time it was closed except during final prelaunch pressurization eliminated the problem. One peculiarity that showed up in flight was a delayed tee-bar withdrawal after bleeddown. The flight telemetry data provided by an event switch on the rotating tee-bar did not trip for a few minutes after the pressure bleed-off. Testing at JPL to check this phenomenon showed the cause to be long-time cold flow of the O-ring seals into the machining imperfections of the mating surface. The breakout force was not overcome immediately by the piston return spring resulting in a delayed release of up to two mintues. No corrective action was taken to change the design once the situation was understood but the event time was increased to allow sufficient time for operation.

For the Viking Program, a complete redesign was undertaken resulting in the cross-section and schematic shown in Figure 3. The items of special note were the double acting piston design that eliminated the time delay phenomenon noted above and weight reduced components that used light metal alloy parts in place of all steel construction. A further departure from previous designs was the use of elastomer sealed bolted connections between the tubing and the cylinders instead of an all welded design. This reduced the cost of parts and made system cleaning and maintenance much easier. The seal in the joint was a special viton face seal washer "Gaskoseal" provided by Parker Seal Company used as shown in Figure 4. It should be noted that although seven of these seals were used in the system, no leakage problems were ever encountered. The double acting piston approach provided extra margin for unlatch because the differential area of the piston developed considerable unlatching force as pressure approached equalization on both sides of the piston. A typical blow down event is shown in Figure 5 where the reduced data indicated a 200-pound (890 N) additional force to move the piston. In the event of a piston bind, the pressure would tend to increase on the large area side of the piston and raise the total unlatching force to approximately 800 pounds (3560 N).

The evolutionary process of the scan platform latch was ongoing for the Voyager spacecraft. In this case a swingout boom mounted scan platform was used that required an axial withdrawal of a collet latch instead of the previously used rotating tee bar. This change was made because the spring deployed boom could introduce forces that prevented a gap from developing between the tee bar and its mating part preventing its movement. The system made use of all the previous developments. The Voyager latch cross-section is shown in Figure 6. Development of this system was uneventful and modifications of the operation were minimal. An item of interest for the mechanism designer is the collet made from titanium with some interesting manufacturing innovations. It was manufactured as a turned part, the nine finger slots were made by a single electro discharge machine pass and it was shotpeened on the inside to open the fingers of the collet to allow easy stud withdrawal. The Voyager spacecraft launched in 1977 unlatched its platform according to plan and all platform mounted science worked successfully.

SAFETY RELATED PROBLEMS

As mentioned earlier in the paper, the methods of calculating stresses in pressure vessels is well known but complications arise when pressurized units are used around personnel. One of the big problems of weight reduction of the pneumatic latch is that it is often under full pressure when the spacecraft is being worked on. Safety requirements are therefore enforced on the design. The latches shown for Viking and Voyager in this paper are admittedly heavy since they met ASME boiler code requirements, i.e., Proof Test to twice working pressure with burst capability of four times working pressure. This seems an undue penalty but if ignored the operational approvals to use the equipment may be a greater problem than the extra weight. No specialized equipment is required to support a pneumatic latch since JPL fills from standard "K" bottles of clean nitrogen.

CONCLUDING REMARKS

The penumatic latch concepts presented in this paper give the mechanism designer a versatile tool for use as a launch latch in space applications. The concepts involved contain no statistical qualification requirements or shock tests as is often the case with direct acting pyro devices. Careful design builds in reliability and functional margin that assures successful operation.

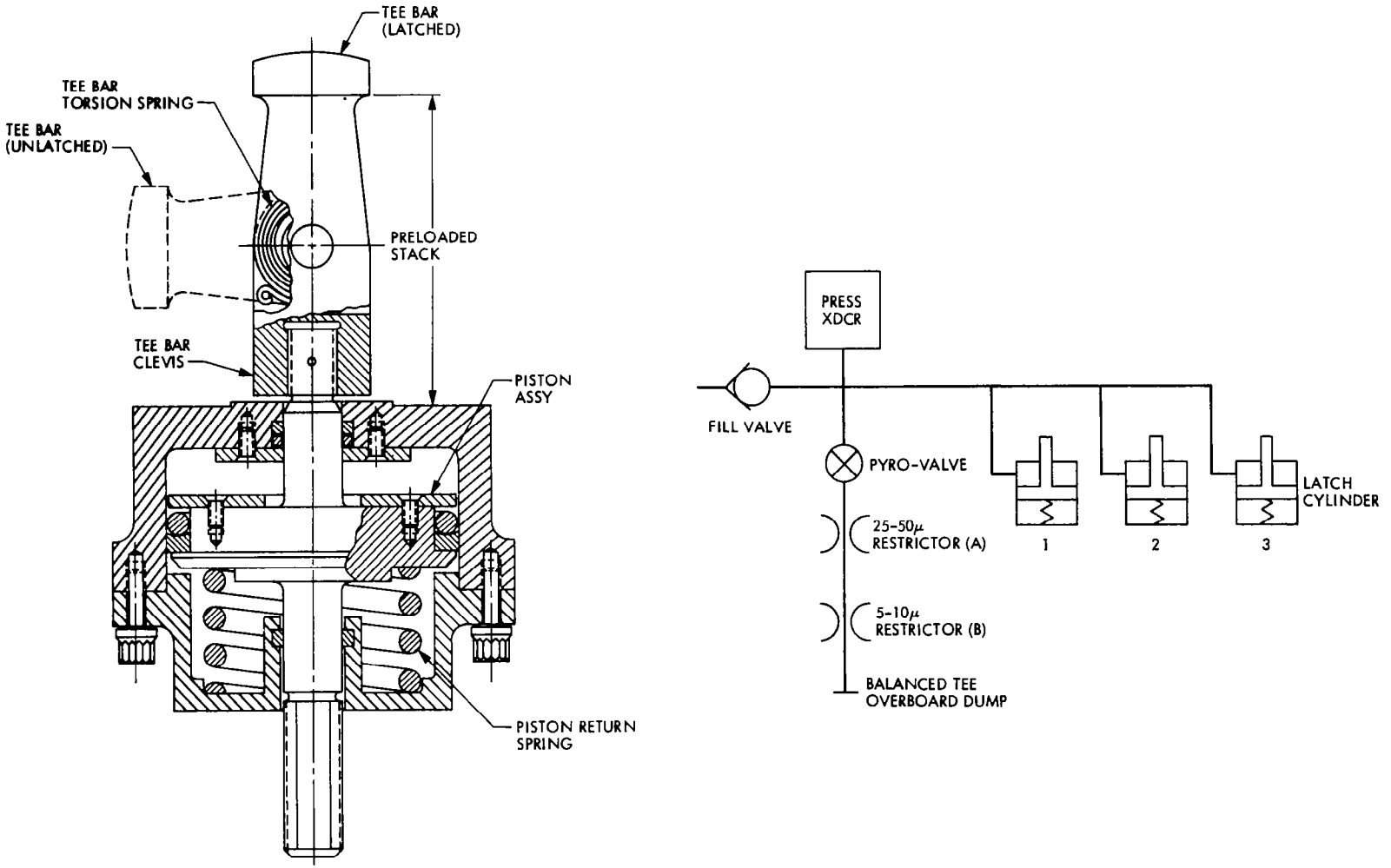

Figure 1. Mariner Pneumatic Latch System and Schematic

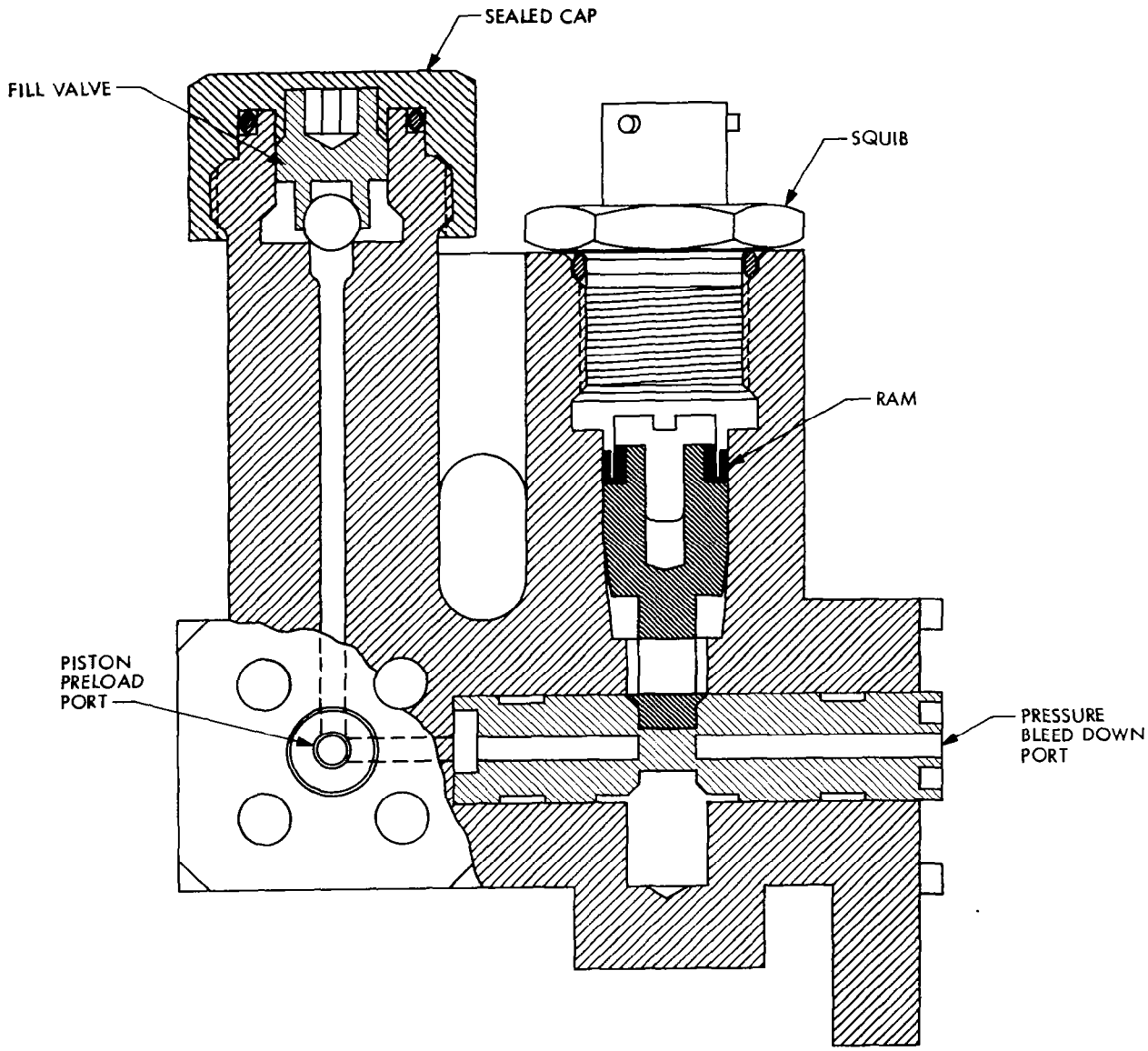

Figure 2. Normally Closed Pyro Valve Assembly

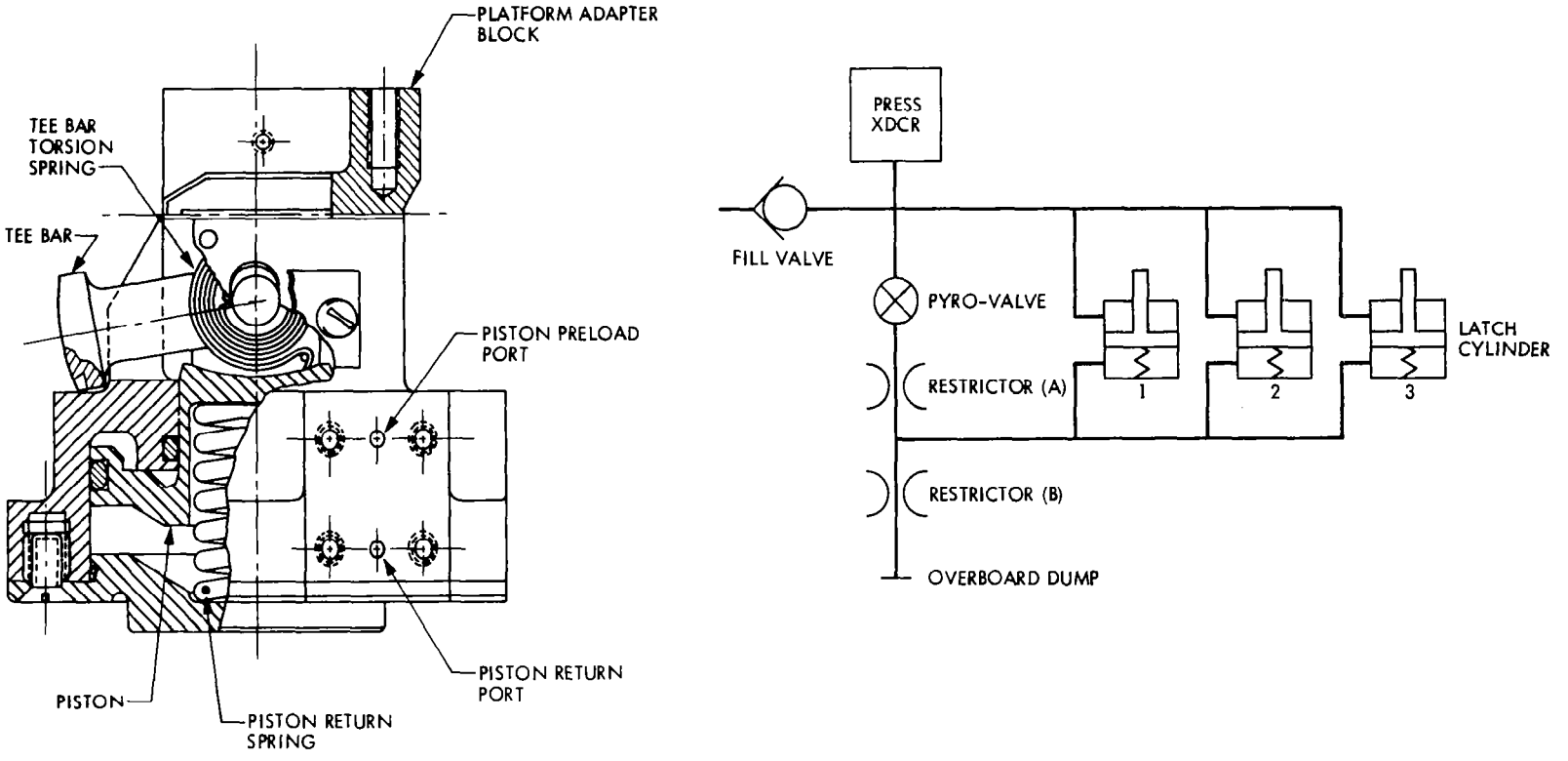

Figure 3. Viking Pneumatic Latch and Schematic

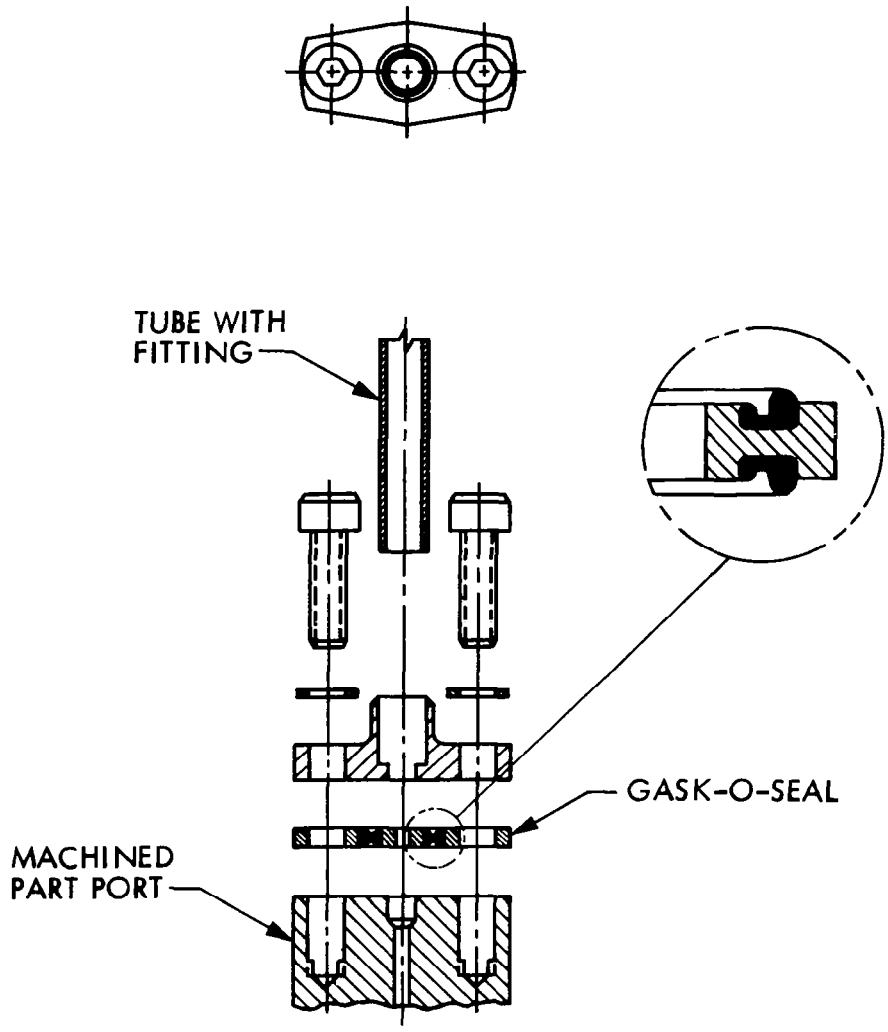

Figure 4. Gask-O-Seal Joint

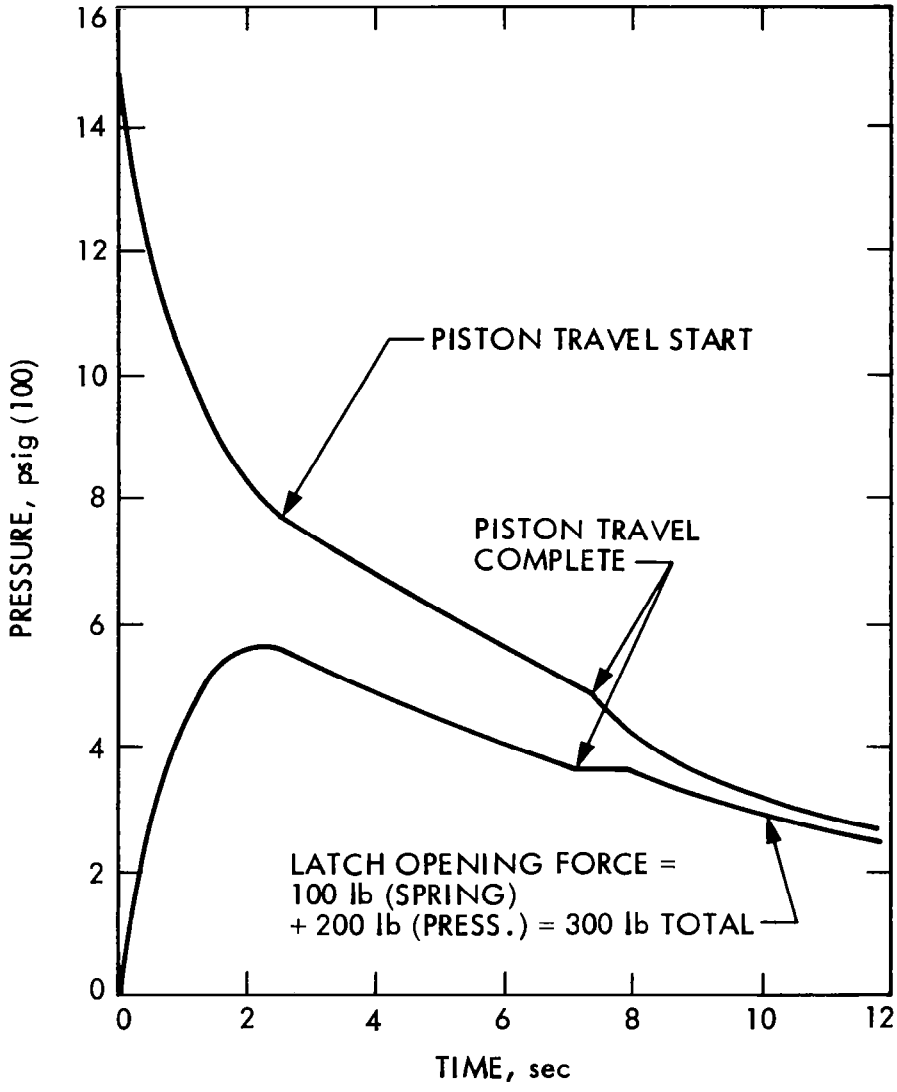

Figure 5. Viking Orbiter System - Struc/Sep Review Scan
Latch Blow Down Cycle

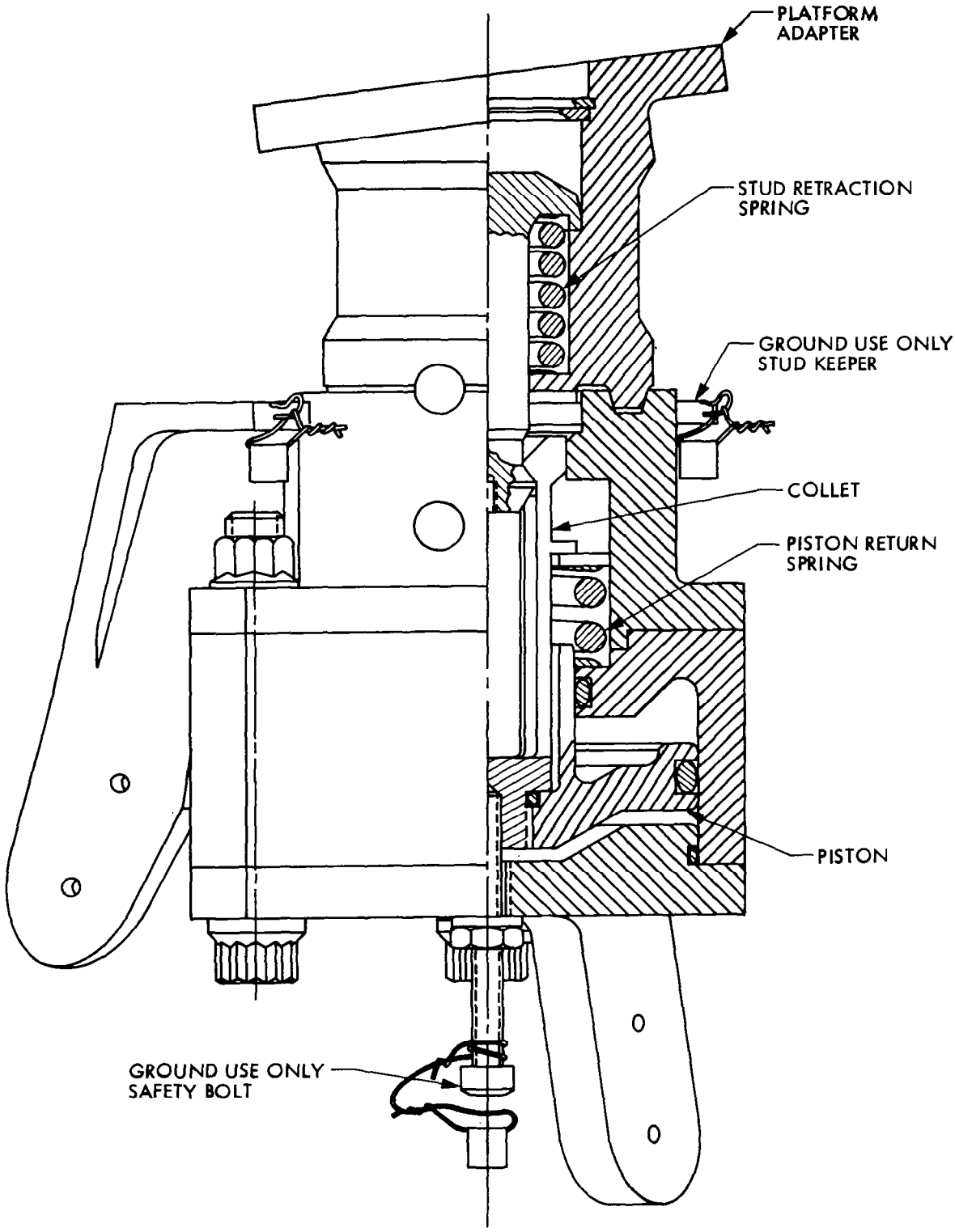

Figure 6. Voyager Scan Platform Latch

SPACE SHUTTLE PAYLOAD HANDLING

ON THE LAUNCH PAD

By Andrew Rado

FMC Corporation

ABSTRACT

The NASA space shuttle launch facility must provide access to a payload in the orbiter payload bay and be capable of installing or removing a payload. To comply with this requirement, launch facility designers conceived of a payload change-out room. The payload change-out room (PCR) will provide a controlled environment and the structural platform for a payload ground handling mechanism (PGHM), which will perform the actual installation or removal of the payload.

Design efforts to develop a PGHM compatible with the free-standing launch vehicle and the payload change-out room housing have had to overcome problems uncommon to the design of material-handling equipment for other uses. The PGHM must compensate for structural deflections resulting from wind forces and the transfer of the payload weight and provide protection for the payload, the orbiter, and the PGHM itself against damaging impacts that could occur during such deflections.

SPACE SHUTTLE LAUNCH FACILITY

The space shuttle launch pad now under construction at the Kennedy Space Center must provide access to the orbiter and its payload from the time the orbiter is emplaced until moments before launch.

Immediate access to the orbiter payload bay or to the payload will be through a payload change-out room (PCR) which will seal the payload bay section of the fuselage and the payload bay doors. Use of airlock systems will continuously maintain the environment in the payload change-out room at clean-room standards to prevent contamination of the orbiter payload bay when the payload bay doors are opened.

The payload change-out room (Figure 1) will house the machinery which will be the access platform to the 60-foot-long payload bay in the orbiter. The machinery will also serve as the payload ground handling mechanism (PGHM) which will emplace the payload within or retrieve the payload from the orbiter.

The PGHM will handle payloads weighing up to 65,000 pounds, measuring up to 15 feet wide by 60 feet long and typically consisting of one to five structurally independent modules.

PGHM PERFORMANCE REQUIREMENT

The launch vehicle, consisting of the orbiter, the external fuel tank, and two solid rocket boosters, is a free-standing structure, which during launch will be supported by a modified Saturn mobile launch pad. Like any free-standing structure, the launch vehicle will deflect under a load, and, if exposed to gusty winds, will oscillate or sway. The swaying motion will occur at a rate equal to the natural frequency of the free-standing structure. The amplitude of the motion will depend on the strength and direction of the prevailing winds. Unfortunately, the orbiter is most flexible in the direction for the payload transfer operations.

The natural frequency of the free-standing launch vehicle is calculated as approximately 30 cycles per minute. Under hurricane conditions, the free-standing launch vehicle will sway 6 to 7 inches from its static position. Payload transfer operations between the orbiter and the PCR, however, will be limited to conditions in which vehicle displacements are 3 inches or less as measured at the top of the payload bay.

The payload change-out room housing the PGHM will similarly respond to wind forces; however, relative to the orbiter displacements the PCR deflections will be negligible. The occurrence of the orbiter displacements dictate the following performance specifications:

- When a payload is to be placed in or retrived from the orbiter on the launch pad, the PGHM supported by the PCR structure, must perform the load transfer operation without exposing the payload or the orbiter to critical impact forces resulting from a collision of the relatively stationary PCR with the swaying orbiter.

- During the load transfer process, the PGHM must yield space for the orbiter deflections to prevent any structural interference between the orbiter and the payload change-out room which could cause undesired strain buildup in either of the structures as the weight of the payload is shifted from the PCR to the orbiter payload bay.

The payloads will be fastened in the orbiter payload bay (see Figure 2) through special payload retention fittings attached to the longerons on both sides of the fuselage. The payload retention fittings resemble conventional journal-bearing pillow blocks. The payloads will mate with the fittings through the 3.25-inch-diameter trunnions which are integral parts of the payload cradle structures. During a load transfer, the payload trunnions must be accurately positioned in line with the payload retention fittings. Bumpig or forcing of the payload trunnions against the retention fittings could result in damage to the payload or to the launch vehicle.

The PGHM must provide continuous position control between the payload and the orbiter during all phases of the load transfer.

DESIGN SOLUTION

Two solutions to the problems caused by the uncontrolled relative motions of the orbiter and the payload change-out room were considered:

- Rigidly clamp the orbiter to the payload change-out room, eliminating any uncontrolled relative motion during load transfer
- By a suitable means, synchronize the movement of payload with the motion of orbiter, thereby preventing any uncontrolled relative motion.

Because early evaluation of the first solution revealed a high potential for damage to the orbiter, the second suggested solution was selected as the basis for the PGHM concept.

The PGHM (Figure 3) will essentially consist of the bridge and stem assemblies, which will position and support the payload, and the load transfer equipment, which will install or retrieve the payload. Coupling devices will fix the load transfer equipment to the stem, to hold the payload in a fixed position, or to the orbiter, so that the payload will move with the orbiter while the weight of the payload is supported by the orbiter and/or the PGHM.

In transferring a load from the PGHM to orbiter, the PGHM, carrying the payload, will move from the rear of the PCR to the front by rolling on support rails with the load transfer equipment coupled to the stem. By completion of this move, the payload will be partially inserted into the swaying orbiter payload bay, a safe distance from the retention fittings on the orbiter.

At this point, four connecting links will be manually attached to the orbiter, and the respective locking mechanisms will couple the load transfer equipment (with the payload) to the orbiter and decouple it from the stem. Thus coupled to the orbiter, the load transfer equipment and the payload will follow the motion of the orbiter, eliminating any significant relative displacement between the payload retention fittings on the orbiter and the trunnions on the payload which remain supported by the PGHM load transfer equipment. Lateral and vertical linear actuators on the PGHM load transfer equipment will then position the payload trunnions coaxial with the payload retention fittings on the orbiter. After the retention fittings are secured, the weight of the payload will be released onto the orbiter.

The PGHM concept thus compensates for relative displacements between the orbiter and the PCR at the PGHM stem and load transfer equipment interface, and eliminates potential impacts between the payload trunnions, the support fittings on the PGHM, and/or the retention fittings on the orbiter.

PGHM LOAD TRANSFER EQUIPMENT

A payload positioned on the PGHM will be supported by support fittings (see Figure 3) which in turn will be supported by two payload support beams, one on either side of the PGHM.

Vertical and horizontal positions of the support beams will be controlled by the top and bottom floating beams. The floating beams will be supported in the vertical position through their housings by two sets of jackscrews. One set will locate the housings relative to the strongback beams supporting the housings; the other set will locate the strongback beams relative to the PGHM stem.

The horizontal or lateral position of the floating beams (Figure 4) will be controlled by linear actuators and the lateral position of the common connecting beam on each side of the PGHM. The floating beams will be connected to the common connecting beams by means of linear actuators. The lateral position of the support fittings relative to the common connecting beams will be adjustable by extending or retracting the actuators. The floating beams will move the support beam, which in turn will change the position of the support fittings.

The common connecting beams will have two modes of operation. In the first mode, they will be locked in a fixed position to the strongback beams through locking mechanisms located at each end (Figure 5). In the second mode, they will be locked to a slide mechanism on each end of the strongback beams.

In the first mode, the lateral position of a payload held by the PGHM will depend on the movement of the stem; in the second mode, it will depend on the motion of the slide mechanisms on the strongback beams. Using a set of connecting links installed between the orbiter and the slide mechanisms, the payload will follow the lateral motion of the orbiter without any significant uncontrolled relative displacement between the orbiter and the payload. Load transfer will thus be smooth and dynamically undisturbed.

COMMON CONNECTING BEAM LOCKING MECHANISM

As described above, the lateral motion of the payload will depend on the freedom of motion of the common connecting beams. The position of the locking mechanisms (Figure 5) will control the motion of the common connecting beams and the dynamic loads imposed on the payload and the orbiter through the orbiter connecting links.

The basic function of the common connecting beam locking mechanisms will be to move the payload and part of the load transfer equipment from a standstill into a harmonic oscillation (or vice versa). In either movement, coupling or decoupling forces will necessarily be applied gradually to minimize dynamic amplification and to maintain the inertia loads on the payload and on the orbiter connecting links below a predetermined limit.

The common connecting beam locking mechanism concept is based on the gradual application of a spring force to couple the end of a common connecting beam to a slide mechanism moving with the orbiter. The locking mechanism will consist of an actuator rod mounted on the common connecting beam through linear bearings and positioned by a linear actuator, also mounted on the common connecting beam. When locked to the strongback beam, the common connecting beam will be restrained in the lateral direction by the engagement of the actuator rod in a slotted cam plate attached to the strongback beam.

When locked to the slide mechanism, the actuator rod will disengage from the slotted cam plate. A pair of cam followers will be pressed by the actuator rod against a V-shaped cam on the slide mechanism through a stack of disk springs. As the force on the springs is increased, proportionately higher lateral forces will move the slide mechanism relative to the common connecting beam. The length of the slotted cam plate will be adjustable so that the common connecting beam will become free of the strongback beam when sufficient force is developed through the spring stack to hold the common connecting beam in static equilibrium by the orbiter connecting link connected to the slide mechanism. As the spring stack force increases, the common connecting beam will move with the slide mechanism and gradually follow the motion of the orbiter. At fully rated spring stack force, there will be no slippage between the common connecting beam and the slide mechanism; therefore, the payload will track the motion of the orbiter.

A common connecting beam locking mechanism will be placed on each end of the two common connecting beams, with each slide mechanism coupled to the orbiter through a separate orbiter connecting link attached to the orbiter near the the forward and aft payload bay bulkheads. Assuming rigid body conditions for both the orbiter payload bay and the PGHM load transfer equipment, a payload supported by the PGHM will have no displacement relative to the retention fittings.

STRAIN-RELEASE MECHANISM

The bottom of the PGHM stem will deflect horizontally as loads increase on the PGHM floors and platforms. This deflection will be accumulative to the relative displacements between the orbiter and the PCR and in some cases could be binding. The PGHM will therefore be clamped to the PCR structure (Figure 3) both at the top support rails and at the PCR floor.

Using the clamps, a change-of-load condition on the PGHM will not cause significant relative displacements when the payload fittings are critically close to the orbiter; however, a locked-in strain condition will be generated which could cause lurching of the PGHM if the clamps are subsequently released without control. The strain-release mechanism will prevent this sudden motion.

The rail clamp will be positioned relative to the bottom of the PGHM stem by means of a jackscrew assembly. To release a locked-in strain, the jackscrew will be actuated in the direction which allows the stem to relax. After the strain between the stem and the rail clamp is eliminated, the rail clamp can be opened without the threat of sudden lurching of the structure.

ACKNOWLEDGEMENT

The author wishes to acknowledge the contributions made by the FMC project team and the assistance of Mr. Bill A. Tolson, NASA Design Engineering Directorate, Kennedy Space Center, Florida.

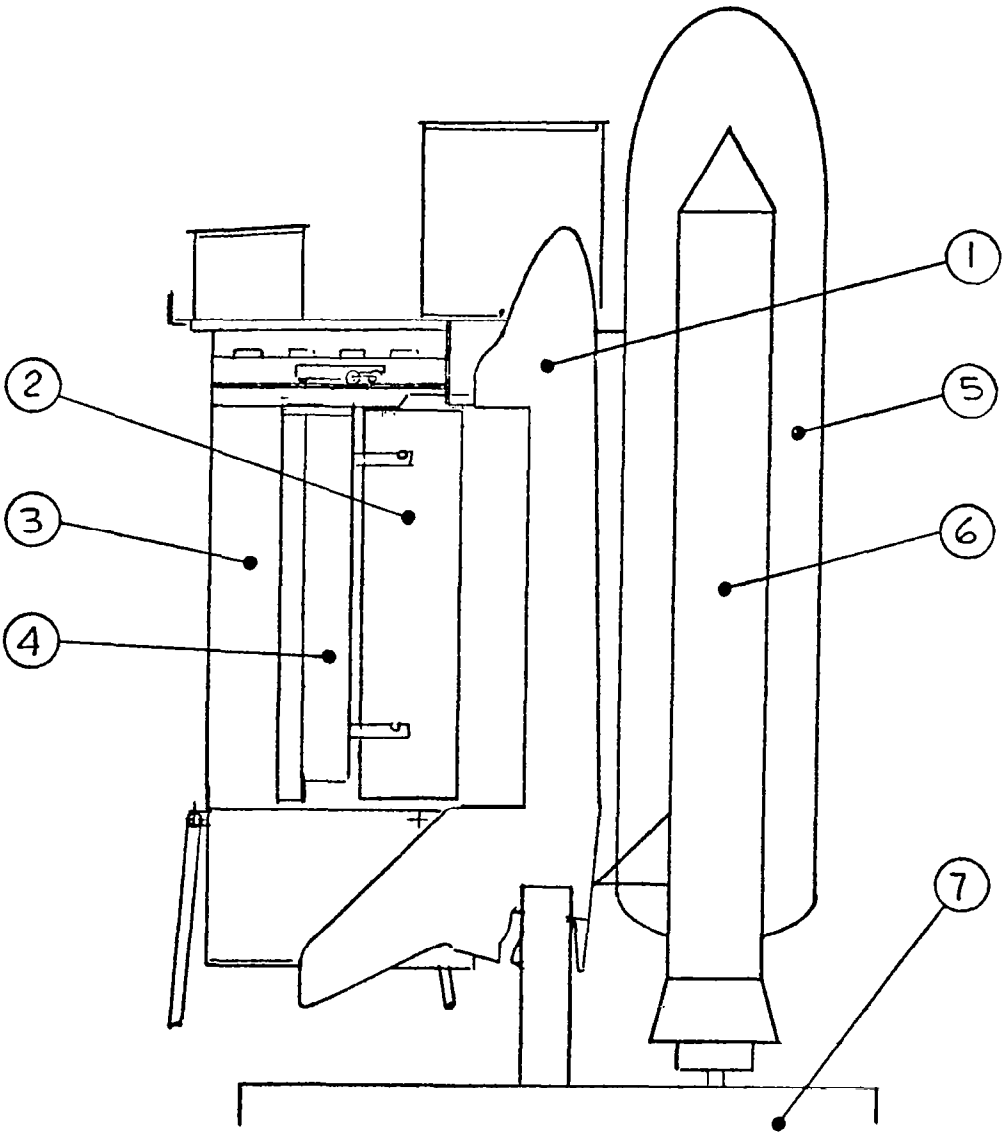

1. ORBITER
2. PAYLOAD
3. PAYLOAD CHANGE-OUT ROOM (PCR)
4. PAYLOAD GROUND HANDLING MECHANISM (PGHM)
5. EXTERNAL FUEL TANK
6. SOLID ROCKET BOOSTER
7. MOBILE LAUNCH PAD

Figure 1. Access to the orbiter

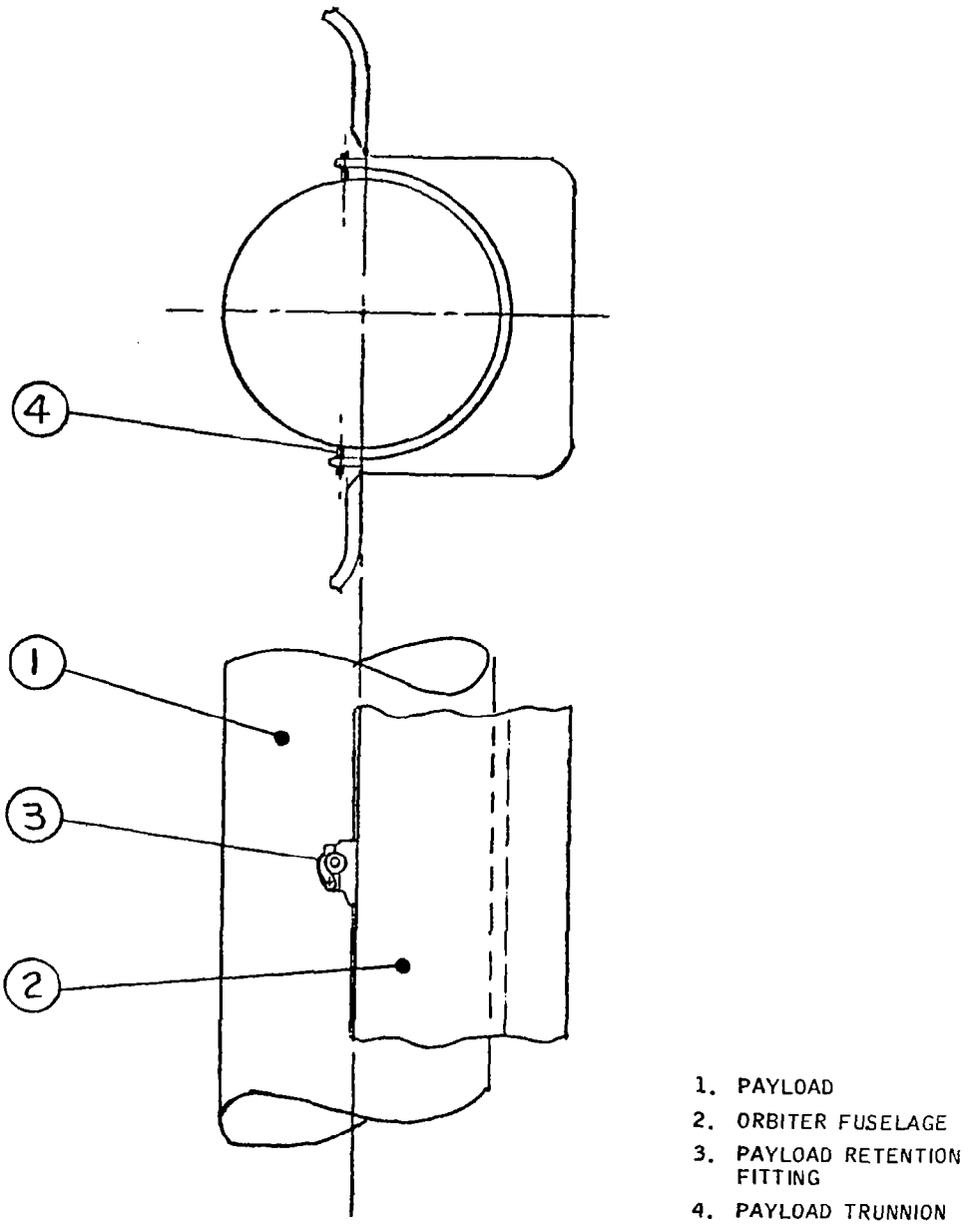

Figure 2. Payload retention method

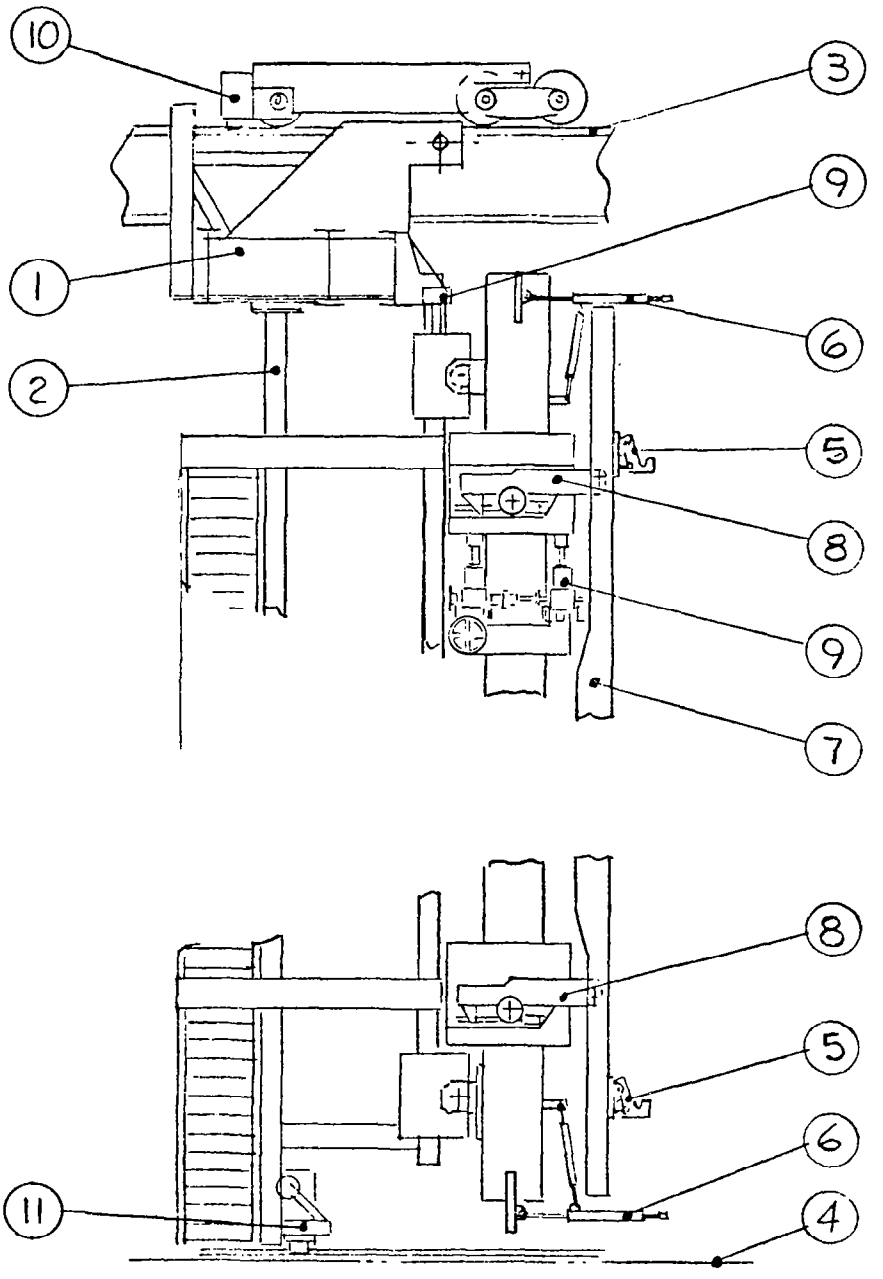

1. PGHM BRIDGE
2. PGHM STEM
3. SUPPORT RAIL
4. PCR FLOOR
5. PAYLOAD SUPPORT FITTING
6. ORBITER CONNECTING LINK
7. PAYLOAD SUPPORT BEAM
8. FLOATING BEAM AND HOUSING
9. VERTICAL POSITION ADJUSTMENT
10. RAIL CLAMP
11. STRAIN-RELEASE MECHANISM

Figure 3. Payload ground handling mechanism

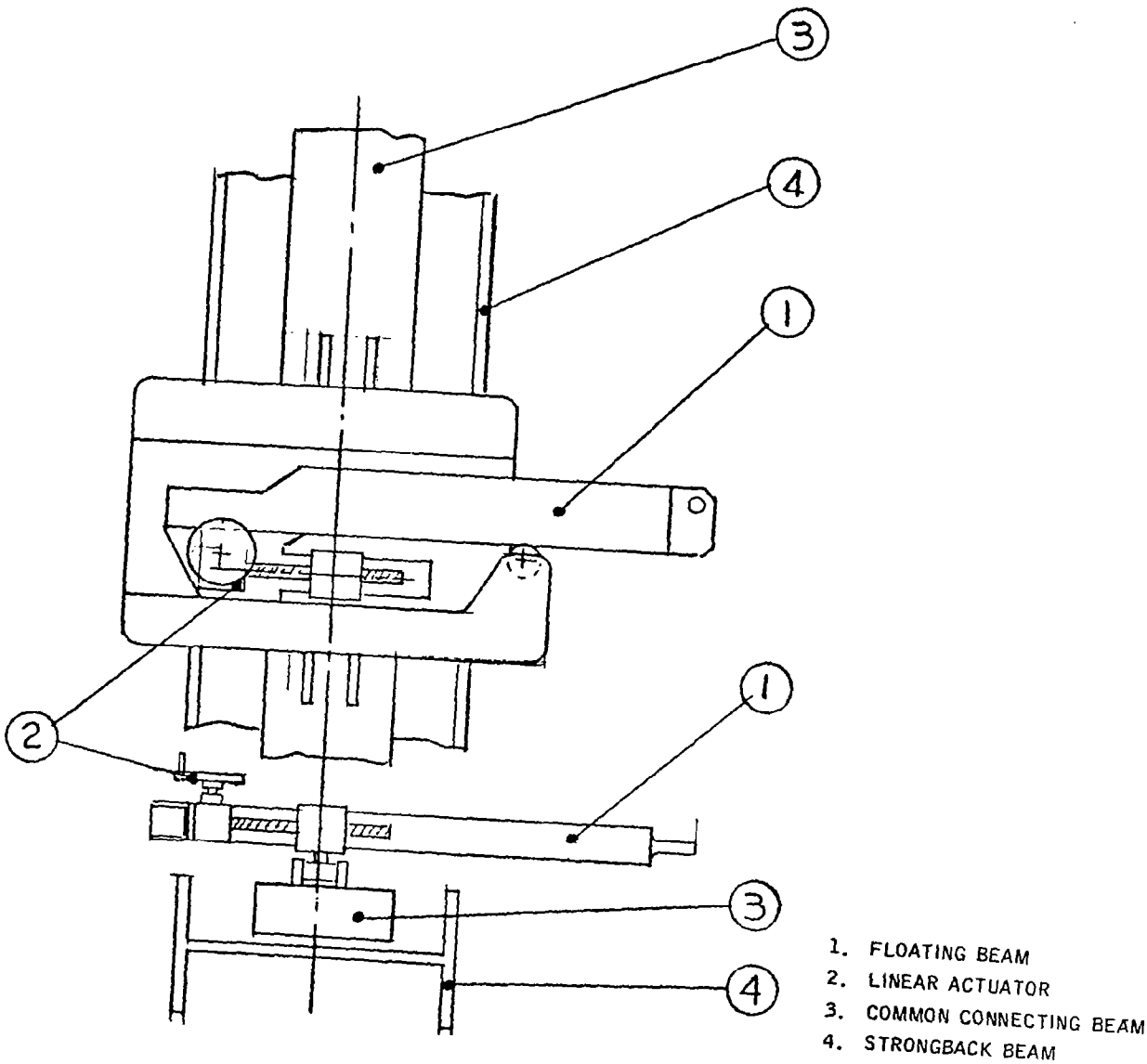

Figure 4. Floating beam positioning

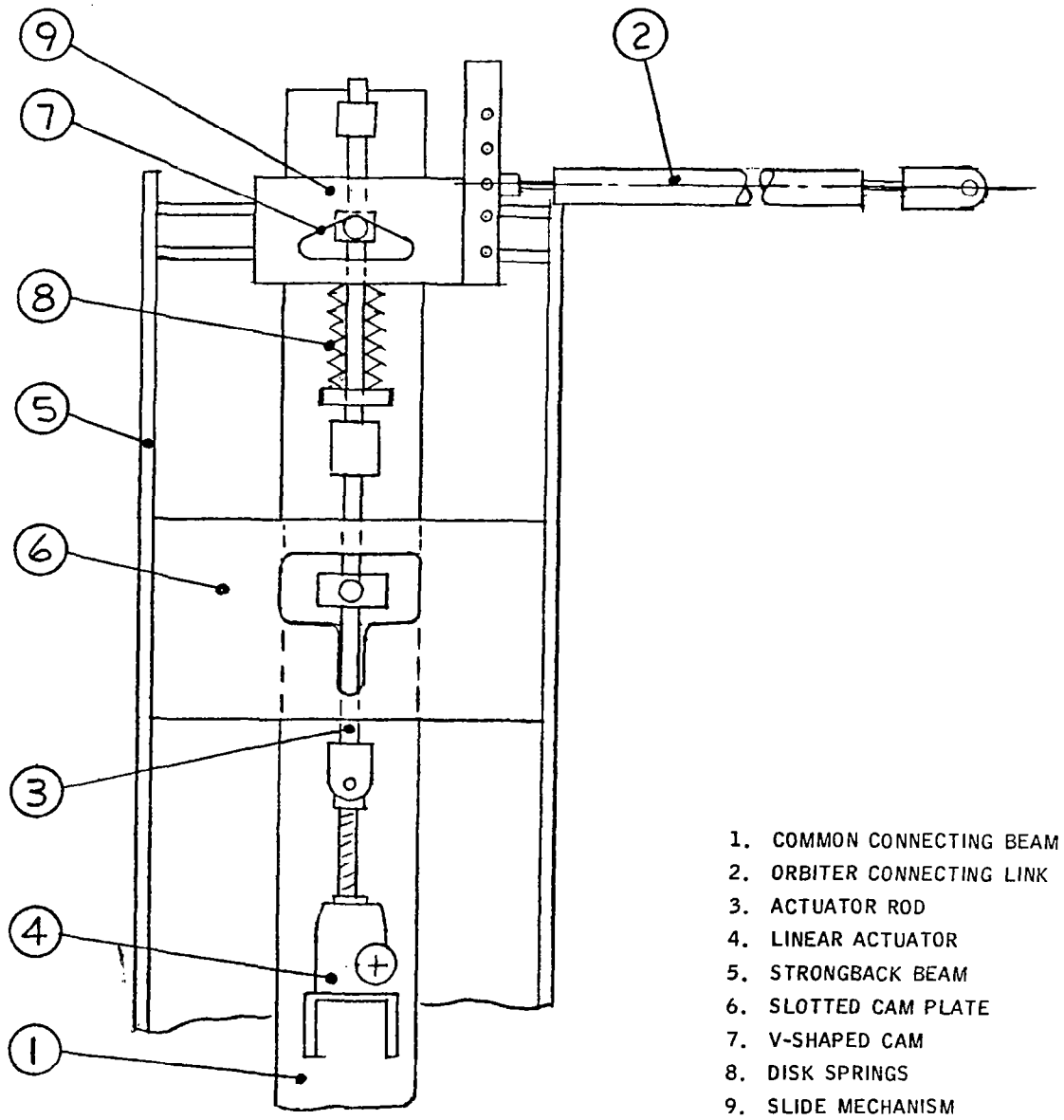

Figure 5. Common connecting beam

DEPLOYMENT/RETRACTION MECHANISM FOR SOLAR MAXIMUM MISSION HIGH GAIN ANTENNA SYSTEM

By

Neal Bennett, Sperry Flight Systems
Peter Preiswerk, ASTRO Research Corporation

ABSTRACT

Accurate steering of a spacecraft communication antenna requires a stable platform. A mechanism called a Deployment/Retraction Assembly (DRA) which provides not only a stable, but a deployable platform for the High Gain Antenna System (HGAS) aboard the Solar Maximum Mission (SMM) spacecraft is described. The DRA also has the capability to retract the system upon command.

INTRODUCTION

The SMM spacecraft scheduled for launch into a 357 mile orbit in October 1979 will have aboard a high gain S-band antenna system capable of communicating with and tracking the TDRS system. This antenna system, called HGAS, must be stowed within a required envelope in the aft end of the spacecraft and withstand launch by a Delta launch vehicle. The spacecraft attitude does not allow the antenna to view the relay satellites when stowed. Consequently, once in orbit, the HGAS must be deployed to a position that allows the antenna to communicate with and track the relay satellites. The HGAS is shown in the deployed condition in **Figure** 1. When deployed, the deploy mechanism must maintain accurate support alignment for the antenna and articulation system while being exposed to the orbital space environment. Space Shuttle recovery of the SMM is planned and to facilitate this the HGAS is required to retract within its launch envelope so that the SMM spacecraft can fit within the Shuttle bay. If retraction is not possible, all portions of the HGAS outside the recovery envelope must be jettisoned from the spacecraft.

The DRA design described in this paper was selected based on the flight experience of the concept and its potential to satisfy the stringent HGAS requirements described above. Similar structures have flown successfully on the Air Force S-3 satellite and NASA's Voyager 1 and 2 as magnetometer booms of 20-foot length, 7-inch diameter and of 43-foot length, 9-inch diameter respectively. The deployable portion of the DRA, the Astromast, provides an ultralight, low profile structure with the deployed stiffness and stability required of HGAS.

DRA DESIGN DESCRIPTION

The DRA is a major subassembly mechanism of the High Gain Antenna System, weighing less than 23 pounds. The total deploy stroke is 60 inches, which

positions the antenna at a point relative to the spacecraft that allows a view of the TDRS system. It has overall stiffness properties that yield major HGAS deployed resonant frequencies in excess of 8 Hz. Deployed alignment stability is expected to be better than .2 degrees over the required temperature range and deploy/retract cycle life. The required cycle life for ground operation will be approximately 30 cycles and for space, 1 cycle.

The DRA itself consists of five major subassemblies: (1) An Astromast Assembly which is the basic deploying and retracting support structure for the antenna and articulation system, (2) A servo assembly, which restrains the Astromast during deployment in a controlled manner, and provides the force required for retraction, (3) hardware that interfaces the HGAS with the SMM spacecraft, (4) a jettison mechanism that is capable of jettisoning certain portions of the HGAS, and (5) an antijettison caging mechanism that inhibits the jettison mechanism in the stowed condition.

ASTROMAST

The Astromast provides the key function in the DRA of structural support to the deployed antenna and articulation system. Its construction provides for maximum stiffness, minimum weight, and minimum volume.

Figure 2 is a layout of the Astromast showing the truss type construction. The basic members are the three main longitudinal members (longerons), triangular frames separating the longerons (batten frames), and pretensioned diagonal members connecting adjacent longerons and batten frames. The diameter through the longerons is 18.5 inches and the length between longeron pivot points is 62.16 inches. There are 5 batten frames, forming 6 bays, each 10.36 inches long. All members are fabricated from unidirectional S-glass/epoxy laminate to take advantage of the inherent high stiffness-to-weight ratio and thermal stability. The total weight of the Astromast is 3.7 pounds.

Stowed, the Astromast is coiled into a height of only 2.3 inches. The longerons develop, like coiled springs, a force tending to deploy the system and are restrained by a central lanyard. Figures 3 through 6 show the deployment sequence, as demonstrated by an engineering model, beginning with the fully stowed condition. Two different stages during the transition from stowed to deployed are shown in Figures 4 and 5. Since all or some portion of the longerons still form a helix, the Astromast is relatively weak during the transition phase. The maximum stiffness and strength properties are not achieved until full deployment, shown in Figure 6. Note the restraining lanyard located in the center. The top plate, representing the interface to the antenna and articulation system, rotates about the longitudinal axis a total of 382.5 degrees as the Astromast deploys.

In the deployed state, the longerons provide axial load capacity and bending stiffness, the battens stabilize the structure while in an elastically buckled condition, and the diagonals provide shear and torsional stiffness. Though the DRA will not be exposed to direct sunlight, the thermal alignment

stability is designed to remain within .2 degrees with as much as 270 degrees R temperature differential between the two diagonals of each bay panel.

SERVO MECHANISM

The DRA servo mechanism controls the rate of deployment and provides the retracting force. A pully containing the restraining lanyard is attached to the output shaft of a simple worm gear assembly. The worm is casehardened steel and the driven helical gear is cast bronze; the mesh as well as the gear bearings are lubricated by Braycote 3L-38RP grease. The worm is driven by a brush type DC gear head motor, producing a total speed reduction of 2433:1. Motor brushes are redundant and of the longlife dry-lube type consisting of 85 percent silver, 12 percent molydisulfide, and 3 percent carbon. Figure 7 shows the location of the servo mechanism on the bottom of the DRA.

For launch the Astromast is not held in position by the lanyard, but by a pyrotechnic pin puller which absorbs the load directly. The pin puller is shown in Figures 7 and 9. Once the spacecraft is stabilized in orbit, the dual initiated pin puller is fired and the deploy sequence is started by commanding the DC motor on. The lanyard is in turn played out at a controlled rate allowing the DRA to deploy. Redundant microswitches are used to indicate the deployed state and are used to switch off the motor. A special bridle system, shown in Figure 8, is used in conjunction with a change in effective lanyard pully radius to prevent the DRA from "snapping" into the deployed state. This bridle system also serves to generate the initial rotation of the DRA about the longitudinal axis when retraction is commanded. Redundant stowed status microswitches, located so that they sense contact of the top structure with the base plate, are used to turn off the servo mechanism once stowage is complete.

INTERFACE HARDWARE

The interface between the DRA mechanism and the SMM spacecraft consists of a lightweight, stiff aluminum cylinder 28.3 inches long and 21 inches diameter, called the canister, shown in Figure 9. Three hat section stringers run the length of the canister carrying loads from the three Astromast longerons directly to three I-beams in the aft end of the spacecraft. The canister not only provides the static and dynamic interface with the spacecraft, but also acts as a guide tube during jettison.

JETTISON MECHANISM

The DRA is capable of jettisoning the antenna, articulation system, Astromast, servo mechanism, and control electronics. The jettison mechanism will only

be activated in the event the DRA cannot be retracted to the fully stowed condition for Shuttle recovery. This capability is provided by three ball release/jettison spring assemblies, shown in Figure 10. A lightweight but structurally sound mechanism has resulted through extensive use of 7075 aluminum. A pyrotechnic cable cutter, shown in Figure 7, severs 3 stainless steel cables that release spring loaded plungers, unloading a set of steel balls in sockets. Once the ball loads are released, 3 jettison springs eject the base plate and all assemblies attached to it out of the canister. The spring stroke is 2.5 inches providing a terminal velocity of 12 in./sec. Spring forces are designed to yield a net force through the HGAS center of gravity to minimize the tendency to rotate. In addition to the jettison release cables, the pyrotechnic cable cutter severs all electrical and RF cables interfacing the HGAS to the SMM spacecraft.

CAGING MECHANISM

To prevent inadvertent jettisoning of the HGAS after Shuttle recovery, the jettison capability is inhibited by a unique but simple caging mechanism shown in Figure 9. Caging occurs only in the stowed condition, but the mechanism allows the DRA to deploy and retract normally. It consists of a pivoted wedge which, when the DRA is fully retracted, will not allow the base plate to move relative to the canister. Consequently, if the cable cutter is accidentally fired, the jettison springs are inhibited from forcing the baseplate out of the canister. After approximately .75 inches of deployment, the caging wedges are released, and jettison is possible.

CONCLUDING REMARKS

A unique mechanism, called a Deployment/Retraction Assembly, has been described that is capable of deploying and retracting the S-band antenna and associated articulation system aboard the SMM spacecraft. Once deployed, it provides a stable and stiff structure from which the antenna can track and communicate with the TDRS system.

At the time of writing, engineering model tests are underway and the protoflight DRA is being fabricated. Engineering models of the worm gear assembly, the jettison mechanism, and the Astromast have been tested and the following has been demonstrated:

- Worm gear design has load/cycle capability in excess of that required for ground and space operation.
- Jettison mechanism ball release concept works successfully.
- The Astromast has adequate cycle life and stiffness to meet mission requirements.

Acceptance testing of the protoflight DRA will begin in late January. At the time of the 12th Aerospace Symposium in April 1978, DRA acceptance tests will be complete and resulting data will be available.

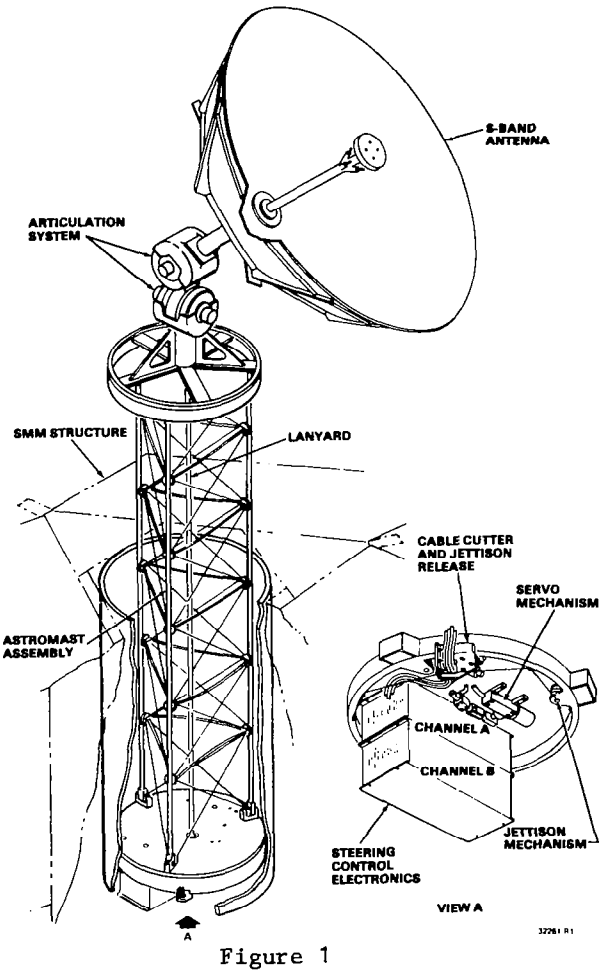

Figure 1
HGAS Deployed

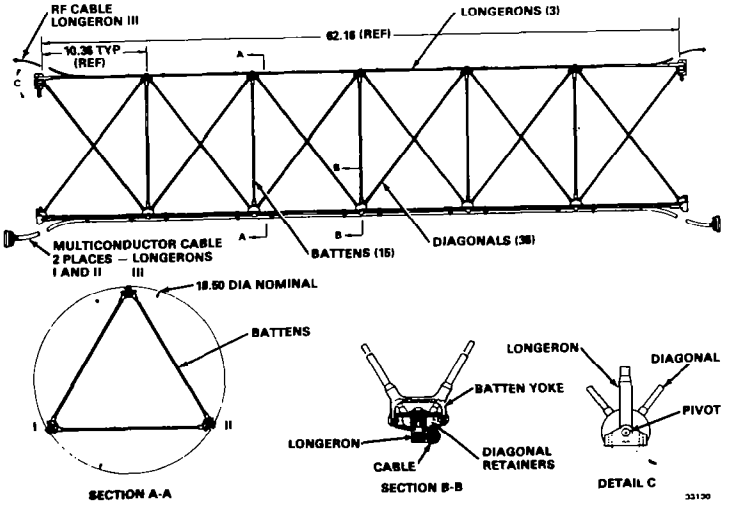

Figure 2
Astromast

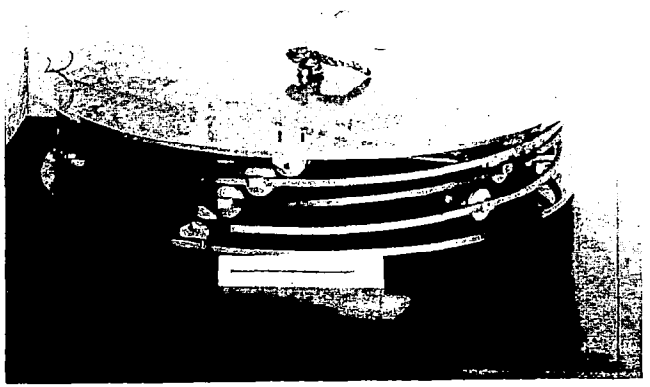

Figure 3 Astromast stowed.

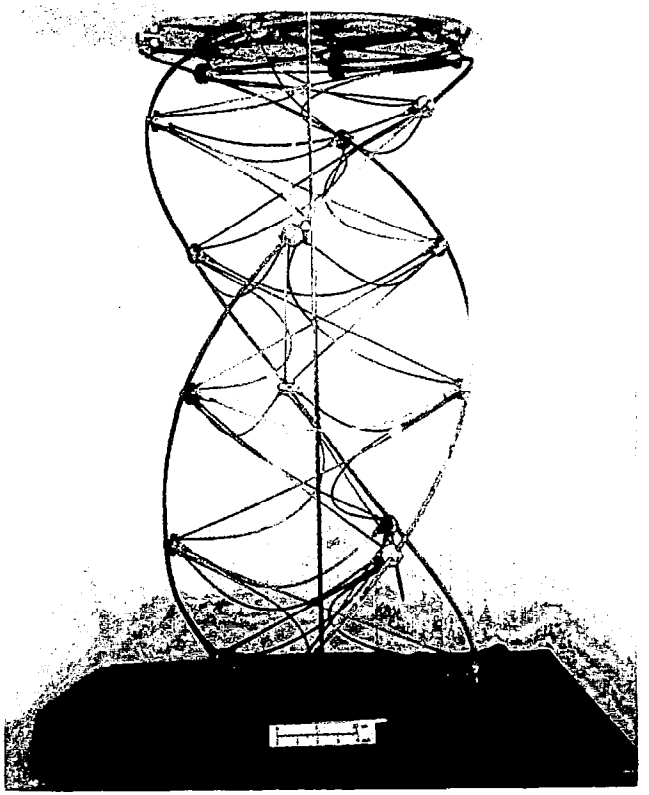

Figure 4 Astromast initial deployment stage.

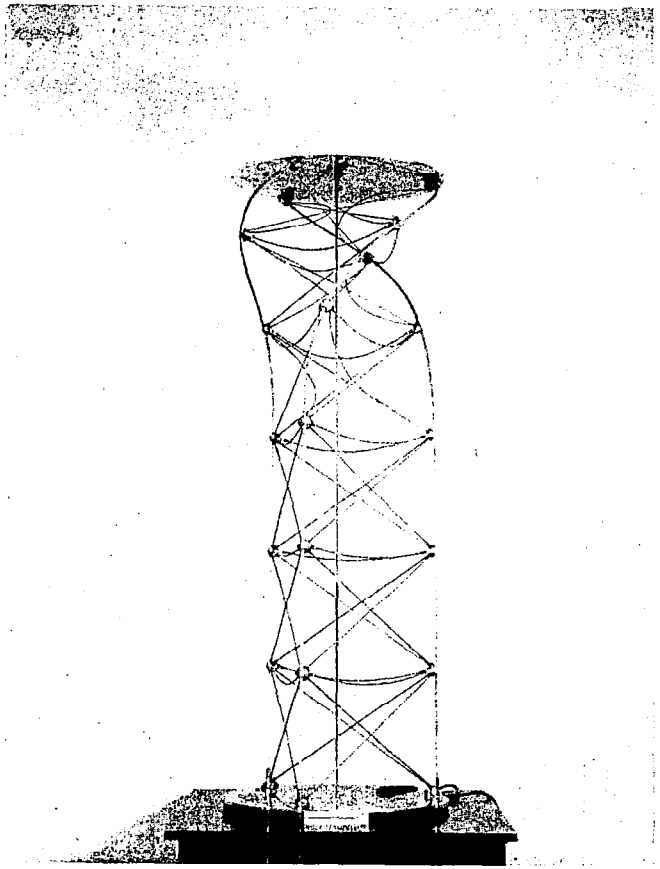

Figure 5 Astromast deploying.

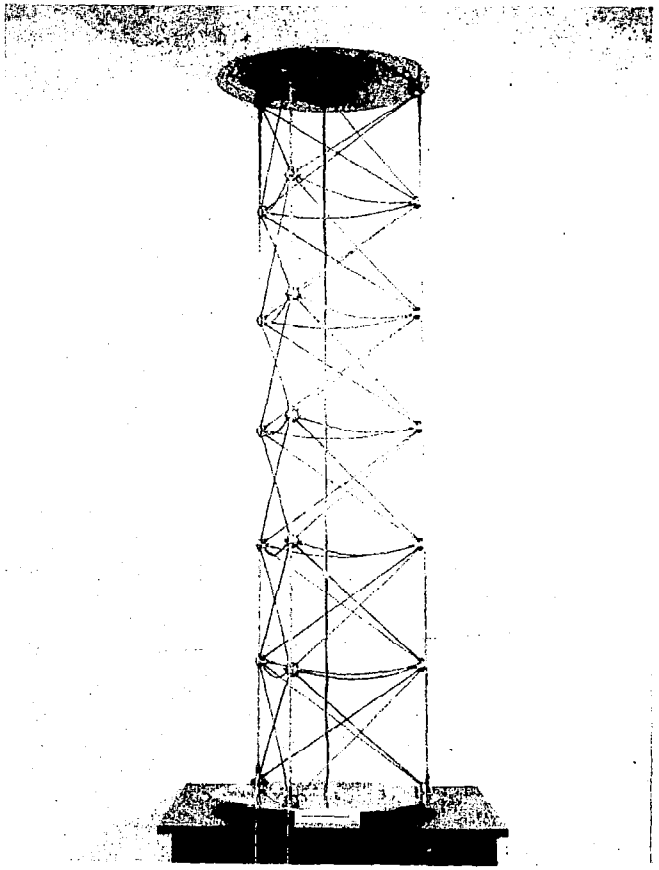

Figure 6 Astromast fully deployed.

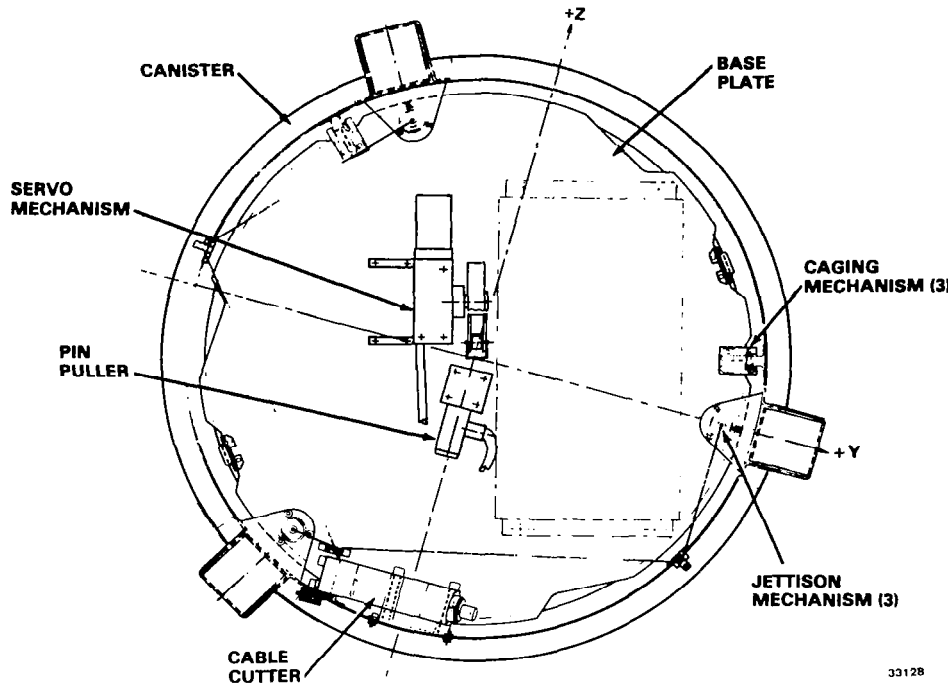

Figure 7
Bottom View of DRA

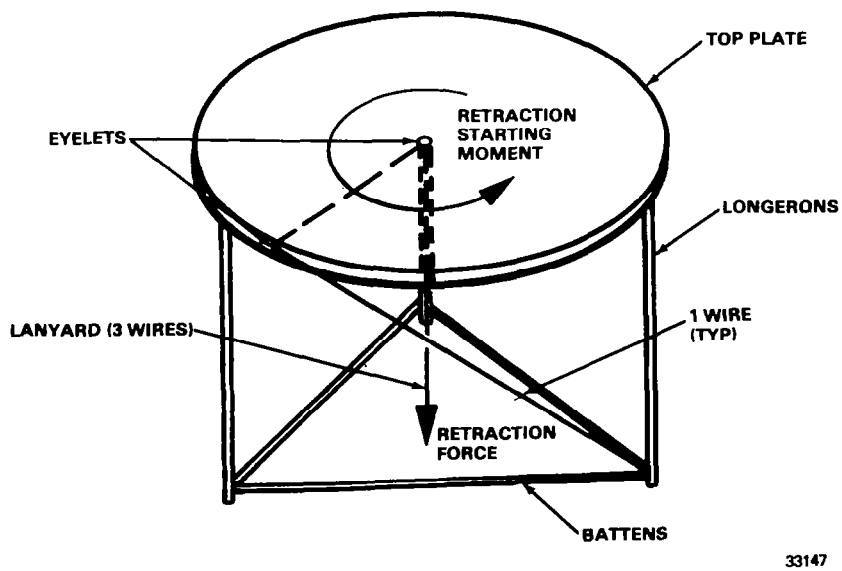

Figure 8
Bridle System

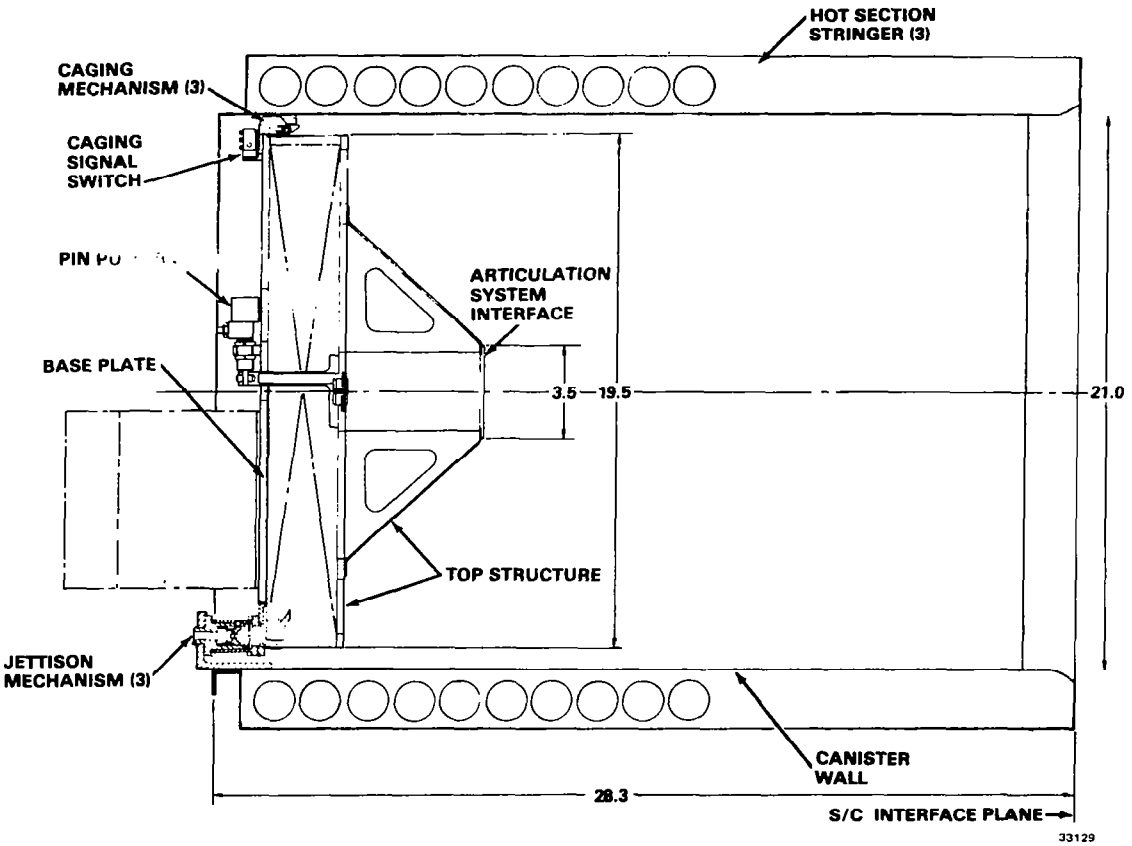

Figure 9
Side View of DRA

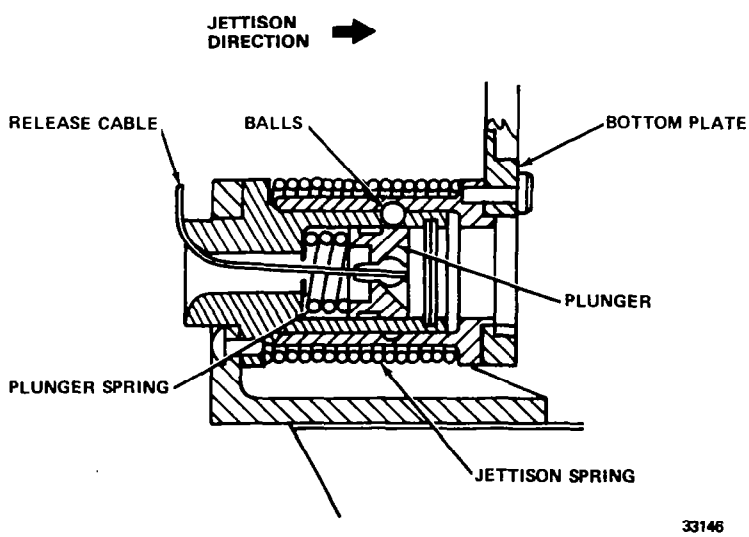

Figure 10
Jettison Mechanism

GEOS Axial Booms

Gunter K. Schmidt, Dornier Systems GmbH, Friedrichshafen, Germany

ABSTRACT

A Booms and Mechanisms Subsystem was designed, developed, and qualified for the geostationary scientific satellite GEOS. The project was sponsered by the EUROPEAN SPACE AGENCY as part of the GEOS development contract. Part of this subsystem are four Axial Booms consisting of one pair of 1 m booms and one pair of 2,5 m booms.
Each of these booms is carrying one "bird cage" electric field sensor. Alignment accuracy requirements led to a telescopic type solution. Deployment is performed by pressurized nitrogen.
The main components of this system are:

- Telescopic Section
- Release Mechanism
- Pressure System
- Triax Cable Harness
- Experiment Canister

At deployment in orbit two of these booms showed some anomalies and one of these two deployed only about 80 %. Following this malfunction a detailed failure investigation was performed resulting in a design modification of some critical components as release mechanism, guide sleeves of the telescopic elements, and pressure system.

INTRODUCTION

Four special telescopic booms were developed for the scientific satellite GEOS as part of the Booms and Mechanisms Subsystem.
GEOS is a spin stabilized satellite with a number of booms extending from the spacecraft body for positioning experiment probes. The experiments measure magnetic and electric fields in the low frequency spectrum.
One of the experiments requires two pairs of wire sphere sensors of 100 mm diameter to be extended 1 m and 2,5 m above the spacecraft body in approximately 70 cm distance parallel to the spin axis. The design requirements led to the development of telescopic booms that are deployed by a nitrogen gas pressure system.
GEOS was launched in April 77. After positioning the spacecraft in a final orbit, its booms were released and deployed. However, one of the "Long Axial Booms" deployed only about 80 to 90 %, resulting in a failure investigation.

This presentation delineates the design details of several critical components and the failure investigation following the partial function failure of the failed "Axial Boom".

FUNCTIONAL CHARACTERISTICS

The four Axial Booms deploy and support GEOS's four wire-sphere electric-field sensors. During launch the experiment spheres are stored at the base of the spacecraft in canister-like containers which are sealed by thin aluminium-foil membranes. The spheres are electrically connected by helically-wound triaxial cables routed within the telescopic booms. (see Fig. 1) Sufficient stiffness was achieved by using aluminium-alloy tubes with a large outer diameter, and thin walls to withstand the bending loads due to centrifugal forces induced by the maximum deployment spin rate of 30 rpm.

Torsional orientation is provided by a keyway. The axial booms are locked by a three-ball mechanism during launch (see Fig. 2) and are released and deployed by pressurised nitrogen, stored in pyrotechnically activated tank valve assemblies at 110 bar. Gas flow during deployment is controlled by orifices at the base of each boom, providing a deployment time of 1 to 4 sec. The gas system maintains a continuous flow for 15 to 20 sec to provide an adequate safety margin. Numerous deployment tests in vacuum were necessary to ultimately define the optimum parameters for this pressure system.
Because of the extreme magnetic and chemical cleanliness required for GEOS, a very careful selection of materials and processes was mandatory.

DESCRIPTION OF THE OBSERVED ANOMALIES

After positioning GEOS in its final orbit, its eight Booms and five Mechanisms were deployed. However, two Axial Booms showed some anomalies during deployment and one of these two, a Long Axial Boom, extended only about 80 to 90 % of its full length.
The table below provides an interpretation of deployment data of the Axial Booms as observed in orbit during April 30. 1977. The observations are based on telemetry data from the accelerometer output and the boom status switches. Several of the interpretations are conclusive, while others remain inclusive (Ref. 1).

Configuration Data:	**Short Axial Booms**		**Long Axial Booms**	
	+X/FS	**-X/PM**	**+Y/FM**	**-Y/FM**
Deployment length	1 m		2,5 m	
overall length	1,6 m		3,1 m	
tip alignment	±0,02 m		±0,02 m	
release delay:	(sec)	(sec)	(sec)	(sec)
t_r nominal	0,5 ±0,05	0,5 ±0,05	0,35 ±0,05	0,25 ±0,05
t_r observed	0,5	0,5 or 10,9	6,6	0,8 ±0,6
deploy time:				
t_d nominal	1,5 ±1	1,5 ±1	2,7 ±1,5	2,7 ±1,5
t_d observed	0,9	10,8 or 0,6	0,8	0,55 ±0,6
Deployment time: $t_D = t_r + t_d$				
t_D nominal	2 ±1	2 ±1	3 ±2	3 ±2
t_D observed	1,4	11,3		1,45 ±0,6
HK – Signal	yes	no	yes	no
achieved deployment lenght	full	full or nearly full	80 to 90 %	full

The information gained from spacecraft data is not totaly unambiguous. The -X PM/SAB data can be interpreted in two ways:

a) Release occurred very late and was followed by a fast deployment.
b) Release occurred for both Short Axial Booms (+X and -X axes) at the same time (ref. 1 Fig. 1a spike A1). This also occurs under normal conditions within a few milliseconds time frame. For the +X SAB release was followed by a nominal deployment. However, deployment of the -X SAB may have momentarily halted after an initial start, due to stiction, and then continued some 11 sec later.

According to the HK-signal the release of the +Y Long Axial Boom occurred approximately 6 to 7 seconds too late. Following the delayed release, a deployment action of this boom was observed at the accelerometer output. However, any conclusions are subject to doubt, as the accelerometer went into saturation when the -Y LAB deployed and as the connection of HK-data and accelerometer readings were considered ambiguous for the Long Axial Boom. The actual deployed length achieved by the +Y Long Axial Boom was determined from attitude manoeuvre and shadow spike data from the LAB experiment sensors.

POSSIBLE EXPLANATIONS FOR THE ANOMALIES

1. Change in friction properties at seals, seal ring, and guide rings, due to:

1.1 effects of hard vacuum
1.2 effects of Van Allen radiation exposure
1.3 temperature effects creating cold flow of the teflon guide rings

2. Reduction of gas flow, due to:

2.1 filter contamination
2.2 orifice choking
2.3 piping leakage

3. Release Mechanism jamming, due to:

3.1 ball-latch tolerances
3.2 piston over travel
3.3 increased friction between ball and ball cage

4. An incident due to launch failure

5. A zero-g Effect

Most of the above explanations are essentially irrelevant since they would have caused different deployment data. Only the effects of 1.3 (stiction), 2.2 (orifice choking), and 3.3 (delayed release) can be considered as valid explanations for the anomalies observed.

FAILURE INVESTIGATION AND SIMULATION TESTS

To gain additional information about the failure behaviour, an investigative test programme was commenced. This programme consisted of three test series.

- Single gas bottle tests
- Release mechanism failure simulation tests
- Orifice choke simulation tests

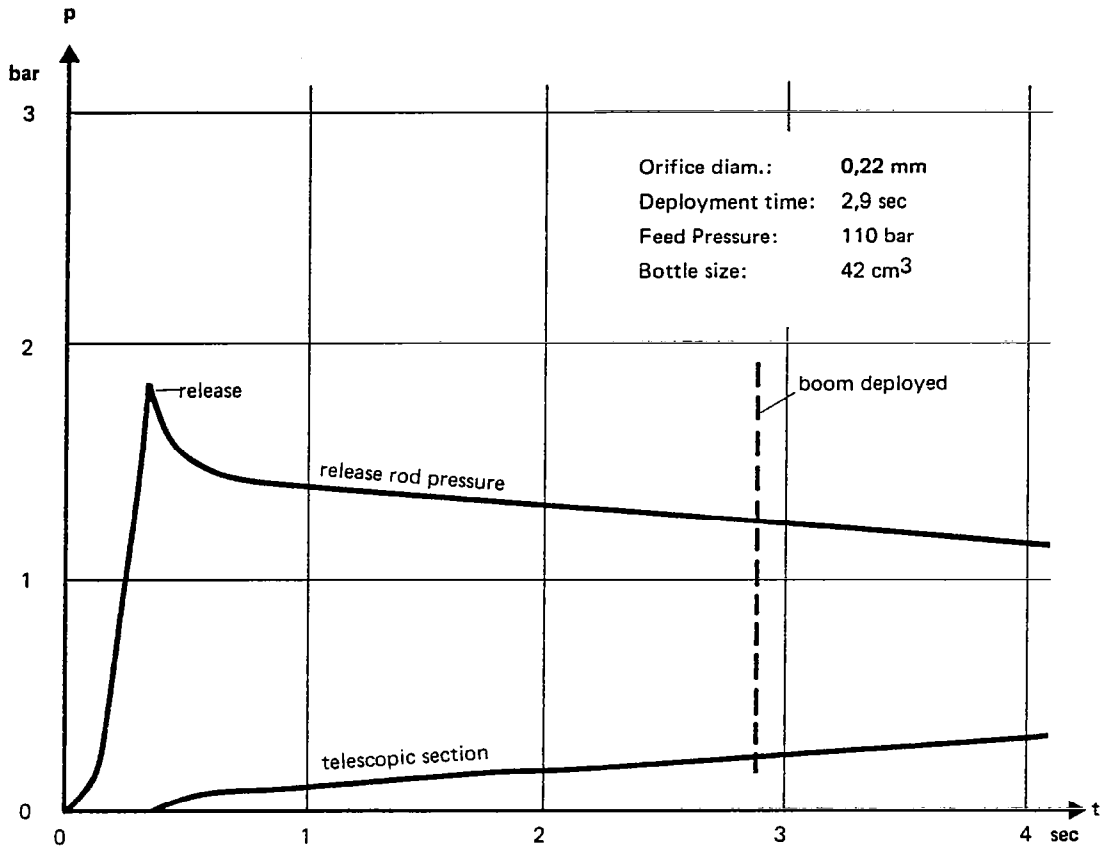

Fig. 3: Long Axial Boom - Pressure Profile

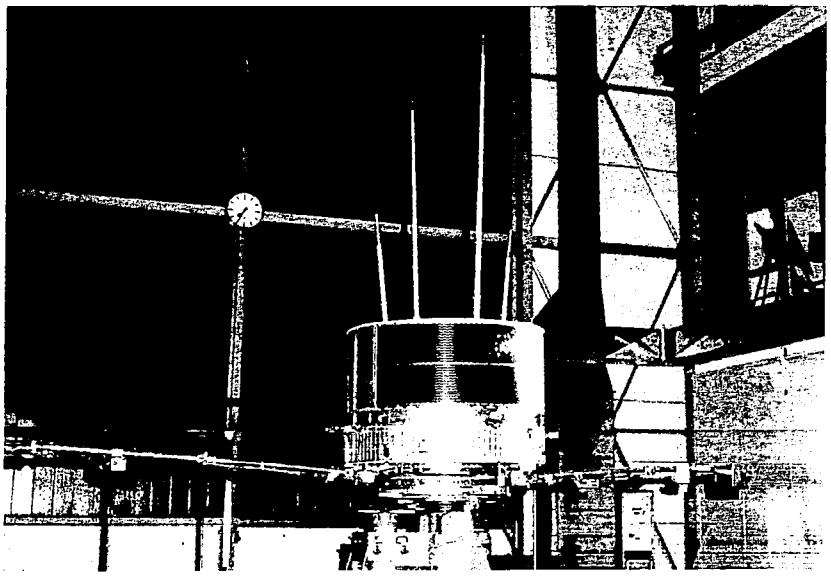

GEOS–Spin Deployment Test of Short Radial and Axial Booms

Approximately one hundred vacuum deployments have been performed in the course of this investigative programme.

1. Tests with a Single Gas Bottle for each pair of the Axial Booms with increased charge pressure. For GEOS–2 it is proposed to keep a second gas bottle for each boom pair in reserve. For this reason, the single bottle pressure had to be determined duplicating deployment times of the GEOS–1 two bottle arrangement charged with 110 bar pressure.
   The tests demonstrated that the deployment times with a single bottle with pressures of 150 to 160 bar are nearly identical to the required deployment time for two bottles with 110 to 115 bar pressure.
2. In a second test series, a jamming of the release balls in the release cage was simulated.
   The test setup allowed the release piston to move, but the release of the boom was delayed by a restraining wire which was melted following the required delay times.
3. In the third test series, an orifice choke was simulated by a thin wire inlay in the orifice channel. During these tests the axial booms were equipped with a special release block which allowed recording of the pressure profiles in the release rod and the telescopic section. A typical pressure profile is shown in Fig. 3.

RESULTS AND EVALUATION

As a result of the above investigations, the release delay t_r and the deploy-time t_d are determined to be the critical parameters. These parameters indicate a characteristic dependency for each of the possible failure explanations. The diagram Fig. 6 illustrates these characteristics.

Curve I shows the relationship attributable to increased friction (1.3). The release delay is not influenced by increased friction in the seal and guide system. Therefore, this failure develops as a vertical line. (see Fig. 6).

Curve II shows the relationship of t_r and t_d for the condition of a reduced gas flow. The reduced gas flow influences the deploy time significantly. Its influence on the release delay is less distinct.

Curve III shows the t_r, t_d dependency for the condition of release mechanism jamming. This failure mode causes the pressure to increase in the release rod and the stowed telescopic sections. When release occurres, there is an increase in deployment speed. This behaviour is more pronounced for the SAB than for the LAB, due to the lower deployed to stowed volume ratio of the SAB.

The full deployment capability is limited by the amount of gas available.

If we apply the orbit data to this diagram, the following can be derived:

The SAB data substantiate a position on either curve I or curve III (point b and a), depending on individual interpretation of the orbit data.
There is no substantive evidence from the orbit data that orifice contamination has to be considered. The diagram demonstrates that any partial orifice choking would cause only a small release delay followed by a slow deployment of the SAB. The orbit data does not support this interpretation.
If the delayed release of the Long Axial Boom has to be considered as definite, any friction has to be excluded, since the +Y LAB still deployed about 80 % following the delayed release. Orifice choking can also be excluded as it was impossible, during the tests, to generate release delays of greater than 4 seconds. The release pressure level could not be achieved for the delayed boom at higher choke rates. This condition is valid also during orbit.
Therefore, a malfunction in the release mechanism can be assumed only for the Long Axial Boom. During the first few seconds of deployment, motion following this delayed release was relatively

Fig. 6 Axial Booms – Deployment Characteristics

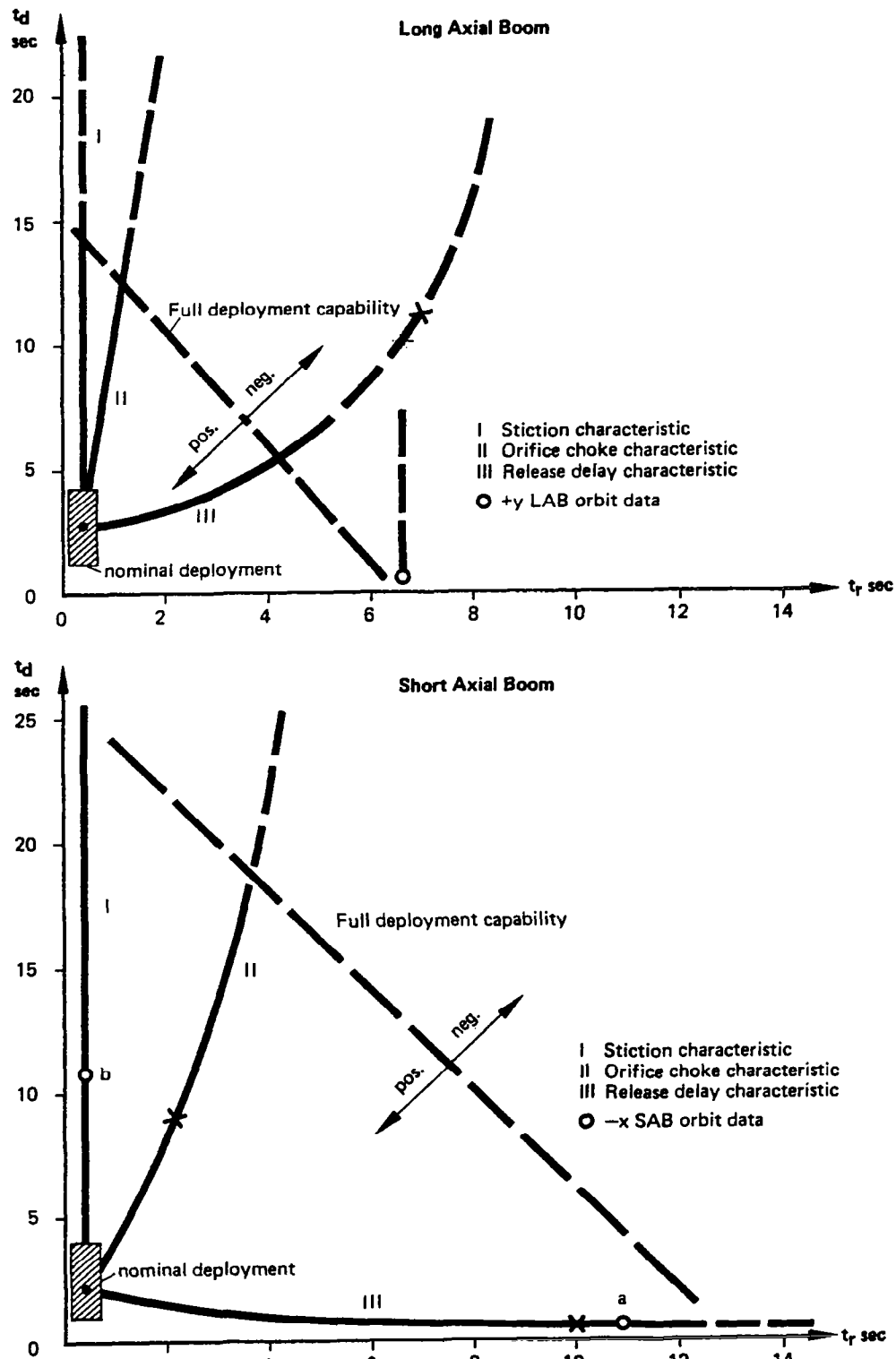

rapid. However, as the accelerometer was in saturation it was not indicated in telemetry data. Following the initial rapid deployment, motion rate was reduced significantly for approximately five seconds and finally came to a stop at about 80 % deployment length.

WHAT MAY HAVE CAUSED THE MALFUNCTION?

Increased deployment times due to stiction (1.3) were observed some ew times during temperature tests. At higher temperatures the teflon guide rings show a cold flow tendency, which can result in a friction increase. However, this friction increase was found within acceptable limits at temperatures below 50°C.

Release Mechanism jamming:

The friction conditions between ball and ball cage had been carefully calculated for GEOS-1. These calculations demonstrated a sufficient safety margin to jamming of 1,5 to 2. However, an indentation caused by the sharp edge of the titanium bushing (Fig. 7 part 1) could have resulted in increased friction, leading to a failure kinematic as indicated in Fig. 7a, b and c.
Inspection of GEOS-1 spare unit release balls proved that the indentations exist. Repeated stowage and release increased the number of indentations and the likelihood of two indentation positions is highly probable; refer to Fig. 7c.
The proper functioning of the +X FS/SAB, Flight Spare Short Axial Boom lends support to this theory, since this boom had not been exposed to repeated testing.

Following actuation of the pyro valves for boom deployment, all four release pistons moved forward and 10 balls moved freely, except for one ball at the +Y LAB and most likely a second ball at the −X SAB may have stuck as shown in Fig. 7c. The gas expanded through the outlet hole into the telescopic sections and decayed as shown by the pressure profile. After some seconds the pressure in the telescopic section nearly equalized to the release rod pressure. At this time, the release spring, which was still compressed may have started to move the release piston in reversed direction due to the reduced pressure differential (see Fig. 2b). It is very likely that due to this piston motion the stuck ball in the jammed mechanism released and movement continued.

DESIGN IMPROVEMENTS

1. To reduce the possibility of friction due to cold flow of guide rings, the tightening torque for the fixation screws has been reduced to decrease the local stress concentrations at the guide ring. In addition, the teflon guide sleeve for RE1 was slightly modified to prevent possible jamming forces caused by cold flow resulting in configuration instability.
2. In GEOS−1 orifice and filter were screwed separately into the release block. During integration of the filter, loose particles may have been created by the screwing operation and trapped between filter and orifice. (Fig. 8a).
   During failure investigation this condition was observed at one time.
   For GEOS−2 a filter-orifice-assembly was developed which is assembled separately during increased cleanliness conditions with careful control under the microscope. This new design reduces significantly the possibility of particle creation and trapping (Fig. 8b).
3. The release mechanism modification mainly concerned the ball release piston and ball cage area. (Fig. 9).
   - The hard edge of the titanium sleeve was replaced by a soft aluminium chamfer to prevent indentation of the balls.
   - The ball cage holes which were cylindrical in GEOS-1 are now conical to improve the ball release. This modification significantly increases the friction safety margin for ball jamming from $\mu 1 = 0{,}41$ to $\mu 2 = 0{,}77$.

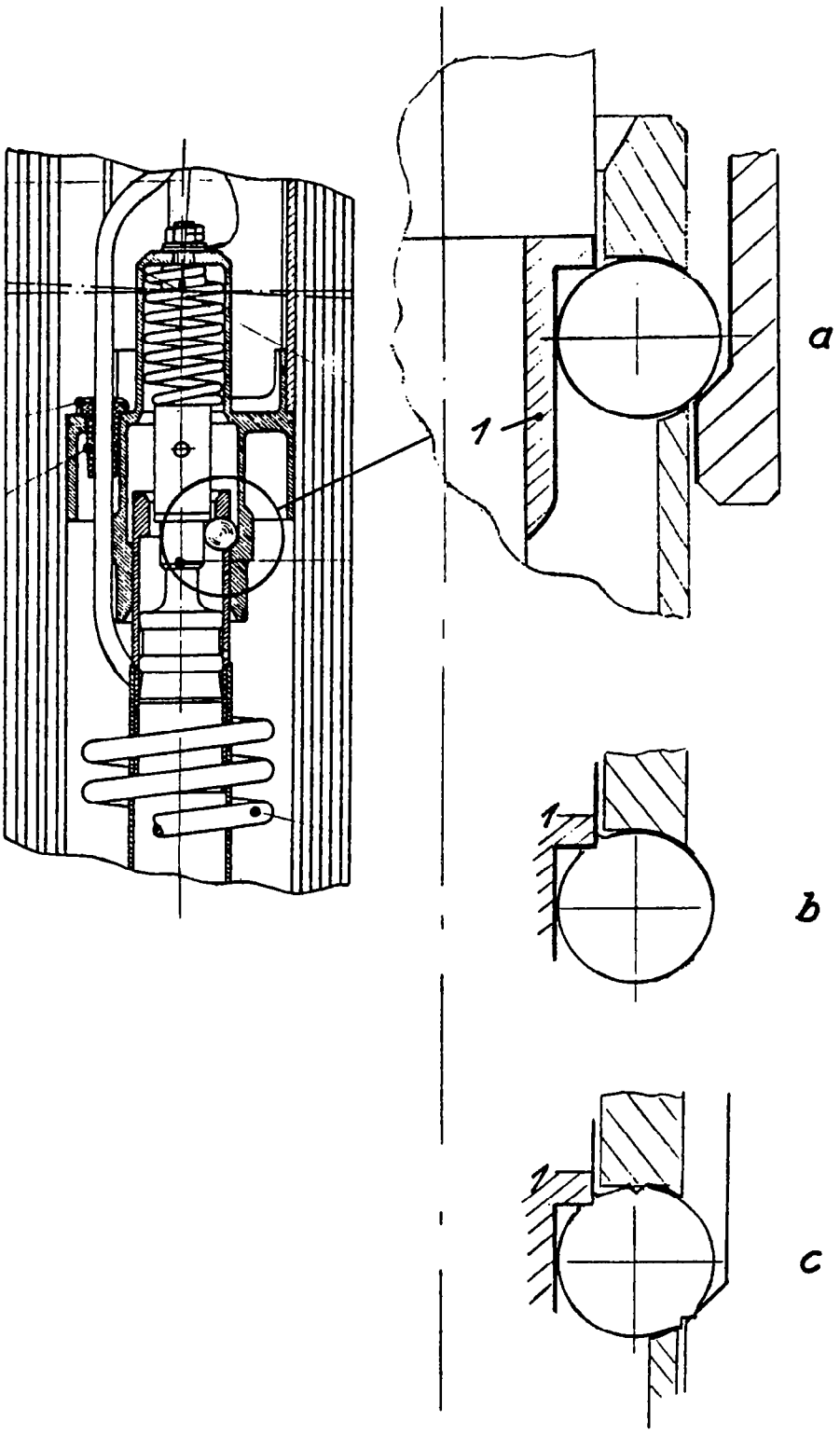

Fig. 7 Release Mechanism – Possible Failure Kinematic

Fig. 8 AXIAL BOOMS – Release Block

a) GEOS–1 design

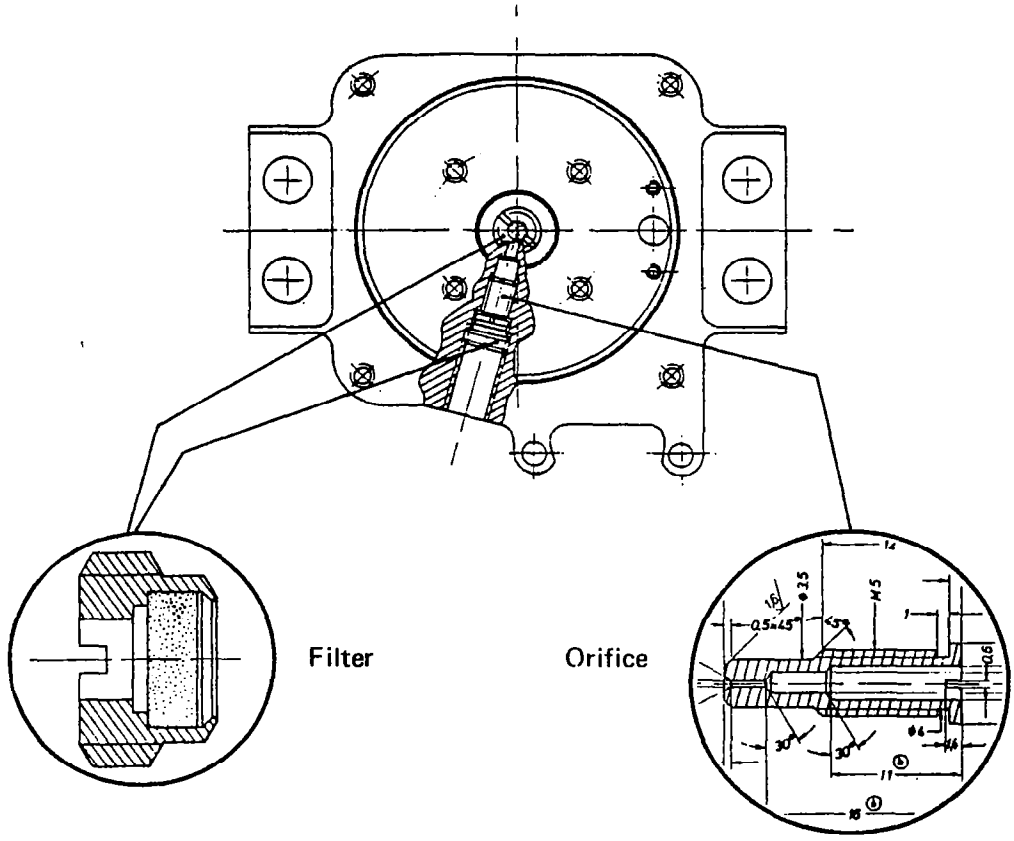

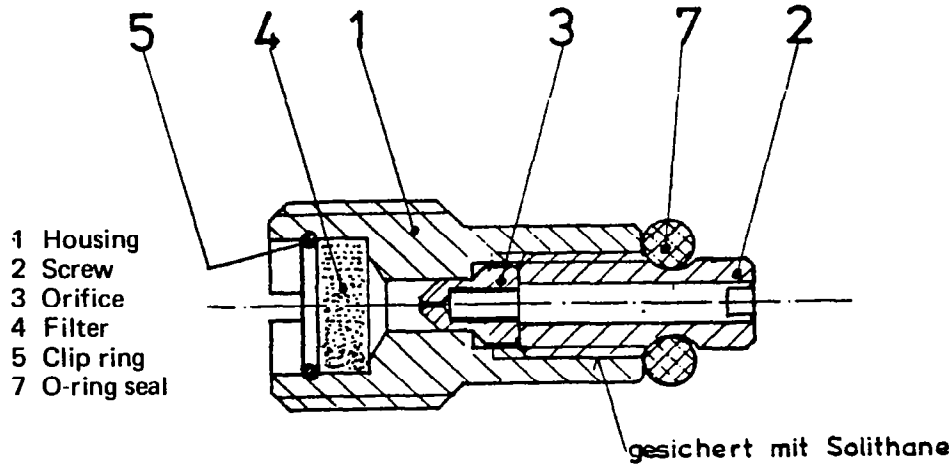

b) GEOS–2 Filter-Orifice-Assembly

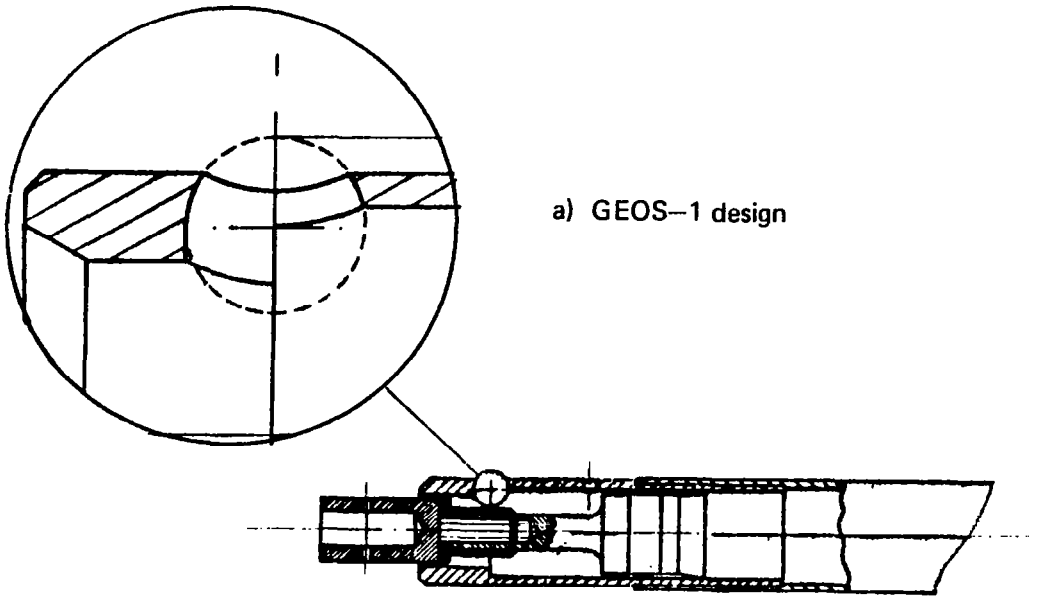

Fig. 9 **AXIAL BOOMS – Release Mechanism**

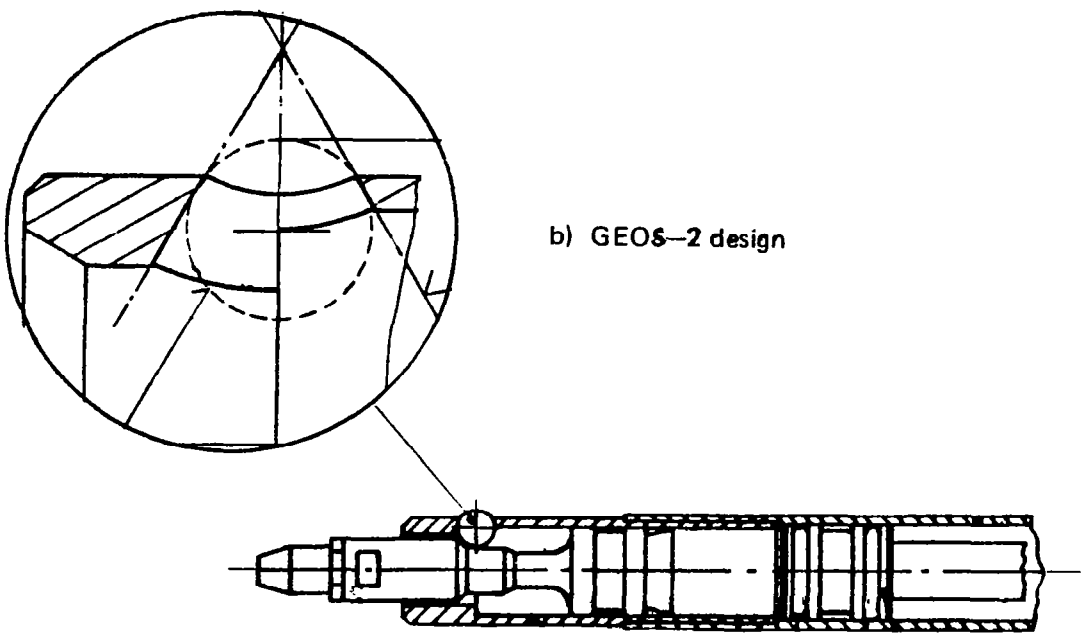

CONCLUSION

Considering the GEOS–1 housekeeping data and accelerometer data and the failure investigation results, the following can be derived:

- there is no indication that an orifice contamination caused the observed anomalies
- the data indicate that the reduced deployment length of the +Y LAB was caused by a malfunction of the release mechanism
- the anomaly in the SAB deployment behaviour was caused either by increased friction of one tube element or also by malfunction of the release mechanism.

REFERENCE

1) ESTEC–DOC. No. PG/01.2/CCK/14.728/JR "GEOS Axial Boom Deployment Sequence – Observations in Orbit" by C.C. Kalweit

2) Dornier – Study Note DO 5C SN 110 "Failure Investigation of FM Axial Boom Damages" by G. Schmidt

3) PM/FM/FS Axial Booms Log Books

4) BAC – "GEOS Axial Booms Improvement Ideas" by P.M. Grosse

5) Dornier – " GEOS Booms and Mechanisms Subsystem Manual " Vol. II Section 3.1.3 Axial Booms – Design and Analysis

6) BAC – Doc. No. GBA 1611 "Axial Booms Deployment Simulation Results" by E. Crellin

7) AERE Harwell–ESTEC Contract No. 2082/73 SK "The effects of radiation on the mechanical and electrical properties of the GEOS Satellite Long Boom Cable materials" by D. Verdin and P.R. Goggin

8) ESTEC–Memorandum ref. PG/01.2/BH/14542/HN "GEOS Axial Booms" by B. Henson

9) ESTEC-Memorandum ref.: PG/146.3/CCK/15.311/JR "GEOS Axial Boom Review Documentation" by C. Kalweit

10) ESTEC-Memorandum ref.: PG/510/BH/15.276/JR "GEOS–2 Axial Booms – Summary of Tests on Flight Model Booms" by B. Henson

DEPLOYABLE ANTENNA REFLECTOR

By William B. Palmer

TRW, Defense and Space Systems Group

ABSTRACT

The first phase in the development of a solid surface, deployable, antenna reflector is outlined and discussed. The deployment concept is described in conjunction with illustrations and photos of the fabricated reflector models. Details and results of the thermal distortion analysis are presented. Results indicate that the discussed reflector concept is an effective approach in satisfying the requirements for large deployable antennas in the 6 GHz to 100 GHz frequency regime.

INTRODUCTION

Spacecraft communication at higher frequencies has led to a need for solid surface, parabolic antenna reflectors. These reflectors must have a high degree of contour accuracy, large diameter apertures and remain thermally stable in a space environment. Stowing larger reflectors inside the restricted envelope of a booster shroud requires developing a deployment concept without sacrificing surface contour accuracy.

An IR&D program was initiated by TRW, Defense and Space Systems Group, Redondo Beach, California in 1976. The first phase of the program was to develop a solid surface, deployable antenna reflector, for spacecraft operation, at frequencies up to 100 GHz. In this paper the progress delineated in developing a deployment concept conjoined with the utilization of the proper materials demonstrates the feasibility of providing a lightweight reflector that is thermally stable in space.

DEPLOYMENT CONCEPT

The deployment concept is illustrated in Figure 1. The center section is a one-piece honeycomb sandwich construction. All folding panels are rigid, honeycomb sandwich structure. The main panels hinge from a support ring under the center section. Two intermediate panels, between the main panels, are connected to the main panels with two or more hinges and to each other with two or more hinges. The hinges have adjustable stops to locate the panels accurately in the deployed position. Springs are used in the hinges to drive the panels to the deployed position. Adjacent inboard hinges of the main panels are interconnected with a compound universal coupling so that all panels deploy simultaneously. Deployment rate is controlled by either a damping device or a geared motor. The folded reflector is restrained by a pin puller, ordnance released, which is supported on one of the tie-down fittings. The tie-down fittings extend beyond the edge of the intermediate panels and are connected at a common joint on the reflector axis.

This concept has several advantages over other systems. For example, all panels are hinged together to insure close control of the parabolic contour.

Further, since the panels are interconnected with hinges, additional hinges or shear joints can be utilized on large reflectors to minimize the relative deflection at the panel joints. Also interconnection of the main panel hinges insures synchronized deployment, minimizing the chance of fouling or damaging panels. In addition insulation on the back of the panels can be used to reduce thermal distortion.

REFLECTOR SIZE AND CONFIGURATION

Although the antenna design and analysis was based on a 16-foot diameter reflector, the deployment concept is applicable for much larger reflectors. The design illustrated with 6 main panels hinged from the center section, is only one of many possible configurations. The number of main panels can be either decreased or increased to fit a particular set of requirements.

The ratios of deployed reflector diameters to stowed envelope dimensions is illustrated in Figure 2. It should be noted that to reduce the stowed envelope diameter requires more panels. The information in Figure 2 is based on preliminary layouts. Other configurations, using similar hinging techniques, may yield larger ratios of deployed/stowed dimensions but is a subject for future study. The graph illustrates the stowed envelope of 4, 6, 9, and 12 main panel configurations.

KINEMATICS

One of the main considerations in establishing the hinge lines was to provide clearance between the backs of the intermediate panels in the stowed position. The other consideration was to locate the hinge lines so that when the reflector was folded the panels would not be warped. Once the hinge lines were located then the shape of the panels was determined so that there would be no interference throughout deployment. A computer program was written to reduce the amount of descriptive geometry required. This program consists of establishing the coordinates of numerous points on the parabolic surface of the deployed reflector and then rotating these points to define the surface at any position during stowage. The paths of points in critical clearance areas were plotted in one degree increments of rotation near the deployed position. Clearance in the stowed position was established by connecting points along the edges of the panels to insure clearance with the contour of the adjacent panels.

REFLECTOR MATERIAL FOR 7-FOOT MODEL

The reflector was constructed of an aluminum honeycomb sandwich with graphite face sheets. The principal requirements were that the sandwich possess a low coefficient of expansion, be dimensionally stable and light as possible. GY70 graphite epoxy (50 ends per inch unidirectional with dacron fill and Narmco 5208 resin) was selected for the 7-foot diameter model. Each ply of the three ply face sheets was .003" thick and was oriented 0 ± 60^{o}. The aluminum core was 1.6 lb/ft^3 with ¼" cell size. A two stage layup was used to reduce panel weight. The face sheets were layed up and cured in an autoclave, then bonded to the core with a roller coating technique. The adhesive used for bonding the face sheets was HT424, a thixotropic paste, supplied by American Cyanamid. This material was selected because when applied with a roller it

forms a bead on the foil edges of the core for excellent bonding to the face sheet. The materials selected and the fabrication techniques used proved to be excellent selections because the completed panels revealed no distortion. The material properties as determined by testing are listed in Table 1.

DESIGN AND ANALYSIS OF 16-FOOT REFLECTOR

A 16-foot diameter reflector was chosen for a "paper" study. The study consisted of preliminary design, structural analysis, thermal distortion analysis and a weight estimate. The ½-inch thick sandwich construction for the reflector utilized three-ply graphite/epoxy face sheets, .009 inches thick, and an aluminum core with a ¼-inch cell size and density of 1.6 lb./ft^3. The support ring under the fixed center section was a rectangular tube cross-section 2 in. X 3 in. X .030 in. thick. The hinges interconnecting the panels were made of aluminum. The main panel inboard hinges which attach to the support ring were made of graphite epoxy composite. Because of weight considerations, no thermal control paint or insulation was used to reduce temperature gradients. Load factors of 12 g lateral and 10 g axial relative to the reflector axis were assumed for the structural analysis. Critical load paths were ascertained and components were sized accordingly.

THERMAL DISTORTION ANALYSIS

The thermal distortion model was a comprehensive model consisting of 1128 triangular plate elements representing the reflector. The support ring, hinges, and feed support struts were simulated by 232 members. Two TRW computer programs were used; the first to determine the deviation of the parabolic contour of each node and the second to determine the best-fit parabola through the nodes. From the Best-Fit Parabola program the ½-path length rms deviation, the focal length, and the bore-sight axis were ascertained.

Thermal distortion was computed for six different sets of conditions applicable for a synchronous orbiting spacecraft:

1. Front face fully illuminated, no insulation on back,
2. Front face ½ shaded, no insulation on back,
3. Front face ½ shaded, with insulation on back,
4. Front face 1/3 shaded, no insulation on back,
5. Front face ½ shaded, no insulation on back, $\alpha = + .3 \times 10^{-6}$ in/in/^{o}F
6. Front face ½ shaded, no insulation on back, $\alpha = - .3 \times 10^{-6}$ in/in/^{o}F
7. Front face ½ shaded, no insulation, inboard hinges of main panels graphite/epoxy composite,
8. Same as 7. except .25" thick core instead of .50"

The results are tabulated in Table 3. The first condition indicates that a symmetrically illuminated reflector has a minimal distortion. Condition 2 shows the effect of unsymmetrical illumination. Condition 3 indicates that adding insulation on the back does not reduce the distortion appreciably. Condition 4 demonstrates that the distortion is only slightly reduced with a small

shaded area. Conditions 5 and 6 show that a significant change in the coefficient of expansion of the graphite face sheets, $\alpha = \pm .3 \times 10^{-6}$ in/in/^{o}F, does not change the distortion drastically. On every other run $\alpha = - .15 \times 10^{-6}$ in/in/^{o}F. (Condition 7) all previous six conditions had aluminum hinges throughout. By changing only the inboard hinges of the main panels to a graphite/epoxy composite the distortion was greatly reduced. The core thickness was reduced from ½" to ¼" (Condition 8) with only a slight increase in distortion.

WEIGHT ESTIMATE

The preliminary weight estimate (Table 2) lists a total weight of 68.5 lbs for the 16-foot diameter reflector. The resultant weight per square foot of reflector surface is 0.299 lb/ft^{2}, including the weight of all components.

MODELS

A partial 7-foot diameter model (Figures 3-6), was designed and constructed of the same materials described for the 16-foot reflector. This model was used to verify that the materials and fabrication techniques would provide reflector panels with the required accuracy. It was also used to demonstrate the deployment concept.

An 11-inch demonstration model (Figures 7 and 8) was also constructed.

CONCLUDING REMARKS

The deployment concept was validated by deployment of the 7-foot diameter model. The accuracy of the surface contour for the panels of the 7-foot model demonstrated that the materials selected and the fabrication techniques were satisfactory for a high performance reflector. Analysis of the 16-foot diameter reflector showed that the distortion due to the worse case temperature distributions encountered in synchronous orbit was less than .002" rms and would be acceptable for frequencies as high as 60 GHz or more.

Future work will establish techniques for assembling, aligning and measuring surface accuracy of the reflector. Design verification tests should be run on flight antennas to demonstrate that the accuracy of the parabolic surface is not affected by launch, deployment or flight environments.

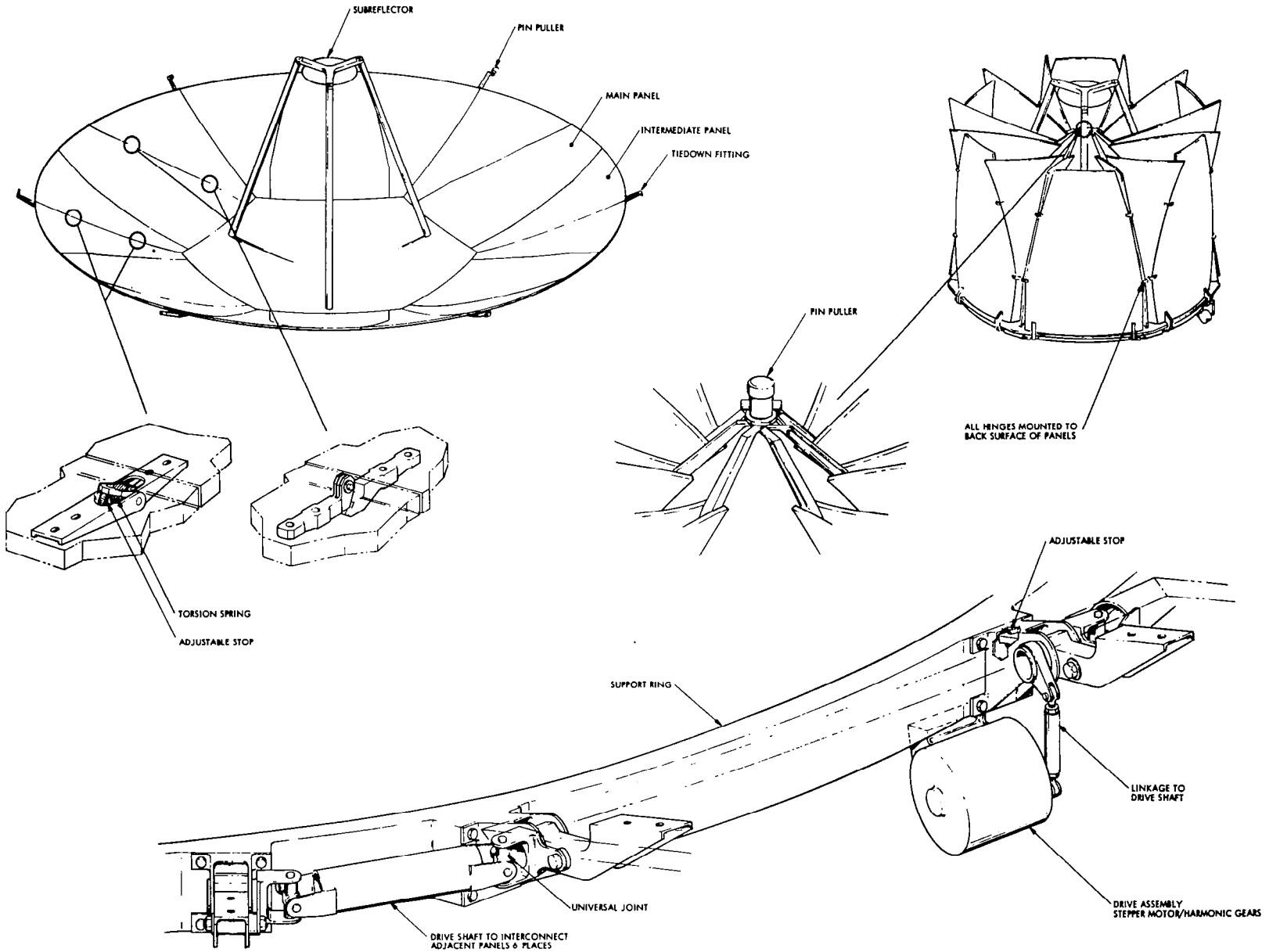

Figure 1 Solid Deployable Reflector

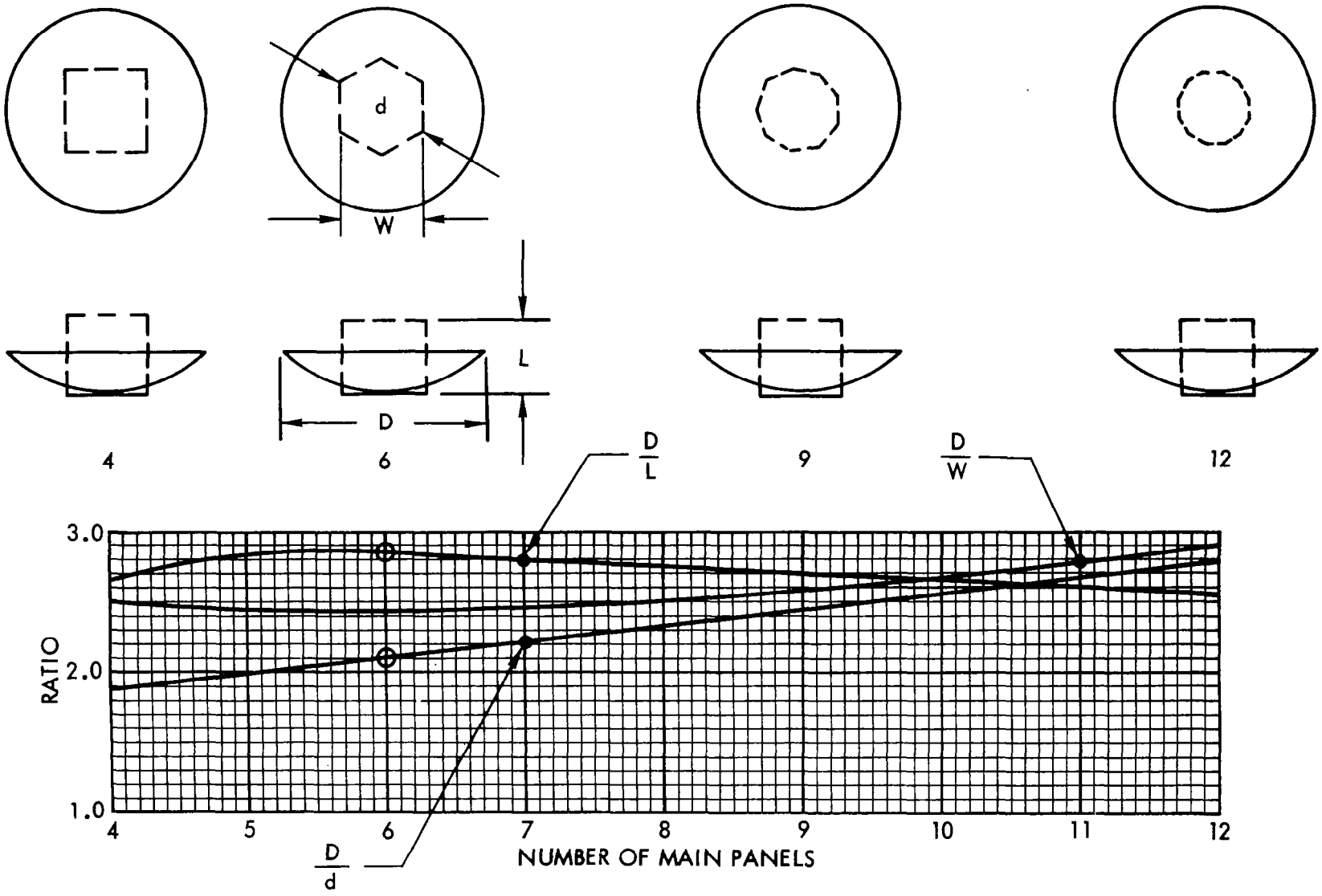

Figure 2 Reflector Configurations and Ratios Of Diameter To Stowed Envelope Dimensions

about 2.5 cm (1 inch) of 0.508 mm (0.020 inch), or about 8 cm (3 inch) of 0.794 mm (1/32-inch) tubing should be helpful for gust filtering without introducing undesirable delays, even if the capacitor volume is small.

FLOW FIELD EFFECTS ON TOTAL ENERGY SENSORS

Obtaining the pressure coefficient for good compensation is best achieved if the sensor can be located in the freestream, unaffected by attitude changes of the aircraft. It is not necessary that the local pressure be the same absolute value as the freestream; it is only necessary that the static pressure, relative to freestream, not vary as the aircraft attitude changes. Because of this, a desirable sensor location must take into consideration local flow field changes during maneuvers. There are several aspects of flow fields which may be important:

1. Boundary layer growth along the body
2. Flow angularities caused by the windshield and the wing body intersection
3. Downwash caused by lifting surfaces deflecting the flow
4. Movable control surfaces which may propagate pressure influences upstream
5. Induced velocities above wing or fuselage

The boundary layer consideration is largely relevant if probes are located on the aft portion of the fuselage. Flows tend to parallel fuselage surfaces aft of the wing, so that a location roughly mid-way between the wing trailing edge and the tail offers relatively constant flow conditions for total energy sensors, provided that the sensor is located far enough from the body to avoid the boundary layer at all angles of attack or yaw. For aft fuselage mounting on the upper side, the sensor element should be located about 7 inches above the surface to insure avoidance of boundary layer fluctuations as attitude changes.

Sensors have been located successfully on the noses of sailplanes; however, for this location there often are significant flow angularities as the flow streamlines are diverted around the body. Canopy bumps may cause local effects which would be undesirable, for example, and when positioning at the proper sweep angle, it should be recognized that streamlines parallel the surface at the surface.

High performance sailplanes usually achieve some laminar flow on the nose portion of the fuselage; a performance penalty may result with a probe in the laminar region which triggers an early transition from laminar to turbulent flow. This is not a problem for training sailplanes or others which do not depend on laminar flow for performance. Judgement must be

used in determining the proper sensor sweep angle on a curving surface, and experimenting with flight tests may be necessary.

The vertical fin location usually offers near freestream conditions, provided the probe is positioned so that the fin, rudder, stabilizer and elevator (especially for Tee Tail configurations) are taken into account.

The principal downwash in the flow field at the fin location is caused by the wing deflecting the air to produce lift. A series of calculations have been made to cover the range of effects for typical sailplanes during cruise and climb conditions. The downwash flow angle is a function of the lift coefficient being achieved at a given time. Reference 16 provides a thorough discussion of the mechanisms affecting the downwash as well as analytical methods for use in calculations. Based on these techniques, and the dimensions for short coupled sailplanes like the 1-26, the downwash angle at the fin tip in degrees is about three times the lift coefficient, C_L . In the cruise condition, the lift coefficient for the 1-26 is about 0.5, making the downwash angle only 1.5 degrees. In the climb condition, the lift coefficient is about 1, making the downwash about 3^o. For high performance sailplanes having longer wings and fuselages, the downwash values decrease to about half those for a 1-26; that is, the range of downwash angles at the fin may be about 1.2 to 1.8 times C_L degrees. The range of lift coefficients may be somewhat greater due to flaps; however, the total downwash variation for high performance sailplanes may still be less than 3^o.

For a fin installation, the sensor should be positioned at least 5 to 10 times the maximum fin thickness ahead of the leading edge (ref. 17). Severe rudder deflections may cause significant lateral flow inclinations; however, the insensitivities of the simple probes described herein are a real advantage. Horizontal tail movements affect the downwash flow field to some extent. When attitude changes are being made, transients may be noticed; however, the effects can be minimized by smooth movements of the control surfaces. Sailplanes that are well balanced will not have very large tail lift coefficients, and therefore small downwash effects.

In summary, a sensor location insensitive to changes in attitude is necessary for operation over a broad range of locations. Aft fuselage and vertical fin locations can be suitable for the probes discussed. Nose installations may be acceptable for low performance sailplanes; however, they must be positioned carefully.

CONCLUDING REMARKS

Experimental pressure coefficients suitable for total energy compensation have been obtained using principles of laminar flow around a small inclined cylinder. To obtain the correct flow relationships, the sensor orifice should be located carefully with respect to the end of a 3-dimensional cylinder; several options for providing the proper relationships have been extended by the current study of probes made of bent-up tubing. Total energy-pressure relationships have been reviewed to explain the principles involved and further explanations of 3-dimensional effects have been presented.

In general, it has been shown that probe sensors with lengths as short as 7 times the outside diameter of the tubing used can be made to work with certain orifice locations. On the other hand, data have shown that sensitivities to manufacturing tolerance and flow incidence angles are reduced when sensor lengths of 11 diameters or greater are used.

Comparative results from a number of experimenters have verified the principles and findings previously presented. The most significant of these probe dimensions are the sensor hole location geometry and the best angle of sweep for compensation that is insensitive to range of angles of incidence.

Damping restrictors are useful to filter gusts and may be simply made by installing a small section of capillary tubing in or near the total energy probe, in series with an appropriate capacitor volume.

Flow field effects around aircraft can affect the compensation of total energy sensors and must be considered. Among the effects are the boundary layer growth, flow angularities, downwash caused by lifting surfaces and movable control surfaces which may propagate pressure influences. The significance of these effects and ways of accounting for them are discussed.

REFERENCES

1. Nicks, Oran W.: A Simple Total Energy Sensor. NASA TMX-73928, March 1976. (Also presented at XV Congress of OSTIV, Rayskala, Finland, June 1976.)

2. Nicks, Oran W.: A Simple Total Energy Sensor. Soaring, Volume 40, No. 9, Sept. 1976.

3. Nicks, Oran W.: How to Make a Total Energy Sensor. Soaring, Vol. 41, No. 3, March 1977.

4. U. S. Patent Office, U. S. Patent No. 4,061,028. Aircraft Total Energy Sensor - Oran W. Nicks, Dec. 6, 1977.

5. Thom, A.: The Flow Past Circular Cylinders at Low Speeds. Proceedings of the Royal Society of London, Series A., Vol. CXLI. Printed for the Royal Society and sold by Harrison and Sons, Ltd., St. Martins Lane, Sept. 1933.

6. Thom, A.: An Investigation of Fluid Flow in Two Dimensions. Reports and Memoranda No. 1194 (AE356). Printed and Published by His Majesty's Stationary Office, London, Nov. 1928.

7. Goldstein, S.: Modern Developments in Fluid Dynamics. Vol. I, Oxford at the Clarendon Press, 1938.

8. Bursnall, William J., and Loftin, Laurence K., Jr.: Experimental Investigation of the Pressure Distribution About a Yawed Circular Cylinder in the Critical Reynolds Number Range. NACA TN 2463, Sept. 1951.

9. Wells, Bill: Calibrating Total Energy Tubes. Soaring, Vol. 41, No. 11, Nov. 1977.

10. Westerboer, Ingo: Die Neue Nicks-Duse: Ein ganz heiber Tip von der OSTIV-Tagung in Finnland. aerokurier, Vol. 9, Sept. 1976.

11. Shaw, Charles: T. E. Sensor, 1-26 Association Newsletter, Jan. 1977.

12. Irving, Frank: A New Total Energy Head. Sailplane and Gliding, Feb.-March 1978.

13. Johnson, Dick: Variometer Time Constants - Soaring Mail - Soaring Vol. 41, No. 6, June 1977.

14. Foster, K., and Parker, G. A.: Fluidics Components and Circuits. Wiley Interscience, A Division of John Wiley and Sons, Ltd., London, New York, Sydney, Toronto.

NASA-ARC 91.5-CM AIRBORNE INFRARED TELESCOPE

By Robert E. Mobley, and Ted M. Brown

NASA Ames Research Center

ABSTRACT

At the 6th Aerospace Mechanism Symposium, September 1971, a paper was presented detailing the planned development of a 91.5 cm aperture telescope to be installed aboard a NASA-Lockheed C-141A aircraft for the performance of infrared astronomy. This airborne observatory is now operational and has exceeded all stability expectations. A unique feature of the telescope is that its entire structure is supported by a 41 cm spherical air bearing which effectively uncouples it from aircraft angular motion, and with inertial stabilization and star tracking, limits tracking errors to less than 1 arc second in most applications. A general description of the system, a summary of its performance, and a detail description of an offset tracking mechanism is presented.

INTRODUCTION

Ground-based observations with an optical telescope are limited by three properties of the terrestrial atmosphere: turbulence, emission and absorption. If a telescope is carried above the troposphere, nearly all turbulence is avoided and both emission and absorption are greatly reduced at many wavelengths in the infrared where water vapor is the source of opacity. To take advantage of high-altitude observations, NASA-ARC has conducted a program of airborne astronomy since 1965, using primarily a CV-990 four engine jet transport and a Lear jet. These aircraft were modified to accept telescopes of up to 30 cm aperture with various stabilizing devices giving long-term line-of-sight stabilities of 10 to 60 arc sec (ref. 1). The intriguing possibility of flying a well-stabilized, large aperture telescope was considered from the beginning of the program and culminated with the 91.5 cm aperture telescope becoming operational in 1974.

The unique feature of the telescope, and the one that, in our opinion, has made the excellent tracking stability possible, was the concept of supporting the telescope on a spherical air bearing and thus effectively uncoupling it from aircraft rotational motions. When this concept was presented at the 6th Aerospace Mechanism Symposium in 1971, it was received (and perhaps rightly so) with some skepticism because of the hostile aircraft environment and the design goal for tracking stability. At that time, the telescope optics were being

figured, equipment components fabricated and the aircraft modified; however, it was still an interesting, but untested concept. Now, after three years of successful operation, we wish to present the airborne infrared telescope as a viable research facility.

SYSTEM DESCRIPTION

Figure 1 shows the telescope installed aboard the StarLifter. The telescope views from an open cavity recessed in the left side of the fuselage forward of the wing and its nominal line of sight is normal to the aircraft longitudinal center line. Movable watertight doors cover the cavity when the system is not in use. For observing, the doors are opened to provide an aperture large enough to preclude vignetting of the telescope over a 4° field of view centered in the orifice. The aperture, or orifice, and the telescope can be moved in-flight over an elevation range of 35° to 75°. Porous spoilers

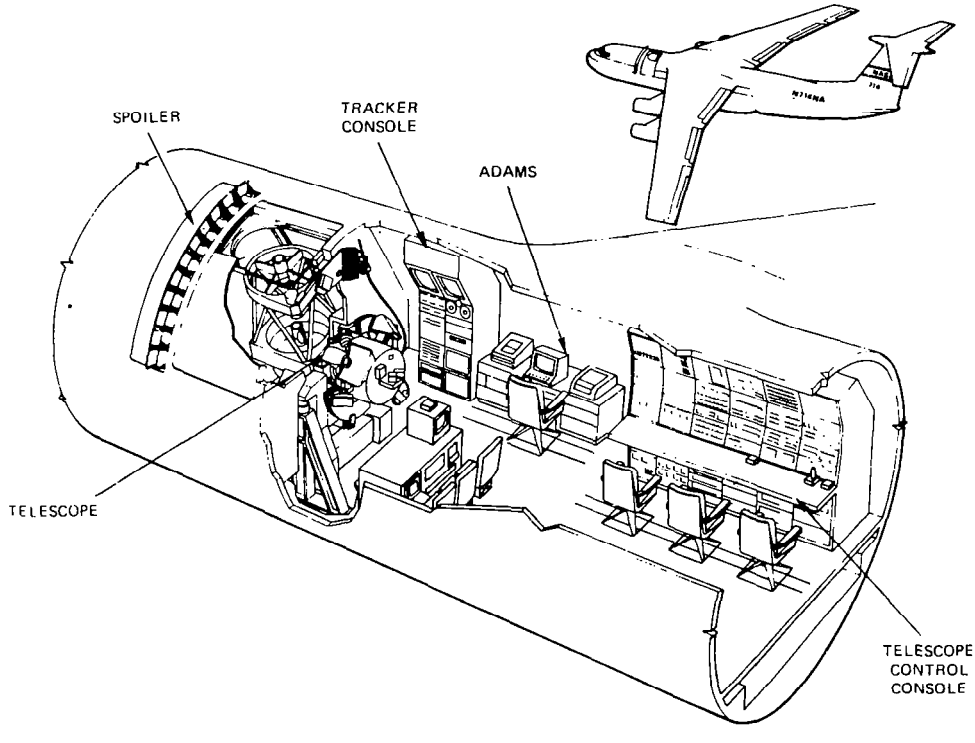

Figure 1 Airborne Observatory

are located in front of the orifice where they control the flow of air across the opening and minimize pressure fluctuations and resonance with the cavity (ref. 2). When the orifice is closed, the spoilers are retracted against the fuselage.

The telescope is a conventional Cassegrain supported in an all-Invar A-frame structure and head ring (fig. 2). The frame and head ring, designed for minimum flexure and low thermal expansion, also support the acquisition and tracking telescopes. The telescope is attached to one side of a 41 cm diameter Invar air bearing that is the single suspension point for the entire telescope system. The air bearing and its matching spherical socket are embedded in the aft pressure bulkhead. A flat mirror located between the primary and secondary mirrors folds the optical axis of the telescope through a hole in the air bearing and on through an equipment mounting flange on the cabin side of the pressure bulkhead.

The primary mirror is a solid CERVIT paraboloid with a 183 cm focal length (f/2). It is supported in its cell by axial and lateral pneumatic bellows and locators. Support for the tertiary mirror and light baffle is through the 20 cm core of the primary to the mirror cell.

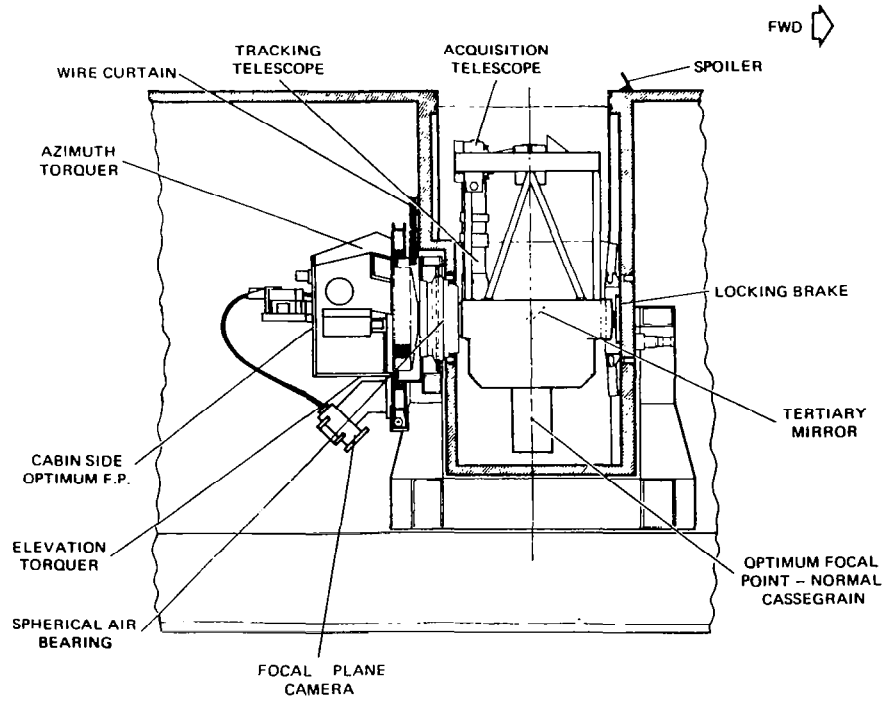

Figure 2 Telescope Installation View Outboard

The secondary mirror, also of solid CERVIT, is a 23 cm diameter hyperboloid figured to yield an overall focal ratio of f/13.5 (12.3m) at final focus. The mirror and step-focus drive are held in the head ring by an orthogonal Invar spider. Some types of radiometry and photometry employ a wobbling secondary mirror as an efficient means of space filtering. Accordingly, an alternate secondary assembly is provided that can be oscillated at frequencies up to 40 Hz.

In the folded mode, optimum focus will fall 61 cm from the mounting flange on the cabin side of the air bearing. Total back-focus will be 76 cm. The hole in the flange contains a disk that can be rotated to five positions interposing different pressure-carrying infrared or visible transmitting windows. With one of the pressure windows in the optical path, instruments can be operated in the cabin environment. With the window removed, the detector package can be operated in the cavity environment, provided a pressure vessel (supplied with the telescope) is installed around the detector package or the detector package itself is designed to carry the pressure differential (0.56 atm). A failsafe interlock will prevent rotating the disk across the open-hole position when a pressure differential exists.

A focal plane monitoring system permits either continuous or command monitoring of the focal plane from the console (closed circuit television display).

The cabin-side mounting flange will support up to 182 kg of observational equipment with a center of mass 61 cm from the flange. The experimenters' equipment weight is interchanged with counterweights to maintain balance of the entire telescope (882 kg) on the air bearing. After initial balance, sensors located on each axis will detect any small imbalances that may occur (e.g., cryogenics depletion) and automatically move small counterweights to rebalance the system.

To prevent drag on the air bearing, all electrical, vacuum, and cryogenic lines will be brought from the cavity wall to the mounting flange and telescope as a single bundle or curtain (fig. 2). The curtain will be servo controlled to follow the telescope's motion. Lines to the telescope are passed through the periphery of the hole in the air bearing.

Conventional Cassegrain focus is available with the tertiary mirror removed. Up to 46 kg of equipment can be mounted to the flange behind the primary mirror cell. However, because of space limitations between the back side of the primary mirror and the cavity floor and walls, the total length of the instrument package cannot exceed 50 cm if the entire elevation range is to be used. In addition, instruments mounted at Cassegrain focus must be operated remotely as there can be no direct access to the cavity during flights.

The air bearing support eliminates all rotational motion potentially transmitted from the airplane. All translatory vibrations are attenuated by an active isolation system. The isolators are designed for a cutoff frequency of 3 Hz. They support the telescope at four points, forming a plane that contains the center of gravity of the telescope and thus eliminating cross

coupling of linear vibrations. The telescope structure is designed for a natural frequency of greater than 30 Hz, while the air bearing has a natural frequency of greater than 150 Hz.

Telescope attitude (relative to the aircraft) is sensed by optical digitizing sensors so located as to indicate telescope position in telescope coordinates of azimuth, elevation and line-of-sight.

OPTICAL PERFORMANCE

The telescope is capable of operating at the ambient pressures and temperatures encountered between 15.2 km and sea level. However, the optical quality of the system is optimized for an average altitude and temperature of 13-15 km and 200°K respectively. Exclusive of aircraft boundary-layer effects on seeing, the overall optical quality is such that at least 85 percent of point-source incident radiation at 0.55 microns is contained within a 1 arc-second blur circle. With the 20.3 cm diameter non-oscillating secondary, the area of obscuration is approximately 8 percent; taking into account effects from the spiders, etc., the system is diffraction-limited at about 1 micron.

Currently, a slightly undersized (18.5 cm diameter) aluminized silicon mirror is mounted on a dual solenoid mechanism oscillating at a maximum frequency of 40 Hz. A second generation oscillating system is under development with a capability of square wave operation at speeds faster than 100 Hz. Appropriate baffles and stops minimize scatter and side-lobe response, and the edges of the spiders facing the primary are gold flashed. Development of a family of mirrors is planned for installation as needed on the oscillating secondary mount. Uncoated pure aluminum is deposited on the primary mirror, and alternate secondary and tertiary mirrors with either aluminum or gold coatings are provided. With all aluminum-coated optics, the threshold visual magnitude at optimum focus is $m_V \geq 17$.

TELESCOPE ENVIRONMENT CONTROL

Beside the use of Invar and CERVIT to minimize thermal flexure, the telescope cavity and the instrument pressure dome can be precooled to near the predicted stagnation temperature at the observing altitude. While on the ground, a portable mechanical refrigerator is used to cool the cavity walls and to trap any water vapor inside the cavity. A slight positive pressure is maintained within the closed cavity to avoid ingestion of water vapor or dust from outside. In-flight cooling is provided by an on-board system.

IMAGE STABILIZATION AND TRACKING

The design goal for image stability at the focal plane was 2 arcsec rms for at least a 30 min interval. Drift between the tracking systems and the main focal plane was not to exceed 1 arcsec during this interval. These goals have been met. Four stages of stabilization are required to achieve this accuracy, the first stage being the StarLifter itself. If the autopilot is tuned for a known airspeed, altitude, and payload, excursions in pitch and yaw are held to within $\pm$ 0.5°. Even in light turbulence, the autopilot can limit aircraft excursions to $\pm$ 2°. The telescope tracking and stabilization systems overcome these latter oscillations.

Inputting a false error signal into the autopilot heading gyro causes the airplane to turn at very slow rates (0.2°/min) and compensate for diurnal motion, thus keeping the observed object centered in the orifice. To view an object at a different azimuth, the airplane is simply turned to a heading that will put the new object athwartship normal to the aircraft or abeam of the telescope.

The air bearing is the second stage of telescope stabilization. Floating on a thin film of high pressure air (the gap between the bearing and its housing will be 1.8 ; air flow will be at 15 scfm at a pressure of 19 atm), the bearing is an almost frictionless support. The air is scavenged to avoid contamination of the cavity. Moreover, the bearing's spherical cross section makes possible three-axis inertial stabilization.

Third-stage stabilization is provided by three gas-bearing gyroscopes and their associated torque motors; each gyro-torquer is tied to one of the telescope's three axes (fig. 2). This system serves as an inertial reference platform for the air bearing. The torque motors can be over-ridden manually to slew the telescope. The segmented dc torque motors are not mechanically coupled between the air bearing and its housing; thus, no static friction is induced into the system. Torque is applied to the telescope by varying the electric field between the "rotor", which is part of the air bearing, and the stator, which is part of the air bearing housing.

The fourth stabilization stage is an image tracking system composed of a 6-inch aperture, f/5 telescope and in the original facility, an image dissector. This system removes gyro drift and other slow random motions, and was originally mounted rigidly to the main telescope and boresighted to its optical axis. Because of the image dissector's modest brightness threshold of mv=+6, it was believed necessary to have offset tracking capability, that is, to be able to center faint stars in the main telescope while tracking on the bright ones. Originally, this was accomplished by incorporating a pair of rotating prisms mounted in front of the tracker. It was felt that this method would afford a much better chance of accomplishing precision setting than actually rotating the tracker itself. This rotating prism mechanism worked well, but had to be discarded because of unexpectedly high thermal distortion of the prisms.

Shortly after this, the original image dissector was replaced with a video camera and a new digital tracker was developed in which the camera output was directly used to develop error signals to feed into the gyro control loop. This new tracker system has been used successfully for two years and has demonstrated a brightness threshold of mv=+12, much improved over the old system. Table I is a summary of the performance of the tracker during a test flight when moderate turbulence was experienced. Because of this improvement, the urgency of developing a successful offset tracking capability was reduced, although not eliminated. Invisible infrared sources could not be observed until offset tracking was incorporated. A new mechanism has now been developed which provides offset tracking by rotating the tracker, telescope/camera assembly itself.

TABLE I

TRACKING ACCURACY, DIGITAL TRACKER

	Stellar Target	Visual Magnitude	Error (sec-rms) Azimuth	Elevation
Pleiades	SAO-076228[1]	3.8	.49	.76
	SAO-076172	4.2	.44	.86
	SAO-076140	4.4	.59	.68
	SAO-076126	5.4	.74	.97
	SAO-076159	5.9	.49	.61
	SAO-076164	6.5	.64	.72
	SAO-076197[2]	6.9	.69	1.40
	SAO-076203[2]	8.6	1.27	1.40
	SAO-076177	9.0	.98	1.80
	Ref. #706[3]	10.1	1.98	2.05

The offset tracking mechanism was to have a range of motion of at least $\pm$ 1/2 degree in both azimuth and elevation motions, and thus, assure having a trackable star within range for any point in the sky. It must hold the tracker steady within 1 arc second in a 0.2 g gust flight environment and have adjustment increments of 1 arc second or less, which could be made frequently during tracking maneuvers. Precision setting approaching a few seconds of arc was necessary. It was estimated that, in most cases, positioning the object within approximately 8 seconds of arc would allow an automatic peaking program to make fine offset corrections, which would pull an invisible object into center. Space limitations were very severe, and the operators could not afford an extended shutdown period to allow modifications necessary to relocate the

tracker to a less cramped area. We had to use the existing tracker's mounting surface which is located on the telescope headring close, radially, to the line-of-sight axis. We could not violate the 36-inch diameter aperture cylindrical space, a difficult feat, because the tracker's existing mounting flange was already up against it. Also, we wished to make use of the old stepping motors (2000 steps/sec) and encoders (10,000 counts/sec) from the rotating prism mechanism, to drive the new mechanism.

Figure 3 shows the mechanism. It is ring shaped and is sandwiched between the tracker's mounting flange and the bottom side of the main telescope's headring. A stack of circular leaf springs serve as a flexure connecting the tracker to the headring. The springs are mounted to the headring at three nearly equally spaced points, around the circle, while the tracker is connected to the springs at points between these. The springs act as a very rigid constraint for three degrees of freedom of motion of the tracker (two lateral translations and axial rotation), but allow flexibility in three others (axial translation, and two lateral rotations). Three screw jacks constrain and adjust the tracker for these flexible degrees of freedom. The jacks, mounted rigidly to the headring through stout shakles and a base ring, bear against the tracker near the points of connection to the springs. They always operate within a range such that the springs produce enough load to the jacks to prevent backlash and separation in a 0.2 g gust environment.

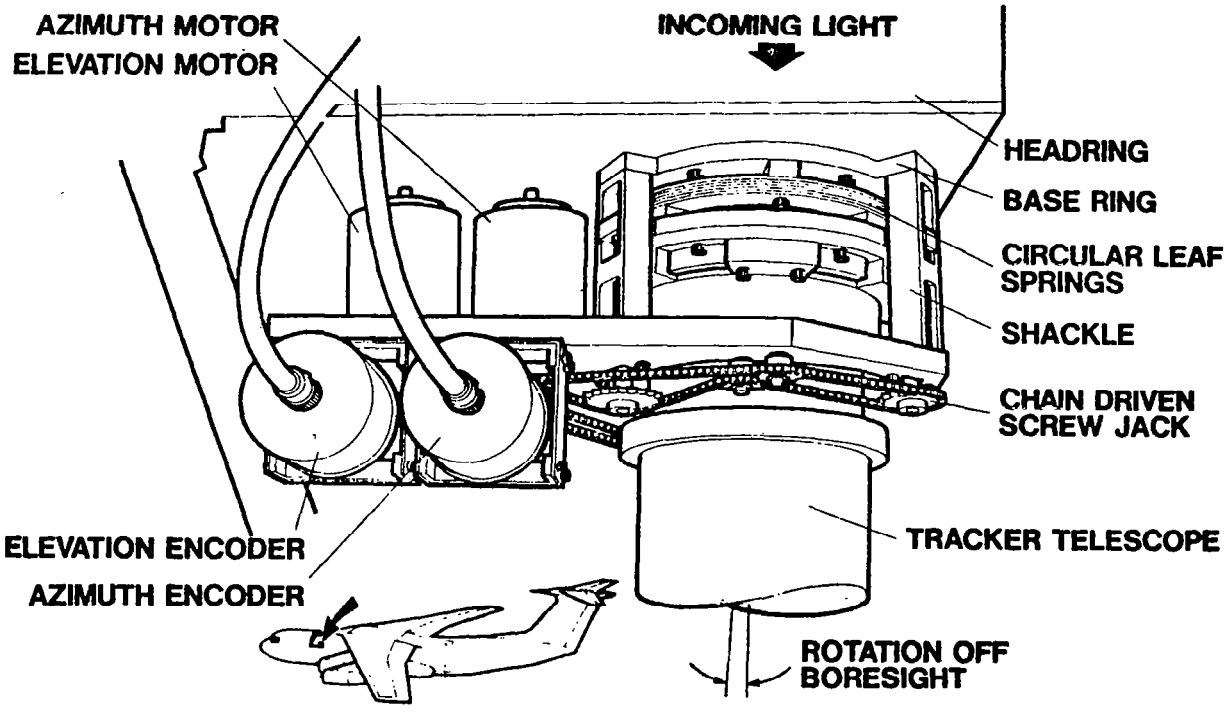

Figure 3 Tracker Offset Mechanism

The jacks are actuated by a pair of stepping motors and a system of chain drive. The elevation rotation is accomplished by driving just one jack, while azimuth rotation requires driving the other two jacks in opposite directions in the same chain loop. This simple combination of jacking motions is possible because there is no requirement to locate the axes of rotation precisely other than to orient them accurately. Encoders sense the jacks' positions.

The mechanism has demonstrated extreme steadiness, no observed degradation from the previous rigid mounting. The chain drive and encoder gearing allow incremental motions of 1/4 arc second. The initial setting precision has been disappointing in that after the mechanism was moved through a dozen offset maneuvers, an RMS setting error of approximately 30 arc seconds occurred. Close examination of the results indicated that a disproportionate amount of the error was in offset direction rather in offset distance. Such a tendency cannot be explained by mechanism imprecision, but only by errors in calculating rotation of the stars relative to the telescope's line of sight (L.O.S.) rotation. Further examination brought to light that, indeed, telescope L.O.S. rotation was not being accurately sensed and used properly by the on-board computer to make the offset direction calculation. The problem is that the telescope L.O.S. has as its only reference the aircraft, which in normal flight is experiencing continual pitch variations (which translate into telescope L.O.S. rotation). There presently exists a control system which can hold the L.O.S. to the aircraft pitch, but the computer makes rotation calculations only every 10 seconds, in which time the aircraft pitch can change markedly. (Parameters used by the computer to calculate offset direction include the star's coordinates, sidereal time, aircraft's longitude and latitude, and aircraft pitch.) What is required is either increasing the frequency of offset direction calculations to every one or two seconds (which would overtax the present on-board computer capacity) or allow the L.O.S. to inertially stabilize over relatively long periods (approximately one minute) and make occasional gross correction when the telescope drifts away from the center of the viewing orifice. This scheme requires a new control system to make this occasional step motion. One of these methods must be used to handle the L.O.S. rotation, and as of this writing, a decision has not been made as to which is most practical.

If one ignores the direction errors in our first tests and only considers offset distance errors, the RMS error was approximately 6 arc seconds, which must all be attributed to mechanism setting imprecision. Two problems have been found which we believe will account for most of this error. We used a miniature roller chain of 0.1475-inch pitch, which turned out to be much more flexible in tension than we had originally estimated (more than ten times). This increased flexibility allows a backlash effect and an effective change in scale factor for different offset position and direction. Scale factor changes apparently occur because the jacking screw torque, and therefore, chain tension varies as the offset positions change. We are presently correcting this problem by replacing the miniature pitch chain with Standard No. 25 roller chains, which is approximately 5 times as stiff. The other problem involved motor shaft bending which primarily resulted in inaccurate encoder readings because of relative motion of the worm and wheel in the worm gear drive. We

are correcting this by mounting outboard bearings to the motor shafts.

Indications are that the future success of the offset tracking mechanism will be more dependent on solving the Line of Sight rotation problem than any setting imprecision of the mechanism itself. While the telescope elevation and azimuth rotation are being stabilized to 1 arc second, all we require in the L.O.S. is knowledge of its position to within approximately a tenth of a degree (or 360 arc seconds).

We believe this can be accomplished. The mechanism itself is proving itself well suited for its application. Over long periods of non-use, it behaves the same as a rigid mounting; the screw jacks are sufficiently loaded that the static friction at the threads allows no motion whatsoever. Its main drawback is in the drive system; considerable torque is required to turn the screw jacks and as a result, components in the drive system experience sufficient elastic deflections to introduce setting errors. We believe the stiffer chain and the outboard bearings on the motor shafts will go a long way to correct this problem.

CONCLUDING REMARKS

The Airborne Observatory has proven to be a very useful facility. It combines a number of unique mechanisms in an unusual application, the most interesting being the use of an air bearing in such a severe environment. It has been most remarkable in that while it performs with such high precision, it remains a very practical and easy to use tool. Rather than being a delicate and fragile device subject to easy failure and malfunction, it is a very sturdy and practical workhorse, capable of undergoing continuous changes to accommodate new experiments, while, at the same time, keeping a busy schedule of two or three flights a week.

REFERENCES

1. Bader, M.; and C. B. Wagoner: NASA Program of Airborne Optical Observations. Appl. Opt. 9.265 (1970).
2. Buell, D. A.: An Experimental Investigation of the Airflow Over a Cavity with Antiresonance Devices. NASA TN D-6205, 1971.
3. Mobley, R. E.; and Cameron, R. N.: NASA-ARC 36-inch Airborne Infrared Telescope, 6th Aerospace Mechanism Symposium, September 9 - 10, 1971.
4. Walter V. Sterling, Inc: Digital Tracker Flight Test Results, WVS Report No. 3-75-06, March 14, 1975.

MR. BOWDEN W. WARD, JR., presents the Dr. George Herzl Award for the best paper to Michael J. Ospring and Ronald E. Mancini

Final Statement

Dr. E. E. Sechler

I wish to thank all participants in this 12th Symposium for making it the success it has been.

Taken in order, the main contributers have been:

1. The members of the Symposium Organizing Committee who read all the many abstracts and made the difficult decision as to the final program.
2. The NASA-AMES Research Center who have been such gracious hosts and in particular Angelo Giovannetti and David Engelbert, plus their competent secretarial assistance and in particular, Pat Daniels for keeping track of all the many details.
3. Al Rinaldo of Lockheed who has spent many hours in worrying about all the many details relating to authors, papers, and organization. We are indebted to him and Angelo for the delightful time we had on Thursday evening.
4. And, finally, the real people who always make successes or failures of Symposia.
   a. Session Chairmen
   b. Authors of papers and the speakers who presented them.
   c. Attendees who not only listened patiently but participated actively with their questions and comments.
   d. Finally, the California Weatherman.

See you all in Johnson S.F.C. in Houston next year at about this time - watch for call for papers.

1. Report No.	2. Government Accession No.	3. Recipient's Catalog No.
NASA CP-2080		

4. Title and Subtitle	5. Report Date
12th AEROSPACE MECHANISMS SYMPOSIUM NASA, CALTECH, LOCKHEED April 27-28, 1978	April 1979
	6. Performing Organization Code
7. Author(s)	8. Performing Organization Report No. A-7737
	10. Work Unit No. 992-22-03
9. Performing Organization Name and Address NASA Ames Research Center Moffett Field, California 94035	11. Contract or Grant No.
	13. Type of Report and Period Covered Conference Publication
12. Sponsoring Agency Name and Address National Aeronautics and Space Administration Washington, D.C. 20546	14. Sponsoring Agency Code

15. Supplementary Notes

Held at Ames Research Center on April 27-28, 1978

16. Abstract

These symposia are the only meetings in the world specifically devoted to the problems of design, fabrication, test, and the operational use of mechanisms. They provide a forum for interchange among those active in the field of mechanism technology.

17. Key Words (Suggested by Author(s))	18. Distribution Statement
Mechanisms Mechanical Engineering	Unlimited STAR Category - 37

19. Security Classif. (of this report)	20. Security Classif. (of this page)	21. No. of Pages	22. Price*
Unclassified	Unclassified	256	$9.00

*For sale by the National Technical Information Service, Springfield, Virginia 22161

NASA-Langley, 1979